

ABSTRACT

Title of Document: VERTICAL DYNAMIC SOIL-PILE
INTERACTION FOR MACHINE
FOUNDATIONS

Ossama Salem Ali Ahmed, Ph.D., 2015

Directed By: Professor, M. Sherif Aggour, Department of
Civil and Environmental Engineering.

The way to achieve satisfactory performance of a machine foundation is to limit its dynamic amplitude to a few micrometers. In using piles for the foundation, the interaction of the pile with the surrounding soils under vibratory loading will modify the pile stiffness and generate damping. This study presents the results of a three-dimensional finite element model of a soil-pile system with viscous boundaries to determine the dynamic stiffness and damping generated by soil-pile interaction for a vertical pile subjected to a vertical harmonic loading at the pile head. The pile was embedded in a linearly elastic, homogeneous soil layer with constant material damping. A parametric study was undertaken to investigate the influence of the major factors of the soil pile system that affect the vertical vibration characteristics of the pile response. These were found to include the dimensionless frequency, a_0 , soil-properties, pile properties, and length and axial load on the pile head.

Pile foundations are generally constructed in groups. A three by three group of piles rigidly capped were used in this study. Three different pile spacings were used, two times, four times and six times the pile diameter. Both the dynamic stiffness and

damping were determined for the whole group. The group effect on the stiffness and damping was determined by group stiffness and damping efficiency factor. The efficiency factor was found to be frequency dependent, could attain values above unity, and was very sensitive to the soil shear modulus. The distribution of forces among the pile group was also determined.

VERTICAL DYNAMIC SOIL-PILE INTERACTION FOR
MACHINE FOUNDATION

By

Ossama Salem Ali Ahmed

Dissertation submitted to the Faculty of the Graduate School of the
University of Maryland, College Park, in partial fulfillment
of the requirements for the degree of
Doctor of Philosophy
2015

Advisory Committee:

Professor M. Sherif Aggour, Chair

Professor Amde M. Amde

Professor Chung C. Fu

Professor Yunfeng Zhang

Professor Sung W. Lee

© Copyright by
Ossama Salem Ali Ahmed
2015

Dedication

To my father, mother, my wife, my daughter, Nour, and my son, Youssef, whom without their continuous support I would not have been able to finish this work.

Acknowledgements

I would like to express my deep appreciation and gratitude to Professor M. S. Aggour whom under his supervision this study was performed. His technical guidance and continuous support and encouragement proved to be invaluable. I would like to thank Professors Amde M. Amde, Chung Fu, Yunfeng Zhang and Sung W. Lee for kindly serving on my advisory committee. I also would like to thank my beloved parents and my wife for the continuous support and encouragement over the years of my study.

Table of Contents

Dedication.....	ii
Acknowledgements.....	iii
Table of Contents.....	iv
Chapter 1: Introduction.....	1
1.1 Statement of the Problem.....	1
1.2 Current Design Method.....	2
1.3 Objective and Scope.....	4
1.4 Structure of the Dissertation.....	5
Chapter 2: Literature Review.....	7
2.1 Background.....	7
2.2 Vibration Limits for Machine Foundation.....	9
2.3 Modeling Techniques for Machine Foundations.....	10
2.4 Machines Supported on Mat Foundations.....	10
2.5 Machine Supported on Piles Foundation.....	14
2.6 Pile Group Interaction.....	30
Chapter 3: Finite Element Model of the Soil Pile System.....	38
3.1 Introduction.....	38
3.2 Generation of the Finite Element Model.....	42
3.3 Model Description.....	49
3.4 Element Types.....	52
3.5 Modeling of the Pile Cap.....	53
3.6 Modeling of the Soil Boundaries.....	55

3.7 Element Size	60
3.8 Damping.....	61
3.9 Soil Properties.....	61
3.10 Pile Properties.....	62
3.11 Loading	63
3.12 Verification of Soil Boundary Location	64
Chapter 4: Vertical Dynamic Response of a Single Pile	68
4.1 Introduction.....	68
4.2 Dynamic Parameters Determined.....	69
4.3 Static Stiffness of a Single Pile.....	72
4.4 Dynamic Stiffness and Damping of a Single Pile.....	75
4.5 Effect of Different Parameter on Dynamic Stiffness and Damping	87
Chapter 5: Dynamic Response of Group of Piles	107
5.1 Introduction.....	107
5.2 Dynamic Stiffness & Damping for a 1.5 ft. Diameter Pile.....	109
5.3 Vertical Static Stiffness of Pile Groups	111
5.4 Dynamic Stiffness, Damping and Resonant Frequency of Pile Groups	114
5.5 Effect of the Ratio G_{soil}/E_{pile} on the Dynamic Stiffness and Damping	132
5.6 Forces and Displacements of Pile Groups	137
5.7 Pile Interaction and Group Efficiency	150
Chapter 6: Model Comparison.....	161
6.1 Comparison of Pile Static Stiffness with Mylonakis and Gazetas Solution ...	161
6.2 Comparison of the Pile Stiffness with DYNA5.....	162

6.3 Comparison of the Pile Stiffness with Novak (1974) and Chowdhury & DasGupta (2009).....	165
6.4 Comparison of the Pile Damping with Gazetas and Dobry.....	170
Chapter 7: Conclusion and Recommendation.....	171
7.1 Single Pile.....	171
7.2 Pile Groups	173
Appendix A: Tables of Single Pile and Pile Groups Analysis.....	178
A.1. Results of Vertical Static Stiffness for Single Pile	178
A.2. Results of Vertical Dynamic Stiffness for Single Pile.....	178
A.3. Effect of G_{soil}/E_{pile} on Vertical Dynamic Stiffness of Single Pile.....	179
A.4. Results of Vertical Damping of Single Pile.....	180
A.5. Results of Vertical Static Stiffness for Pile Groups.....	182
A.6. Results of Vertical Dynamic Stiffness for Pile Groups	184
A.7. Effect of G_{soil}/E_{pile} on Pile Group Dynamic Stiffness.....	186
A.8. Damping of a Group of Piles	188
Appendix B: Derivation of Compliance Functions	191
B.1. Vertical Vibration of Foundation on Elastic Half Space	191
B.2. Rocking Vibration of Foundation on Elastic Half Space.....	209
B.3. Sliding Vibration of Foundation on Elastic Half Space.....	211
B.4. Torsional Vibration of Foundation.....	215
Appendix C: Static and Dynamic Efficiency Calculation	217
C.1. Comparison of Static Efficiency Factors between FE Solution and Randolph and Poulos.....	217

C.2. Comparison of Dynamic Efficiency Factors between FE Solution and Dobry and Gazetas	219
References.....	221

LIST OF FIGURES

Figure 1-1: Machine waves transmitted into soil continuum.....	2
Figure 2-1: Turbo-Generator Machine Supported on Rigid Block Foundation	8
Figure 2-2: Turbo-Generators Machine with Frame Foundation	9
Figure 2-3: Finite Element Model for Mat Foundation	11
Figure 2-4: Foundation Lumped Mass Model (Fixed Base).....	13
Figure 2-5: Three Dimension Foundation Model with Soil Springs	13
Figure 2-6: Smith (1960) Lumped Mass Pile Soil Reaction Model	16
Figure 2-7: Smith (1960) Shaft and Base Soil Reaction Model	17
Figure 2-8: Lysmer and Richart (1966) Soil Reaction Base Model	18
Figure 2-9: Randolph and Simons (1986) Soil Reaction Shaft Model	18
Figure 2-10: Randolph and Simons (1986) Soil Reaction Base Model.....	19
Figure 2-11: Holeyman (1988) Soil shaft reaction model	20
Figure 2-12: El-Naggar and Novak (1994) Pile Shaft Model.....	21
Figure 2-13: Deeks and Randolph (1995) Soil Reaction Base Model.....	22
Figure 2-14: Novak Model for a Single Pile.....	24
Figure 2-15: Variation of $fz1$ with LR and EpG for Friction Piles.....	26
Figure 2-16: Variation of $fz2$ with LR and EpG for Friction Piles.....	26
Figure 2-17: Sub-Structuring Method (Gazetas 1984)	27
Figure 2-18: Holeyman (1985) shaft and base model.....	29
Figure 3-1: Soil Pile Model for a Single Pile.....	39
Figure 3-2: Pile Foundation with Piles Spaced at $2D_{pile}$	40
Figure 3-3: Pile Foundation with Piles Spaced at $4D_{pile}$	41

Figure 3-4: Pile Foundation with Piles Spaced at $6D_{pile}$	41
Figure 3-5: Three Dimension View of Soil Pile System	42
Figure 3-6: Global Coordinate Systems in ANSYS	44
Figure 3-7: Soil Volumes in ANSYS.....	46
Figure 3-8: ANSYS Free Meshing	48
Figure 3-9: ANSYS Mapped Meshing	48
Figure 3-10: Soil Volumes Meshed using Mapped Meshing	49
Figure 3-11: Finite Element Model for Soil-Pile-Soil Interaction.....	51
Figure 3-12: Solid 186 Elements Global and Local Axis.....	53
Figure 3-13: Pile Group Foundation Model for Piles Spaced at $2D_{pile}$	54
Figure 3-14: Pile Group Foundation Model for Pile Spaced at $4D_{pile}$	54
Figure 3-15: Pile Group Foundation Model for Pile Spaced at $4D_{pile}$	55
Figure 3-16: Damper Element at the Edge of Soil Boundaries (Viscous Boundary) .	57
Figure 3-17: Dynamic Forces Acting on Unit Soil Volume	58
Figure 3-18: Sectional View of a Single Pile in Soil Continuum.....	63
Figure 3-19: Sectional View of Pile Groups in Soil Continuum	64
Figure 3-20: Effect of Soil Edge on Pile Vertical Dynamic Response.....	66
Figure 3-21: Vertical Pile Response Due to Change in Soil Lateral Boundaries	66
Figure 4-1: Single Pile Finite Element Model 3D View.....	68
Figure 4-2: Single Pile Finite Element Model Sectional View.....	69
Figure 4-3: Vertical Dynamic Amplitude	70
Figure 4-4: Dynamic Magnification Factor at Pile Head.....	71
Figure 4-5: Static Stiffness of a Pile as a Function of the Soil Shear Modulus (G_{soil})	73

Figure 4-6: Comparison of Static Stiffness for Pile With and Without Surrounding Soils	74
Figure 4-7: Stiffness of Pile Based on Average Amplitude for $f_c = 3000$ psi.....	75
Figure 4-8: Stiffness of Pile Based on Maximum Amplitude for $f_c = 3000$ psi.....	76
Figure 4-9: Stiffness of Pile Based on Average Amplitude for $f_c = 4000$ psi.....	76
Figure 4-10: Stiffness of Pile Based on Maximum Amplitude for $f_c = 4000$ psi.....	76
Figure 4-11: Stiffness of Pile Based on Average Amplitude for $f_c = 5000$ psi.....	77
Figure 4-12: Stiffness of Pile Based on Maximum Amplitude for $f_c = 5000$ psi.....	77
Figure 4-13: Stiffness of Pile Based on Average Amplitude for $f_c = 6000$ psi.....	77
Figure 4-14: Stiffness for Pile Based on Maximum Amplitude for $f_c = 6000$ psi.....	78
Figure 4-15: Stiffness for Steel Pile.....	78
Figure 4-16: Damping of a Single Pile with $f_c = 3000$ psi.....	79
Figure 4-17: Damping Ratio of a Single Pile with $f_c = 3000$ psi.....	79
Figure 4-18: Damping of a Single Pile with $f_c = 4000$ psi.....	79
Figure 4-19: Damping Ratio of a Single Pile with $f_c = 4000$ psi.....	80
Figure 4-20: Damping of a Single Pile with $f_c = 5000$ psi.....	80
Figure 4-21: Damping Ratio of a Single Pile with $f_c = 5000$ psi.....	80
Figure 4-22: Damping of a Single Pile with $f_c = 6000$ psi.....	81
Figure 4-23: Damping Ratio of a Single Pile with $f_c = 6000$ psi.....	81
Figure 4-24: Response of a Pile Embedded in Strong Soil at Resonance.....	84
Figure 4-25: Response of a Pile Embedded in Weak Soil at Resonance.....	86
Figure 4-26: Vertical Displacement of Pile in Strong and Weak Soil.....	87
Figure 4-27: Effect of G_{soil}/E_{pile} on Pile Dynamic Stiffness at Frequency of 50 Hz...	90

Figure 4-28: Effect of G_{soil}/E_{pile} on Damping at Frequency of 50 Hz.....	92
Figure 4-29: Effect of G_{soil} on Dynamic Stiffness at Frequency of 50 Hz	93
Figure 4-30: Effect of G_{soil} on Pile Damping at Frequency of 50 Hz.....	94
Figure 4-31: Effect of Load on Dynamic Stiffness.....	95
Figure 4-32: Effect of Load on System Damping.....	96
Figure 4-33: Effect of Load on Resonant Frequency.....	96
Figure 4-34: Effect of Pile Length on Stiffness for Pile in a Strong Soil	97
Figure 4-35: Effect of Pile Length on Damping for Pile in a Strong Soil	98
Figure 4-36: Effect of Pile Length on Stiffness for Pile in a Weak Soil	98
Figure 4-37: Effect of Pile Length on Damping for Pile in a Weak Soil.....	98
Figure 4-38: Vertical Displacement Distribution at Resonance in Strong Soils	100
Figure 4-39: Vertical Displacement Distribution at Resonance in Weak Soils,.....	101
Figure 4-40: Effect of Concrete Strength on Pile Stiffness	102
Figure 4-41: Effect of Concrete Strength on Pile Damping	102
Figure 4-42: Soil-Pile System Resonant Frequency	103
Figure 4-43: Resonant Frequency for a Single Pile with $f_c = 3000$ psi.....	104
Figure 4-44: Static and Dynamic Stiffness for Pile with $f_c = 3000$ psi.....	105
Figure 5-1: Pile Foundation with Piles Spaced at $2D_{pile}$	108
Figure 5-2: Pile Foundation with Piles Spaced at $4D_{pile}$	108
Figure 5-3: Pile Foundation with Piles Spaced at $6D_{pile}$	109
Figure 5-4: Dynamic Stiffness Based on Average Amplitude.....	109
Figure 5-5: Dynamic Stiffness Based on Maximum Amplitude	110
Figure 5-6: Damping of the Pile as a Function in a_o	110

Figure 5-7: Damping Ratio of the Pile as a Function of a_0	110
Figure 5-8: Resonant Frequency of the Pile as a Function of a_0	111
Figure 5-9: Vertical Static Stiffness for Pile Groups with $f_c = 3000$ psi	112
Figure 5-10: Vertical Soil Stresses for a Group of Piles and Axial Pile Forces in Soil with Shear Modulus (G_s) = 1000 ksf	113
Figure 5-11: Vertical Soil Stresses for a Group of Piles and Axial Pile Forces in Soil with Shear Modulus (G_s) = 6000 ksf	114
Figure 5-12: Vertical Soil Stresses for a Group of Piles and Axial Pile Forces in Soil with Shear Modulus (G_s) = 11000 ksf	114
Figure 5-13: Dynamic Stiffness for a 3 x 3 Group of Piles with $f_c = 3000$ psi.....	115
Figure 5-14: Dynamic Stiffness for a 3 x 3 Group of Piles with $f_c = 4000$ psi.....	116
Figure 5-15: Dynamic Stiffness for a 3 x 3 Group of Piles with $f_c = 5000$ psi.....	117
Figure 5-16: Dynamic Stiffness for a 3 x 3 Group of Piles with $f_c = 6000$ psi.....	118
Figure 5-17: Response of a Group of Piles with $f_c = 3000$ psi	119
Figure 5-18: Response of a Group of Piles with $f_c = 4000$ psi	120
Figure 5-19: Response of a Group of Piles with $f_c = 5000$ psi	121
Figure 5-20: Response of a Group of Piles with $f_c = 6000$ psi	122
Figure 5-21: Displacement of Pile Groups Spaced at $2D_{pile}$ in Strong Soil ($a_0 = 0.2$)	126
Figure 5-22: Displacement of Pile Groups Spaced at $2D_{pile}$ in Weak Soil ($a_0 = 2.0$)	127
Figure 5-23: Displacement of Pile Groups Spaced at $4D_{pile}$ in Strong Soil ($a_0 = 0.2$)	128
Figure 5-24: Displacement of Pile Groups Spaced at $4D_{pile}$ in Weak Soil ($a_0 = 2.0$)	129

Figure 5-25: Displacement of Pile Groups Spaced at $6D_{pile}$ in Strong Soil ($a_0 = 0.2$)	130
Figure 5-26: Displacement of Pile Groups Spaced at $6D_{pile}$ in Weak Soil ($a_0 = 2.0$)	131
Figure 5-27: Effect of G_{soil}/E_{pile} on Group Stiffness for Piles with $f_c = 3000$ psi.	132
Figure 5-28: Effect of G_{soil}/E_{pile} on Group Stiffness for Piles with $f_c = 4000$ psi.	132
Figure 5-29: Effect of G_{soil}/E_{pile} on Group Stiffness for Piles with $f_c = 5000$ psi.	133
Figure 5-30: Effect of G_{soil}/E_{pile} on Group Stiffness for Piles with $f_c = 6000$ psi.	133
Figure 5-31: Effect of G_{soil}/E_{pile} on Group Damping for Piles with $f_c = 3000$ psi.	134
Figure 5-32: Effect of G_{soil}/E_{pile} on Group Damping for Piles with $f_c = 4000$ psi.	134
Figure 5-33: Effect of G_{soil}/E_{pile} on Group Damping for Piles with $f_c = 5000$ psi.	135
Figure 5-34: Effect of G_{soil}/E_{pile} on Group Damping for Piles with $f_c = 6000$ psi.	135
Figure 5-35: Unit Load Applied to Pile Cap.....	138
Figure 5-36: Static Force in Middle Pile for Pile Groups in Strong Soils	139
Figure 5-37: Static Force in Corner Pile for Pile Groups in Strong Soils.....	140
Figure 5-38: Static Force in Edge Pile for Pile Groups in Strong Soils	140
Figure 5-39: Static Displacement of Pile Groups in Strong Soils	143
Figure 5-40: Static Displacement of Pile Groups in Weak Soils.....	144
Figure 5-41: Case 1-a 2 x 2 group of pile	145
Figure 5-42: A Group of Piles 3 x 3 Spaced at 9 ft.....	146
Figure 5-43: Vertical Force Distribution in the Soil Pile System in Strong Soil.....	147
Figure 5-44: Displacement of Pile Group for Weak Soil	148
Figure 5-45: Force Time History for Pile Group in for Weak Soil	149

Figure 5-46: Static Stiffness for Single Pile for Pile Diameter = 1.50 ft. and Concrete Strength = 3000 psi	151
Figure 5-47: Static Stiffness for Pile Groups Spaced at $2D_{pile}$, $4D_{pile}$ and $6D_{pile}$ for a Pile Diameter = 1.50 ft. and Concrete Strength = 3000 psi	152
Figure 5-48: Static Efficiency Factors	153
Figure 5-49: Static Efficiency Factors Based on AASHTO and FE.....	154
Figure 5-50: Stiffness Efficiency Factors	155
Figure 5-51: Damping Efficiency Factors	156
Figure 5-52: Group Stiffness Efficiency Factors as Function in (G_{soil}).....	157
Figure 5-53: Group Damping Efficiency Factors as Function in (G_{soil}).....	157
Figure 5-54: Vertical Stress in Soil-Pile Elements and Axial Load in Piles	159
Figure 5-55: Vertical Stress in Soil-Pile Elements and Axial Load in Piles	159
Figure 5-56: Vertical Stress in Soil-Pile Elements and Axial Load in Piles	160
Figure 6-1: Comparison between Mylonakis and Gazetas and FEA Solution for Static Stiffness.....	162
Figure 6-2: Modified ANSYS Finite Element Model.....	163
Figure 6-3: Vertical Displacement for Pile Group 2x2 and Spacing = 3.0 ft.at Resonance	164
Figure 6-4: Vertical Displacement Amplitude of the Piles.....	164
Figure 6-5: Block Foundation Supported on Piles.....	166
Figure 6-6: Comparison of Response between FEA and Novak at $a_0 = 0.25$	168
Figure 6-7: Comparison of Response between FEA and Novak at $a_0 = 0.30$	168
Figure 6-8: Comparison of Response between FEA and Novak at $a_0 = 0.35$	169

Figure B-1: Vertically Loaded Foundation.....	191
Figure B-2: Coefficient f_1 for Flexible Foundation (Reissner1936).....	192
Figure B-3: Coefficient f_2 for Flexible Foundation (Reissner1936).....	193
Figure B-4: Coefficient f_1 for Rigid Foundation (Reissner1936).....	193
Figure B-5: Coefficient f_2 for Rigid Foundation (Reissner1936).....	194
Figure B-6: Uniform Pressure Distribution.....	196
Figure B-7: Pressure Distribution under Rigid Foundation.....	196
Figure B-8: Parabolic Pressure Distribution.....	196
Figure B-9: Compliance Functions f_1 and f_2 for Rigid Base.....	198
Figure B-10: Compliance Functions f_1 and f_2 for Uniform Loading.....	198
Figure B-11: Compliance Functions f_1 and f_2 for Parabolic Loading.....	199
Figure B-12: Plot of Z Versus a_0 for Flexible Circular Foundation.....	201
Figure B-13: Plot of Z Versus a_0 for Rigid Circular Foundation.....	201
Figure B-14: Variation of Z' with a_0 for Flexible Circular Foundation.....	202
Figure B-15: Variation of Z' with a_0 for Rigid Circular Foundation.....	202
Figure B-16: Variation of the Displacement Functions with a_0 and Poisson's Ratio.....	204
Figure B-17: Soil Idealization as Determined by Lysmer and Richart.....	206
Figure B-18: Soil and Foundation Idealization as Determined by Lysmer and Richart	206
Figure B-19: Plot of F_1 - F_2 Versus a_0 for Rigid Circular Foundation Subjected to Vertical Vibration (Lysmer and Richart).....	207
Figure B-20: Foundation Rocking Mode of Vibration.....	209
Figure B-21: Foundation Sliding Mode of Vibration.....	211

Figure B-22: Foundation Torsional Vibration	215
Figure C-1: Comparison of Efficiency Factors Between FE and Randolph and Poulos for Piles Spaced at $6D_{pile}$	218
Figure C-2: Comparison of Efficiency Factors Between FE and Randolph and Poulos for Piles Spaced at $4D_{pile}$	219
Figure C-3: Comparison of Efficiency Factors Between FE and Randolph and Poulos for Piles Spaced at $2D_{pile}$	219

LIST OF TABLES

Table 4-1: Pile Axial Stiffness	74
Table 5-1: Static Loads on Piles Embedded in Strong Soils	141
Table 5-2: Static Loads on Piles Embedded in Weak Soils.....	143
Table 5-3: Forces Amplitude for Piles in Strong Soils at Resonance (12Hz)	147
Table 5-4: Forces amplitude in the piles for weak soil at resonance (7.0Hz).....	149
Table 5-5: Wave Length in Soils with Different Shear Modulus	158
Table 6-1: Comparison of Stiffness and Damping between ANSYS and DYNA5..	165
Table 6-2: Comparison between FEA Solution and Novak Closed Solution.....	169
Table 6-3: Comparison between FEA and Chowdhury and DasGupta Solution.....	170

Chapter 1: Introduction

1.1 Statement of the Problem

Dynamic vibrations resulting from machine operations cause the foundation soil system to vibrate, inducing cyclic stresses in the soil. The nature of such cyclic oscillations depend on the deformation characteristics of the supporting soil, the geometry of the foundation system (Block foundation or Frame foundation), the inertia loads of the machine foundation system, the type of dynamic excitation forces (Harmonic excitation, Impulsive...etc.), and the supporting base of the machine foundation, i.e., whether the machine is directly supported on a mat foundation or supported on piles.

For machines to have a satisfactory operation, the dynamic amplitude of the machine at the location where the machine is anchored to the foundation should be limited to very small values. Usually these limits should not exceed a few microns (10 to 12 microns). If the dynamic amplitude at the machine bearings exceeds such limits, excessive vibrations occurs and at a certain vibrational limits the machine trips, i.e., it stops working. In addition, due to the presence of machine vibration, dynamic loads are emitted into the soil in the form of excitation forces that are transmitted to adjacent buildings from the soil continuum, as shown in Figure 1-1. Consequently, this jeopardizes the integrity of the adjacent structures. The main goal of machine foundation engineering is to limit both the motion amplitudes and the vibrations transmitted into the soil continuum within an acceptable limits in order to achieve satisfactory machine operation. In many cases, this can be achieved by using deep foundations such as piles or drilled shafts. In general, the use of pile groups can increase the natural frequency of the system and decrease the amplitude of vibration.

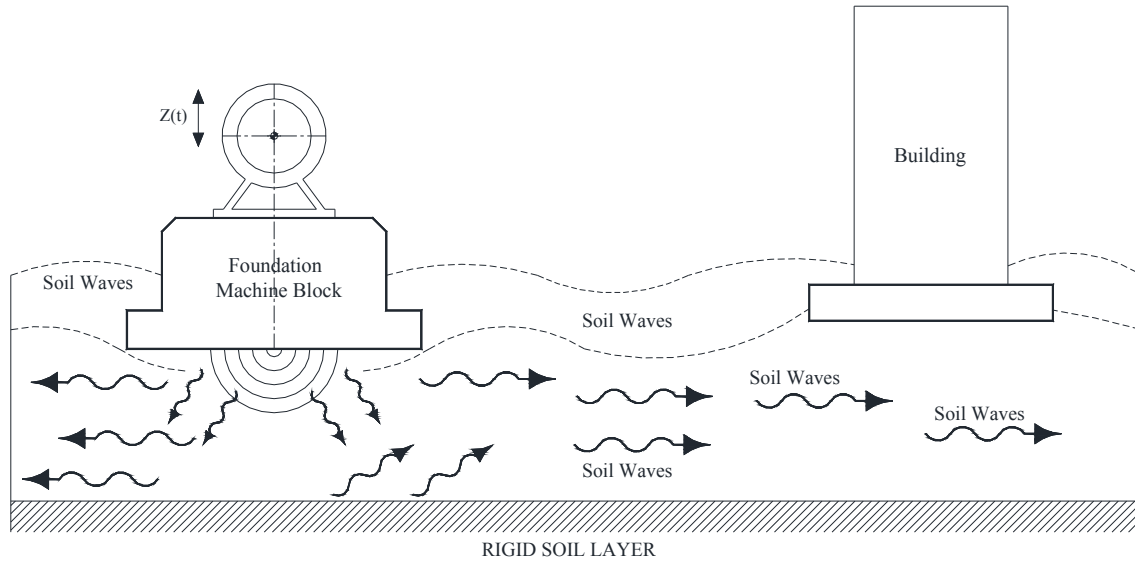


Figure 1-1: Machine waves transmitted into soil continuum

Using piles to support machine foundations has increased significantly in the past few years. Piles are used to transfer the dynamic loads generated by the machine to a stronger soil stratum and dampen the machine dynamic loads in the soil continuum by either friction or bearing or both. Thus, introducing piles reduces the motion amplitudes at the machine bearing support to an acceptable values.

1.2 Current Design Method

In design both the stiffness and the damping of the soil pile system are to be determined. Damping occurs because the stress waves occurred at the machines location will travel away from the foundation results in large amount of energy loss through geometric damping. Currently the most used method for determining the stiffness and damping for piles are determined based on a closed form continuum solution developed by Novak (1974). He developed charts that relate the pile dynamic stiffness and damping with the dimensionless frequency parameter (a_0), where:

$$a_o = \frac{\omega r_o}{V_s} \quad (1-1)$$

Where: ω = Machine operating frequency in rad/sec, r_o = pile radius, V_s = soil shear wave velocity $V_s = \sqrt{G_{soil}/\rho_{soil}}$

These charts are based on a two-dimensional plane strain analytical continuum solutions, and do they not take into consideration the three-dimensional effects of the pile-soil interaction. In addition, Novak stated that the values of pile stiffness and damping based on the continuum solution are accurate for dimensionless frequency parameter (a_o), equal to 0.3. Around this value, the stiffness and damping are “reasonably stationary and the numerical results values within this range are suitable for most applications...” thus limiting the applicability of these charts to certain machine operating frequencies. Operating speed for machines can range from 200 rpm (app. 3Hz), as in the case of small pumps and compressors, to 12000 rpm (200 Hz), as in the case of high speed rotary compressors, medium pressure turbines (5000 rpm - 83 Hz), extraction turbines and combustion and steam turbines used in generating electric power, the operating frequency is around 3000 rpm to 3600 rpm (50 to 60 Hz). In addition, stiffness and damping of piles have been found to be frequency dependent, however, Novak’s solution is assuming frequency independent stiffness and damping values. Since piles are generally constructed in group the interaction between the pile to pile and pile to soil, i.e., pile-soil-pile interaction must be considered, which cannot be considered in the two dimensional plane strain solution.

During machine vibration, the machine-foundation-pile system interacts with the soil in two mechanisms that occur simultaneously in a small time lag. Kinematic interaction, which is the difference in motion of the foundation system and the free field motion due to

the presence of a stiff foundation system, waves inclination, waves incoherence, and foundation embedment, and Inertial interaction, which is the additional inertial dynamic forces and displacements that are imposed on the soil foundation system during machine foundation oscillation. Both kinds of interaction must be considered in the design of a machine foundation system in order to achieve proper design.

1.3 Objective and Scope

For the design of foundation for vibrating machinery, an equivalent spring-damper system for the pile group is needed. This system may then be applied to the structure at the appropriate supports for the purpose of analysis of the structural response. This dissertation is a study of the vertical dynamic response of a single pile and pile groups embedded in a soil continuum having different soil properties. The vertical dynamic stiffness and damping for a single pile and pile groups are determined for a range of the dimensionless frequency parameter (a_0) from 0.2 to 2.0, thus covering the range of most machines operating frequencies. Pile-supported-machine foundations (such as foundations used to support a Combustion Turbine Generator (CTG), Steam Turbine Generator (STG), and Feed Water Pumps (FWP)) are widely used in the industry, especially in the power industry and have a frequency in the range of 50 to 60 Hz. Emphasis on these frequencies was undertaken in this study. The effect of pile strength on the vertical dynamic stiffness and damping of the pile is also considered by using piles having different concrete compressive strengths (i.e., 3000 psi, 4000 psi, 5000psi and 6000 psi).

In this study, a three dimensional finite element solution was utilized to determine the vertical dynamic stiffness and damping for a single pile and pile groups embedded in a homogeneous soil continuum. The soil continuum was modeled using three-dimensional

brick elements, and the piles were modeled using six degrees of freedom beam elements. The analysis is performed in a fully coupled manner between the soil and the pile groups considering the three-dimensional nature of the soil-pile-interaction problem. The vertical dynamic stiffness and damping for the pile is generated as a function in the dimensionless frequency parameter (a_0), as well as the shear modulus of the surrounding soil. The system was excited by a vertical harmonic force. The effect of the interactions between the piles in the pile groups was also studied. The efficiency factors were developed for piles spaced at twice the pile diameter, four times the pile diameter, and six times the pile diameter ($2D_{pile}$, $4D_{pile}$ and $6D_{pile}$). Charts relating the dimensionless frequency parameter (a_0) with pile vertical dynamic stiffness and damping were developed that can be readily used in the selection of vertical dynamic pile stiffness and damping to be used in a design.

1.4 Structure of the Dissertation

Chapter 2 presents a literature review on the design process of machine foundations and the current method analysis techniques of the soil-pile-soil-interaction. Chapter 3 presents the development of the finite element modeling of the single pile and of the pile groups. It presents the basic theory used by the ANSYS computer code, the types of the elements used to model the pile and the soil continuum, and the modeling of the soil viscous boundaries. It also presents the range of the variables used in the study. Chapter 4 presents the results of dynamic analysis of a single pile embedded in a soil continuum having different soil properties. The dimensionless frequency parameter (a_0) used ranges from 0.2 to 2.0. The effect of soil shear modulus, pile elastic modulus, length and axial load on the pile head on the vertical dynamic stiffness and damping of the pile is also presented.

Chapter 5 presents the results of dynamic analysis for pile groups in a soil continuum having different soil properties. The analysis included in this chapter is for a group of 3 x 3 piles spaced at $2D_{pile}$, $4D_{pile}$ and $6D_{pile}$. The stiffness and the damping of the group of piles were computed for different values of dimensionless frequency parameter (a_0). Dynamic efficiency factors were developed for all pile groups as well as the distribution of forces among the pile groups was also presented. Chapter 6 presents a verification of the model used to confirm the reasonableness of the computer results. Chapter 7, the conclusion and recommendations are summarized.

Chapter 2: Literature Review

2.1 Background

Foundations subjected to dynamic loads are widely used in industry, especially in the power industry for both nuclear and fossil power generation plants. Examples of foundations that support machines are boiler-feed-pump foundations and turbo-generator machines foundations. Both foundations are used to support machines used in the power generation industry. Generally, machines are classified based on their operating speed, type of dynamic excitation forces, type of foundation (block or framed foundation), and load transfer mechanism (i.e., either the machine foundation system is directly supported on a mat, or supported on piles).

2.1.1 Classification of Machines Based on Machine Operating Speed

Machines are classified based on machine operating speed into the following groups:

1. Low-speed machines. These include machines used in paper industry, printing machines and steam mills. They operate at a speed in the range of 50 rpm to 600 rpm.
2. Moderate speed machines. This set includes machines that operate at 600 to 1500 rpm such as boiler feed pumps and small fans used in the power industry.
3. High speed machines. These are machines that operate at a speed higher than 1500 rpm. Among this group of machines are the turbines and compressors that are commonly referred to as turbo-machines.

2.1.2 Classification of Machines Based on Type of Excitation Forces

Generally machines can be classified according to the type of dynamic excitation forces that they develop into rotating machines such as turbo-machinery, steam generators,

and compressors, reciprocating machines that include steam engines, piston compressors and pumps, and impact machines such as forging hammer machines and stamping machines. Rotating or reciprocating parts develop time varying dynamic forces. During start up, the machine passes through varying operating speeds until it reaches its final operating frequency, i.e., steady state operation. For reciprocating machines, dynamic forces are developed due to secondary unbalance forces that exist in the machine.

2.1.3 Classification of Machines Based on Foundation Type

Two types of foundation systems are typically used for machines: 1) rigid block foundation systems (Figure 2-1), which are typically used to support Combustion Turbine Generator (CTG) machines, and 2) framed structure foundation systems (Figure 2-2), which are used to support Steam Turbine Generator (STG) machines. These two foundation systems exist in most industrial facilities, fossil power generation plants, and nuclear power generation plants.

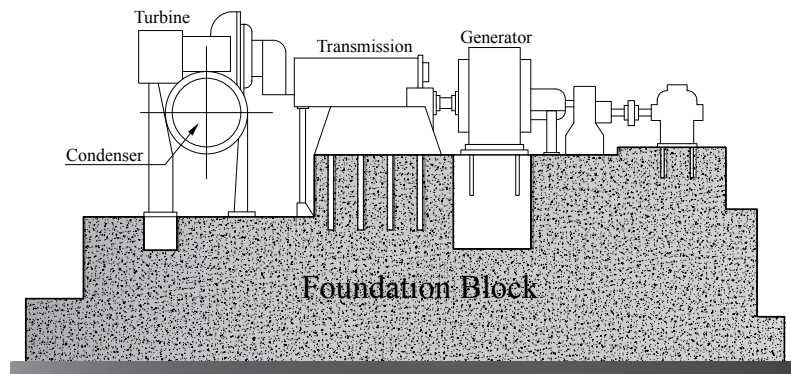


Figure 2-1: Turbo-Generator Machine Supported on Rigid Block Foundation

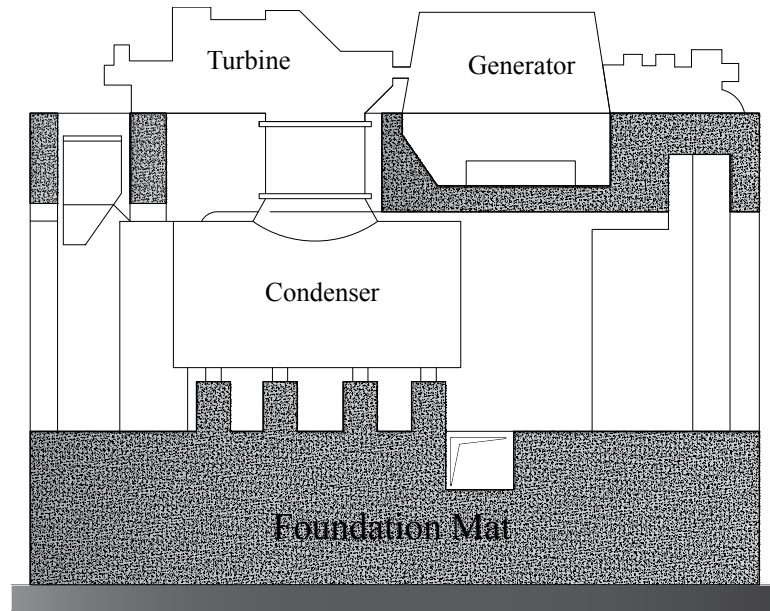


Figure 2-2: Turbo-Generators Machine with Frame Foundation

2.1.4 Classification of Machines Based on Load Transfer Mechanism

Most machines are supported by a mat foundation. However, piles are introduced under the foundation when soil conditions are not adequate to directly support machine loads, or when the soil deformations due to dynamic load exceed the allowable machine vibration limits. Piles are used to not only transmit the machine loads to more adequate soil layers, but also to limit the vertical dynamic response of the foundation system to an allowable vibration amplitude.

2.2 Vibration Limits for Machine Foundation

The analysis and the design of a machine supporting foundation are governed by the dynamic requirements of the machine. These dynamic requirements involve limiting the foundation response to predetermined vibration limits at the machine bearing support. The maximum allowable dynamic amplitude response at the machine bearing support is limited to 10-12 micro meters, which is equivalent to 0.01 inch/sec. Richart (1962)

recommended that the maximum acceleration due to machine operation should not exceed 0.5 times the acceleration due to gravity.

2.3 Modeling Techniques for Machine Foundations

The dynamic analysis of structures is performed through the selection of an idealized model consisting of springs with adequate stiffness to capture the actual stiffness of the foundation, lumped masses representing the machine and the foundation weight, and damping elements to model the energy dissipation mechanism. There are many techniques used in the idealization of a machine foundation. Some of these techniques adopt mathematical modeling and others adopt the finite element method. Many researchers followed the concept of mathematical models to develop the system equations of motion using dynamic equilibrium equations in order to determine the response of the physical system.

2.4 Machines Supported on Mat Foundations

Mat foundations are used in cases where several small vibrating units are placed close to each other. This type of foundation is characterized by its ability to damp the vibration from the machines due to its high flexibility. The flexibility of the mat depends on the relative stiffness between the mat foundation and the supporting soil. As the flexibility of the mat increases, the ability of the foundation to damp the vibration from the machines increases in the horizontal and rocking mode. However, the vertical modes for these types of foundations must be investigated. In the case of one machine supported on a rigid foundation, a single mass is lumped in the machine's center of gravity and the foundation combined modes of vibration are investigated for this mass. However, if a flexible foundation mat is used to support a set of machines, the masses of these machines are

lumped as a set of masses on the foundation. Figure 2-3 shows a finite element model used to model a flexible foundation mat with the masses of the machines lumped at the intersection between the mat elements. The soil underneath the foundation is modeled as an equivalent system of spring damper elements to model the soil stiffness and damping properties. This modeling technique is appropriate for the analysis of thin concrete slab foundations directly supported on the soil. The mat is divided into triangular or rectangular finite elements that have bending capabilities. The masses of the machines are lumped on the elements intersecting joints.

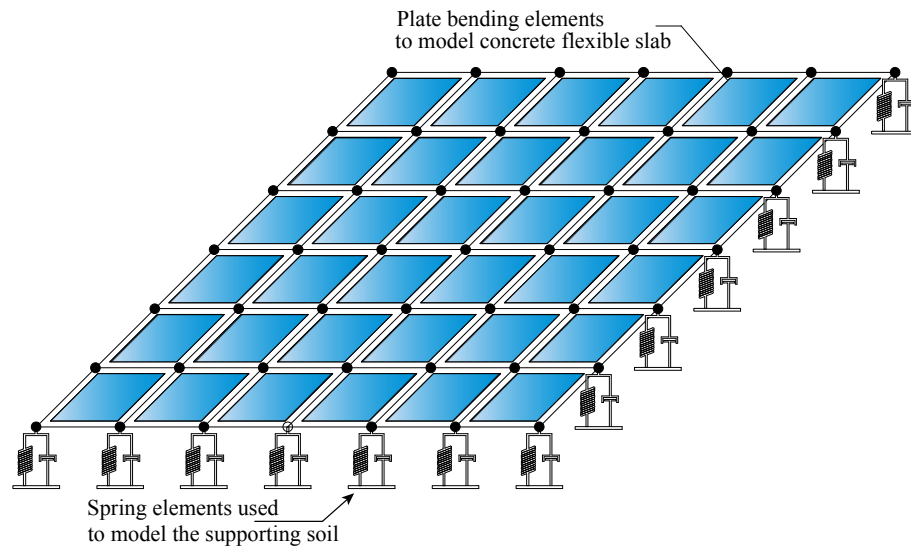


Figure 2-3: Finite Element Model for Mat Foundation

A Multi-Lumped mass is another modeling technique used to analyze an elevated foundation. This model is usually used when the foundation base mat is supported by a stiff soil or rock since the effect of the soil is completely ignored. The machine and superstructure dead weight is calculated and applied as a static load in the direction of the structure's deflected shape. The mass of the machine and the structure are lumped in the points where the foundation dynamic response is required to be calculated. The model used to describe this foundation is shown in Figure 2-4. The main problem of this model is that

each element acts independently of each other, which means that the global foundation response is not accurately captured. In addition, the coupled effect of the soil structure interaction is not calculated. The effect of soil on the foundation response can be very influential in many aspects. For example, if the foundation is constructed on a stiff soil, the soil will not damp the vibration resulting from the machine and will shift the foundation's natural frequency close to that of the machine, which makes the structure vulnerable to resonance that might cause damage to the foundation and the machine. On the other hand, if the foundation is constructed on a flexible soil, the soil will damp the vibration from the structures in the form of inelastic deformation in the soil medium causing a differential deflection of the tabletop beams, which will result in the machine's rotor misalignment. Therefore, the effect of the soil medium is a crucial factor in the dynamic response of the foundation. In most practical cases, the pedestal column bases are fixed into the base mat. This conservative approach of modeling the column-foundation-soil connectivity excludes the effect of the soil medium on the foundation tabletop response and shifts the system's whole natural frequency towards the machine operating speed.

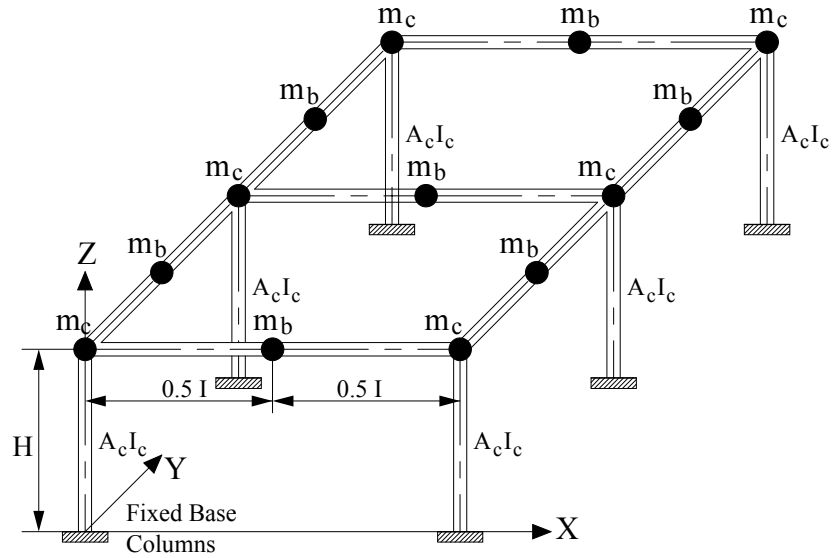


Figure 2-4: Foundation Lumped Mass Model (Fixed Base)

Figure 2-5 shows an enhanced version of the model presented in Figure 2-4. The effect of the soil structure interaction on the response of the elevated foundation is captured by modeling the soil as an equivalent spring damper element in order to represent the stiffness and damping characteristics of the soil medium.

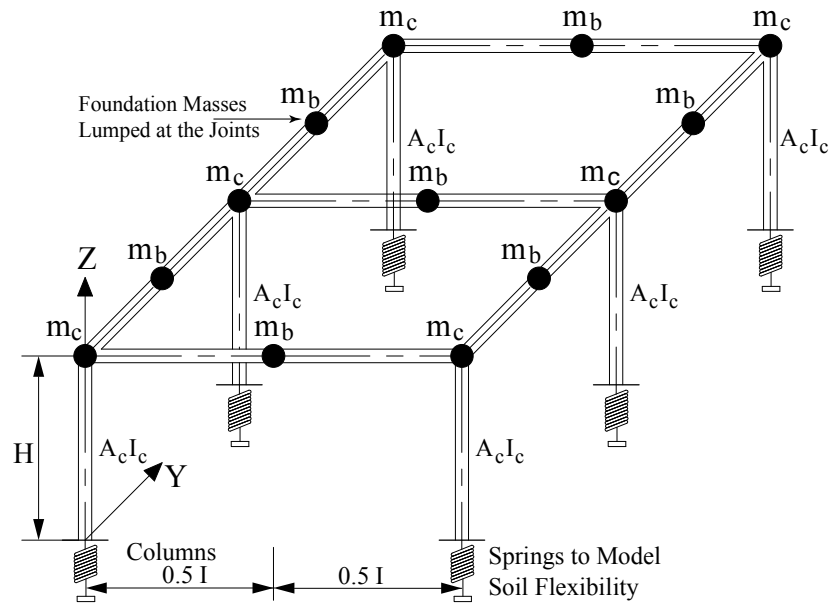


Figure 2-5: Three Dimension Foundation Model with Soil Springs

2.5 Machine Supported on Piles Foundation

Piles are used as a foundation under several conditions, such as, where the soil is weak in bearing capacity to withstand pressures due to dynamic loads or the soil loses its strength due to the presence of a ground water table or when the soil dynamic deformation exceeds the allowable machine vibration limits. Under these conditions, using piles under the foundation have the advantage of (1) transmitting the machine loads to more adequate soil layers, (2) limiting the vertical dynamic response of the foundation system, especially for a block type foundation, (3) increasing the natural frequency of the machine foundation system, thus shifting the overall machine foundation's natural frequency outside the operating frequency of the machine, and (4) reducing the dynamic amplitudes of the foundation system. Understanding the interaction between the soil and the piles is an important aspect in determining the actual response of the foundation system. The general practice for machine foundations supported over piles is to ignore the effect of the soil and to depend only on the stiffness of the piles to limit the vibration amplitudes. Selection of the pile type, diameter, depth and number of piles is an involved process, and the evaluation of dynamic characteristics of piles is a complex task and suffers with many associated uncertainties. The machine foundation block itself serves as a rigid pile cap that connects piles at their head. Evaluation of dynamic characteristics of a single pile is a difficult task and evaluation of dynamic characteristics of a group of piles connected by a rigid pile cap becomes complex and calls for many assumptions, resulting in added levels of uncertainties.

Several researchers modeled the pile vertical dynamic response considering the effect of soil pile interaction by either adopting the Beam-on-Dynamic-Winkler-

Foundation (BDWF) approach or by using the continuum approach. In the BDWF approach, each layer of soil is assumed to respond independently to adjacent layers. The soil-pile contact is discretized to a number of points where combinations of springs and dashpots represent the soil-pile stiffness and damping at each particular layer. The disadvantage of the BDWF model is the two-dimensional simplification of the soil-pile contact, which ignores the three dimensional components of interaction. The continuum approach accounts for the part of soil mass surrounding the pile and is considered in the analysis instead a system of spring-damper elements.

2.5.1 Soil Pile Interaction Based on Beam-on-Dynamic-Winkler-Foundation

In the BDWF approach, each soil layer is assumed to respond independently from the adjacent layers. The soil-pile contact is discretized to a number of points where a combination of springs and dashpots representing the soil-pile stiffness and damping are added at each particular layer. The numerical procedure to analyze the response of the pile under the effect of dynamic loading was first proposed by Smith (1960). Smith modeled the pile in the form of a series of lumped masses connected by vertical springs, as shown in Figure 2-6. Smith solved the equation of motion and computed the response of the pile due to impact loading resulting from the hammer drop on the top of the pile. The approach developed by Smith is defined as a one dimensional approach. The effect of the soil elastic-plastic and damping properties was accounted for in the form of reaction models consisting of spring-slider-dashpot elements connected in parallel.

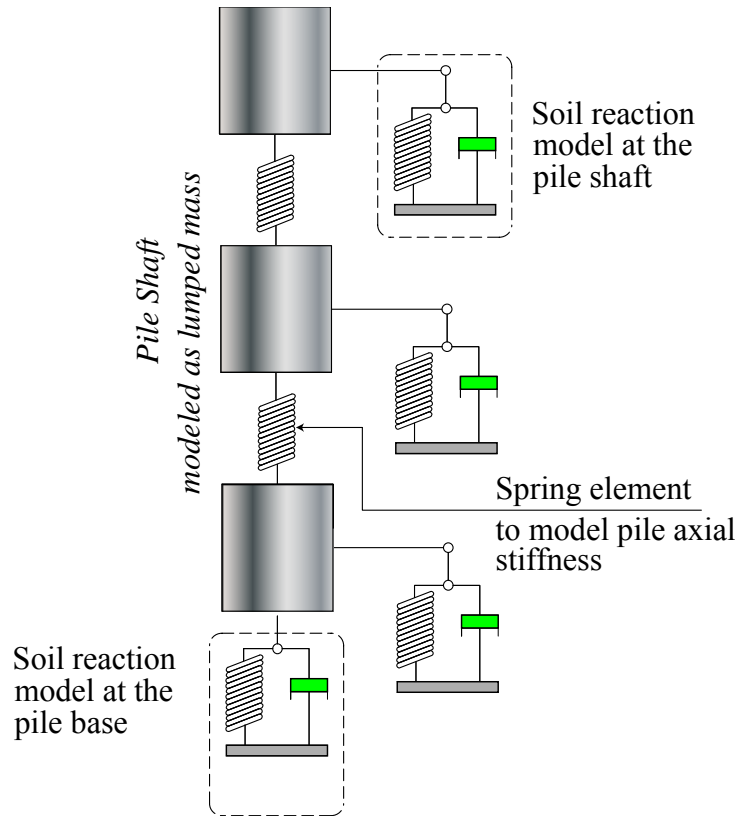


Figure 2-6: Smith (1960) Lumped Mass Pile Soil Reaction Model

The soil reaction is approximated using a series of isolated soil springs, and the method neglected the interaction between such soil springs. The spring stiffness is determined from the load-settlement relationship along the pile shaft and the pile tip. The load settlement relationship along the pile shaft is commonly referred to as the t-z response and the pile tip load settlement relationship as the Q-Z response (API 2003). Smith proposed the soil reaction model at the pile shaft and at the pile base, as shown in Figure 2-7.

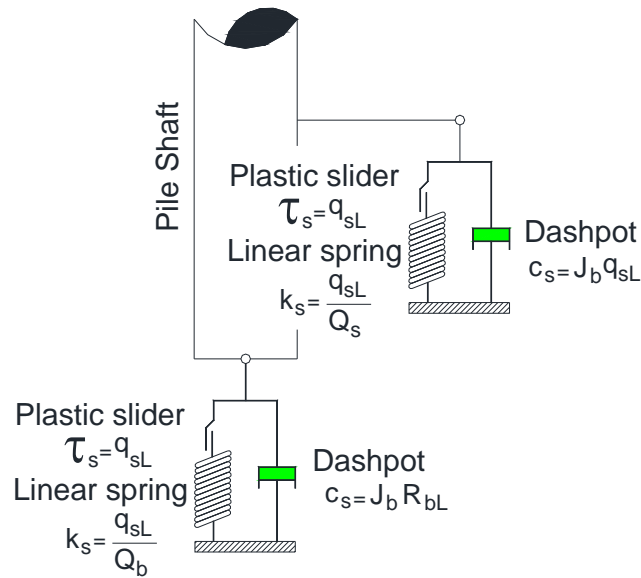


Figure 2-7: Smith (1960) Shaft and Base Soil Reaction Model

Several researchers updated the damping empirical constants (J_b) in Smith's soil reaction models. Forehand and Reese (1961) proposed different values for Smith's damping constant for sand and clay. The proposed values accounted for the increased damping in clay resulting from the higher viscosity that exists in cohesive soil than that existing in sand.

Lysmer and Richart (1966) developed a closed form solution for the motion of a circular rigid foundation on the surface of an elastic half space subjected to vertical dynamic loading. Simons and Randolph (1985) extended Lysmer and Richart's model to compute the soil reaction model at the base of end bearing piles. As long as the soil strains are within the elastic limits, and no plastic deformations are developed within the soil continuum, Lysmer and Richart's model is accurate in capturing the soil elastic properties at the base of the pile, especially for steady state machine operational loading and due to impact type loading. Based on Simons and Randolph solution, the total soil reaction at the

base of the pile is composed of the total spring reaction and the dashpot, as shown in Figure 2-8.

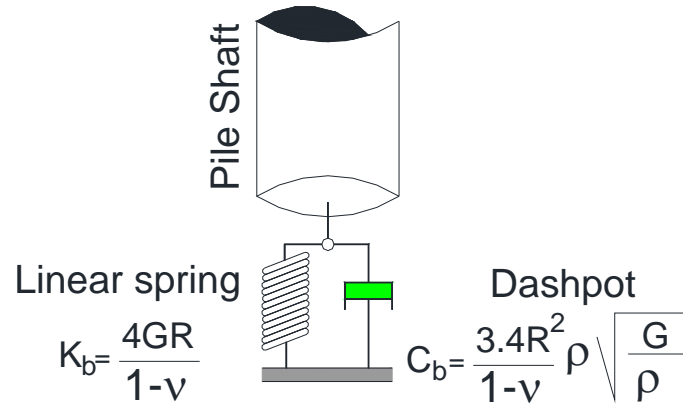


Figure 2-8: Lysmer and Richart (1966) Soil Reaction Base Model

Randolph and Simons (1986) also proposed a model for the soil shaft reaction. The model consisted of two systems connected in series, as shown in Figure 2-9. The first system is composed of a spring and dashpot connected in parallel to represent soil radiation damping. This system is then connected to another system composed of a slider and dashpot connected in parallel to represent soil viscous properties.

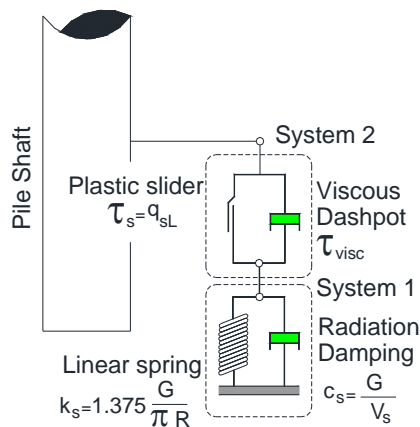


Figure 2-9: Randolph and Simons (1986) Soil Reaction Shaft Model

Based on Randolph and Simons, pile slippage will occur only when the stresses in the linear spring and the radiation dashpot are below the shaft unit resistance (τ_{static}). As long as the stresses in the pile are below this value, the pile and the soil will move together and pile slippage will not occur. If slippage occurs, the motion of the system will be governed by the slider and the viscous dashpot. To account for the plastic deformation developed at the base of the pile due to high dynamic impact loading resulting from driving hammer loading, Randolph and Simons enhanced the Lysmer and Richart base model by adding a slider, as shown in Figure 2-10, in order to decouple the soil plastic zone from the rest of the soil once the strain plastic strain is reached.

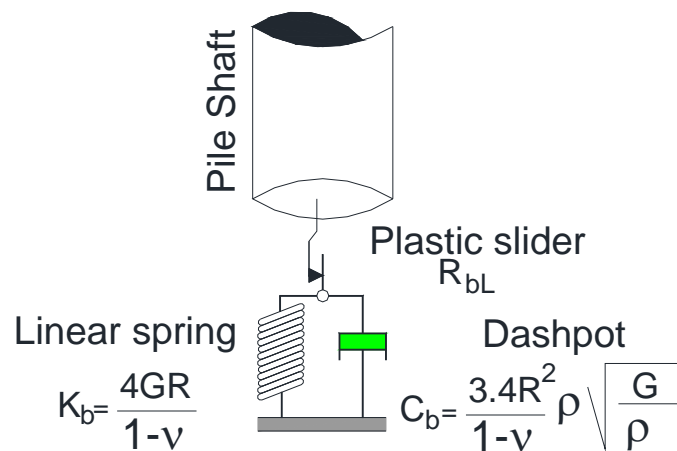


Figure 2-10: Randolph and Simons (1986) Soil Reaction Base Model

Holeyman (1988) proposed a soil reaction model as shown in Figure 2-11. The model consists of a viscous dashpot and radiation dashpot connected in parallel. Holeyman's model assumed that the soil viscous damping is active before sliding, which is different than Randolph and Simon's assumption. This means that the soil elastic and damping characteristics will only initiate once the pile shaft slips. Holeyman considered that the spring is only active under static loading of the pile. The model also proposed that

the slider will be activated once the sum of the reaction of the elastic springs and the dashpots exceeds the slider strength (τ_{sf}).

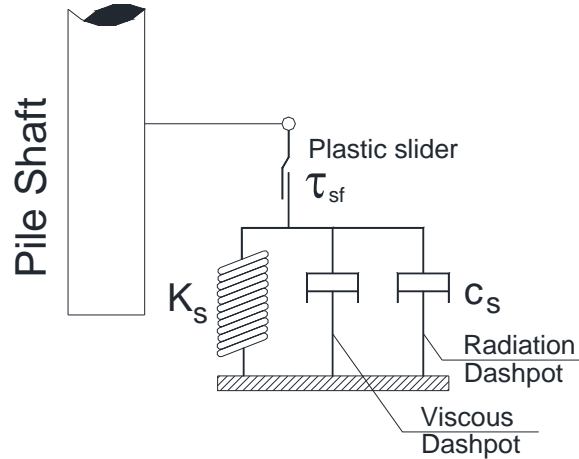


Figure 2-11: Holeyman (1988) Soil shaft reaction model

Kagawa (1991), in the study of an axially loaded pile under dynamic loading using the beam-on-Winkler foundation analysis proposed dynamic t-z and Q-Z models. The proposed t-z and Q-Z models include four elements, a spring, a dashpot, a mass and a slider element. El-Naggar and Novak (1994) used the model developed by Randolph and Simons and included the effect of soil nonlinearity for the soil band in direct contact with the pile shaft. Under the effect of impact loading such as the impact loading resulting from the pile driving, El-Naggar and Novak divided the soil zone around the pile into two zones. The first zone is the inner zone, which is in direct contact with the pile element that will exhibit strong nonlinear deformation at the pile soil interface. The second zone is the outer zone where the soil will behave elastically and will not exhibit any nonlinear behavior. The model developed by El-Naggar and Novak is shown in Figure 2-12. At the interface with the pile, El-Naggar and Novak provided a slider element to capture the slip and the relative motion between the pile and the soil due to the soil nonlinear behavior.

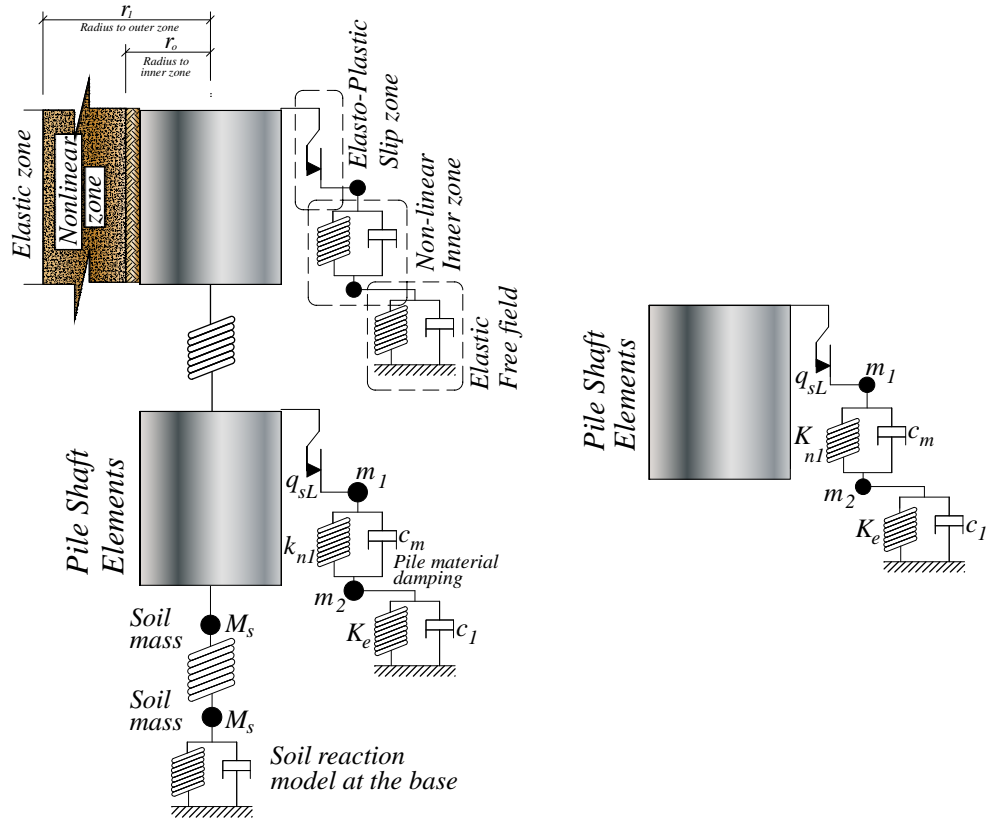


Figure 2-12: El-Naggar and Novak (1994) Pile Shaft Model

The model proposed by El-Naggar and Novak included all the features of the model developed by Randolph and Simons and added to it the effect of soil nonlinear behavior in the vicinity of the pile. However, the extension of the slippage zone from the pile and the inner zone diameter was not clear. El-Naggar and Novak proposed to define the extent of the soil outer zone to be 1.1 pile diameters.

Deeks and Randolph (1995) validated the base model developed by Lysmer and Richart by matching the results of a finite element modeling of the pile with several rheological model configurations. The model proposed by Deeks and Randolph was able to validate the base model proposed by Lysmer and Richart for impact loading on an elastic half space when the soil's Poisson's ratio is less than 1/3. Deeks and Randolph tried to

capture the soil vibrating mass by including two masses m_0 , and m_1 , as shown in Figure 2-13.

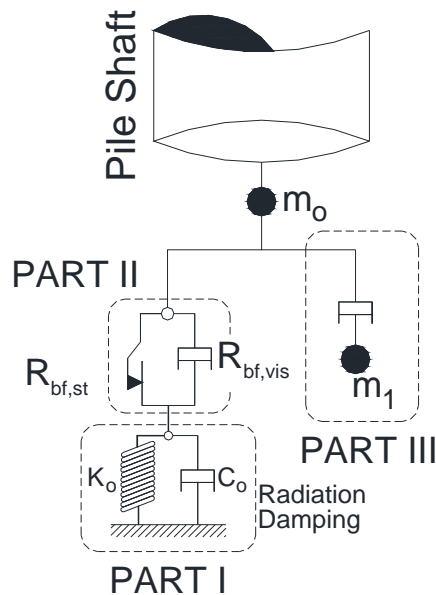


Figure 2-13: Deeks and Randolph (1995) Soil Reaction Base Model

The model proposed by Deeks and Randolph was able to validate the base model proposed by Lysmer and Richart for impact loading on an elastic half space when the soil's Poisson's ratio is less than 1/3. Mylonakis (2001) provided an approximate analytical solution for the determination of a depth dependent Winkler modulus for the elastic modeling of the soil pile interaction. Seidel and Coronel (2011) in assuming the response of offshore piles subjected to cyclic loading, they idealized the pile as a lumped mass connected with springs and the surrounding soils were idealized as load transfer curves along the pile shaft (t-z curves), and the pile base (Q-Z curves).

The disadvantage of applying the BDWF approach is its two-dimensional simplification of the soil-pile interaction and ignoring the generation of geometric damping. Geometric damping (or radiation damping) represents dissipation of vibration energy from the soil-pile systems into the semi-infinite soil medium. On the other hand,

the continuum approach accounts for the soil mass in contact with the pile instead of a system of spring-damper elements.

2.5.2 Soil Pile Interaction Based on Continuum Approach

This analytical method is based on Mindlin's (1936) closed form solution for the application of point loads to a semi-infinite mass. Its accuracy depends to a great extent on the evaluation of the Young's modulus and other elastic soil parameters. This method cannot incorporate the nonlinear soil-pile behavior however; the equivalent linear method is used to model the soil pile interaction. The elastic continuum method is more appropriately applied for small strain, steady-state vibration problems. However, the method is also limited in modeling layered soil profiles, and the solutions are only available for constant soil modulus and linearly increasing soil modulus. Tajimi (1966) was able to describe a dynamic soil-pile interaction using the elastic continuum theory. He developed a solution using a linear Kelvin-Voigt visco-elastic stratum to model the soil elements. However the model ignored the vertical component of the pile response. Baranov (1967) idealized the three dimensional soil domain as a stack of independent infinitesimal thin soil slices with each particular soil slice behaving under plane-strain conditions. In his solution, the soil material is assumed to be homogenous, isotropic, and viscoelastic.

Novak (1974) presented an approximate analytical expression for the dynamic stiffness of piles based on linear elasticity. Novak assumed the following:

1. The pile is assumed to be vertical, cylindrical and moving as a rigid body.
2. The pile is perfectly connected to the soil (no separation is allowed between the rigid cylinder and the soil medium).

3. The soil above the pile tip behaves as elastic layers composed of infinite thin independent layers, plane strain soil with elastic waves propagating only in the horizontal direction.
4. Soil reaction acting on the pile tip is equal to that of an elastic half space.
5. The motion of pile is small, and excitation is harmonic i.e. the exciting force = $Q_0 e^{i\omega t}$

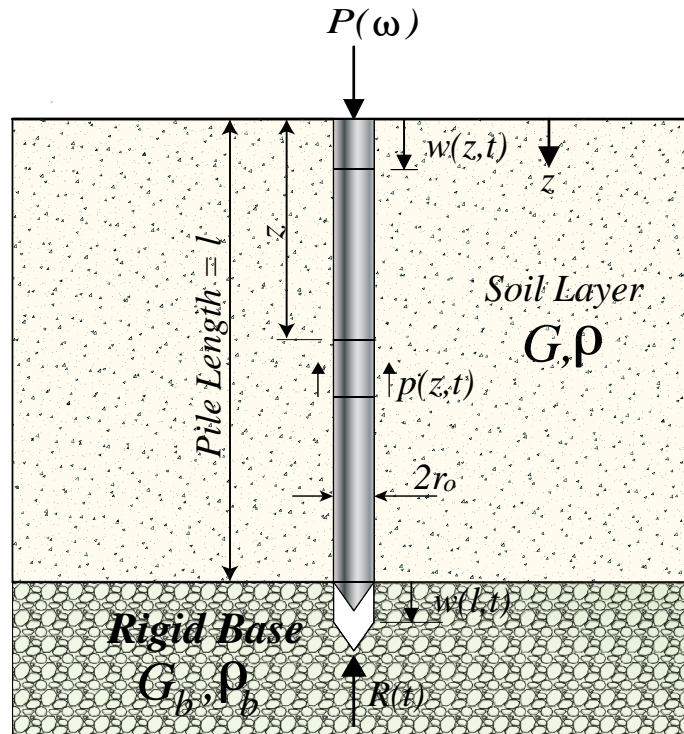


Figure 2-14: Novak Model for a Single Pile

The complex stiffness is the force that produces unit dynamic displacement of the pile head.

Vertical vibration of the pile

$$w(z, t) = w(z) e^{i\omega t} \quad (2-1)$$

Soil reaction at the pile tip

$$p(z, t) = G(S_{w1} + iS_{w2}) w(z, t) dz \quad (2-2)$$

Where:

$$S_{w1} = \frac{J_1(a_o)J_0(a_o) + Y_1(a_o)Y_0(a_o)}{J_0^2(a_o) + Y_0^2(a_o)} \quad (2-3)$$

$$S_{w2} = \frac{4}{J_0^2(a_o) + Y_0^2(a_o)} \quad (2-4)$$

Where: J_0 and J_1 are Bessel functions of a first kind of order 0 and 1, Y_0 and Y_1 are Bessel functions of a second kind of order 0 and 1.

The equation of motion of the pile/soil system is given by

$$m \frac{\partial^2 w(z, t)}{\partial t^2} + c \frac{\partial w(z, t)}{\partial t} - E_p A \frac{\partial^2 w(z, t)}{\partial z^2} + G(S_{w1} + iS_{w2})w(z, t) = 0 \quad (2-5)$$

Solution yields:

$$w(z) = \cos \Lambda \frac{z}{l} + C(\Lambda) \sin \Lambda \frac{z}{l} \quad (2-6)$$

$$\Lambda = l \sqrt{\frac{1}{E_p A} [m\omega^2 - GS_{w1} - i(c\omega + GS_{w2})]} \quad (2-7)$$

$$N(z) = E_p A \frac{dw(z)}{dz} \quad (2-8)$$

Where l = pile length

The complex stiffness is the force that produces unit dynamic displacement of the pile head.

$$F(0) = E_p A \frac{dw(0)}{dz} = \frac{E_p A}{l} F(\Lambda) \quad (2-9)$$

$$F(\Lambda) = -\Lambda C(\Lambda) = F(\Lambda)_1 + iF(\Lambda)_2 \quad (2-10)$$

Where: C_{w1} and C_{w2} are Bycroft coefficient, $F(\Lambda)_1$ is the pile's real stiffness, and $F(\Lambda)_2$ is the pile damping.

Novak defined the pile equivalent spring constant and damping coefficient as shown in equations (2-11) and (2-12).

$$k_z = (E_p A / R) f_{z1} \quad (2-11)$$

$$c_z = (E_p A / \sqrt{G / \rho}) f_{z2} \quad (2-12)$$

Where: E_p is the pile elastic modulus, R is the pile radius, A is the pile cross section area, G is the soil shear modulus, and ρ is the soil density, f_{z1} and f_{z2} are non-dimensional parameters.

The coefficients f_{z1} and f_{z2} are given in Figures 2-15 and 2-16 for friction piles.

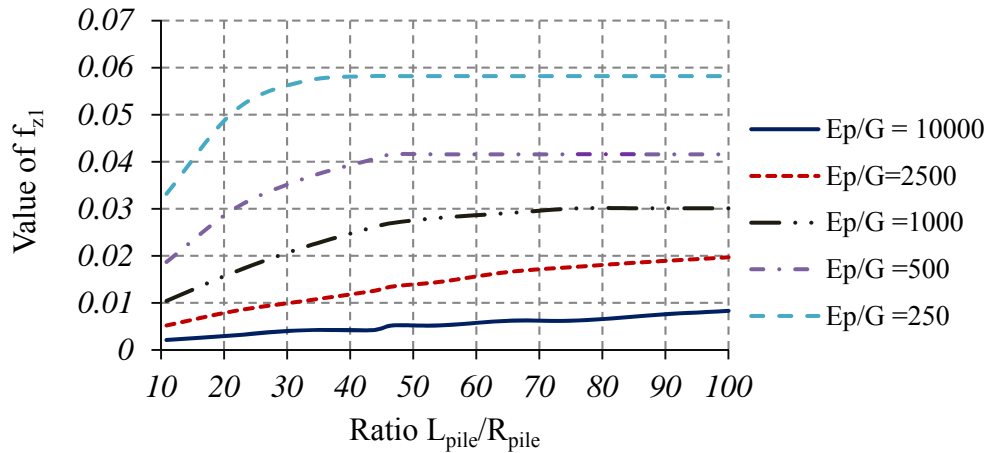


Figure 2-15: Variation of f_{z1} with L/R and E_p/G for Friction Piles

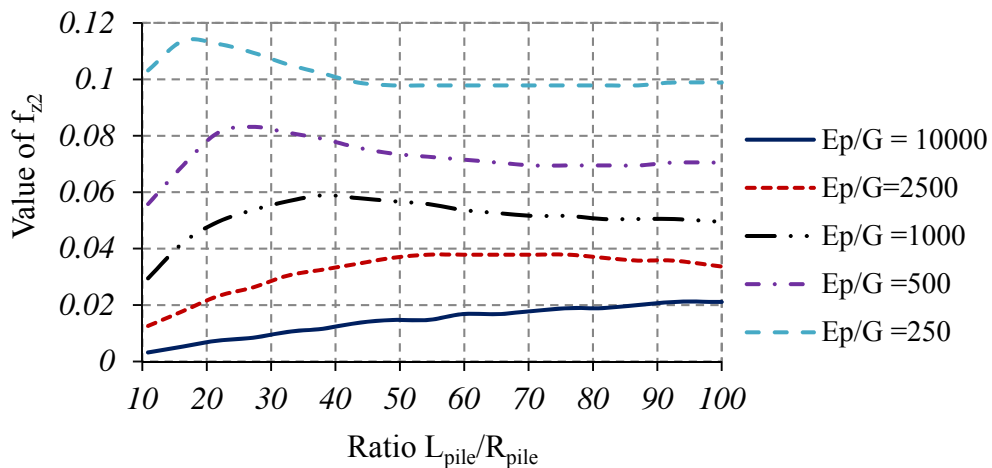


Figure 2-16: Variation of f_{z2} with L/R and E_p/G for Friction Piles

Novak (1974) mentioned that the values of stiffness and damping coefficient are accurate for dimensionless frequency parameters around $a_0=0.3$, around this value, “the stiffness and damping are reasonably stationary and the numerical results values within this range are suitable for most applications”.

Gazetas (1984) introduced the concept of sub-structuring as shown in Figure 2-17 to compute the soil pile interaction impedance function.

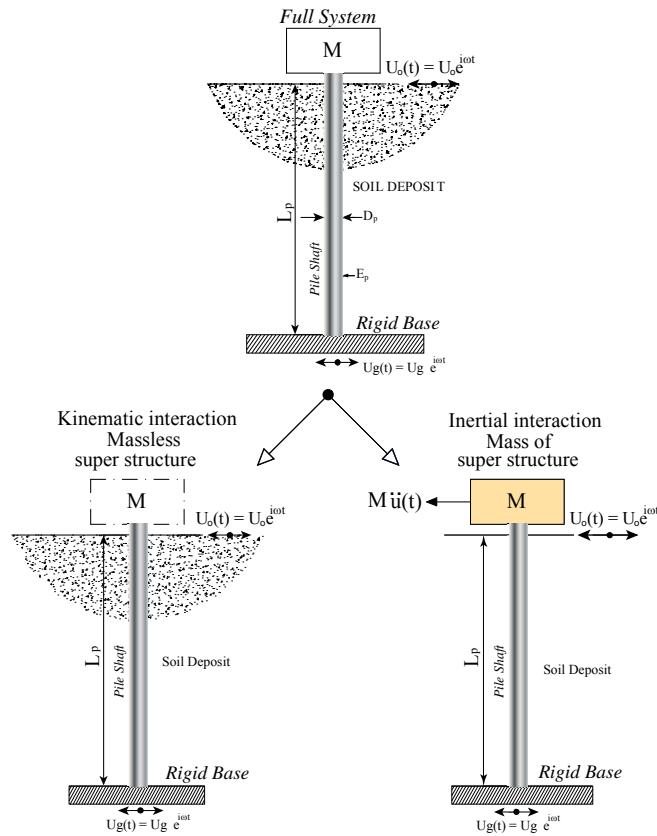


Figure 2-17: Sub-Structuring Method (Gazetas 1984)

Based on this concept, the pile interacts with soil in two different mechanisms that occur within small laps of time, kinematic interaction, and inertial interaction. The major assumption in this approach is that the soil will remain elastic and that the concept of superposition is valid. Kinematic interaction of the soil pile system is the difference between the soil motion in the free field and the soil motion at the foundation. The free

field is a point in the soil continuum far from the foundation. This difference in motion arises from the existence of a stiff member within the foundation continuum, wave incoherency and wave inclination. The kinematic interaction is determined by calculating the response of the soil pile system assuming a massless foundation. This is usually accomplished using the concept of transfer function. The transfer function is defined as the ratio of the foundation motion to the motion in the free field. Due to the effect of the kinematic interaction forces, the foundation will oscillate. Thus the foundation inertial forces are excited, adding additional moments at the base of the foundation, which results in additional forces at the soil foundation interface. To modify the response of the pile foundation system to account for the kinematic interaction, the amplified response resulting from kinematic analysis of the massless foundation is used as an input motion in the inertial interaction analysis. The dynamic impedance function of the foundation is computed based on the response of the foundation and the associated damping at the soil foundation interface.

Holeyman (1988) developed a pile shaft and base model to consider the effect of the soil mass vibrating with a pile during pile driving, as shown in Figure 2-18. In his model, Holeyman included part of the soil during pile driving analysis as a continuum instead of considering the soil effect in the form of spring and dashpot. In his pile base model, Holeyman considered a truncated cone of soil under the pile base, which will control the reaction model. The truncated cone is then discretized into a lumped mass connected to each other by a nonlinear spring. For the shaft model, Holeyman discretized the soil surrounding the pile into a series of cylinders each having its mass lumped in its center. The only mode of deformation considered between these cylinders was the shearing

develop a formulation of the vertical dynamic stiffness and damping value for a single pile in a soil continuum and included the inertial effect of the pile mass that Novak's (1974) continuum solution did not take into account. The response was also determined for the first mode with both the stiffness and damping equations taken as frequency independent. They defined the vertical dynamic stiffness (K_1) and damping coefficient (C_1) for an end bearing pile as follows:

$$K_1 \approx \left(\frac{EA}{8L} + \frac{GS_1 L}{2} \right) \quad (2-13)$$

$$C_1 \approx \frac{1}{2} r_o \sqrt{\rho G S_2} L \quad (2-14)$$

Where: S_1 and S_2 are stiffness and damping coefficients, $S_1 = 2.7$ and $S_2 = 6.05a_o + (0.7022a_o)/(a_o + 0.01616)$

2.6 Pile Group Interaction

Piles are almost always used in groups and the effect of pile to pile interaction is an important parameter in the dynamic performance of the pile group, especially pile foundations subjected to dynamic loading such as those supporting machines. Under the effect of machine induced dynamic loading, elastic waves are transmitted from piles adjacent to each other. These waves interact with each other and result in modification of the dynamic response of the pile group foundation and thus affect the performance of the supported machine. The distance between the individual piles influences the behavior of the pile group. According to ACI (2004), when the distance between the individual piles is more than 20 times the pile diameter, the piles do not affect each other and the group stiffness and damping are the same as the sum of the contributions from the individual piles. For closely spaced piles, similar to the static response, the pile-soil interaction will

affect the group stiffness and damping. However, the dynamic group effects differ considerably from the static group effects. The methods available for the dynamic analysis of pile groups are of two types, the first type, which is the one mostly used, where the response of the single pile, i.e., stiffness and damping are determined using the static or dynamic interaction factor. The second type uses the finite element method to model the whole pile group and from it the effect of the pile spacing on the group response can then be determined.

2.6.1 Static Interaction Factors

Novak (1977), in a solution of a group of piles indicated that when the piles are closely spaced, the displacement of one pile is increased due to the displacement of all the other piles, and conversely, the stiffness and damping of the group are reduced. With no analytical solution available for the dynamic interaction of the piles he proposed that the interaction factors can be obtained from the static solution of Poulos (1968). The concept of pile to pile interaction was introduced by Poulos (1968) using Mindlin's equation of elasticity to solve for the stresses and displacement between piles due to horizontal loading. Poulos defined the interaction factor (α) as follows:

$$\alpha_r = \frac{\text{additional displacement due to adjacent pile displacement}}{\text{pile displacement due to direct loading on the pile}} \quad (2-15)$$

Novak (1977) proposed the following formula to account for the pile to pile interaction and to compute the pile groups stiffness and damping:

$$K_{\text{group}} = \frac{\sum_1^n K_{\text{pile}}}{\sum_1^n \alpha_r} \quad (2-16)$$

$$C_{\text{group}} = \frac{\sum_1^n C_{\text{pile}}}{\sum_1^n \alpha_r} \quad (2-17)$$

Randolph and Poulos (1982) defined the interaction (α_r) factor for pile groups as a function in pile length (l_p), pile spacing (s) and soil shear modulus at the pile base and in contact with the pile.

$$\alpha_r = \text{Group interaction factor} = \frac{0.5 \ln \left(\frac{l_p}{s} \right)}{\ln \left(l_p d \frac{G_{\text{avg}}}{G_b} \right)} \quad (2-18)$$

where: K_{pile} = the stiffness of the pile group, G_{avg} = the average shear modulus along the pile length, G_b = the shear modulus at the pile base, l_p = the pile length and d is the pile diameter.

Under a dynamically loaded pile foundation, the interaction between the pile groups is greatly influenced by the frequency of excitation of the forcing function. Both dynamic stiffness and damping of pile groups are frequency dependent and their values may increase or decrease based on the frequency of excitation of the forcing function. In addition, unlike static loading, the effect of pile spacing is also affected by the frequency of excitation of the forcing function.

Wolf and von Arx (1978) were the first to study the effect of pile-soil-pile dynamic interaction. They used finite element axisymmetric modeling formulation to establish the dynamic displacement field resulting from a line load. Wolf and von Arx utilized the finite element procedures to calculate the displacement at any point within the soil mass due to a line load acting on the surface of half-space. The displacement field was then used to determine the flexibility matrix of the soil at each frequency. The results presented by Wolf and von Arx showed a high dependence of the pile interaction on the number of piles within

the pile groups and on piles spacing within the group. Waas and Hartmann (1981) analyzed the motion and the forces on the pile groups subjected to earthquake loading. In their model, the soil was analyzed as a viscous elastic layered medium subjected to point and ring loading. Waas and Hartmann calculated the kinematic and the inertial response of the pile-soil system to determine the dynamic stiffness matrix of the complete system. The pile groups were modeled as a semi rigid linear beam element with the tip of the pile pinned and the head fixed to the pile cap. The flexibility matrix was computed by applying a unit harmonic load acting on each node within the soil continuum at the node where the soil and the pile are connected to determine the frequency dependent on the flexibility matrix of the soil medium. Waas and Hartmann concluded that the dynamic stiffness of pile groups are highly dependent on the frequency of excitation of the forcing function, the soil layering and the ratio of the shear wave length and the pile cap. Sheta and Novak (1982) investigated the effect of the soil nonlinearity on the axial dynamic response of pile groups. In their model, Sheta and Novak weakened the soil ring in direct contact with the pile to account for the high strain condition within this soil layer. The soil was modeled as horizontal layers with varying soil properties. The piles were modeled as vertical linear elastic members and the masses of piles were lumped at the pile head, center and tip. The piles lumped masses were connected with massless circular elements. The soil flexibility matrix was computed based on the plane strain conditions with a softer cylindrical zone around the pile where its mass was neglected to avoid wave reflection at the boundaries. Using this composite model, Sheta and Novak calculated the displacement field in each soil layer and formulated the flexibility matrix. Sheta and Novak concluded that the dynamic group stiffness is considerably different than the static stiffness; the dynamic stiffness and damping of the

pile groups are more dependent on the frequency of excitation than is a single pile, and the weak zone around the pile increases the group stiffness and damping of the pile groups by limiting their interaction.

Nogami (1983) showed that the concept of Winkler soil model could be applicable to the pile group problems for a frequency range higher than the fundamental natural frequency of the soil deposit. The dynamic group effect is frequency dependent due to the effect of the wave interference. The group effect is governed by the ratio between the pile spacing and the shear wave length of the soil. The dynamic group effect can either increase or decrease the response of the group of piles.

Etouney et al (1983), presented a semi analytical solution for the dynamic behavior of vertical pile groups where the soil is modeled as a plane strain continuum and the piles as a set of beam elements. They showed that dynamic coupling between the piles in the group is important in the low frequency range and less important at higher frequencies and that the correction factors due to pile groups is frequency dependent.

Han (2010), for the design of large pump foundation, performed a dynamic analysis and compared a shallow block foundation, deep block foundation and cast-in-place concrete piles foundations. The group effects of the piles was accounted for using vertical static interaction factors. He found that the stiffness and damping were higher for the pile foundation and thus the vibration amplitude was reduced by the pile foundation.

2.6.2 Dynamic Interaction Factors

Dobry and Gazetas (1992) modeled the soil as linear hysteric material, and the piles were modeled as circular piles. They assumed that under harmonic excitation, cylindrical waves are emitted from an oscillating pile, or active pile, radially along the pile length in

the horizontal direction towards the adjacent pile defined as the receiving pile, or the passive pile. They also assumed that the variation of the amplitude with depth for the receiving pile is attuned to the active pile. Based on these assumptions, Dobry and Gazetas defined the dynamic interaction factor as follows:

$$\alpha_v = \left(\frac{S}{r_0}\right)^{-1/2} e^{\left(\frac{-\xi\omega S}{V_s}\right)} e^{\left(\frac{-i\omega S}{V_s}\right)} \quad (2-19)$$

where: S and r_0 = pile spacing and radius, V_s = soil shear wave velocity and ζ = material damping ratio.

They mentioned that the proposed interaction formula overestimates the peak value for stiffness and damping for a pile group in stiff soil, i.e., soil having a Young's modulus greater than 300 times the pile's Young's modulus. Gazetas and Makris (1991) developed a simple method for calculating the dynamic steady state axial response of floating pile groups embedded in a homogeneous and non-homogenous soil continuum. Gazetas and Makris concluded that the interaction between piles are generally due to the interference of wave fields generated from one pile along the pile shaft and speeding outwards and exciting the adjacent pile. For homogenous soil, the wave fields emitted from the active pile are cylindrical and are independent from pile flexibility and slenderness. However, for nonhomogeneous soil, Gazetas and Makris concluded that the wave fronts are non-cylindrical and used the ray theory to compute the piles group dynamic stiffness and damping. Gazetas et al (1993) compared the use of the static interaction factor and the dynamic interaction factor in their study of the dynamic response of pile groups using Beam-on-Dynamic-Winkler foundation approach. They indicated that the use of static interaction factor are acceptable for static and low frequency cases and that the dynamic

interaction factors approach is the only way that can be recommended in engineering practice. Fan et al (1991) conducted a numerical study for the kinematic response of groups of vertical floating piles. The piles were connected through rigid massless caps and subjected to vertically propagating harmonic S-waves. In their study, the soil profile was modeled as a homogeneous material with the shear modulus proportional to depth. Fan et al showed that under soil-pile-kinematic interaction the influence of the nature of the soil profile is profound at all frequencies, the effects of pile groups configuration, number of piles in the group, and relative spacing between piles are usually insignificant for lateral displacements, but quite important for pile cap rotations.

Reese and Wang (2008), in the design of the foundation for a wind turbine using a group of drilled shafts used static response of the group since the natural frequency range of the wind turbine foundation is in the lower range and when the piles are close together to form a circle the soil contained within the circle moves with the piles. The load transfer model of the axial side resistance uses the t-z curves and for the axial tip resistance uses the Q-Z curves to represent the response of the soil. Ashkinadze and Fang (2014), using the Monte Carlo simulation of the pile group response with different soil shear modulus treated as a fuzzy parameter and used the dynamic interaction factor. They determined that the equivalent pile group stiffness in the $S/D = 3$ to 5 was in the range of 1.82 to 2.33 times the sum of the stiffness of individual piles, i.e. the group resulted in a stiffer response. Whereas the damping was reduced by a factor of 0.64 to 0.82, i.e., the group interaction tends to reduce damping due to multiple reflection of the elastic waves in the soil.

2.6.3 Dynamic Efficiency Factor

ACI (2004) indicated that the dynamic group effect differs from the static group effect, the dynamic stiffness and damping of pile groups vary with frequency, and group stiffness and damping can be either reduced or increased by the pile-soil-pile interaction. The stiffness and damping group effect can be determined by the group stiffness and damping efficiency factor ($\alpha_{\text{stiffness}}$ and α_{damping}) defined by ACI (2004) as:

$$\alpha_{\text{stiffness}} = \frac{\text{Group Stiffness}}{\text{Sum of Stiffness of Individual Pile}} = \frac{K_{\text{group}}}{N_{\text{pile}}K_{\text{single}}} \quad (2-20)$$

$$\alpha_{\text{damping}} = \frac{\text{Group Damping}}{\text{Sum of Damping of Individual Pile}} = \frac{C_{\text{group}}}{N_{\text{pile}}C_{\text{single}}} \quad (2-21)$$

Where: K_{single} and C_{single} are the stiffness and damping of individual pile considered in isolation.

Chapter 3: Finite Element Model of the Soil Pile System.

3.1 Introduction

The finite element code ANSYS 13 (2011) is used to model the soil-pile interaction problem for a single pile and a group of piles. ANSYS is multi-purpose software that has multiple capabilities to perform linear and nonlinear transient dynamic analysis in the frequency domain. In addition, the ANSYS element library contains a wide range of element types that are suited to model the soil pile interaction problem. This chapter presents and discusses the details of the numerical modeling of the pile soil interaction problem. It describes the elements used to model the soil and the pile, the connectivity between the pile and the soil and modeling of the soil's viscous boundaries. The chapter also presents a parametric study on the effect of the extent of the soil boundary on the results of the vertical dynamic response of the pile.

Two finite element models are presented; the first model is for a single pile embedded in a soil continuum. The pile diameter is set at 3.0 ft. and the pile length is set at 30 ft. This model is used to study the vertical dynamic stiffness and damping of a single pile due to a variation of the dimensionless frequency dependent parameter (a_0) that ranges from 0.2 to 2.0. The parameter a_0 is a dimensionless frequency parameter that includes the effect of the pile radius (r_0), the machine operating angular frequency (ω) and the soil shear wave velocity (V_s). The soil shear wave velocity is also a function of the soil shear modulus (G_{soil}) and the soil mass density (ρ). Therefore, all parameters that affect the dynamic response of the soil pile interaction problem are defined in this dimensionless frequency parameter (a_0). The pile material is another parameter that affects the vertical dynamic stiffness and damping of the pile. Four pile materials are

used to calculate the dynamic stiffness and damping for a single pile and for pile groups. These materials are based on concrete compressive strengths of 3000, 4000, 5000 and 6000 psi. In order to determine the vertical dynamic stiffness and damping of the pile, the pile head is excited using a harmonic loading having the following form

$$Q = Q_0 e^{i\Omega t} \quad (3-1)$$

Where: Q_0 is a constant force amplitude = 1.0 lb. and Ω is the frequency of the forcing function varies from 1.0 to 50 Hz.

The vertical pile response due to this exciting force is calculated for different pile concrete strengths and for a frequency dependent parameter (a_0) that ranges from 0.2 and 2.0. The model is shown in Figure 3-1.

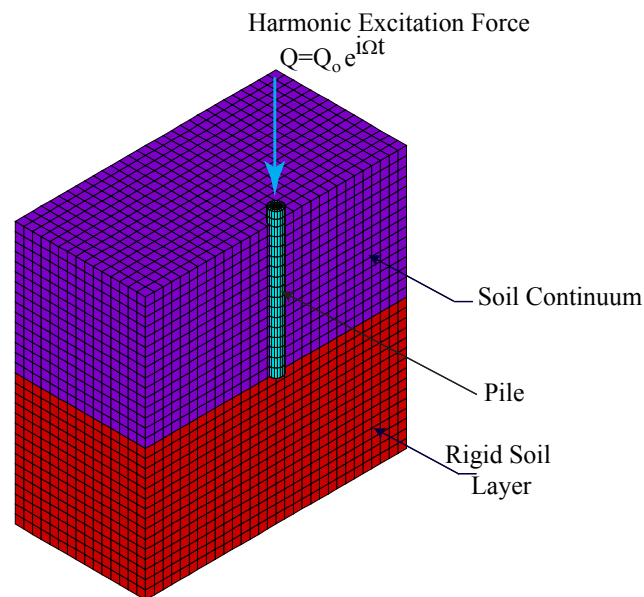


Figure 3-1: Soil Pile Model for a Single Pile

The second finite element model is modeling a pile cap supported on a group of piles and embedded in a soil continuum. This model is generated to determine the effect of the soil-pile interaction on the vertical dynamic stiffness and damping of pile

groups. In this model, the pile diameter is set at 1.5 ft. and the pile length is set at 30 ft. Three foundation configurations are modeled to calculate the pile group vertical dynamic stiffness, damping, and dynamic interaction factors. The first foundation configuration is for a pile group spaced at a spacing equal to a $2D_{pile}$, as shown in Figure 3-2, where D_{pile} is the pile diameter and equal to 1.5 ft. The second model is a pile group spaced at spacing equal to $4D_{pile}$, as shown in Figure 3-3. The third finite element model is to model a pile foundation configuration where the piles are spaced equal to a $6D_{pile}$, as shown in Figure 3-4. The analysis is performed for the pile groups for different values of the dimensionless frequency parameter (a_0) that ranges from 0.2 to 2.0.

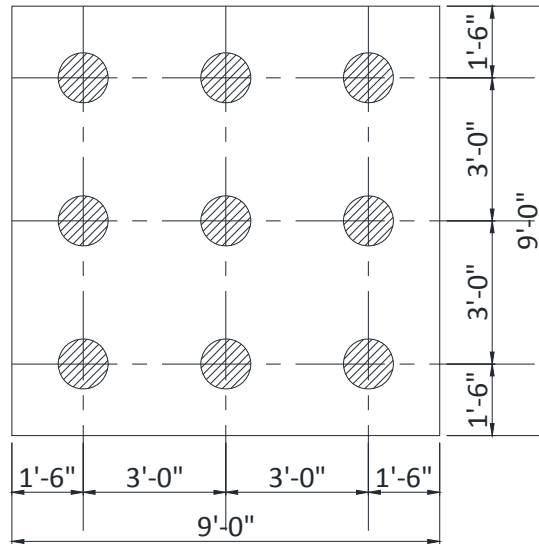


Figure 3-2: Pile Foundation with Piles Spaced at $2D_{pile}$

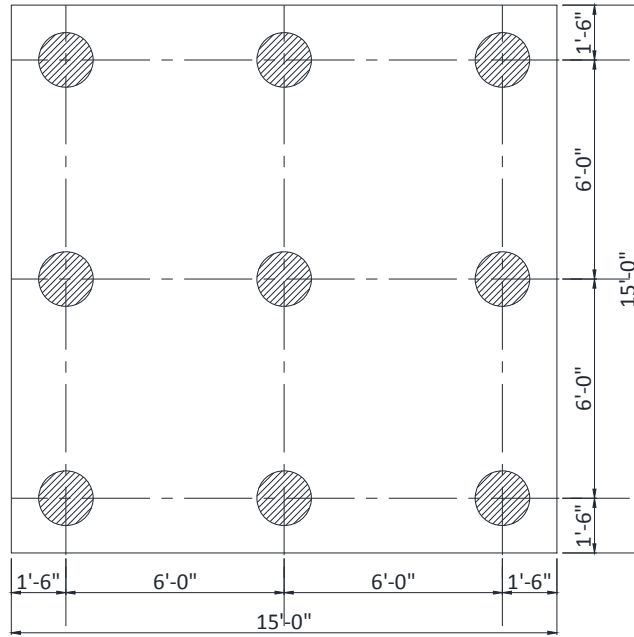


Figure 3-3: Pile Foundation with Piles Spaced at $4D_{pile}$

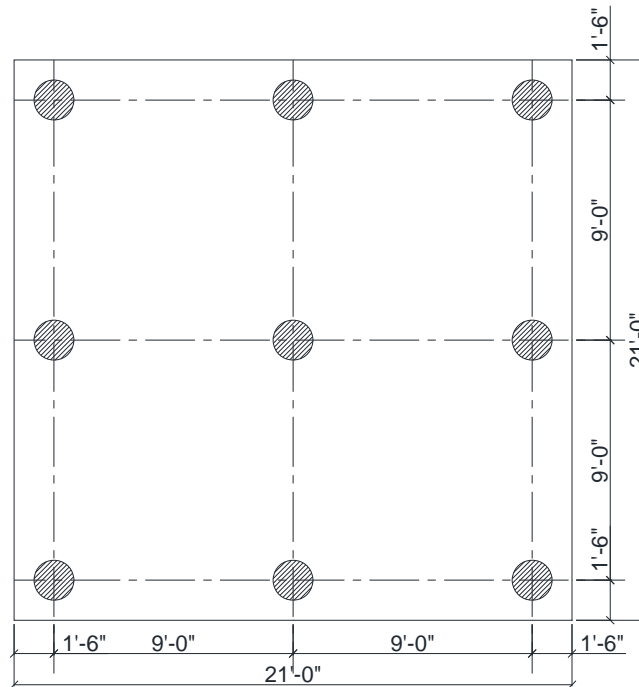


Figure 3-4: Pile Foundation with Piles Spaced at $6D_{pile}$

To consider the effect of pile concrete compressive strength on the pile groups vertical dynamic stiffness and damping, different concrete compressive strengths are

considered in the analysis, 3000 psi, 4000 psi, 5000 psi, and 6000 psi. These models are also used to study the effect of the soil shear modulus, pile elastic modulus and pile spacing on the vertical dynamic stiffness and damping of the pile groups. A three dimensional view of the soil-pile system is shown in Figure 3-5.

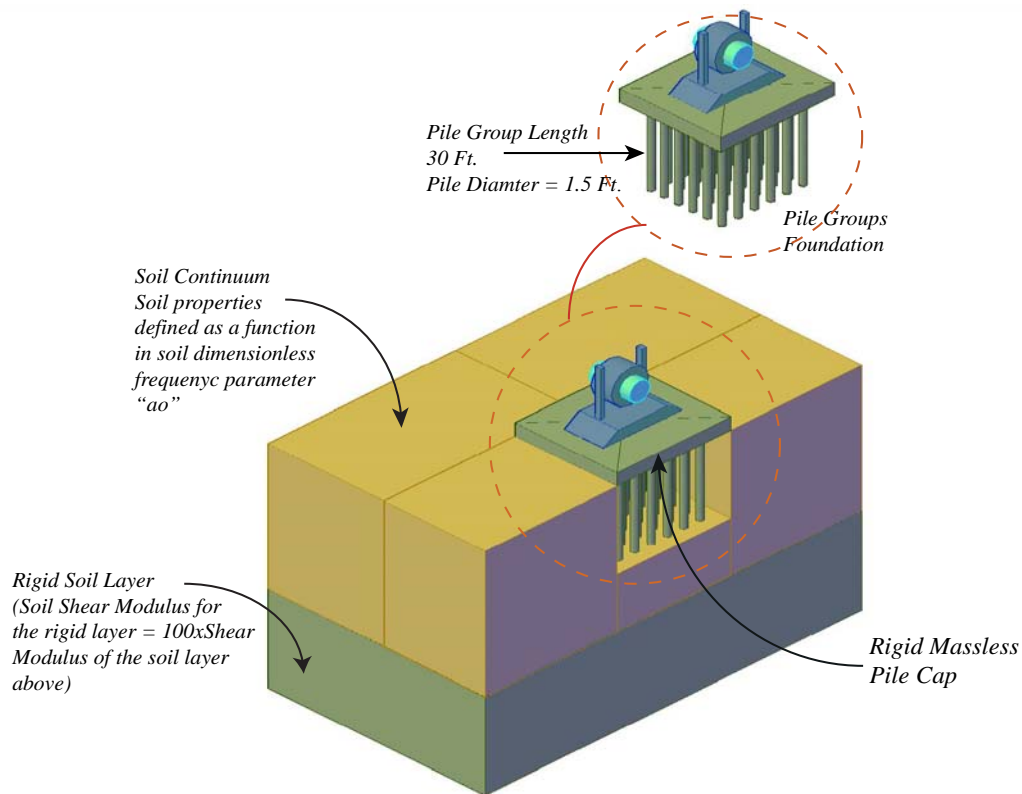


Figure 3-5: Three Dimension View of Soil Pile System

3.2 Generation of the Finite Element Model

Finite element modeling is a numerical representation of a physical engineering system. Therefore, the model should accurately capture the geometric detail of the system, the actual boundary conditions and the excitation environment of the dynamic system in order to simulate the real behavior of the problem. Generally, a dynamic finite element analysis consists of three major steps:

1. Idealization of geometry, materials and loading.

2. Formulation of stiffness, mass and damping matrices.
3. Solution of the resulting equations of motion.

A fundamental kinematic assumption of all finite element methods is that the displacement field $u(x, y)$ is completely defined by the displacement vector $\{u\}$ of the nodal points of the system. Several parameters affect the finite element results of the model, such as the element type, element length and boundary conditions. Selection of these parameters is discussed in the following sections.

ANSYS offers a wide variety of element library suitable for different application. Each element has specific properties. The behavior of these elements is defined through the use of element real constants. Generally, there are two methods to generate models in ANSYS, Direct generation method and Solid modeling. For large models, the direct generation method is less powerful since it requires the user to input and define all the joint coordinates and element connectivity in advance. The solid modeling, on the other hand does not require the user to manually input the coordinates of each joint. The general geometry of the model is generated through the use of geometric entities, then these geometries are meshed using ANSYS auto-meshing capabilities. Thus it offers more flexibility in generating and modifying the finite element model. Finite element analysis is performed in ANSYS in three major steps:

1. Building the model, the Preprocessing Phase.
2. Applying loads and obtaining the solutions, the Solution Phase.
3. Review the results, the Post Processing Phase.

3.2.1 ANSYS Coordinates Systems

There are multiple coordinate systems offered by ANSYS that are suitable for different shapes and geometries:

1. Global and local coordinate systems.
2. Nodal coordinate system that defines the nodes, their directions and degrees of freedom.
3. Element coordinate system that describes the element results output and its material properties orientation.

ANSYS has three built-in global coordinate systems that share the same origin:

Cartesian, cylindrical, and spherical, as shown in Figure 3-6.

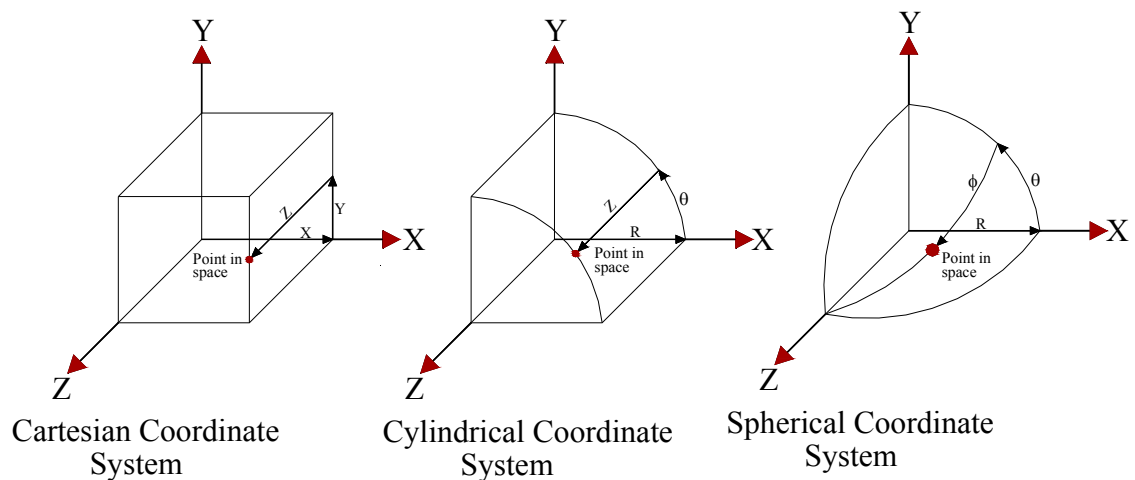


Figure 3-6: Global Coordinate Systems in ANSYS

The appropriate coordinate system is chosen according to the geometry of the problem.

The Global Cartesian coordinate system is used to generate the pile-soil model and the pile group-soil models.

3.2.2 Generation of the Solid ANSYS Model

The solid modeling method is considered the most convenient method to generate the finite element model and is used in this study. This is due to its flexibility to generate the geometry of the soil-foundation-pile system and its ability to easily incorporate changes in the model. In this research, solid modeling is developed using the ANSYS parametric programming language (APDL).

The main steps to generate a solid model are summarized as follows:

1. Define key points and lines. The Key points are considered the lowest order of the solid model entities. They define the vertices of the model and are used by the program to determine the location of the finite elements nodes. The key points work as a foundation for the solid model that locates the position of the model in the global coordinate system. Key points are defined in the global Cartesian coordinate system by the three major coordinates; X, Y, and Z.
2. Create areas and volumes to define the model geometry using the previously defined key points and lines. Volume and area elements can be created directly through key points and line generation can be skipped. Figure 3-7 shows an isometric view of the soil volume created through key points.

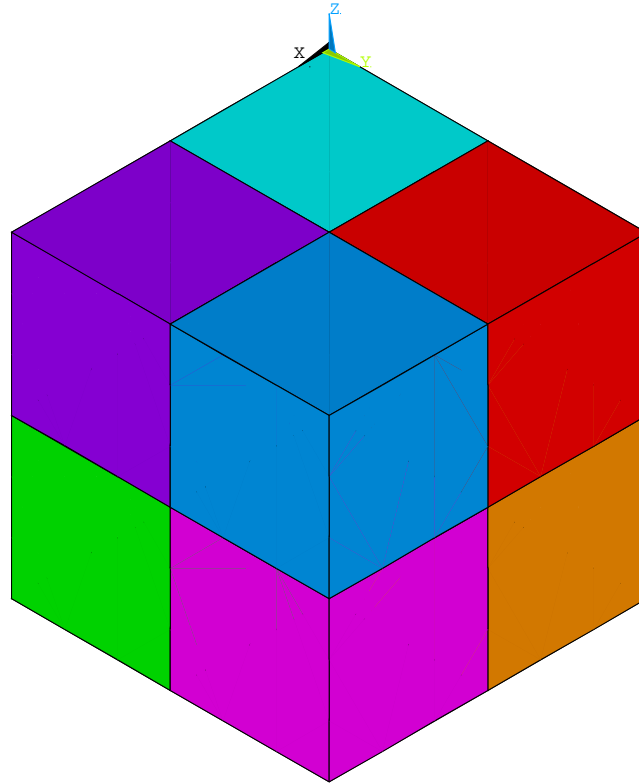


Figure 3-7: Soil Volumes in ANSYS

3. The next step after the model geometry is created is to select the element types that will be used to discretize the geometry and generate the finite element idealization of the problem. The selection of the element types depends on the required accuracy of the analysis. Generally, there are two methods to increase the accuracy of the finite element model, either to increase the number of elements, called h-refinement, or to use higher order elements, called p-refinement. Higher order elements (solid elements) with quadratic element formulation are more accurate in modeling soil elements, while beam elements are used to model the pile elements. The element behavior in ANSYS is defined by using elements attributes such as the elements real constants and the elements material properties. The elements real constants are used to define the

element's geometrical properties and to define the elements behavior. These properties, such as elements thicknesses, added masses to the element and nonlinearity of the elements are defined through the use of real constants. The elements material properties are also defined before the model is meshed into finite elements. Material properties such as the element elastic modulus, shear modulus, and the element poisson's ratio are required to create the element constitutive laws and generate the element elasticity matrix.

4. After the element type real constants and material properties are defined, the geometrical entities are meshed to generate the finite element model. ANSYS offers two types of meshing capabilities, depending on the complexity of the geometry and the required accuracy of the solution, free or mapped mesh. The elements of the free mesh are randomly distributed in the domain of the geometric elements with different elements sizes, such as shown in Figure 3-8. This type of meshing usually results in element distortion and reduces the accuracy of the results. On the other hand, mapped meshing, shown in Figures 3-9 and 3-10, have more organized elements and consistent element sizes along the domain of the geometric entities that are being meshed. The element size and the distortion of elements are fully controlled by the user in the computational domain. Mapped meshing is used in this research to increase the accuracy of the results and control the element sizes for best computational accuracy.

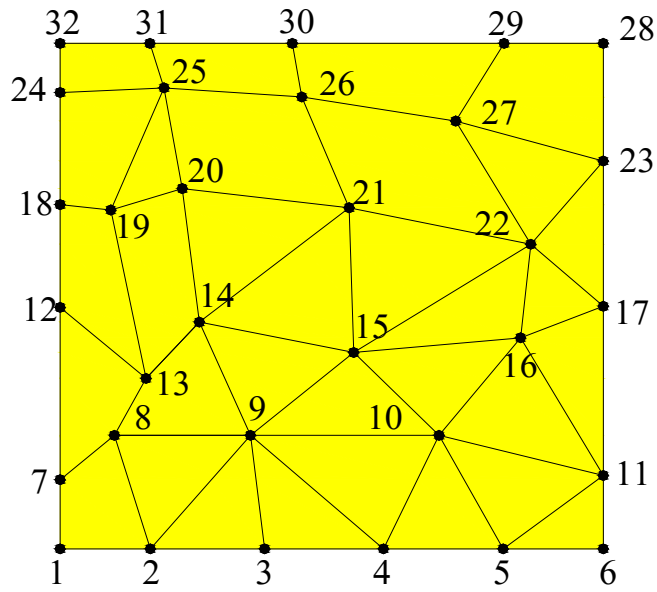


Figure 3-8: ANSYS Free Meshing

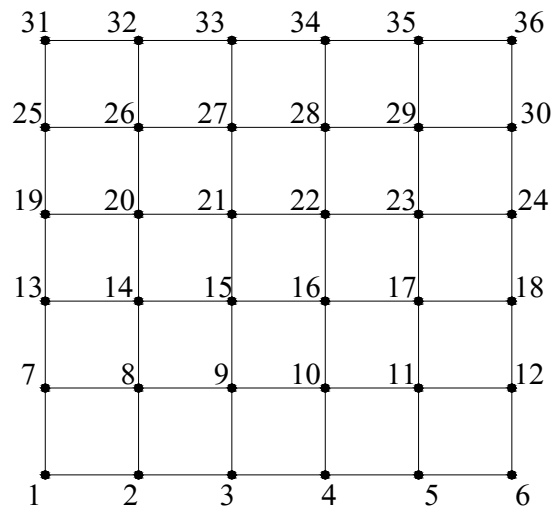


Figure 3-9: ANSYS Mapped Meshing

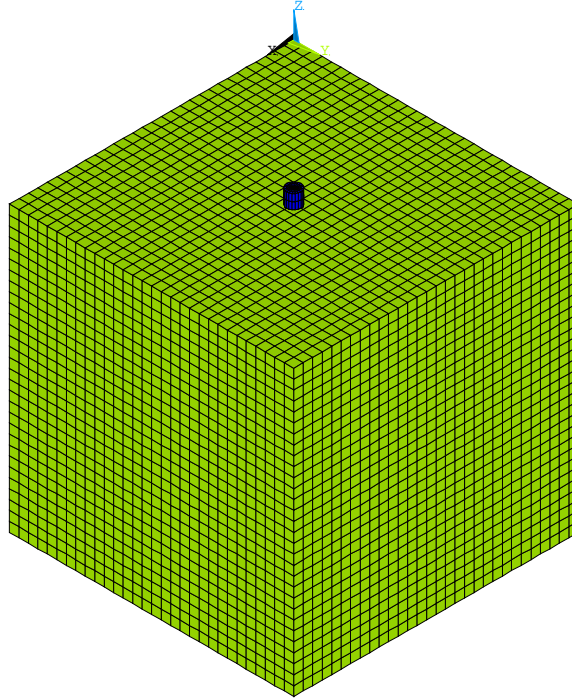


Figure 3-10: Soil Volumes Meshed using Mapped Meshing

3.3 Model Description

Two models are created to analyze the vertical dynamic response of the soil pile interaction. The first model considered a single pile in a soil continuum, while the second model is used to study the interaction between piles in the pile groups under the effect of vertical dynamic excitation. The analysis is performed for a pile having different concrete compressive strength and for a dimensionless frequency parameter (a_0) that ranges from 0.2 to 2.0, where:

$$a_0 = \frac{\omega r_0}{V_s} \quad (3-2)$$

Where: ω is the machine operating frequency, r_0 is the pile radius and V_s is the soil shear wave velocity.

Based on the size of the machine, the applied static and dynamic loading and the supporting foundation is a block type or frame type foundation, the piles diameter under the foundation for these machines can range from 1.5 ft. to 5.0 ft. (usually auger piles are used). The pile diameter used in this analysis is 3.0 ft. for the analysis of a single pile and 1.5 ft. for the analysis of a group of piles. The soil continuum is modeled using ANSYS element SOLID186 and the pile element is modeled using ANSYS beam element BEAM188. In order to capture the inertial interaction between the soil and the pile elements, a weight of 10^5 lbs. is added at the top of the pile element using ANSYS element MASS21. Since the soil continuum is infinite and it is not practical to model the total unbounded soil medium using a finite number of finite elements, an artificial boundary is introduced at distance equal to the pile length in each direction (30 ft.). Viscous boundaries are introduced at the edge and base of the soil continuum to allow transmitting the waves without it being reflected back into the computational domain. ANSYS spring-damper element COMBIN14 is used to model the soil viscous boundaries. Figure 3-11 presents the finite element model of the single pile embedded in the soil continuum. The top of the pile is subjected to a harmonic excitation force and the response is measured for a range of dimensionless frequency parameter (a_0) from 0.2 to 2.0.

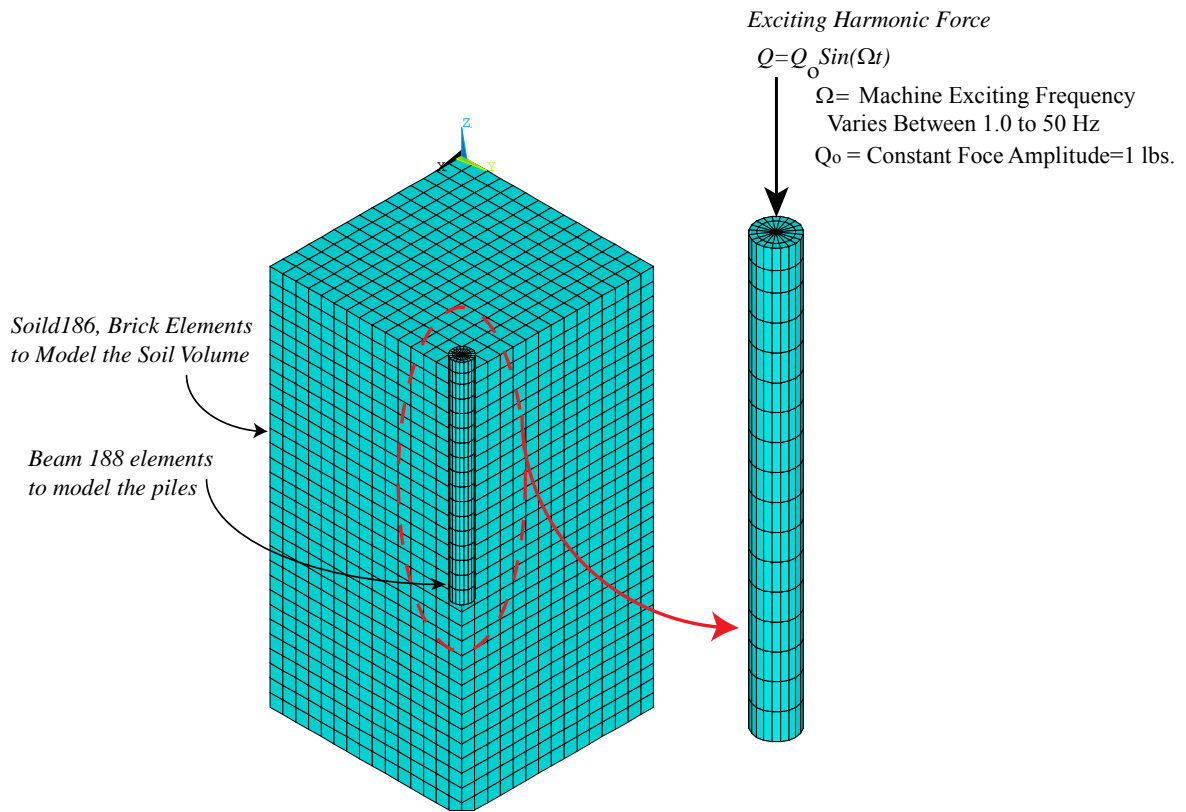


Figure 3-11: Finite Element Model for Soil-Pile-Soil Interaction

The single pile finite element model is composed of 43,500 nodes, and 27,100 solid elements to model the soil continuum and 14,000 damper elements to model the soil's viscous boundaries. For each concrete compressive strength a total of 10 analyses cases were performed and for each analysis case, a total of 50 load steps were performed (from 1 Hz to 50 Hz). Therefore, the total analysis cases performed to the single pile are 40 analysis cases with total of 2,000 load steps. The average solution time is 20 minutes per load step. The total solution time for the 40 analysis cases of the single pile finite element model on a machine having an Intel Core i7 Processor, 24GB RAM and 64-bit operating system was approximately 22 days. The total analysis runs for the pile groups were ten runs per pile concrete compressive strength per pile groups spacing. This means that for pile groups spaced at $2D_{pile}$ the pile concrete material is 3,000 psi,

a total of 10 analysis cases are performed (from $a_0 = 0.2$ to $a_0=2.0$) and for each analysis case a total of 50 load steps were performed (from 1.0 Hz to 50 Hz). Therefore, for pile groups spaced at $2D_{pile}$, $4D_{pile}$ and $6D_{pile}$ and pile concrete compressive strength of 3000 psi, 4,000 psi, 5,000 psi, and 6,000 psi, a total of 120 analysis cases were performed, and a total of 6,000 load steps were analyzed.

The finite element model generated to model the pile groups spaced at $2D_{pile}$ consisted of 19,000 nodes, 10,500 solid elements to model the soil continuum and 7,500 elements to model the soil viscous boundaries. To model pile groups spaced at $4D_{pile}$, the finite element model consisted of 41,341 nodes, 25,728 solid elements to model the soil continuum and 12,866 elements to model the soil viscous boundaries. Finally, the finite element model generated to model the soil-pile system for pile groups spaced at $6D_{pile}$ consisted of 54,794 nodes, 35,568 elements to model the soil continuum and 15,626 elements to model the soil viscous boundaries.

3.4 Element Types

ANSYS element SOLID186 is used to model the soil continuum. Solid 186 is a higher order 3-D 20-node solid element that exhibits quadratic displacement behavior. As shown in Figure 3-12, the element is defined by 20 nodes having three degrees of freedom per node: translations in the nodal x, y, and z directions.

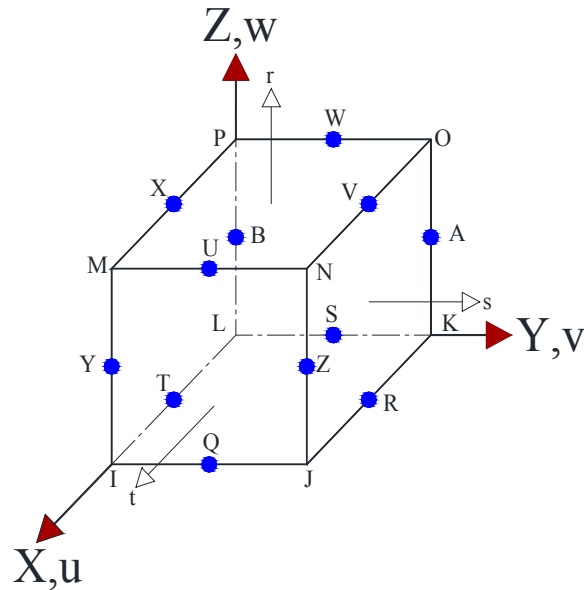


Figure 3-12: Solid 186 Elements Global and Local Axis

The pile element is modeled using ANSYS element BEAM188. The BEAM188 element has six degrees of freedom at each node, translations in the x, y, and z directions and rotations about the x, y, and z directions. The element formulation is based on the Timoshenko beam theory, which includes shear-deformation effects. The element formulation assumes that the transverse shear strain is constant throughout the cross section, which means that the beam cross sections remain plain after deformation.

3.5 Modeling of the Pile Cap

The pile cap was modeled using ANSYS element SOLID186. The pile groups are connected by a rigid massless pile cap for uniform distribution of the excitation force on the pile groups without adding additional masses or stiffness to the pile groups. The pile foundation system was excited using a unit constant force harmonic excitation force acting at the center of the pile cap. Figures 3-13, 3-14, and 3-15 show the finite element mode for pile groups spaced at $2D_{pile}$, $4D_{pile}$ and $6D_{pile}$.

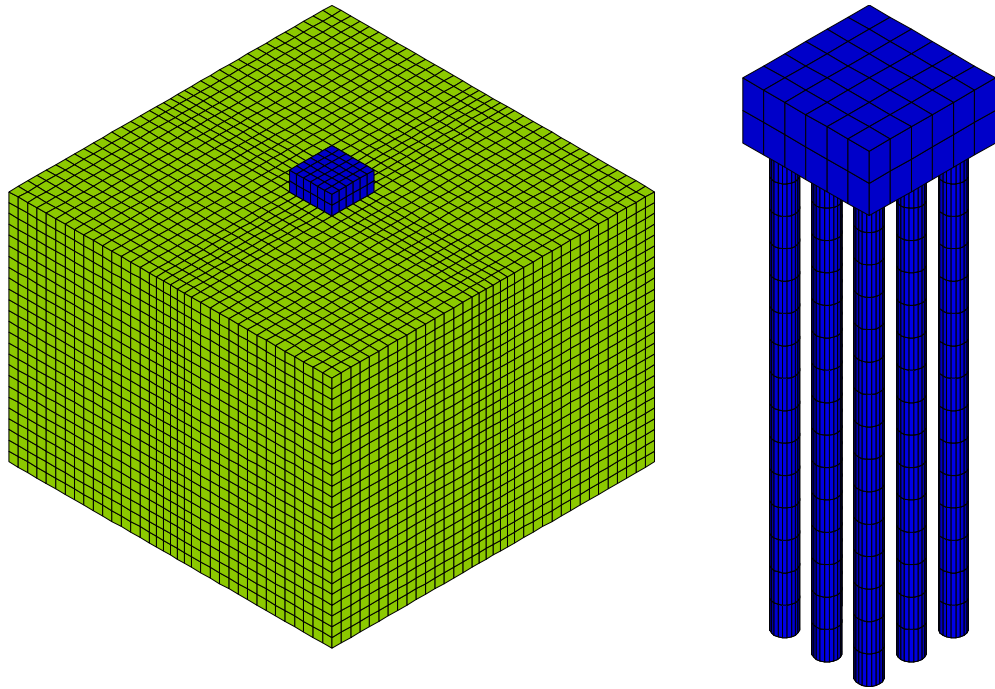


Figure 3-13: Pile Group Foundation Model for Piles Spaced at $2D_{pile}$

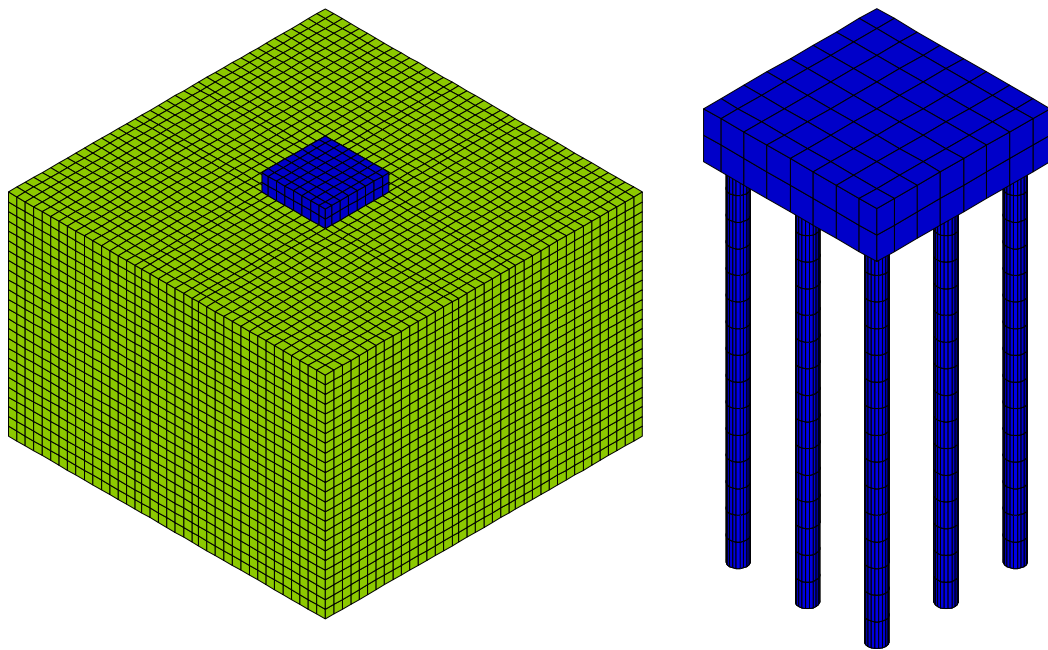


Figure 3-14: Pile Group Foundation Model for Pile Spaced at $4D_{pile}$

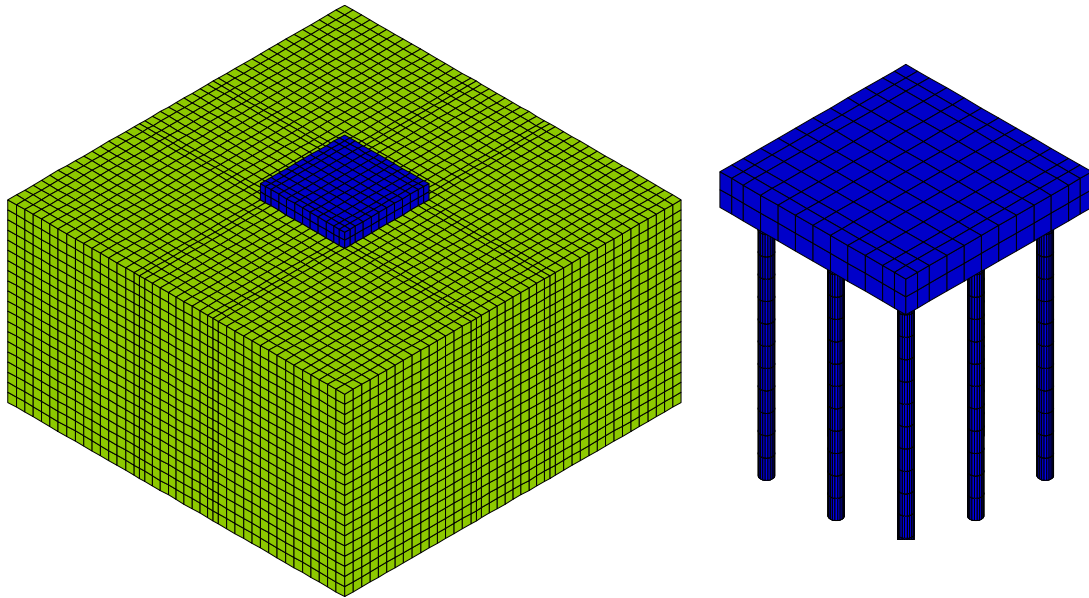


Figure 3-15: Pile Group Foundation Model for Pile Spaced at $4D_{pile}$

3.6 Modeling of the Soil Boundaries

To model the soil-pile interaction problem using the finite element method, the soil unbounded domain has to be truncated to a finite size. In static analysis, since the displacement field decreases with increasing distance from the structure, simple boundary conditions such as a fixed boundary condition is introduced at a sufficient distance from the structure, usually in the range of 3 to 5 times the soil depth. Thus, the unbounded soil system is converted into a bounded system. This truncation process is not applicable in a soil dynamic application because of the effect of wave reflection at the truncated boundaries. During vertical dynamic excitation of a foundation pile soil system, elastic waves are transmitted into the soil medium in all directions towards infinity. At the surface of the soil boundary, reflection of the elastic waves occurs back into the foundation pile system. In addition, at the interface of the soil layers, refraction of the elastic waves also occurs. In dynamic analysis of the machine foundation soil

pile system, introducing rigid boundaries will reflect the wave originating from the machine foundation system back into the discretized model. Thus, lead to a factious amplification of the waves within the computation continuum. Therefore, the soil boundaries should be modeled to allow the elastic waves emitted from the machine foundation system to pass through the soil bounded boundary elements toward infinity without reflecting the waves into the computational domain. Therefore, viscous boundaries composed of dashpots oriented in a direction normal and parallel to the soil lateral boundaries, as shown in Figure 3-16, are provided using ANSYS spring-damper element “COMBIN14”. The damper elements are provided at the edge of the soil continuum at a distance of 20 times the pile radius (30 ft.).

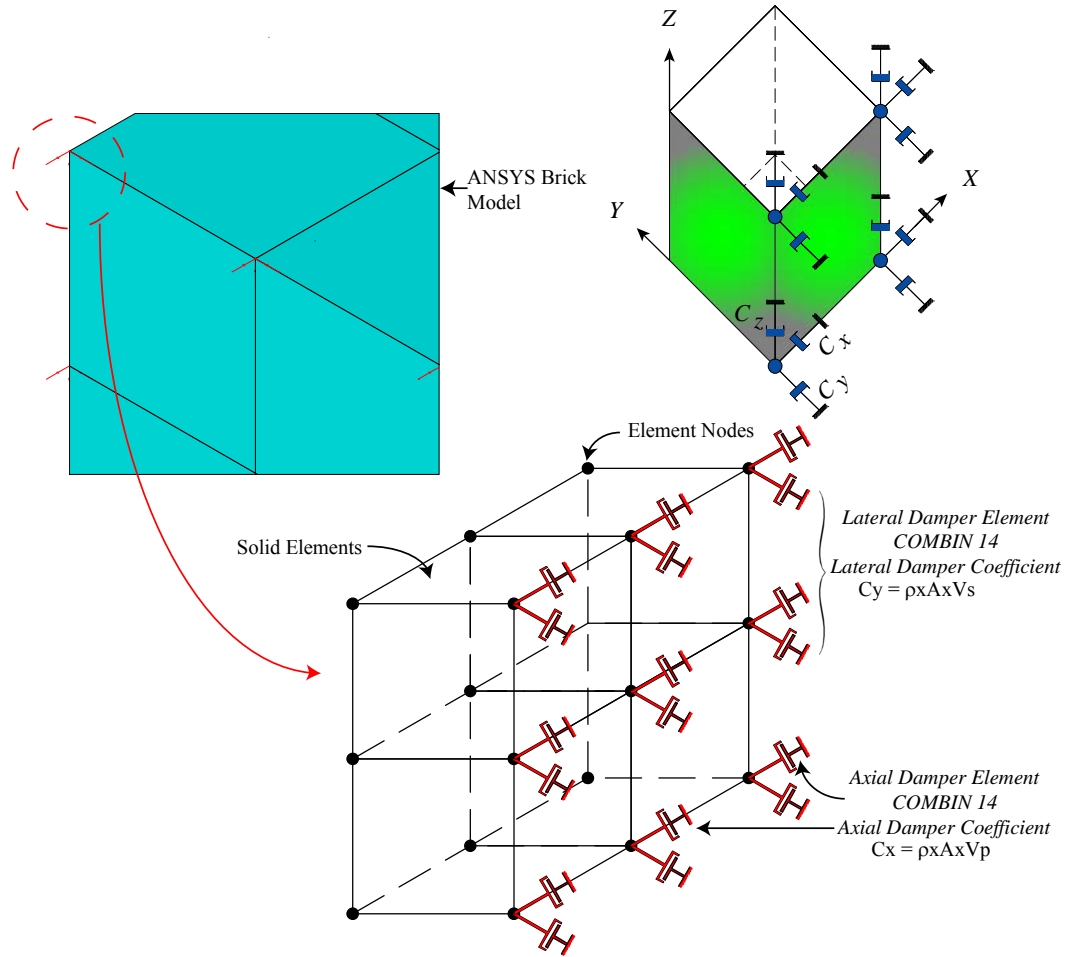


Figure 3-16: Damper Element at the Edge of Soil Boundaries (Viscous Boundary)

The damper coefficient used in the direction perpendicular to the element (C_y) and along the element side (C_x and C_z) is calculated as presented by Wilson (2002). The dynamic equilibrium for a soil unit volume, as shown in Figure 3-17, through which waves are propagating in the positive x direction equation of motion as per De Alembert's theory is;

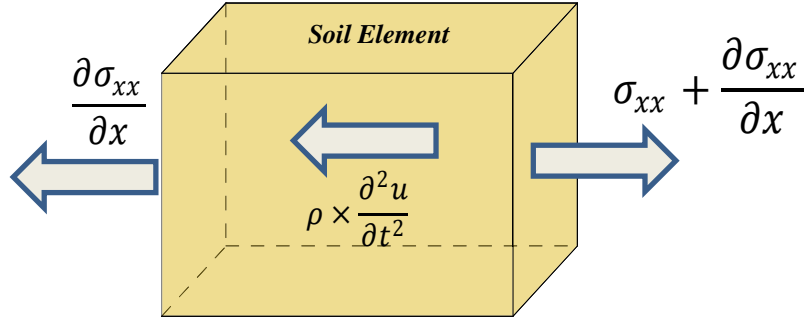


Figure 3-17: Dynamic Forces Acting on Unit Soil Volume

$$-\sigma_{xx} - \rho \times \frac{\partial^2 u}{\partial t^2} + \sigma_{xx} + \frac{\partial \sigma_{xx}}{\partial x} = 0 \quad (3-3)$$

$$\frac{\partial \sigma_{xx}}{\partial x} = \rho \times \frac{\partial^2 u}{\partial t^2} \quad (3-4)$$

Since $\sigma_{xx} = \lambda \times \epsilon_{xx}$ and $\lambda =$ Lamé's constant, Therefore, σ_{xx}

$$= \lambda \times \frac{\partial u}{\partial x} \text{ and } \frac{\partial \sigma_{xx}}{\partial x} = \lambda \times \frac{\partial^2 u}{\partial x^2}$$

$$\rho \times \frac{\partial^2 u}{\partial t^2} = \lambda \times \frac{\partial^2 u}{\partial x^2} \Rightarrow \frac{\partial^2 u}{\partial t^2} = V_p^2 \times \frac{\partial^2 u}{\partial x^2} \quad (3-5)$$

Where $V_p =$ P wave propagating through the medium

The solution of the above wave equation is given by

$$u(x, t) = U \left[\sin \left(\omega t - \frac{\omega x}{V_p} \right) + \cos \left(\omega t - \frac{\omega x}{V_p} \right) \right] \quad (3-6)$$

$$\frac{\partial u(x, t)}{\partial t} = U \omega \left[\cos \left(\omega t - \frac{\omega x}{V_p} \right) + \sin \left(\omega t - \frac{\omega x}{V_p} \right) \right] \quad (3-7)$$

$$\text{Since the soil axial strain} = \epsilon_{xx} = \frac{\partial u}{\partial x} \quad (3-8)$$

$$\epsilon_{xx} = -U \left(\frac{\omega x}{V_p} \right) \left[\sin \left(\omega t - \frac{\omega x}{V_p} \right) + \cos \left(\omega t - \frac{\omega x}{V_p} \right) \right]$$

$$\varepsilon_{xx} = \frac{1}{V_p} \times \frac{\partial u(x, t)}{\partial t}$$

The soil stress is computed as $\sigma_{xx} = -\lambda \times \varepsilon_{xx}$ (3-9)

$$= -\lambda \times \frac{1}{V_p} \times \frac{\partial u(x, t)}{\partial t}$$

Where $\lambda = \text{Lame's Constant} = \rho \times V_p^2$

$$\sigma_{xx} = \rho \times V_p \times \frac{\partial u(x, t)}{\partial t} \quad (3-10)$$

$$F_{xx} = \sigma_{xx} \times A = \rho \times V_p \times A \times \frac{\partial u(x, t)}{\partial t} \quad (3-11)$$

F_{xx} is the force that is identical to the force in a simple viscous damper whose value is equal to $\rho V_p A$. Therefore, a boundary condition can be created that will allow the P waves to pass without any reflection and allow the strain energy to radiate away from the source. Similarly, a boundary condition can be created that will allow the S waves to pass without any reflection and allow the strain energy to radiate away from the source using the same procedure

$$F_{zz} = \sigma_{zz} \times A = \rho \times V_s \times A \times \frac{\partial w(x, t)}{\partial t} \quad (3-12)$$

Where: V_s is the soil shear wave velocity = $\sqrt{G_{\text{soil}}/\rho_{\text{soil}}}$

Therefore, the damper coefficient perpendicular to the soil boundary is given by:

$$C_y = \rho V_p A \quad (3-13)$$

Damper coefficient along to the element side

$$C_x = C_z = \rho V_s A \quad (3-14)$$

where: $A = \text{Area served by each node}$, $\rho = \text{mass density of soil material}$, $V_p = \text{Soil compression wave velocity}$ and $V_s = \text{Soil shear wave velocity}$

3.7 Element Size

Selection of correct element size is an important parameter in the soil pile interaction problem since the accuracy of the solution depends on the ability of the displacement field in the discretized model, which is defined by the nodal displacement and element interpolation function, to approximate the actual behavior of the soil continuum. Based on the recommendation of Lysmer (1978), the elements size S_{element} , must be chosen based on the maximum frequency content of the applied loads, i.e., the maximum element size is governed by the highest frequency of the applied dynamic load. Therefore, to model a shear wave, the maximum dimension of the elements must be chosen smaller than the shorter wave length of the wave to be transmitted in the soil continuum.

$$S_{\text{element}} \leq \lambda_{\text{shear}} \quad (3-15)$$

where: S_{element} is the maximum element dimension, and λ_{shear} is the shorter wave length P-waves are not considered since they travel faster than the shear wave and thus have longer wave lengths than shear waves.

Lysmer (1978), proposed the following criteria for selecting the finite element size

$$S_{\text{element}} \approx \frac{1}{5} \lambda_{\text{shear}} \quad (3-16)$$

Based on this criterion, for a range of soil shear wave velocities of 250 ft./sec to 2,300 ft./sec, and machine operating frequency of 50Hz, the shear wave length is 5.0 ft. to 46.0 ft. and the minimum element length should be 1.0 ft. to 9.4 ft., respectively. Therefore, the size of elements used to model the soil elements and pile elements are chosen equal to 1.0 ft., which is the distance between element nodes.

3.8 Damping

A 5% constant damping ratio is used in the model to account for material damping of the soil/pile system.

3.9 Soil Properties

3.9.1 Surrounding Soil

The effect of variation of the soil properties is captured by utilizing the dimensionless frequency dependent parameter (a_0). The soil medium is modeled as linear elastic material. This is because, for satisfactory machine operation, the maximum dynamic displacement amplitudes at the location of the machine bearing supports are limited to 10-12 microns. These limits on the machine maximum dynamic amplitudes maintain the strains in the soil within the elastic limits. The soil properties are computed at different values of the dimensionless frequency parameter (a_0) that range from 0.2 to 2.0. The dimensionless frequency parameter (a_0) is related to the soil dynamic shear modulus and Young's modulus by the following relations

Since $a_0 = \omega r_0 / V_s$ and $V_s = \sqrt{G_{soil} / \rho}$. Thus the soil shear modulus:

$$G_{soil} = \frac{(2\pi f r_0)^2 \gamma_{soil}}{(a_0)^2 g} \quad (3-17)$$

and Soil Young's Modulus

$$E_{soil} = 2G_{soil}(1 + \mu_{soil}) \quad (3-18)$$

where: γ_{soil} = Unit weight of soil material, assumed equal to 100 pcf, f = machine operating frequency in Hz, r_0 = pile radius, $g = 32.2 \text{ ft. /sec}^2$ and μ_{soil} = soil material Poisson's ratio = 0.25

The range of soil properties for different (a_0) values can be determined as follows, for a machine operating frequency, f of 50 Hz:

When $a_0 = 0.20$, $G_{soil} = 17.2 \times 10^3$ ksf and $V_s = 2,353$ ft./sec, i.e., the soil will have a high shear modulus (strong soil).

When $a_0 = 2.0$, $G_{soil} = 0.172 \times 10^3$ ksf and $V_s = 235.3$ ft./sec, i.e., the soil will have a lower shear modulus (weak soil).

3.9.2 Soil at the pile tip

The pile tip rests on a rigid soil layer. The thickness of the layer used is 20 ft.

The properties of this layer are:

Soil Base Shear Modulus:

$$G_{base} = 100G_{soil} \quad (3-19)$$

Soil Base Young's Modulus:

$$E_{base} = 2G_{base}(1 + \mu_{soil}) \quad (3-20)$$

where: G_{base} = Shear modulus at the pile tip and E_{base} = Young's modulus at the pile tip

3.10 Pile Properties

The pile properties used in the model are determined based on the concrete compressive strength of the pile material where the Young's modulus and Shear modulus for the pile material is computed using the following equations:

Pile Young's modulus (ACI 318):

$$E_{pile} = 57000\sqrt{f_c} \quad (3-21)$$

Pile Shear Modulus:

$$G_{pile} = \frac{E_{pile}}{2(1 + \mu_{pile})} \quad (3-22)$$

where: μ_{pile} = Pile material Poisson's ratio = 0.17 and γ_{pile} = 150 lb./ft³

3.11 Loading

The finite element model for the single pile is excited with a vertical dynamic harmonic excitation force acting at the pile head equal to

$$Q = Q_o \sin(\Omega t) = Q_o e^{i\Omega t} \quad (3-23)$$

Where: Ω is the frequency of the forcing function = 1 to 50 Hz and Q_o = constant force amplitude = 1 lbs.

A load of 10^5 lb. is added on the top of the pile to represent part of the weight of the machine and to capture the inertial interaction between the soil and pile elements. Figures 3-18 and 3-19 show a section view of the soil pile system for a single pile and pile groups.

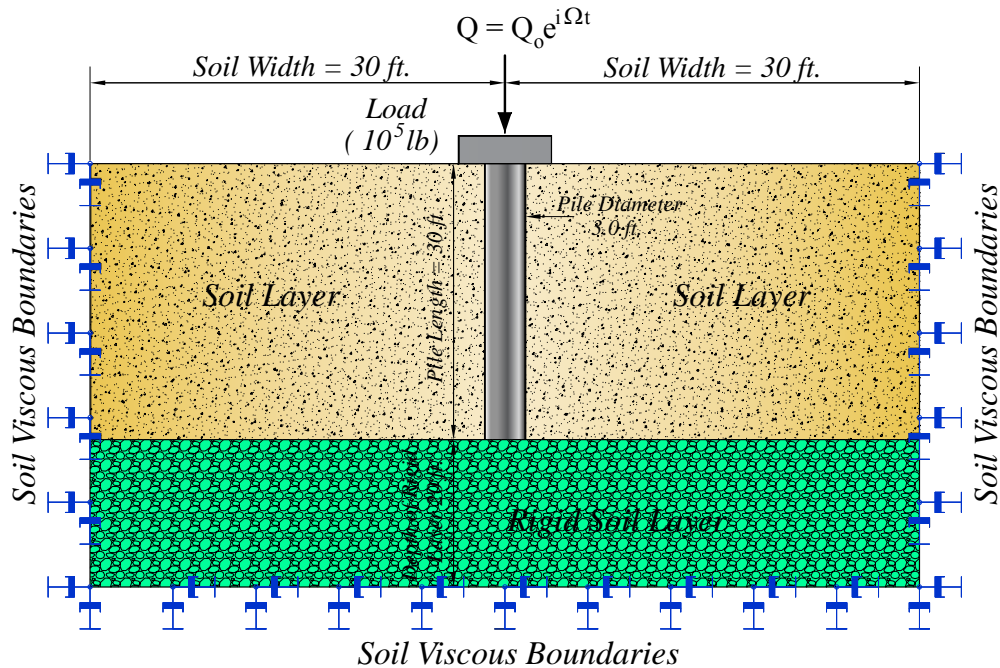


Figure 3-18: Sectional View of a Single Pile in Soil Continuum

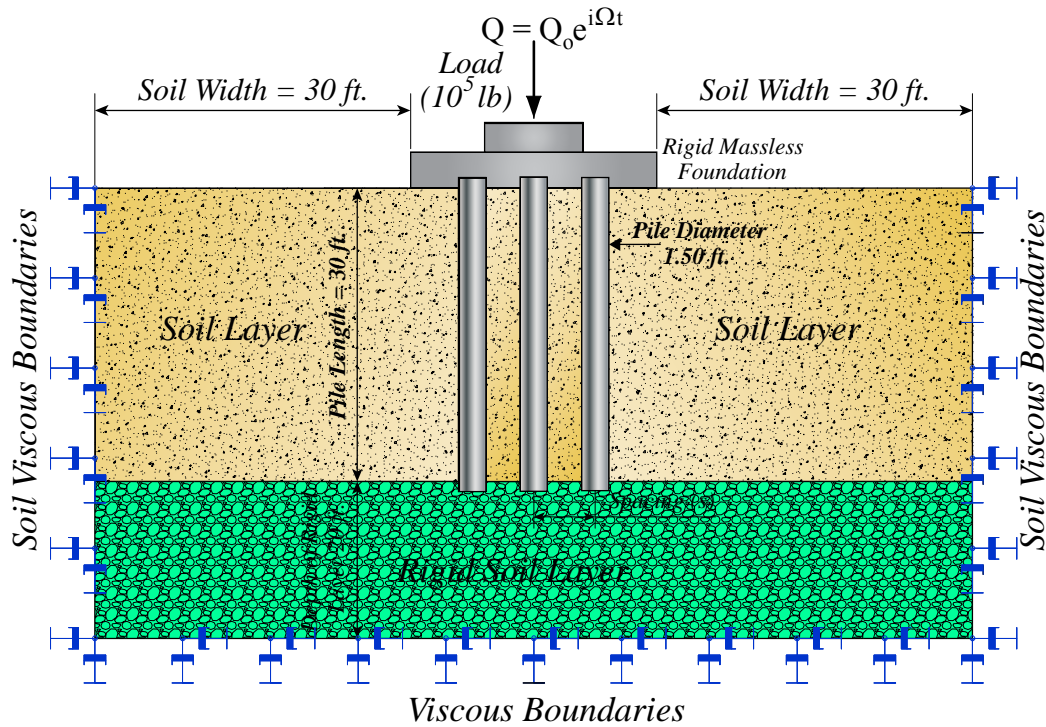


Figure 3-19: Sectional View of Pile Groups in Soil Continuum

3.12 Verification of Soil Boundary Location

Selection of the location of the soil lateral boundaries plays an important role in the pile vertical dynamic response. The location of the soil lateral boundaries must be selected so as not to reflect the soil waves into the computation continuum and thus amplify the response of the soil-pile-foundation system. Generally there are two types of boundaries that are used to model the soil lateral boundaries.

- Elementary Boundaries
- Viscous Boundaries

Elementary boundaries can be fixed boundaries or free boundaries. The location of the elementary boundaries depends on the soil's natural frequency, and damping characteristics of the soil continuum. Usually the location of the soil boundary is determined based on trial and error. An initial estimate of the soil lateral boundary

within the range of three to five times the soil depth is usually used as an initial estimate, then the location of the soil lateral boundary increases incrementally until the response converges.

Viscous boundaries, on the other hand, are composed of dashpots oriented in a direction normal and parallel to the soil lateral boundaries. Kuhlemeyer and Lysmer (1973) recommended the location of the soil lateral viscous boundaries at four to five times the pile diameter. In the analysis of pile vertical response, the location of the soil boundaries are defined at distances equal to 20 times the pile radius ($20r_0$), which is consistent with the recommendation of Kuhlemeyer and Lysmer. To ensure convergence of the vertical dynamic amplitudes and the accuracy of the solution, two additional conditions for the location of the soil lateral boundaries are checked at $30r_0$ and $40r_0$ respectively, where r_0 is the pile radius. Therefore, to check the effect of the location of the soil lateral viscous boundaries on the soil-pile vertical dynamic response, a total of three cases were checked. In all three cases, the dimensionless frequency parameter (a_0) is set equal to 0.2. The soil lateral boundaries are modeled using viscous boundaries having the formulation as shown in Section 3.6. The three models are excited using a constant amplitude harmonic excitation force having the form $Q = Q_0 e^{i\Omega t}$ acting on the pile head. The vertical dynamic displacement amplitude response is computed at the top of the pile. Figure 3-20 shows the vertical dynamic displacement response of the pile head for each case of the soil boundaries ($20r_0$, $30r_0$ and $40r_0$) with respect to the forcing function exciting frequency. The maximum displacement amplitude for each of the soil boundary cases are plotted in Figure 3-21.

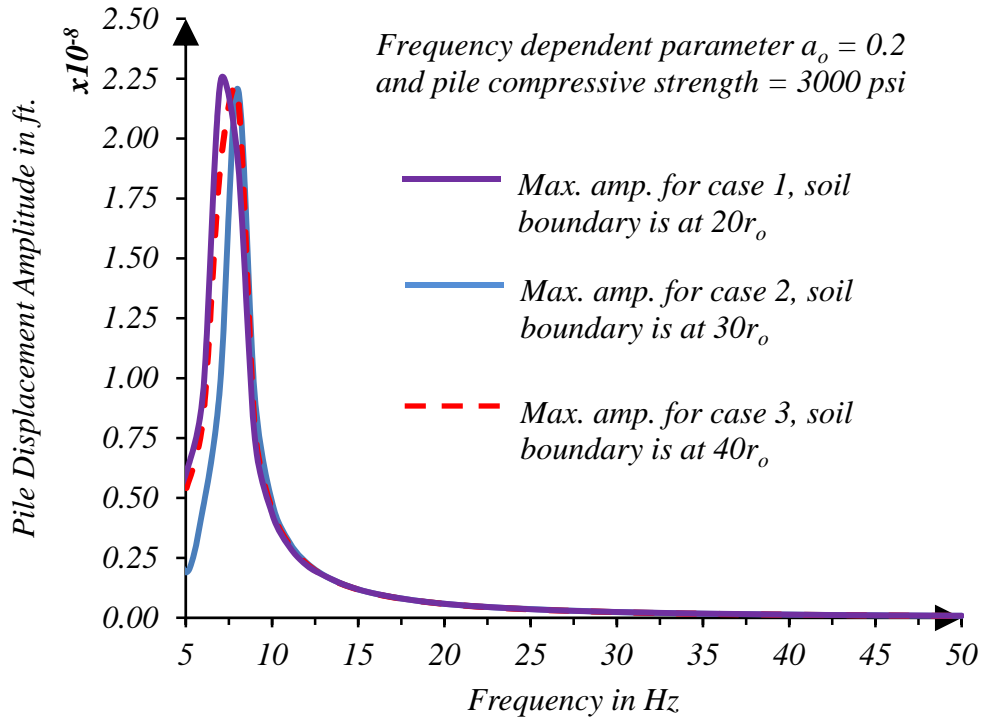


Figure 3-20: Effect of Soil Edge on Pile Vertical Dynamic Response

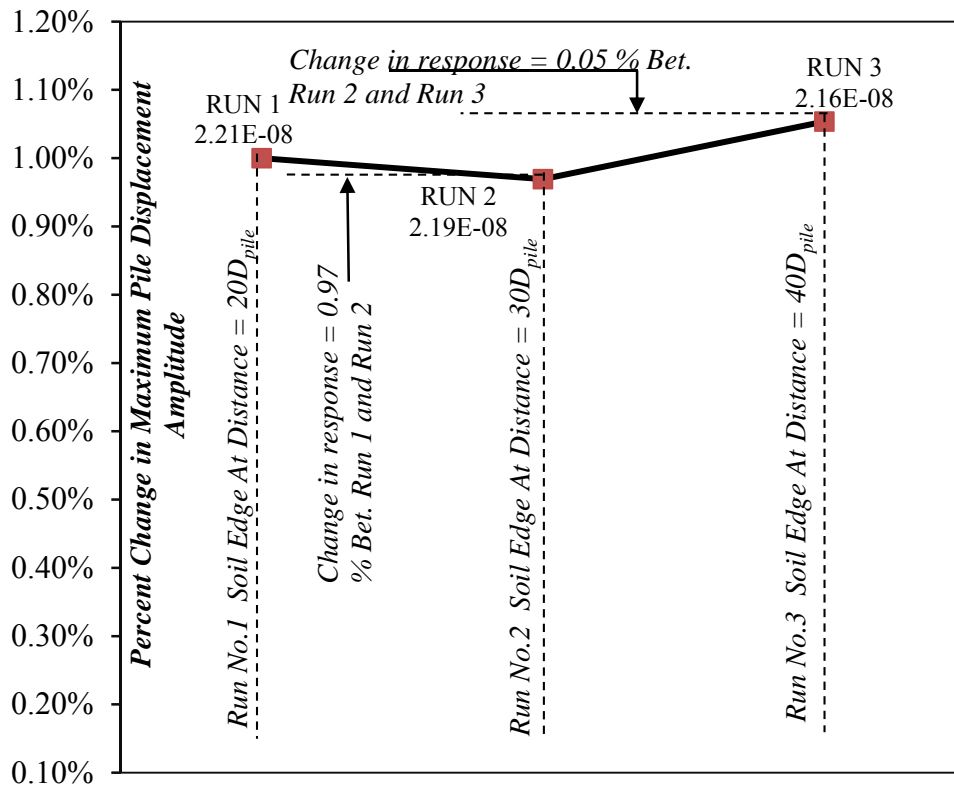


Figure 3-21: Vertical Pile Response Due to Change in Soil Lateral Boundaries

The maximum displacement amplitude for the soil boundary at a distance of $20r_0$ is 2.21×10^{-8} ft., and for soil boundary at a distance of $30r_0$ is 2.19×10^{-8} ft., and finally, for the soil boundary at a distance of $40r_0$ is 2.16×10^{-8} ft. The differences between all three cases are within 1%. Therefore, it is concluded that locating the soil lateral boundaries at a distance equal to $20r_0$ using viscous boundary elements is acceptable and the effect of increasing the lateral soil boundary more than $20r_0$ has a negligible effect on the pile amplitude response.

Chapter 4: Vertical Dynamic Response of a Single Pile

4.1 Introduction

To calculate the vertical dynamic stiffness and damping for a single pile, the finite element model for the single pile described in Chapter 3 and shown in Figures 4-1 and 4-2 is excited using a vertical dynamic harmonic excitation force acting at the pile head equal to the following:

$$Q = Q_o \sin(\Omega t) = Q_o e^{i\Omega t} \quad (4-1)$$

where: Ω is the frequency of the forcing function = 1 to 50 Hz and Q_o = constant force amplitude = 1 lbs.

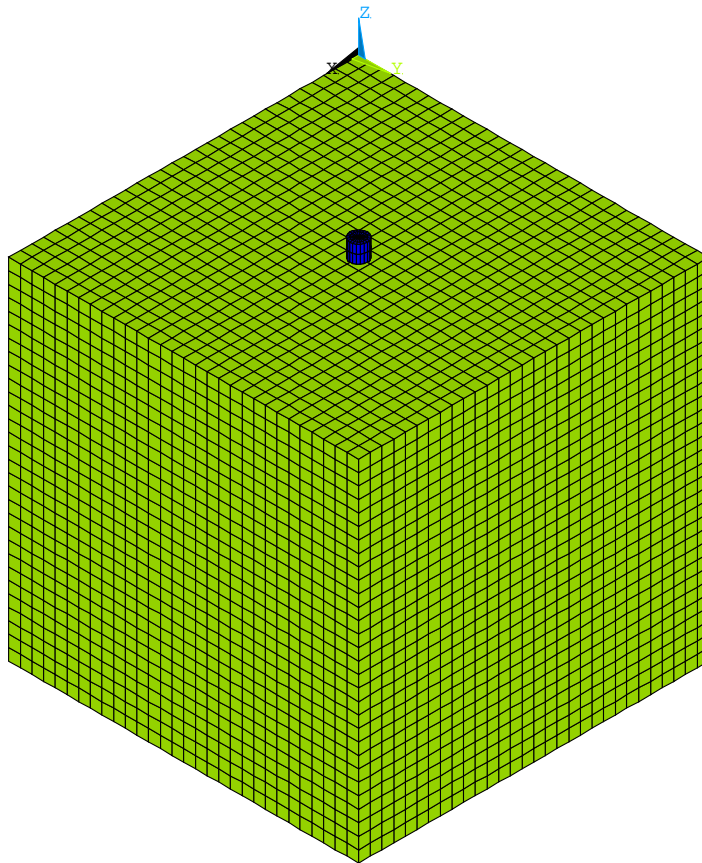


Figure 4-1: Single Pile Finite Element Model 3D View

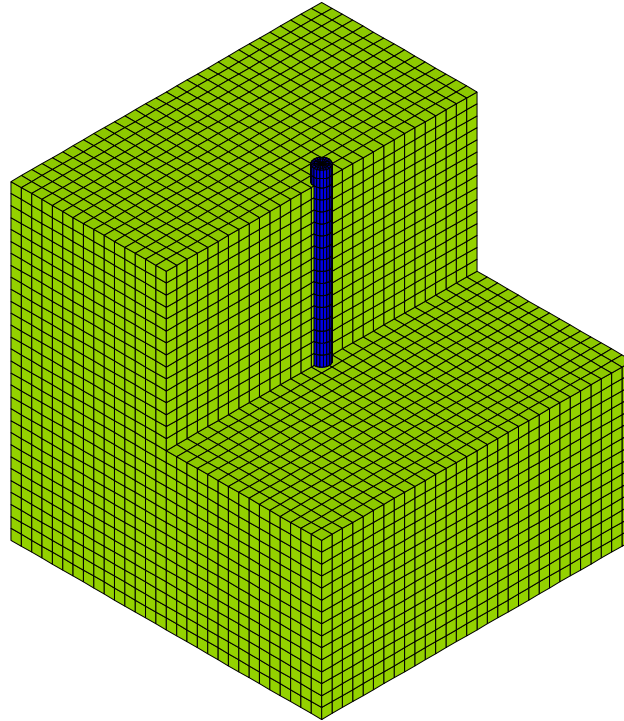


Figure 4-2: Single Pile Finite Element Model Sectional View

The vertical dynamic amplitude response for the pile due to the vertical dynamic force is calculated for different values of pile concrete compressive strength ($f_c = 3000$ psi, 4000 psi, 5000 psi, 6000 psi and for a steel pile) for the dimensionless frequency parameter (a_0) that ranges from 0.2 to 2.0.

4.2 Dynamic Parameters Determined

4.2.1 Dynamic Stiffness of a Single Pile

The vertical dynamic stiffness of a concrete pile is calculated at the pile head at various frequencies of excitation. The vertical dynamic stiffness at each value of the dimensionless frequency parameter (a_0) is determined as the inverse of the average vertical dynamic amplitude, as shown in Figure 4-3 and Equation (4-2).

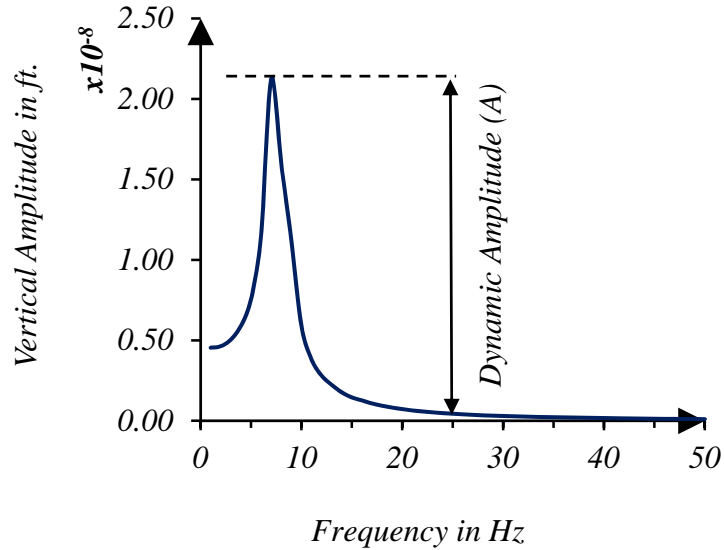


Figure 4-3: Vertical Dynamic Amplitude

Average vertical dynamic stiffness is given by equation (4-2)

$$K_{\text{average}} = \frac{1}{A_{\text{average}}} \quad (4-2)$$

where: A_{average} is the average dynamic amplitude for the frequency range from 1 Hz to 50 Hz.

Also, the minimum vertical dynamic stiffness is determined from equation (4-3).

$$K_{\text{minimum}} = \frac{1}{A_{\text{max}}} \quad (4-3)$$

where: A_{max} is the maximum dynamic amplitude at resonance

The vertical amplitude as a function of frequency, as shown in Figure 4-3, shows a sharp peak at resonance and very small response at other frequencies. Defining the stiffness at resonance, which in this study is between 5 to 10 Hz and the fact that the machine operating frequency is around 50 Hz will produce a very small stiffness. Whereas defining an average stiffness, i.e., incorporating the effect of frequencies of 1 Hz to 50 Hz would produce a more realistic value of the dynamic stiffness.

4.2.2 Damping of a Single pile

The damping of the concrete pile is calculated using the soil-pile system Dynamic Magnification Factor (DMF). The calculation of damping was undertaken at resonance where it is the most critical. The DMF for the pile soil system at each dimensionless frequency parameter (ω_0) is calculated as shown in Figure 4-4 and Equations 4-3, 4-4 and 4-5:

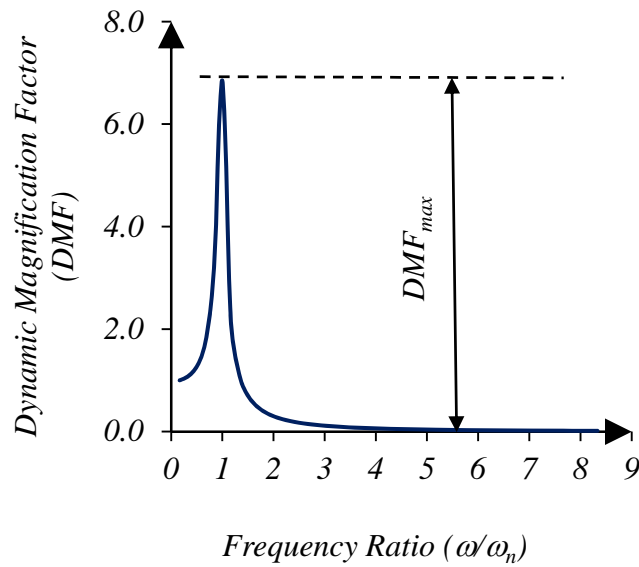


Figure 4-4: Dynamic Magnification Factor at Pile Head

DMF (is the dynamic displacement over static displacement)

$$DMF_{\max} = \frac{1}{2\zeta\sqrt{1-\xi^2}} \quad (4-4)$$

$$\zeta = \frac{c}{c_{cr}} \quad (4-5)$$

$$c = \zeta(2M_{\text{eff}}\omega_n) = \zeta\left(2\frac{K_{\text{pile}}}{(2\pi f_n)^2}(2\pi f_n)\right) = \zeta\left(\frac{K_{\text{pile}}}{\pi f_n}\right) \quad (4-6)$$

where: ζ = damping ratio, c_{cr} = system critical damping, ω = circular frequency, ω_n = soil pile system resonant frequency in rad/sec, K_{pile} = pile vertical dynamic stiffness (K_{min}) and f_n = soil-pile system natural frequency in Hz.

4.2.3 Soil Pile System Resonant Frequency

The resonant frequency of the pile soil system is the frequency where the maximum vertical dynamic amplitude response occurs. The resonant frequency is computed for the pile soil system at different values of the dimensionless frequency parameter (a_0) and for piles having a concrete compressive strength of 3000, 4000, 5000, and 6000 psi.

4.3 Static Stiffness of a Single Pile

Using the finite element model the vertical static stiffness for a single pile is determined as a function of the soil shear modulus (G_{soil}). The pile head is subjected to a static unit vertical load and the vertical displacement of the soil-pile system is determined at the pile head at different values of the soil shear modulus. The results of the vertical static stiffness are shown in Figure 4-5.

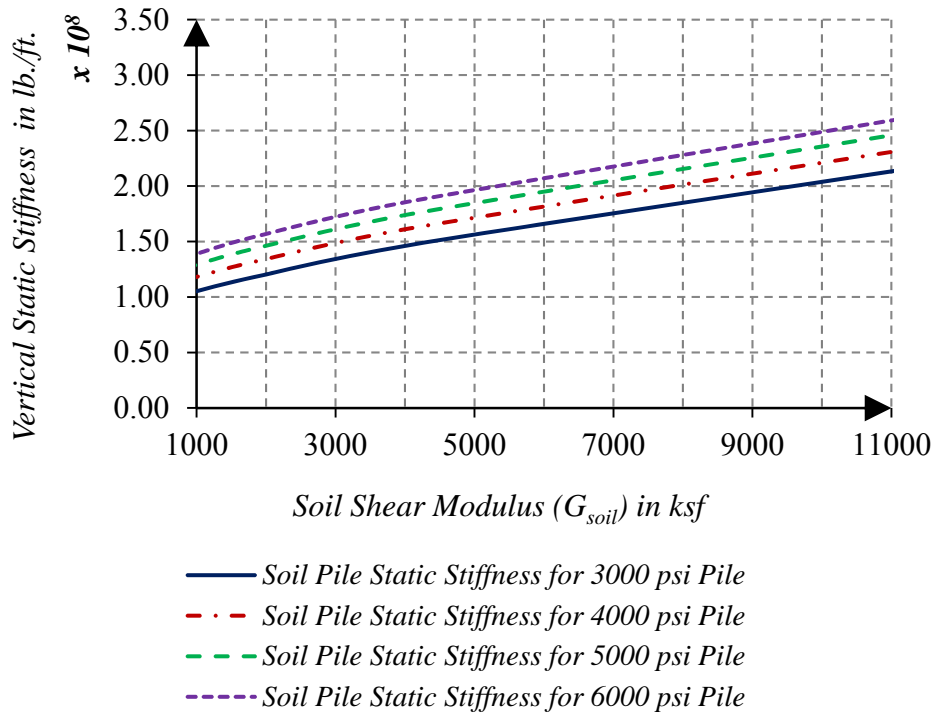


Figure 4-5: Static Stiffness of a Pile as a Function of the Soil Shear Modulus (G_{soil})

The axial stiffness of the pile element was also calculated assuming the pile as a vertical element without considering the effect of the soil. The axial stiffness of a circular member is given by equation (4-7)

$$K_{axial} = \frac{E_{pile}A_{pile}}{L_{pile}} \quad (4-7)$$

Where: E_{pile} is pile elastic modulus, A_{pile} is the pile cross section area and L_{pile} is the pile length = 30ft.

For different pile material, the axial stiffness is summarized in Table 4-1.

Table 4-1: Pile Axial Stiffness

Pile Concrete Compressive Strength (f_c)	Young's Modulus of Pile Material in lb./ft ²	Pile Cross Section Area ($r_o= 1.50$ ft.)	Pile Length (L_{pile}) in ft.	Axial Stiffness K_{axial} in (lb/ft.)
3000 psi	4.496×10^8	7.069	30	1.059×10^8
4000 psi	5.191×10^8	7.069	30	1.223×10^8
5000 psi	5.804×10^8	7.069	30	1.368×10^8
6000 psi	6.358×10^8	7.069	30	1.498×10^8

The results of the vertical axial static stiffness from the finite element model for the piles are compared with the axial stiffness of a vertical member calculated based on equation (4-7). The axial static stiffness is determined for a strong soil having a soil shear modulus of 17.20×10^3 ksf. The results are shown in Figure 4-6.

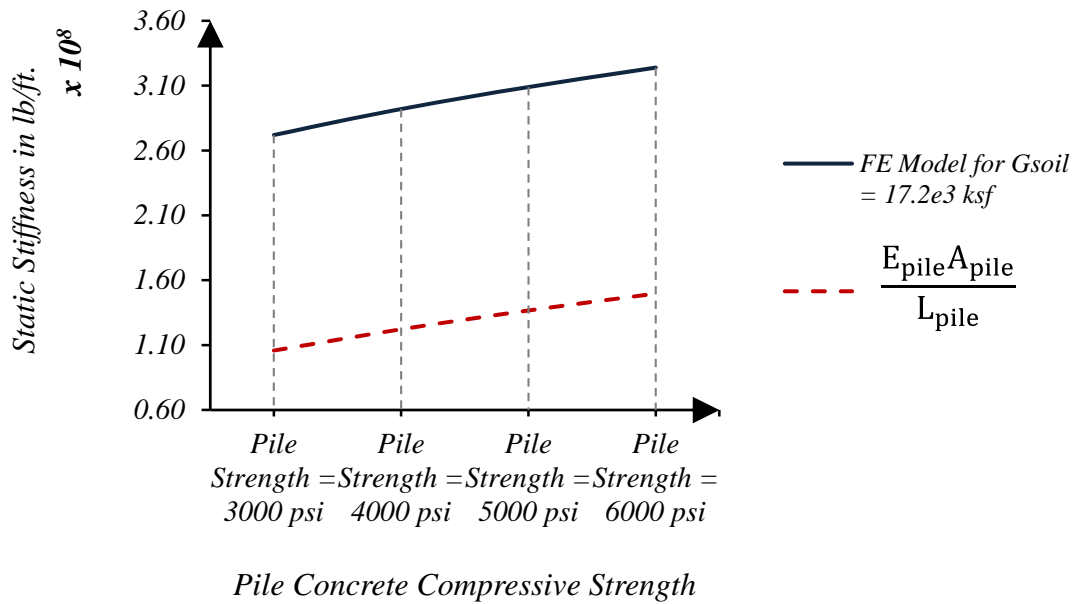


Figure 4-6: Comparison of Static Stiffness for Pile With and Without Surrounding Soils

The difference in the vertical static stiffness between the finite element model and the axial stiffness, assuming the pile as an axially loaded member for a pile in

strong soil, is 61% for a pile having a concrete compressive strength equal to 3000 psi, 58% for a pile having a concrete compressive strength equal to 4000 psi, 55% for a pile having a concrete compressive strength equal to 5000 psi, and 54% for a pile having a concrete compressive strength equal to 6000 psi. The increase in static stiffness for the pile in strong soil is due to the effect of the soil in increasing the overall pile-soil static stiffness.

4.4 Dynamic Stiffness and Damping of a Single Pile

4.4.1 Dynamic Stiffness for a Single Pile

Using the finite element model the vertical dynamic amplitude response was determined. The average dynamic stiffness of a single pile is determined based on the average amplitude using equation (4-2) and the minimum dynamic stiffness of the single pile is determined based on equation (4-3). Figures 4-7 to 4-15 show the average and minimum dynamic stiffness for a single pile with a concrete compressive strength of 3000, 4000, 5000, 6000 psi and for the steel pile. These figures show the variation of the dynamic stiffness as a function of the dimensionless frequency parameter (a_0).

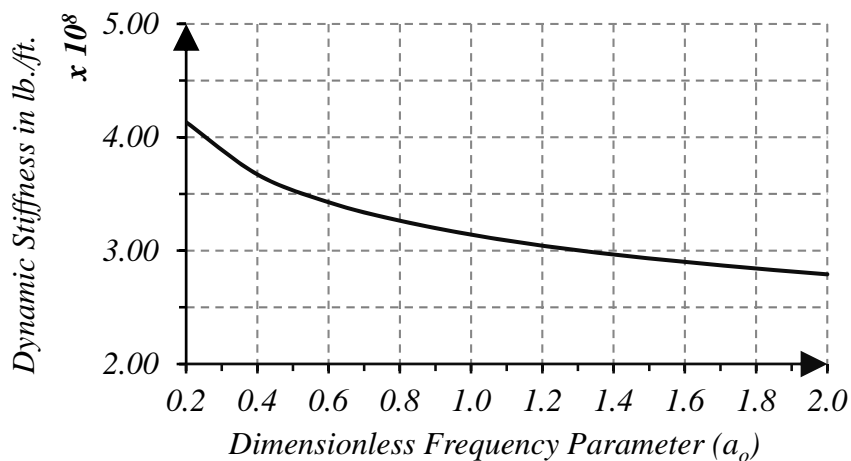


Figure 4-7: Stiffness of Pile Based on Average Amplitude for $f_c = 3000$ psi

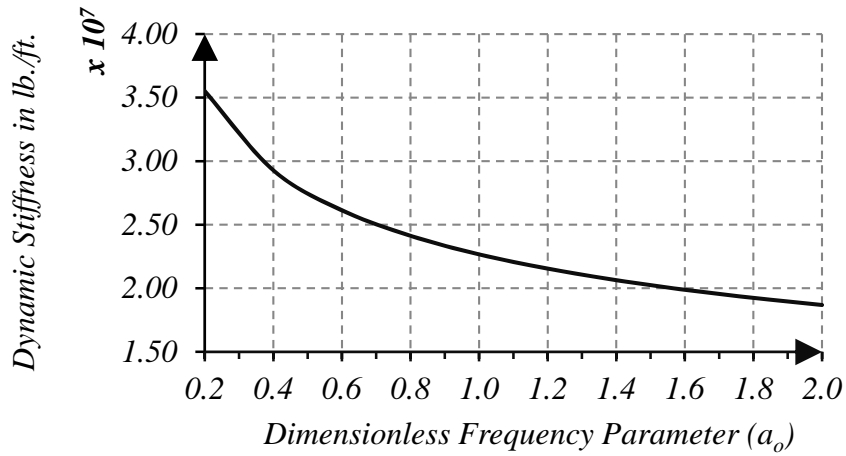


Figure 4-8: Stiffness of Pile Based on Maximum Amplitude for $f_c = 3000$ psi

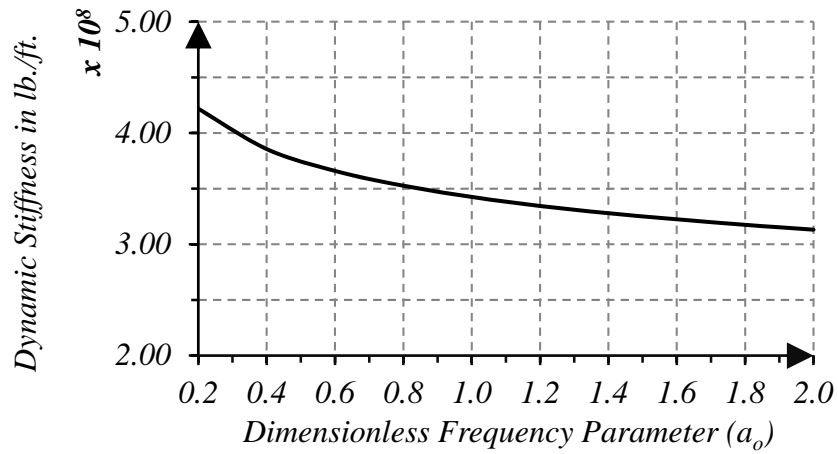


Figure 4-9: Stiffness of Pile Based on Average Amplitude for $f_c = 4000$ psi

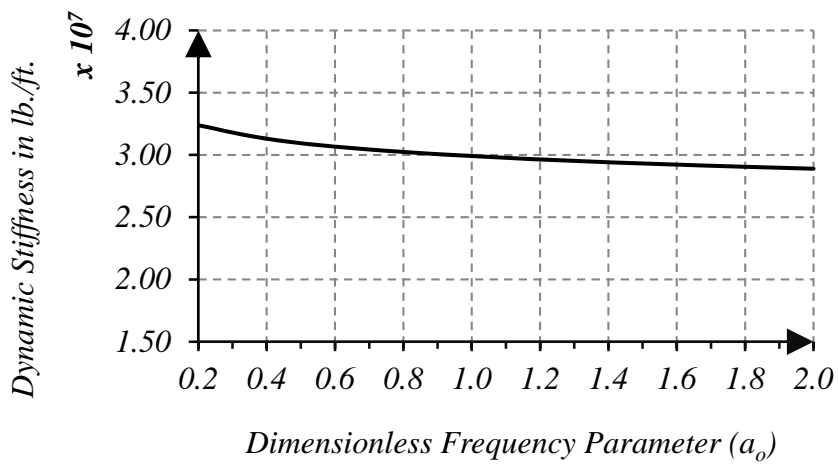


Figure 4-10: Stiffness of Pile Based on Maximum Amplitude for $f_c = 4000$ psi

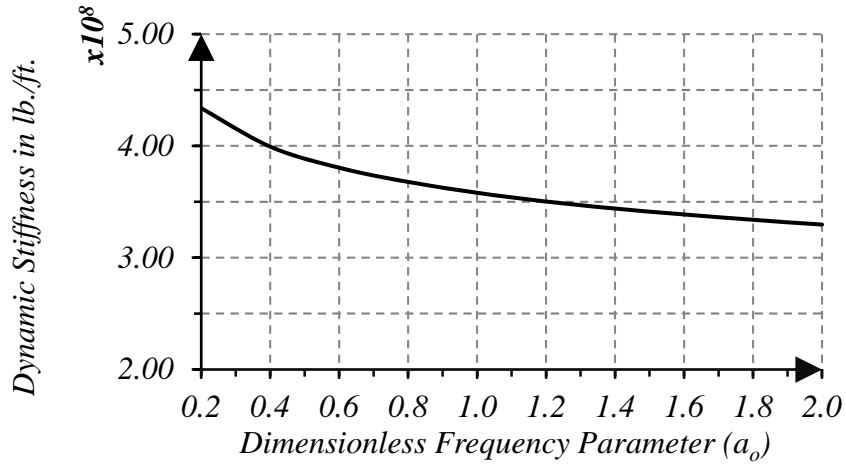


Figure 4-11: Stiffness of Pile Based on Average Amplitude for $f_c = 5000$ psi

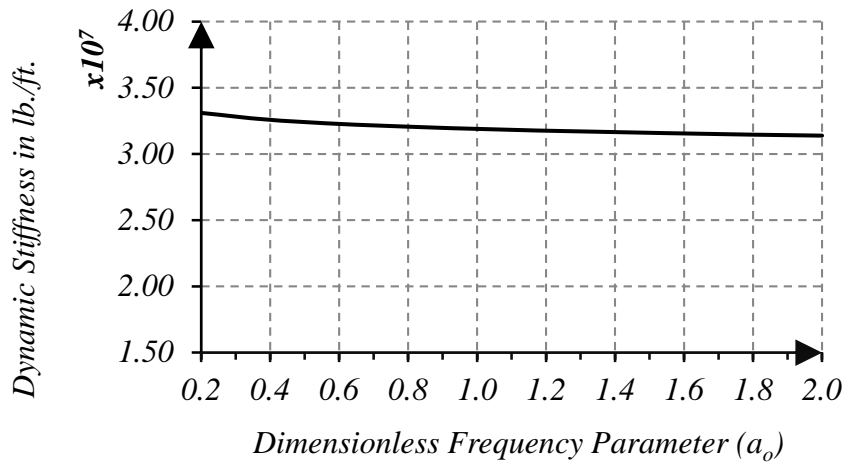


Figure 4-12: Stiffness of Pile Based on Maximum Amplitude for $f_c = 5000$ psi

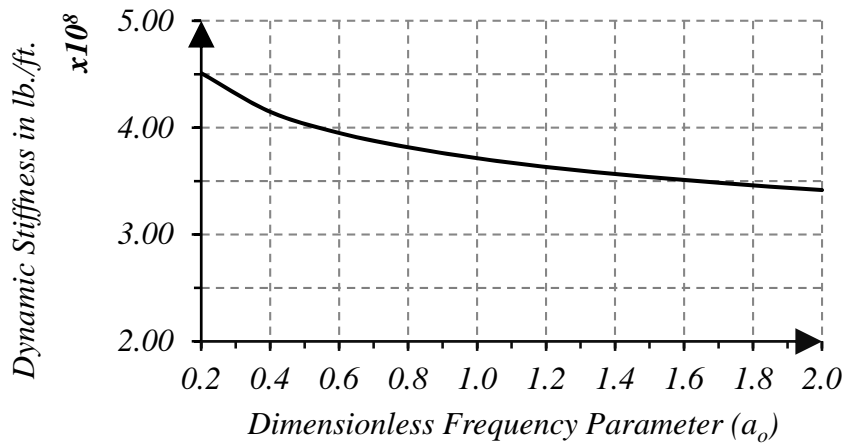


Figure 4-13: Stiffness of Pile Based on Average Amplitude for $f_c = 6000$ psi

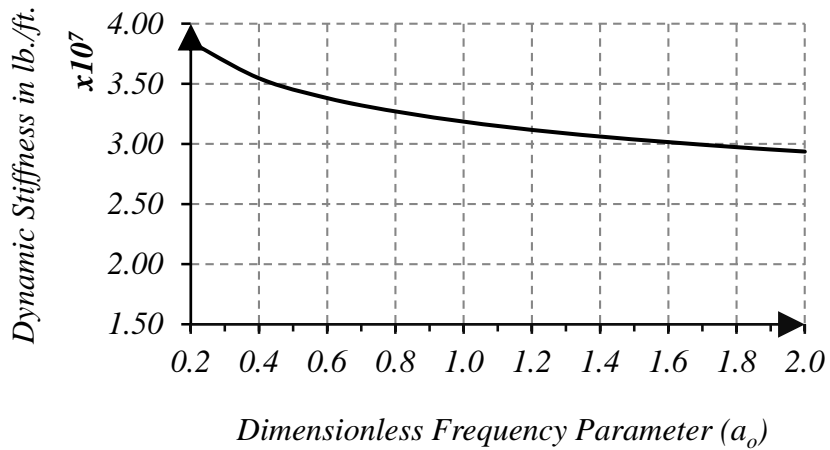


Figure 4-14: Stiffness for Pile Based on Maximum Amplitude for $f_c = 6000$ psi

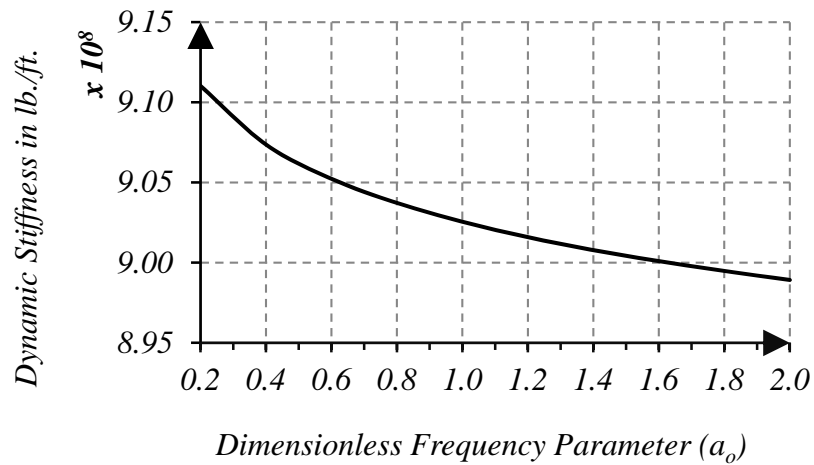


Figure 4-15: Stiffness for Steel Pile

4.4.2 Damping for a Single Pile

The variation of the soil-pile system damping and damping ratios with the dimensionless frequency parameter (a_o) are shown in Figures 4-16 and 4-17 for a single concrete pile with a concrete compressive strength of 3000 psi, Figures 4-18 and 4-19 for a single pile with a concrete compressive strength of 4000 psi, Figures 4-20 and 4-21 for a single pile with a concrete compressive strength of 5000 psi and Figure 4-22 and 4-23 for a single concrete pile with a concrete compressive strength of 6000 psi.

The pile damping is calculated based on the minimum stiffness from the maximum amplitude of the pile-soil system, i.e., K_{\min} .

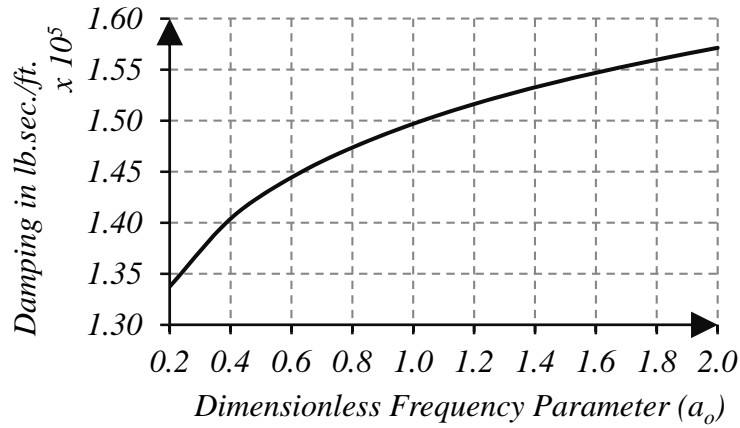


Figure 4-16: Damping of a Single Pile with $f_c = 3000$ psi

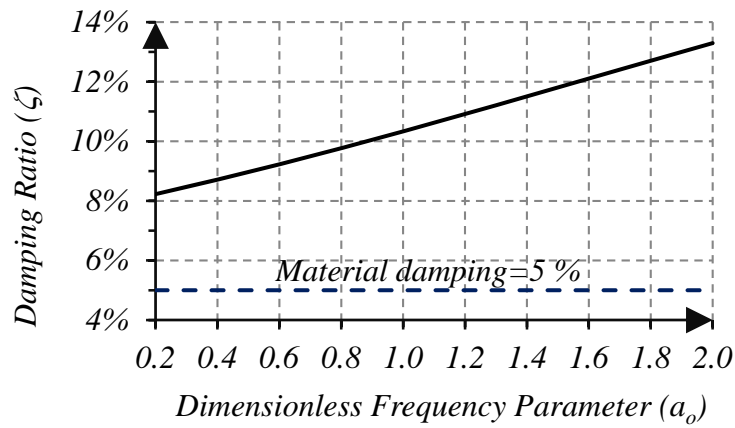


Figure 4-17: Damping Ratio of a Single Pile with $f_c = 3000$ psi

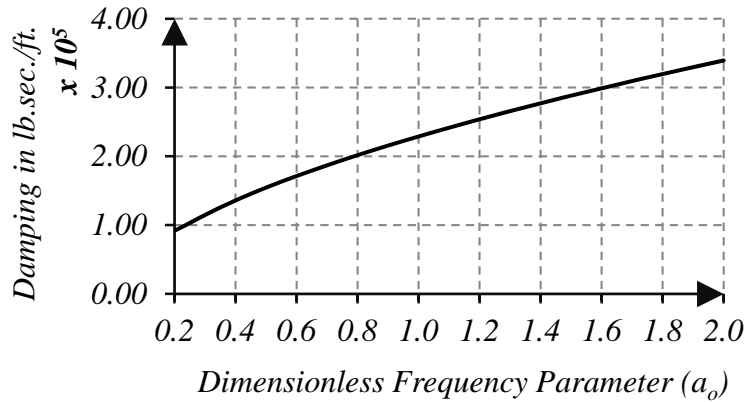


Figure 4-18: Damping of a Single Pile with $f_c = 4000$ psi

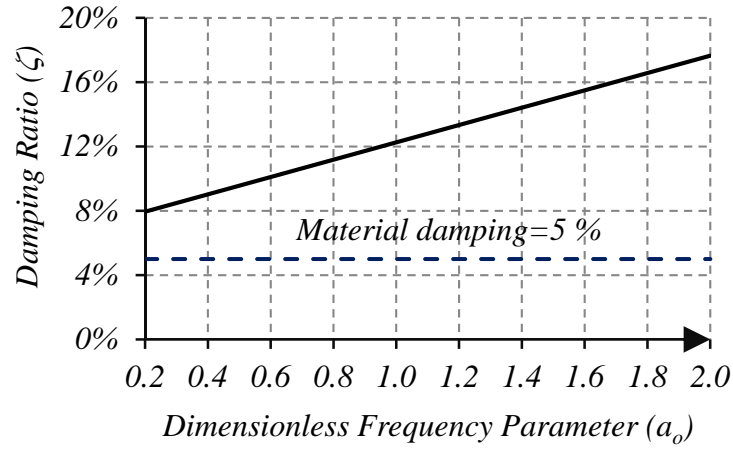


Figure 4-19: Damping Ratio of a Single Pile with $f_c = 4000$ psi

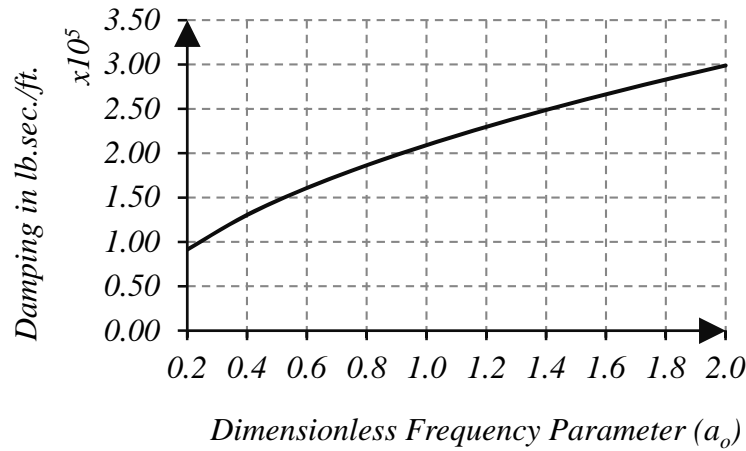


Figure 4-20: Damping of a Single Pile with $f_c = 5000$ psi

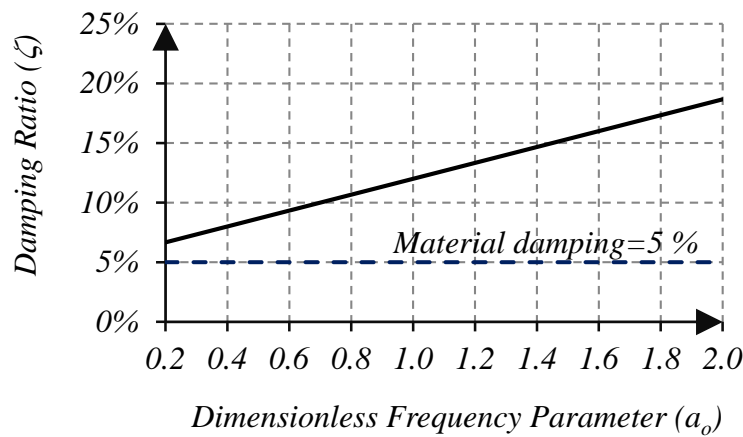


Figure 4-21: Damping Ratio of a Single Pile with $f_c = 5000$ psi

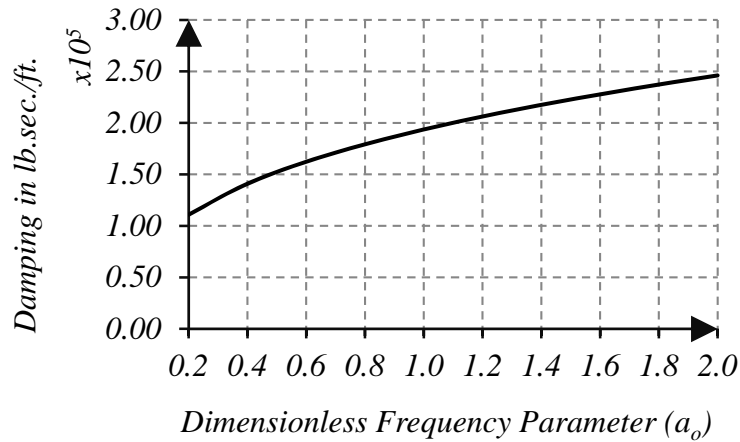


Figure 4-22: Damping of a Single Pile with $f_c = 6000$ psi

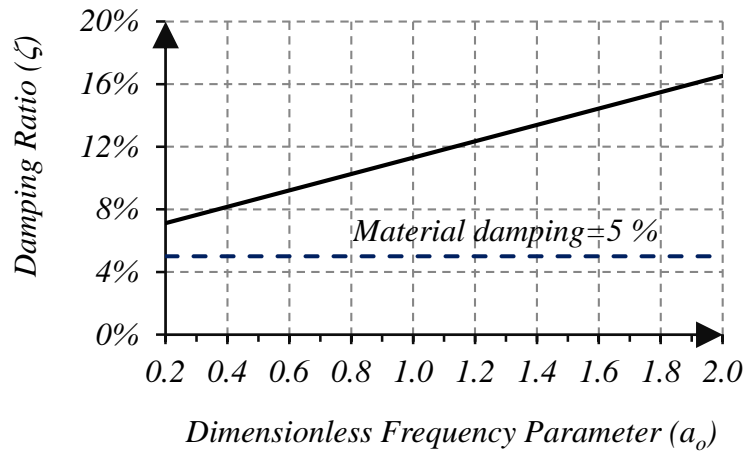


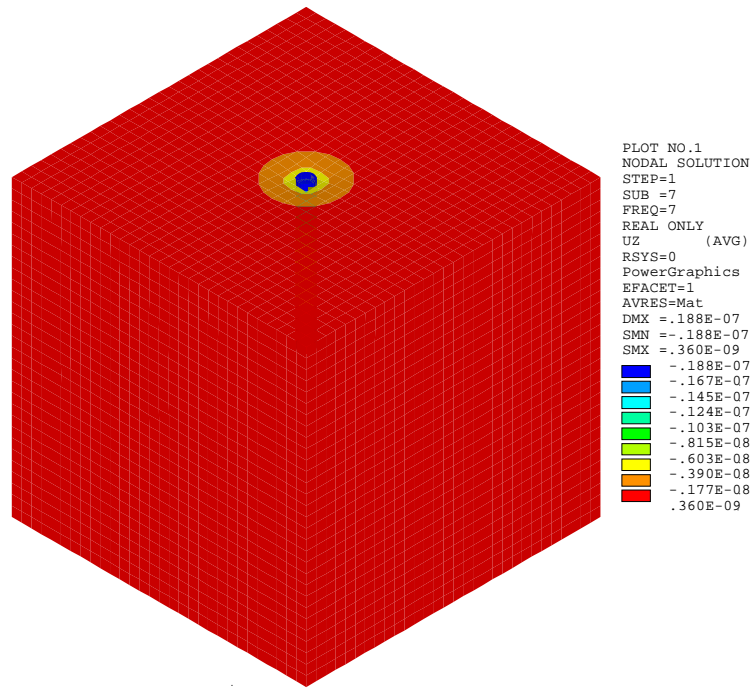
Figure 4-23: Damping Ratio of a Single Pile with $f_c = 6000$ psi

4.4.3 Discussion of the Results

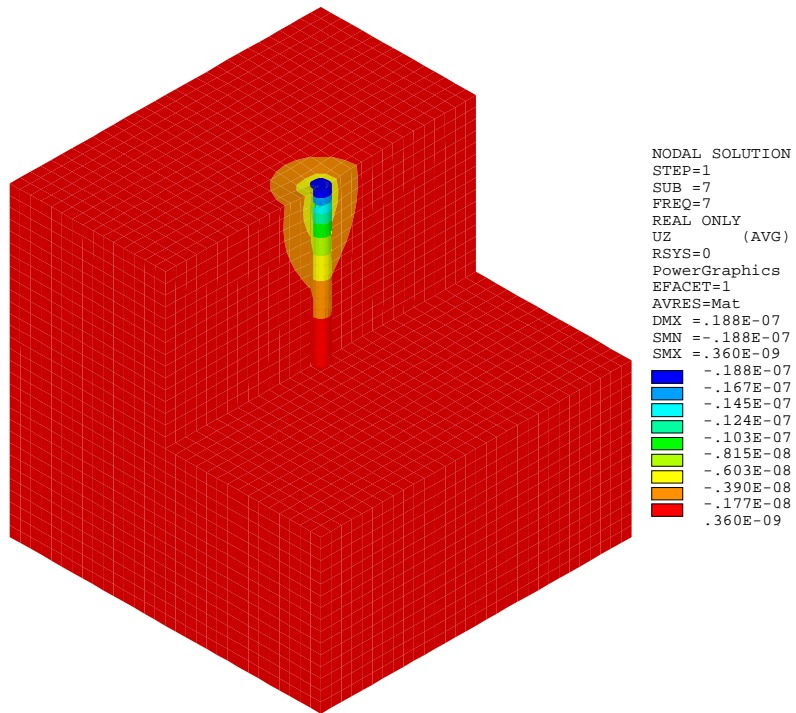
The vertical dynamic response of the pile under vertical dynamic excitation depends on the operating frequency of the machine, the pile vertical stiffness and the soil shear wave velocity. These parameters are defined in the dimensionless frequency parameter (a_o). For a lower range of the dimensionless frequency parameter (a_o) indicating a dense soil material, and for the same machine steady state operating frequency, the amplitude response of the combined soil-pile system is reduced, indicating an increase in the soil-pile vertical dynamic stiffness. As the dimensionless

frequency parameter (a_0) increases indicating a reduction in the soil shear wave velocity characterizing loose soil material, the vertical dynamic amplitude response of the soil-pile system is increased and the soil pile system stiffness is reduced by approximately 50% when (a_0) changes from 0.20 to 2.0.

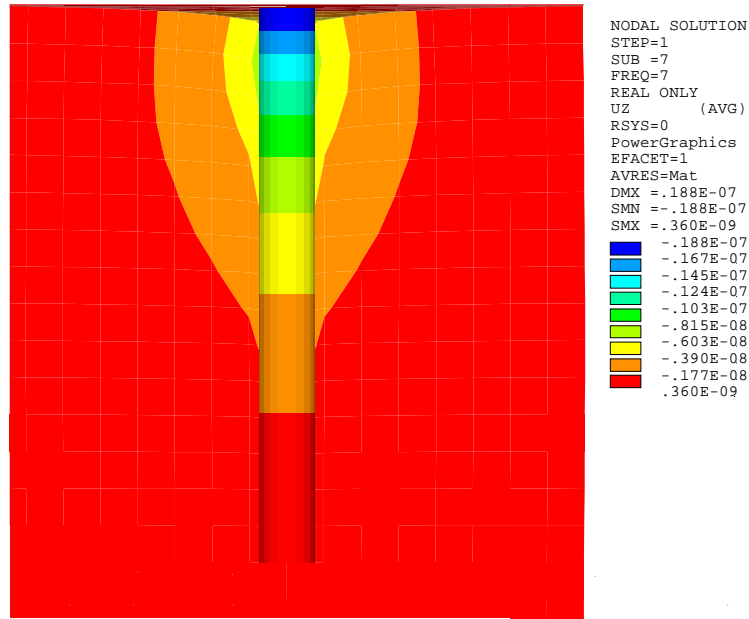
As shown in Figures 4-16, 4-18, 4-20 and 4-22, the vertical damping increase with the increase in the dimensionless frequency parameter (a_0), the damping ratio increase with (a_0) although the material damping was constant at 5%. The total damping, which includes the geometrical damping increased from 8% to about 13%. To explain such a response, Figures 4-24 and 4-25 are provided. Figure 4-24 shows that the response of the pile soil system in strong soil material is well defined within a certain influence diameter around the pile. This influence diameter was found to be approximately equal to five times the pile diameter ($5D_{pile}$), as shown in the plan view. Beyond the influence diameter, the response of the soil is almost negligible. Conversely, the response of the pile in a weak soil continuum, shown in Figure 4-25, extends to the whole soil medium without a definitive influence diameter, i.e., in weak soil conditions, waves will emanate simultaneously from all points along the whole pile length and thus geometrical damping will be more in the vibration of a pile in a weak soil than a pile vibrating in a strong soil.



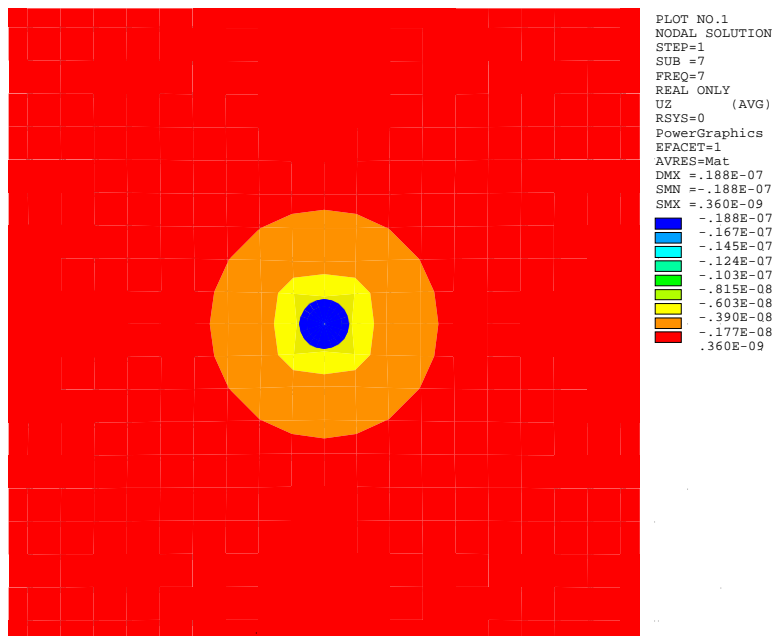
(a)



(b)



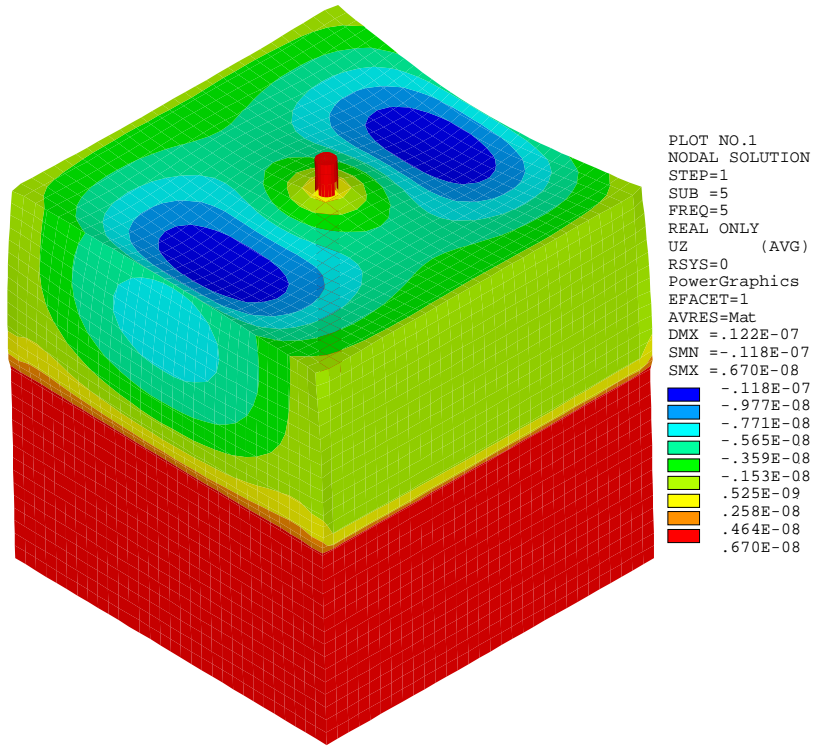
(c)



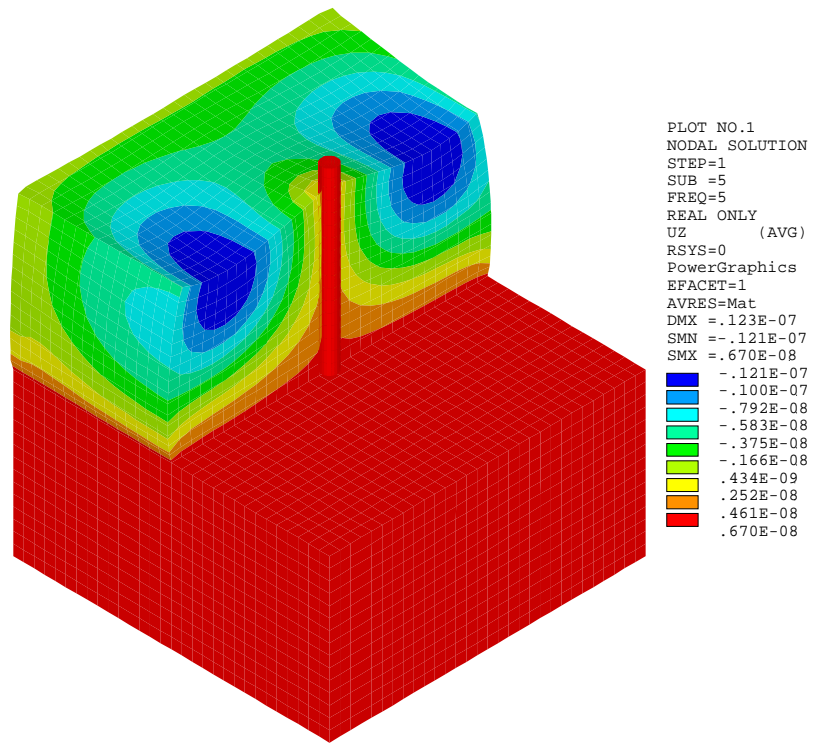
(d)

Figure 4-24: Response of a Pile Embedded in Strong Soil at Resonance
 ($G_{\text{soil}} = 17.20 \times 10^3$ ksf)

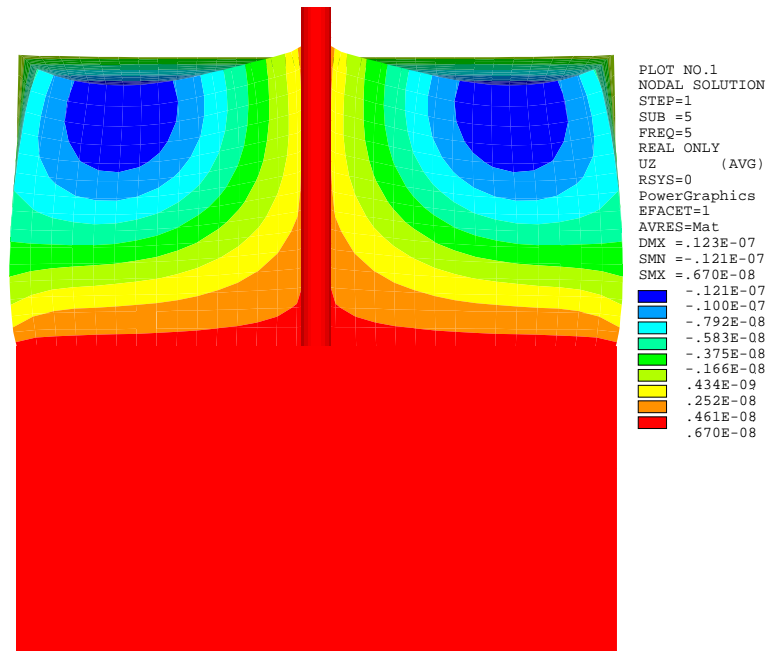
- (a) 3D view
- (b) 3D section view of vertical displacement
- (c) Section view of vertical displacement
- (d) Plan view of vertical displacement



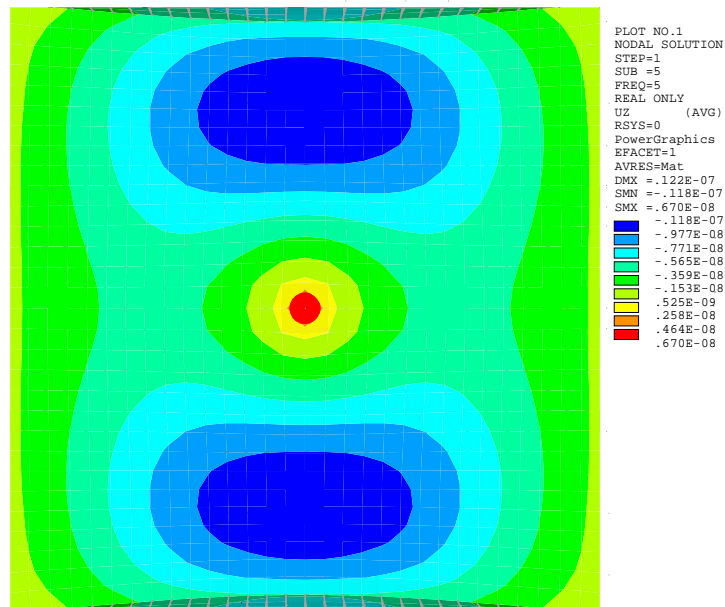
(a)



(b)



(c)



(d)

Figure 4-25: Response of a Pile Embedded in Weak Soil at Resonance
 ($G_{soil}=0.172 \times 10^3 \text{ksf}$)

- (a) 3D view
- (b) 3D section view of vertical displacement
- (c) Section view of vertical displacement
- (d) Plan view of vertical displacement

Figure 4-26 shows the vertical displacement of pile in strong and weak soils. For strong soil, it can be seen that the vertical motion of the pile damped rapidly with depth. Conversely, for pile in a weak soil, the vertical motion of the pile is almost constant along the pile length as the soil does not damp the motion.

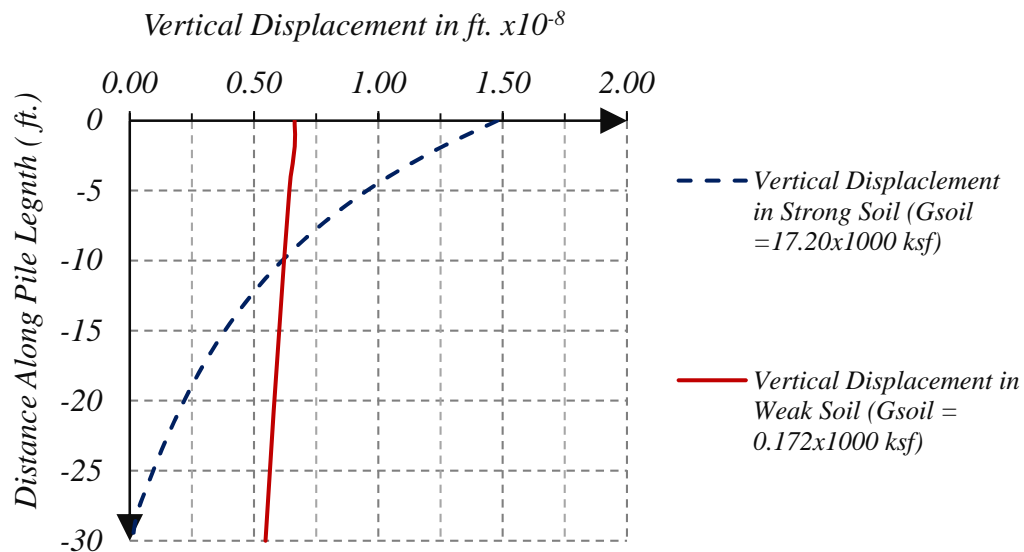


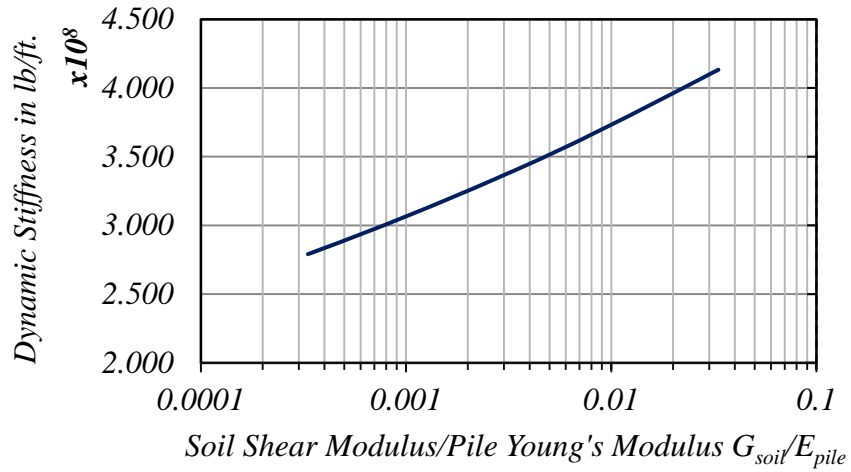
Figure 4-26: Vertical Displacement of Pile in Strong and Weak Soil

4.5 Effect of Different Parameter on Dynamic Stiffness and Damping

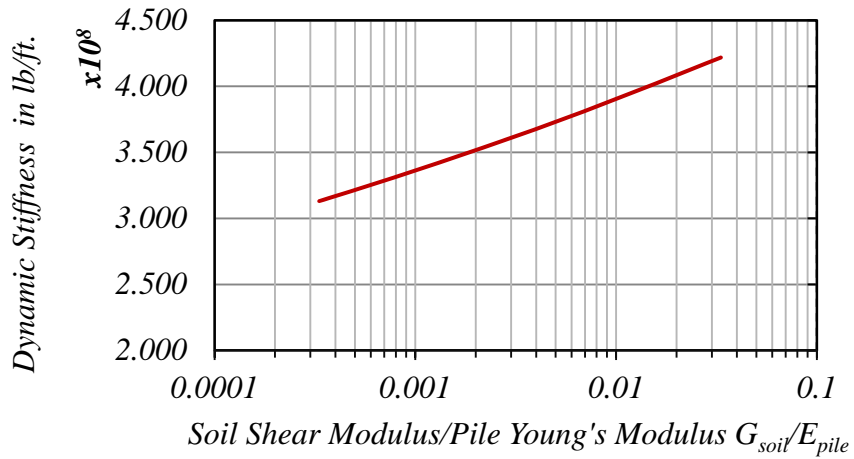
4.5.1 Effect of G_{soil}/E_{pile} on the Vertical Dynamic Stiffness & Damping

The effect of an increased soil shear modulus with respect to the pile elastic modulus on the vertical dynamic stiffness and damping of the soil pile system is shown for all piles. The ratio of the soil shear modulus to the pile elastic modulus has a significant effect on the dynamic response of the pile-soil system. An increase in the ratio of the soil shear modulus to the pile's Young's modulus, indicating an increase in soil shear wave velocity, which is associated with a reduction in the vertical displacement response of the soil-pile system, consequently increases the soil-pile system stiffness, as shown in Figure 4-27. The pile damping is also influenced by the

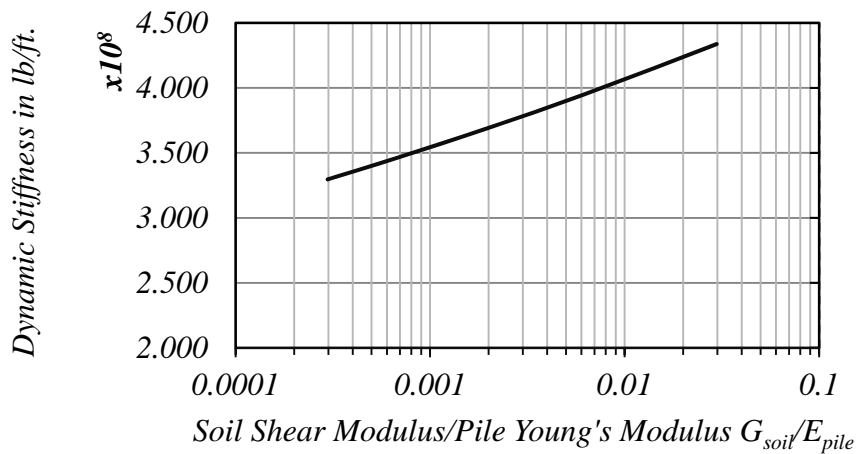
ratio of the soil shear modulus and the pile's Young's modulus. With an increase of the ratio of that of the soil shear modulus to the pile's Young's modulus indicating stronger soil material the pile damping is reduced, since geometrical damping is less for a pile vibrating in strong soils than for a pile vibrating in weak soils.



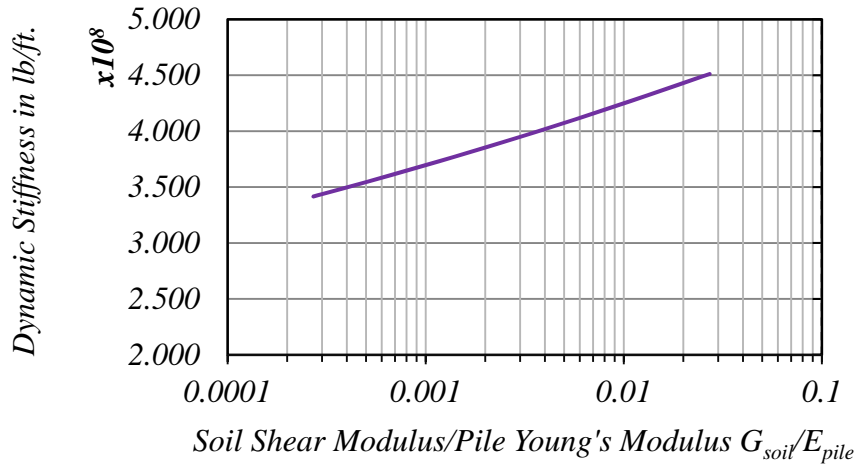
(a) Pile Concrete Compressive Strength = 3000 psi



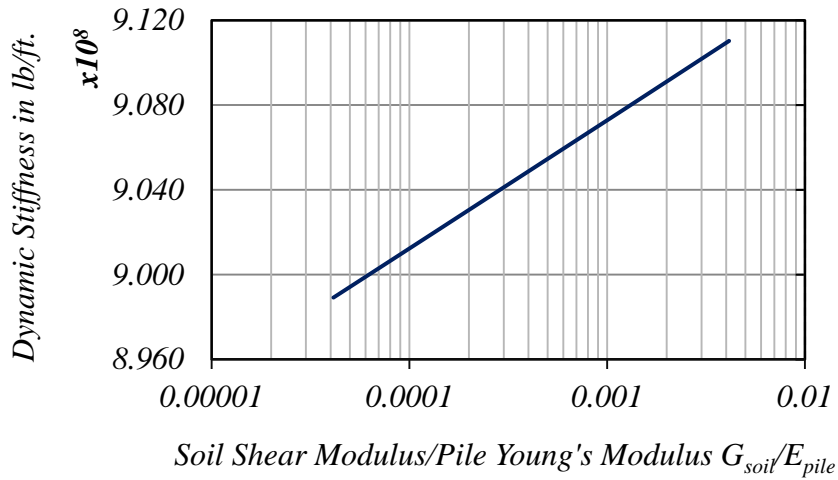
(b) Pile Concrete Compressive Strength = 4000 psi



(c) Pile Concrete Compressive Strength = 5000 psi



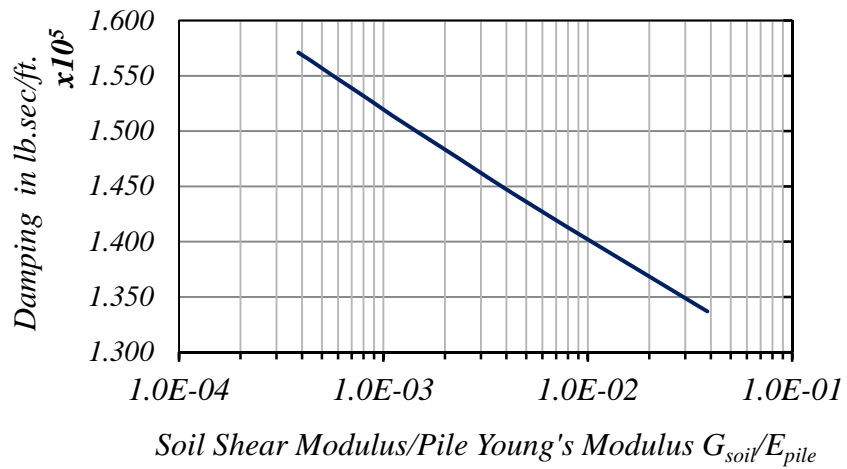
(d) Pile Concrete Compressive Strength = 5000 psi



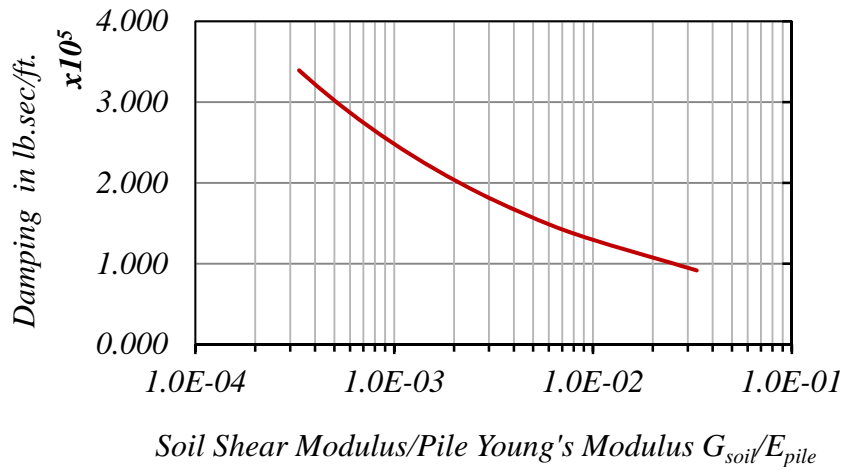
(e) Steel Pile

Figure 4-27: Effect of G_{soil}/E_{pile} on Pile Dynamic Stiffness at Frequency of 50 Hz

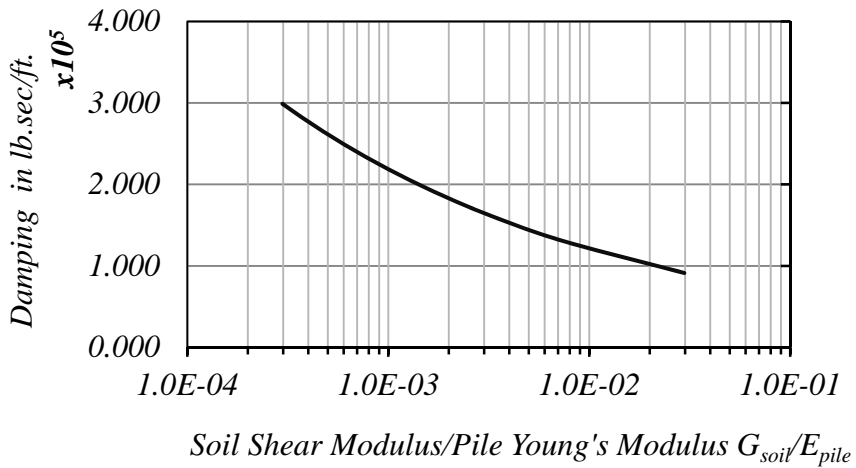
- (a) Pile Concrete Compressive Strength = 3000 psi
- (b) Pile Concrete Compressive Strength = 4000 psi
- (c) Pile Concrete Compressive Strength = 5000 psi
- (d) Pile Concrete Compressive Strength = 6000 psi
- (e) Steel Pile



(a) Pile Concrete Compressive Strength = 3000 psi



(b) Pile Concrete Compressive Strength = 4000 psi



(c) Pile Concrete Compressive Strength = 5000 psi

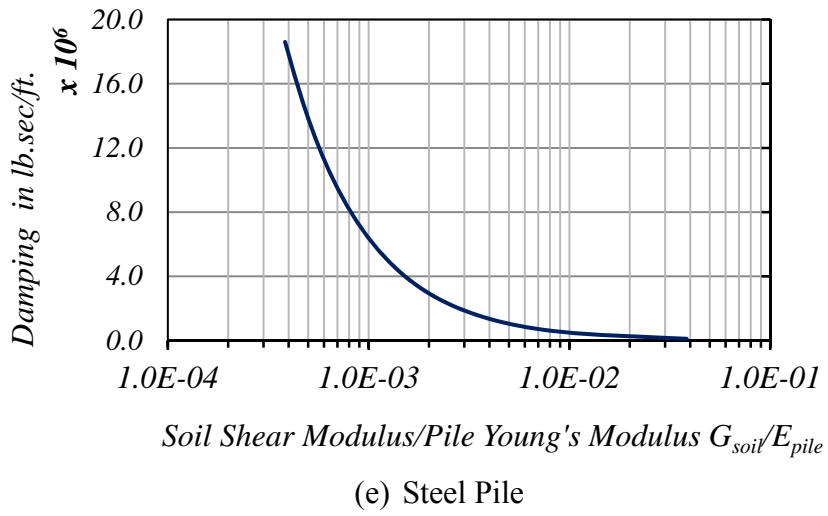
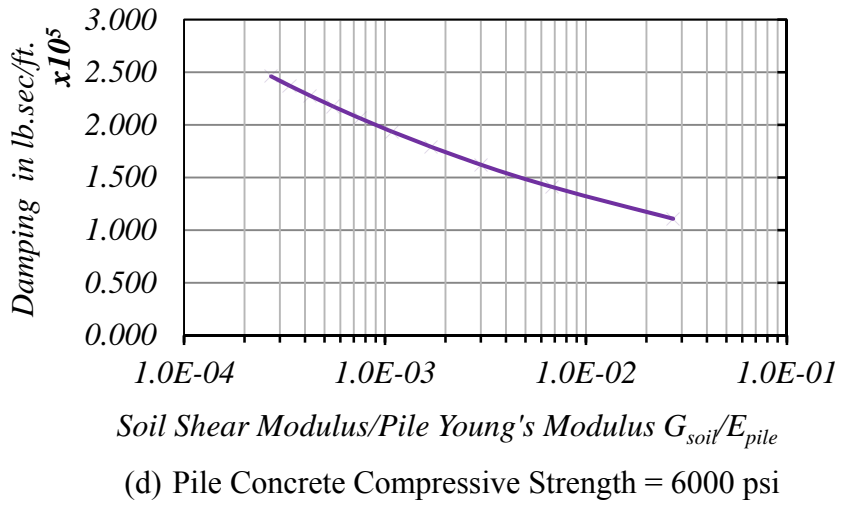


Figure 4-28: Effect of G_{soil}/E_{pile} on Damping at Frequency of 50 Hz
 (a) Pile Concrete Compressive Strength = 3000 psi
 (b) Pile Concrete Compressive Strength = 4000 psi
 (c) Pile Concrete Compressive Strength = 5000 psi
 (d) Pile Concrete Compressive Strength = 6000 psi
 (e) Steel Pile

4.5.2 Effect of G_{soil} on the Vertical Dynamic Stiffness & Damping

The effect of the soil shear modulus on the soil pile vertical dynamic stiffness and damping is shown in Figures 4-29 and 4-30 for piles with different concrete compressive strengths.

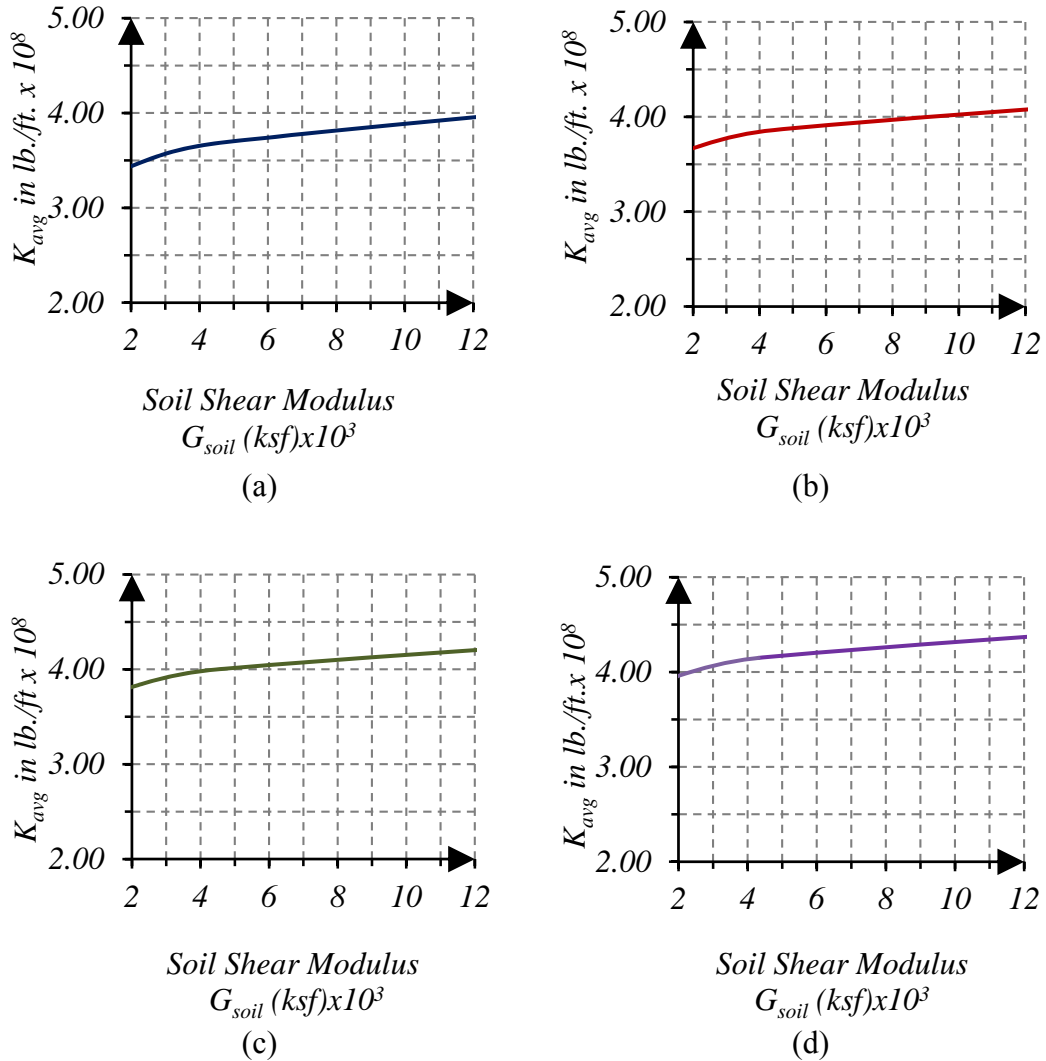
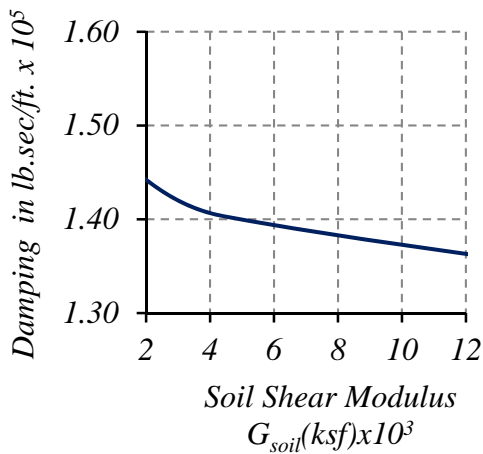
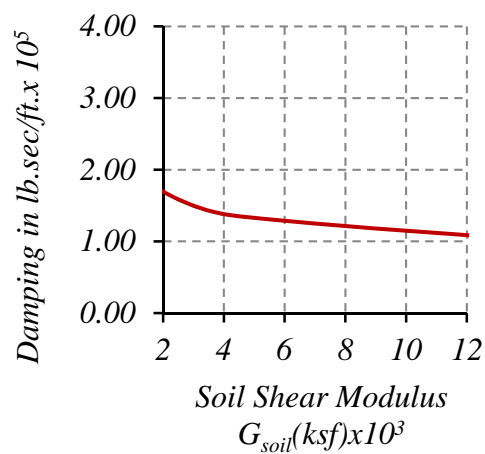


Figure 4-29: Effect of G_{soil} on Dynamic Stiffness at Frequency of 50 Hz

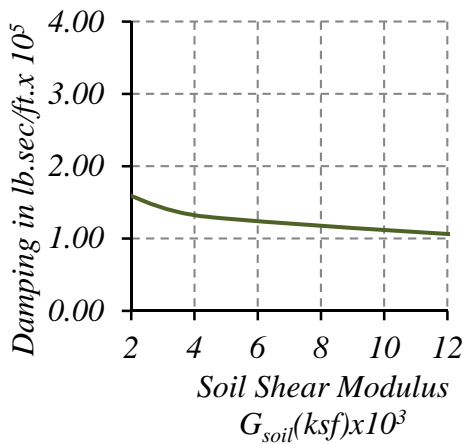
- (a) Pile Concrete Compressive Strength = 3000 psi
- (b) Pile Concrete Compressive Strength = 4000 psi
- (c) Pile Concrete Compressive Strength = 5000 psi
- (d) Pile Concrete Compressive Strength = 6000 psi



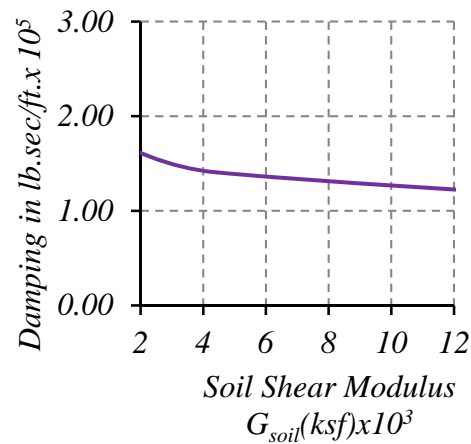
(a)



(b)



(c)



(d)

Figure 4-30: Effect of G_{soil} on Pile Damping at Frequency of 50 Hz

- (a) Pile Concrete Compressive Strength = 3000 psi
- (b) Pile Concrete Compressive Strength = 4000 psi
- (c) Pile Concrete Compressive Strength = 5000 psi
- (d) Pile Concrete Compressive Strength = 6000 psi

Pile vertical dynamic stiffness and damping depends on the interaction of the pile and the surrounding soil. An increase in the soil shear modulus indicates an increase in the soil pile stiffness. As an example, when the soil shear modulus increases from 1×10^3 kip/ft² to 12×10^3 kip/ft², the pile vertical dynamic stiffness increases by approximately 25%. Whereas, the reduction in the soil pile damping is 20 %.

4.5.3 Effect of an Axial Load on the Stiffness, Damping and Frequency

The analysis of the soil pile system considered a load of 10^5 lb. acting on the top of the pile. This load is considered to account for that portion of the total weight of the machine assigned to each pile. The load also produces inertial interaction in the soil pile system and thus affects its performance. The effect of the load on the pile soil system stiffness, damping and resonant frequency, were determined by using different loads on the pile head and computing the stiffness, damping and system resonant frequencies. The effects of the change in the load on the pile stiffness, damping and resonant frequency are shown in Figures 4-31, 4-32 and 4-33.

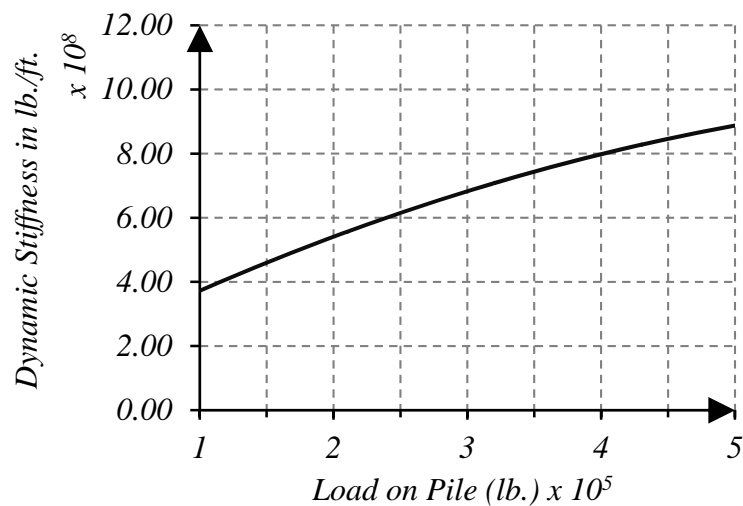


Figure 4-31: Effect of Load on Dynamic Stiffness

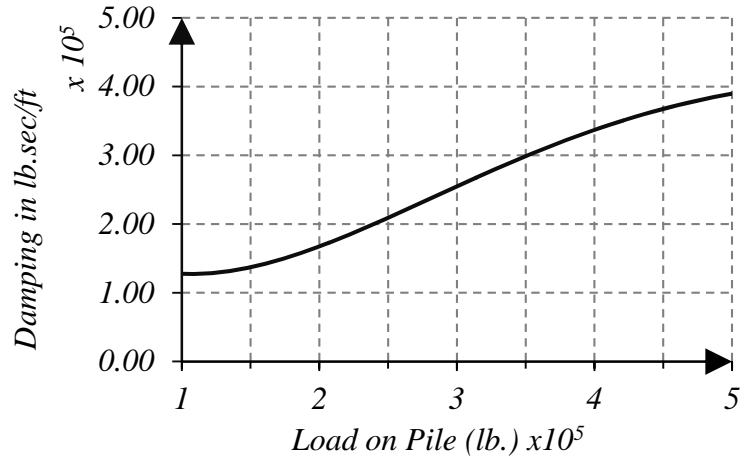


Figure 4-32: Effect of Load on System Damping

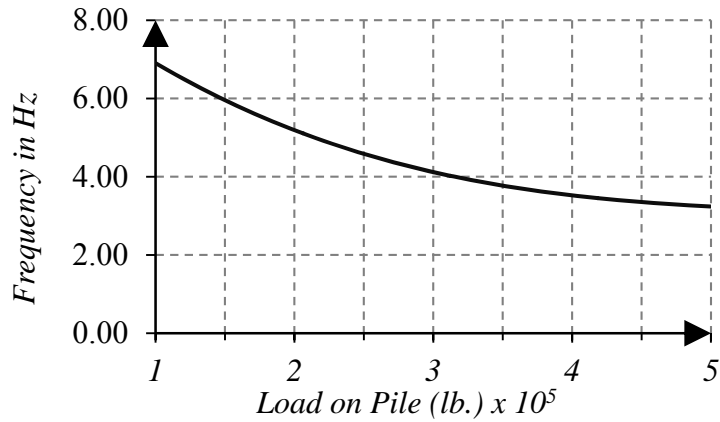


Figure 4-33: Effect of Load on Resonant Frequency

As shown in the figures, increasing the load increases the stiffness and damping but decreases the resonant frequency of the soil pile system. The increase in the load on the pile made the system stiffer, however, a stiffer system produces more geometric damping. For the resonant frequency, as shown by Richart (1962), as the axial load increases on a pile of a given length, the resonant frequency is reduced. Manna and Baidya (2009) in their experimental study of the vertical vibration of a full scale pile that both the resonant frequency and the resonant amplitude decreased as the static load on the pile increased.

4.5.4 Effect of Pile Length on the Dynamic Stiffness and Damping

The effect of the pile length on the vertical dynamic stiffness and damping is determined for piles having lengths of 20 ft., 25 ft., 30 ft., 35 ft. and 40 ft. The pile head was excited with a unit amplitude excitation force. A load on the pile head of 10^5 lbs. was also applied. Two soil types were considered in the analysis. The first soil type was for a strong soil material with soil a shear modulus $G_{\text{soil}} = 17.2 \times 10^3$ ksf. The second soil type was for a weak soil material with soil a shear modulus $G_{\text{soil}} = 0.172 \times 10^3$ ksf. Figures 4-34 and 4-35 show the vertical dynamic stiffness and damping of the pile as a function of length for the strong soil while Figures 4-36 and 4-37 show the dynamic stiffness and damping for the pile in the weak soil material.

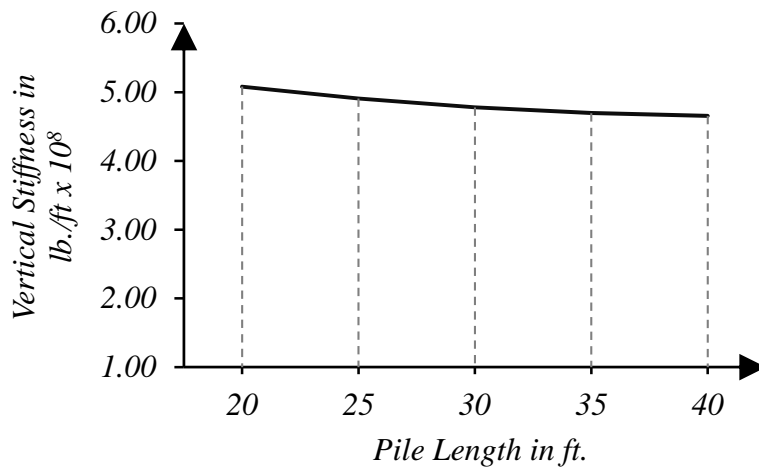


Figure 4-34: Effect of Pile Length on Stiffness for Pile in a Strong Soil ($G_{\text{soil}} = 17.20 \times 10^3$ ksf)

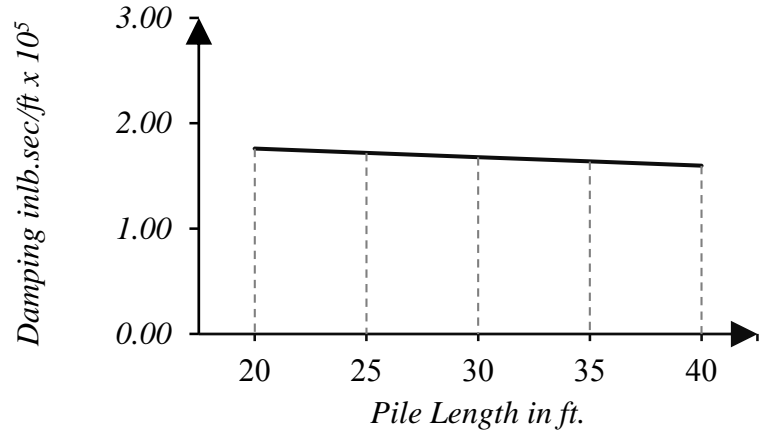


Figure 4-35: Effect of Pile Length on Damping for Pile in a Strong Soil ($G_{\text{soil}} = 17.20 \times 10^3$ ksf)

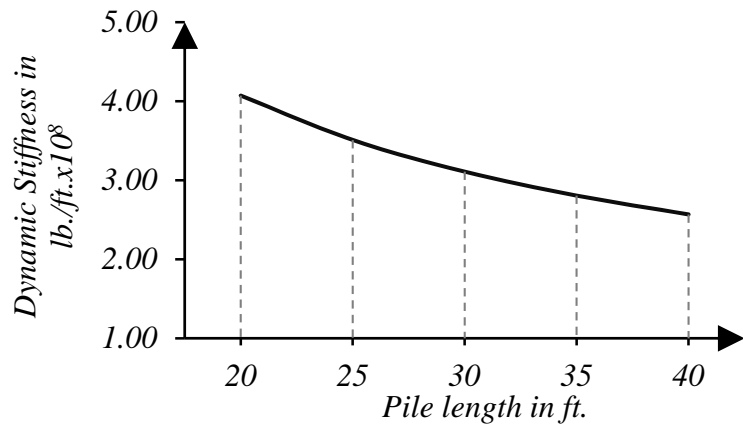


Figure 4-36: Effect of Pile Length on Stiffness for Pile in a Weak Soil ($G_{\text{soil}} = 0.172 \times 10^3$ ksf)

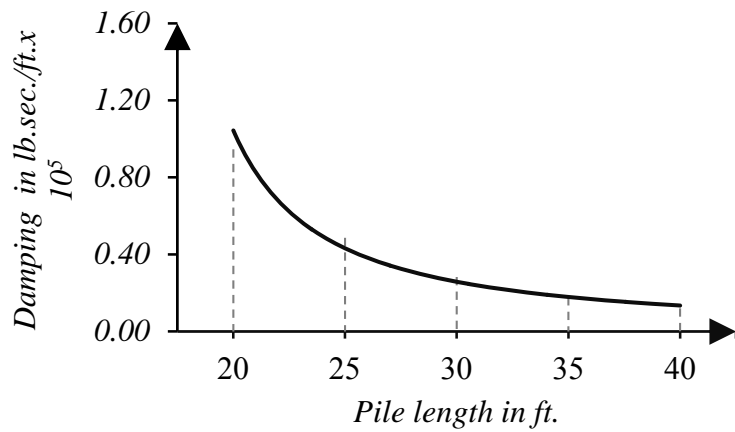
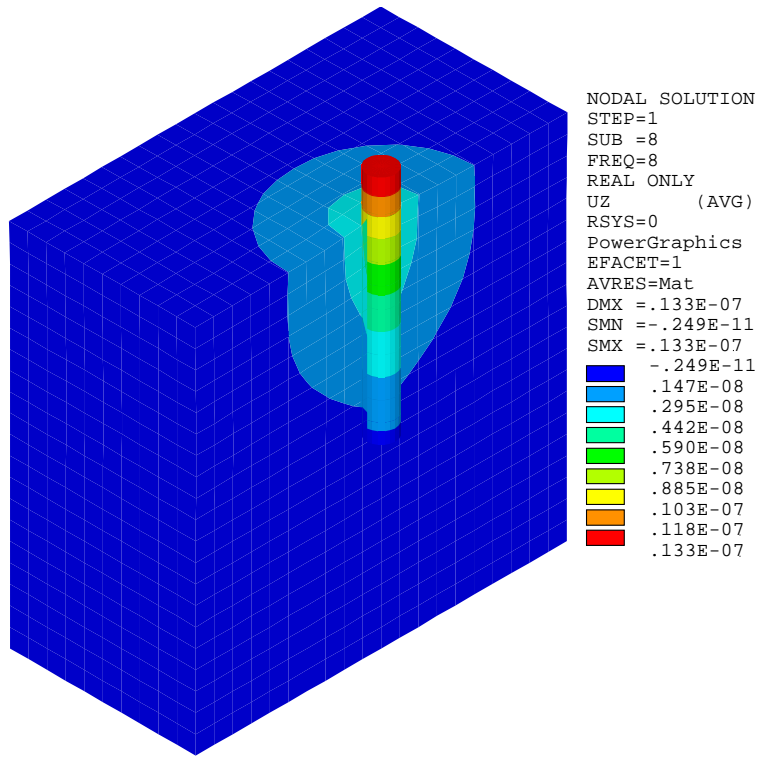
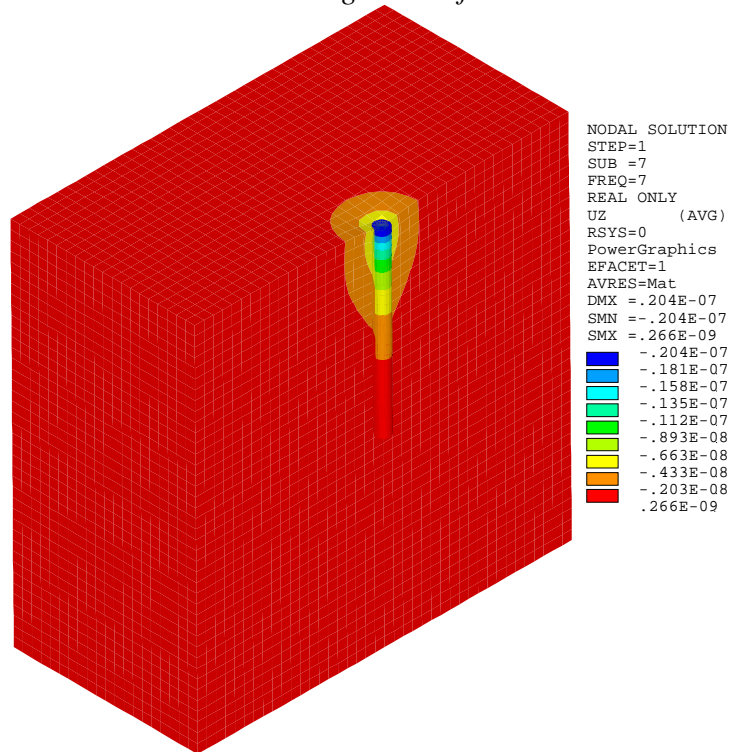


Figure 4-37: Effect of Pile Length on Damping for Pile in a Weak Soil ($G_{\text{soil}} = 0.172 \times 10^3$ ksf)

As shown in Figures 4-34 and 4-35, the change in pile length from 20 ft to 40 ft in strong soils had a small effect on both the dynamic stiffness and damping where both parameters changed by less than 10%, whereas in Figures 4-36 and 4-37 where the piles were in weak soils, both the dynamic stiffness and damping were markedly reduced by increasing the pile length from 20 to 40 ft. This can be explained by Figures 4-38 and 4-39. In Figure 4-38 a pile in a strong soil at a length 20 ft and the one of 40 ft shows that only the upper part in the pile undergoes significant displacement, i.e., an active length of the pile provides the stiffness and damping, hence increasing the length of the pile has a minimum influence in the response. Whereas, in Figure 4-39, for piles in a weak soil at a length of 20 ft the displacement in Figure 4-39(a) is smaller than the displacement in Figure 4-39(b), and the pile vibrated as a rigid body. Thus the longer a pile in weak soils produces less stiffness and less damping. A change in pile length from 20 ft to 40 ft reduced the stiffness by 40 % and the damping by 85%. Thus, depending on the soil stiffness the effect of the pile length in a weak soil would decrease the stiffness and damping and the pile length had no effect on the stiffness and damping in strong soils.

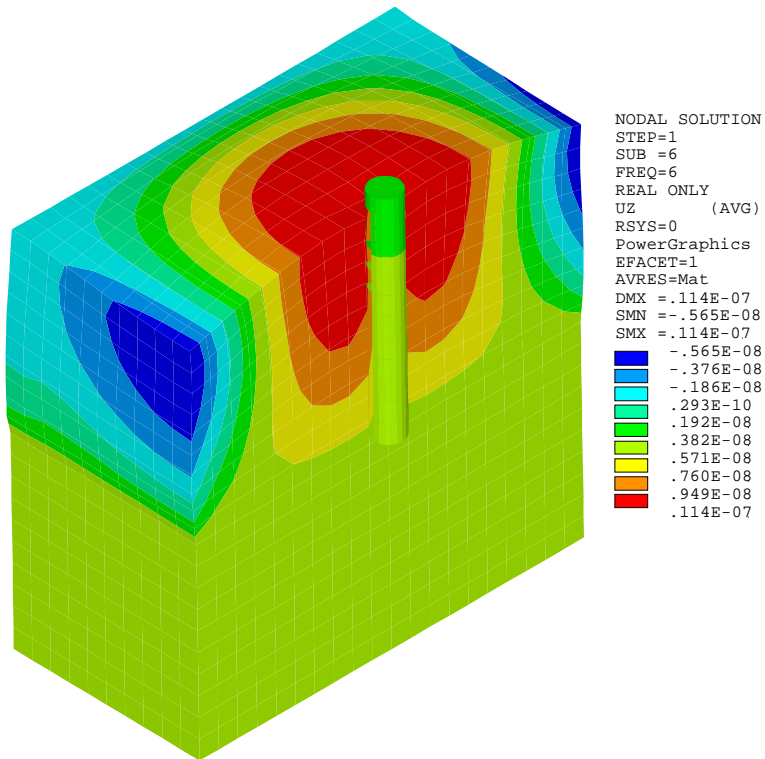


Pile length = 20 ft

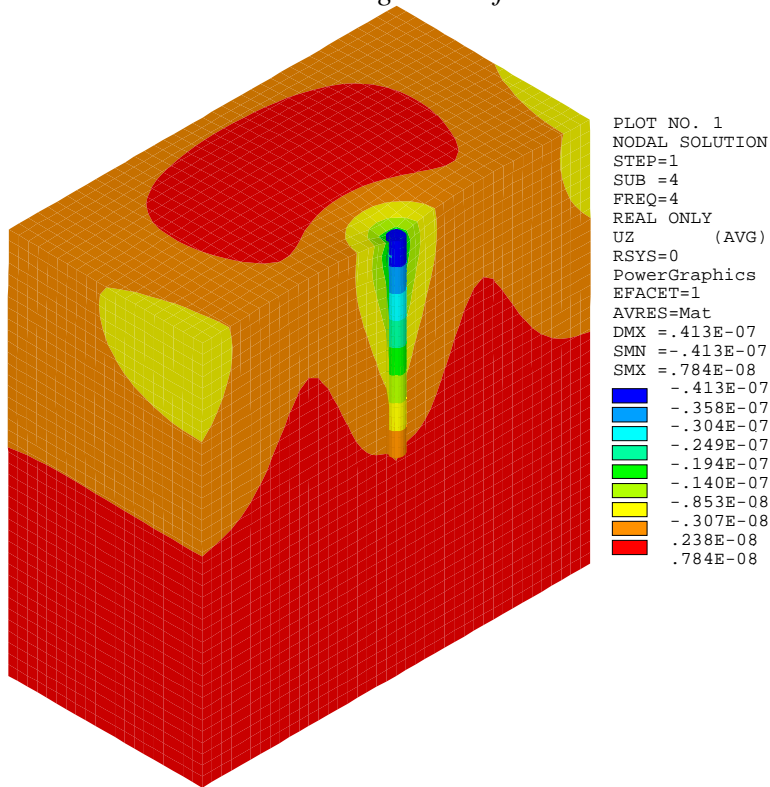


Pile length = 40 ft

Figure 4-38: Vertical Displacement Distribution at Resonance in Strong Soils ($a_0 = 0.2$)



Pile length = 20 ft



Pile length = 40 ft

Figure 4-39: Vertical Displacement Distribution at Resonance in Weak Soils, ($a_0 = 2.0$)

4.5.5 Effect of Pile Strength on the Dynamic Stiffness and Damping

The effect of the pile's compressive strength on the pile dynamic stiffness and damping is presented in Figures 4-40 and 4-41 for a dense soil material with a soil shear modulus, $G_{\text{soil}} = 17.3 \times 10^3 \text{ kip/ft}^2$.

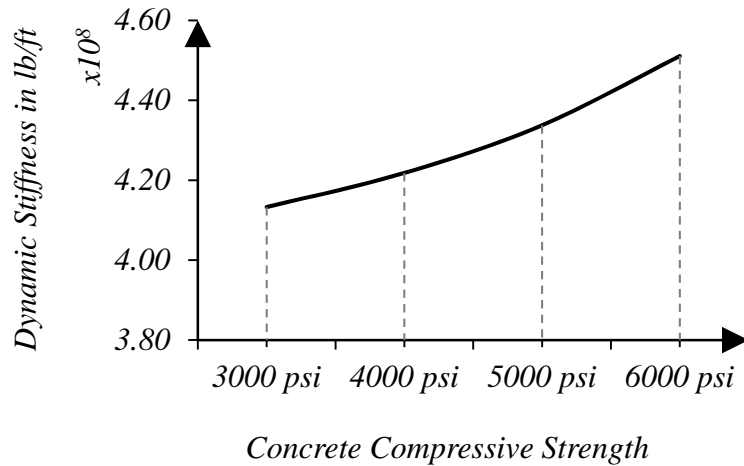


Figure 4-40: Effect of Concrete Strength on Pile Stiffness ($G_{\text{soil}} = 17.3 \times 10^3 \text{ kip/ft}^2$).

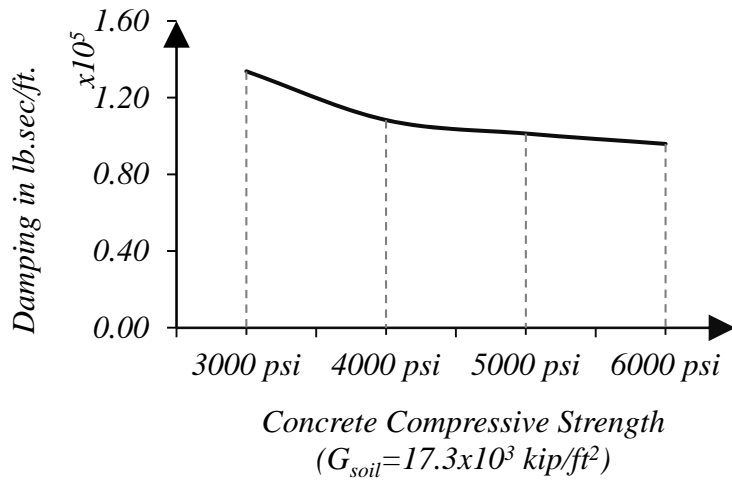


Figure 4-41: Effect of Concrete Strength on Pile Damping ($G_{\text{soil}} = 17.3 \times 10^3 \text{ kip/ft}^2$).

As the pile concrete strength increases from 3,000 psi to 6,000 psi, the average increase in the piles vertical dynamic stiffness is about 15% and the reduction in the pile damping is about 11%.

4.5.6 Effect of Soil Shear Wave Velocity on Resonant Frequency

The effect of the soil shear wave velocity on the soil-pile system's resonant frequency is shown in Figure 4-42 for piles having different compressive strengths.

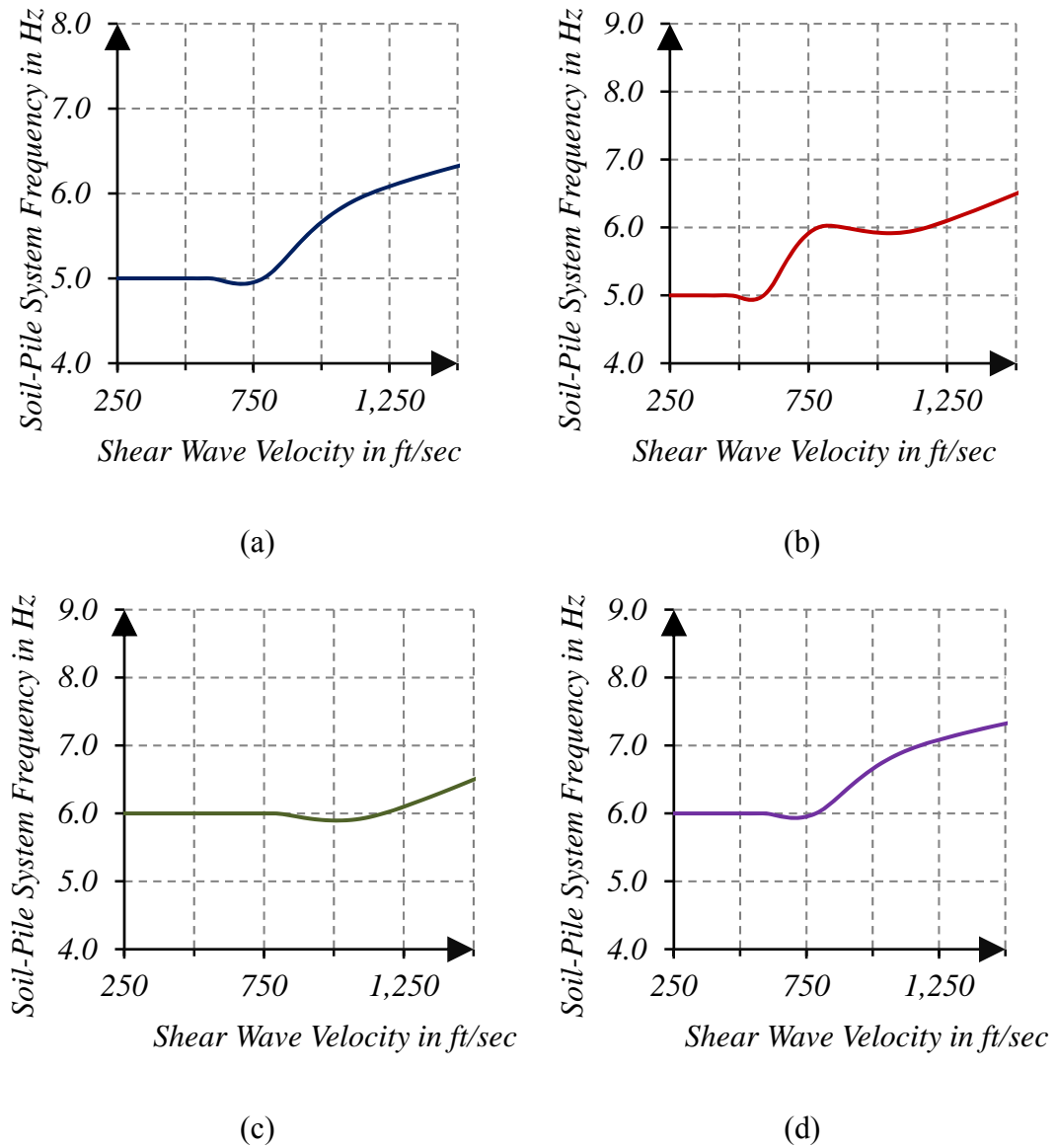


Figure 4-42: Soil-Pile System Resonant Frequency

- (a) Pile Concrete Compressive Strength = 3000 psi
- (b) Pile Concrete Compressive Strength = 4000 psi
- (c) Pile Concrete Compressive Strength = 5000 psi
- (d) Pile Concrete Compressive Strength = 6000 psi

With higher values of shear wave velocity, indicating dense soil material, the soil pile system is stiffer and consequently the system resonant frequency is increased.

4.5.7 Effect of Pile Diameter on Pile-Soil Resonant Frequency

The effect of pile diameter on the pile-soil system resonant frequency is shown in Figure 4-43. Three pile diameters are studied 3.0 ft., 1.50 ft. and 0.75 ft. The weight considered on the pile head for all three pile diameters was $1/9 \times 10^5$ lb. The pile head was excited by harmonic excitation forces and the pile-soil system resonant frequency was determined at different values of the dimensionless frequency parameter (a_0).

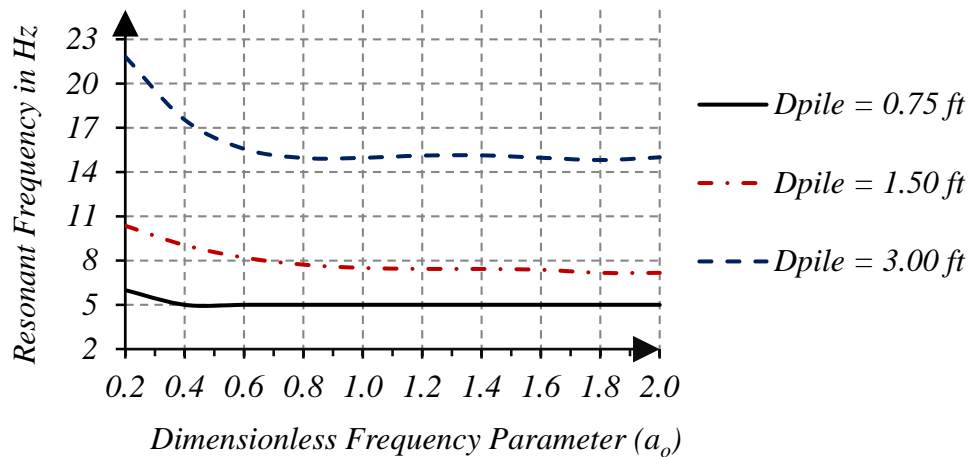


Figure 4-43: Resonant Frequency for a Single Pile with $f_c = 3000$ psi

The pile-soil system resonant frequency is sensitive to the pile diameter. As shown in Figure 4-43 the resonant frequency is almost doubled as the pile diameter increases from 0.75 ft. to 1.50 ft. and from 1.50 ft. to 3.0 ft. This means that for all soil types, the increase in the pile-soil system resonant frequency is directly proportional to the pile diameter without consideration of the soil type. The frequency value, on the other hand, depends on the type of soil.

4.5.8 Comparison Between the Static Stiffness and Dynamic Stiffness

Using the finite element model, the vertical static stiffness for a pile is determined as a function of the soil shear modulus. The head of the pile element is subjected to a unit vertical load and the displacement of the soil-pile system is determined at the pile head. The pile has a concrete compressive strength of 3,000 psi. The effect of the soil contribution on the static stiffness is determined by assuming the pile as a compression member that has an axial stiffness of:

$$K_{\text{axial}} = \frac{E_{\text{pile}}A_{\text{pile}}}{L_{\text{pile}}} \quad (4-8)$$

where: E_{pile} is the Young's modulus of the pile material, A_{pile} is the pile cross section area and L_{pile} is the pile length

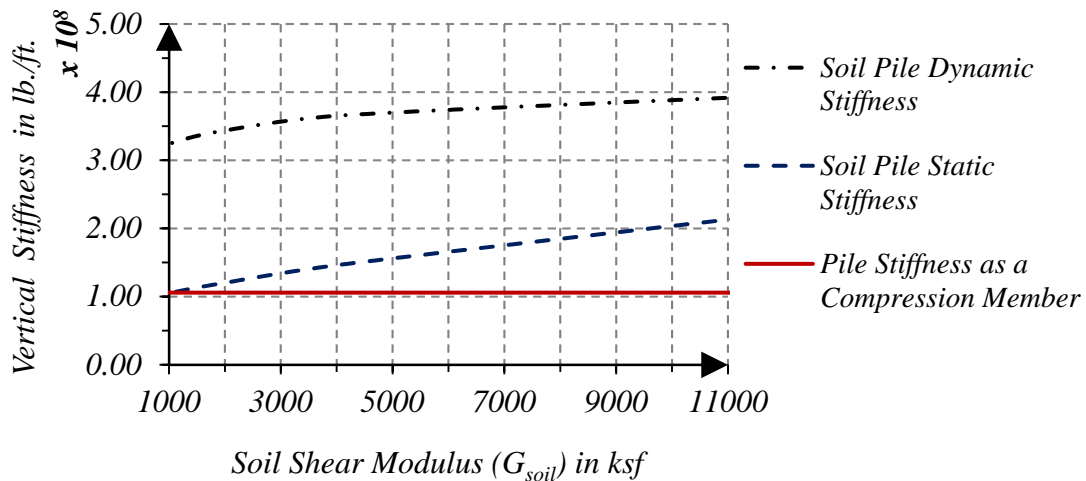


Figure 4-44: Static and Dynamic Stiffness for Pile with $f_c = 3000$ psi

Figure 4-44 shows a plot of the pile stiffness when the pile is acting as a compression member, soil pile static stiffness and soil pile dynamic stiffness. The plot shows that the dynamic stiffness is about three times the static stiffness. The plot also shows that at a shear modulus of 1,000 ksf, the static stiffness is the same as the stiffness

of a compression member, i.e., the surrounding soil has no contribution towards the static stiffness at such a low soil shear modulus. Also, a pile embedded in denser soil has almost twice the static stiffness than piles embedded in a loose soil material. The dynamic stiffness of a single pile is almost two to three times its static stiffness for the range of soil shear modulus used in this study.

Chapter 5: Dynamic Response of Group of Piles

5.1 Introduction

The effect of interaction between piles in a pile group on the vertical dynamic stiffness and damping was studied in this chapter. To study such an effect, three pile foundation configurations were considered. The first configuration considered a pile group spaced at two times the pile diameter, as shown in Figure 5-1, the second configuration considered a pile group spaced at four times the pile diameter, as shown in Figure 5-2, and the third configuration considered a pile group spaced at six times the pile diameter, as shown in Figure 5-3. The three pile configurations were used to calculate the response of a pile foundation system using concrete piles having compressive strength of 3000 psi, 4000 psi, 5000 psi and 6000 psi. The pile groups were connected by a rigid massless pile cap for uniform distribution of the excitation force on the pile group without adding additional masses or stiffness to the pile group. The pile foundation system was excited using a unit constant force harmonic excitation acting at the center of the rigid massless pile cap having the following form:

$$Q = Q_o \sin(\Omega t) = Q_o e^{i\Omega t} \quad (5-1)$$

Where: Ω is the frequency of the forcing function = 1 to 50 Hz, and Q_o = constant force amplitude = 1 lbs.

The dynamic soil properties were defined as a function in the dimensionless frequency parameter (a_o) that ranged from 0.20 to 2.0.

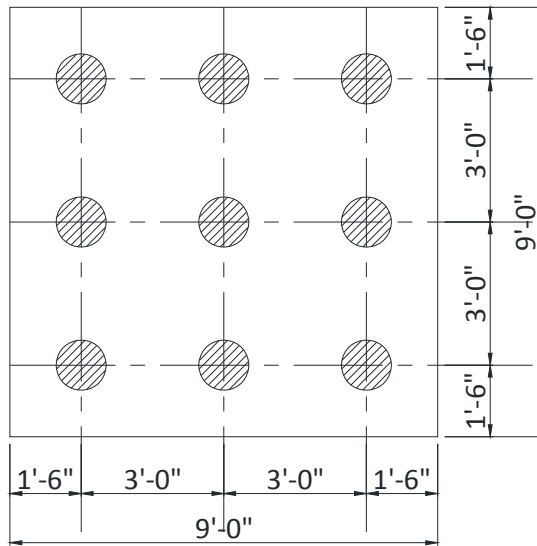


Figure 5-1: Pile Foundation with Piles Spaced at $2D_{pile}$

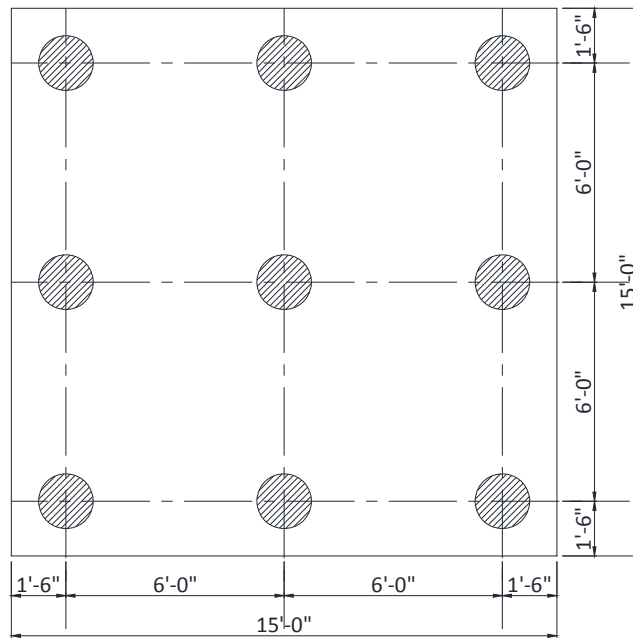


Figure 5-2: Pile Foundation with Piles Spaced at $4D_{pile}$

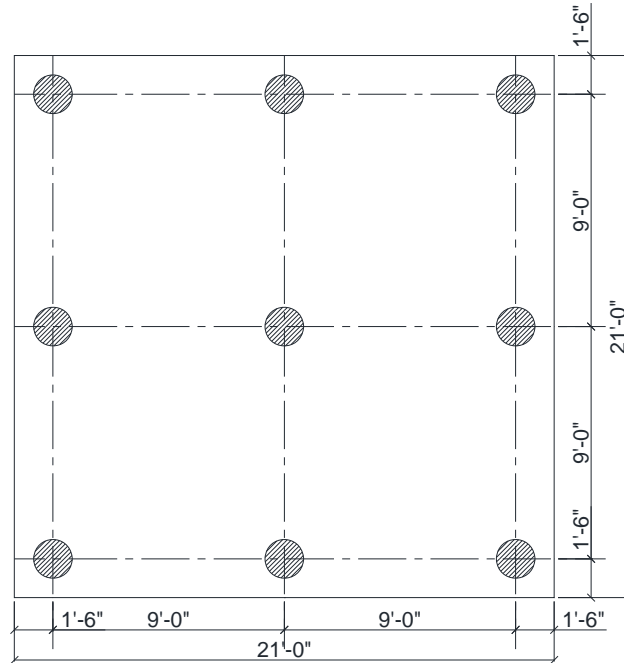


Figure 5-3: Pile Foundation with Piles Spaced at $6D_{pile}$

5.2 Dynamic Stiffness & Damping for a 1.5 ft. Diameter Pile

The vertical dynamic stiffness based on the average and maximum amplitude, damping, damping ratio and resonant frequency are shown in Figures 5-4 to 5-8 for a pile having a concrete compressive strength of 3000 psi and a diameter of 1.5 ft.

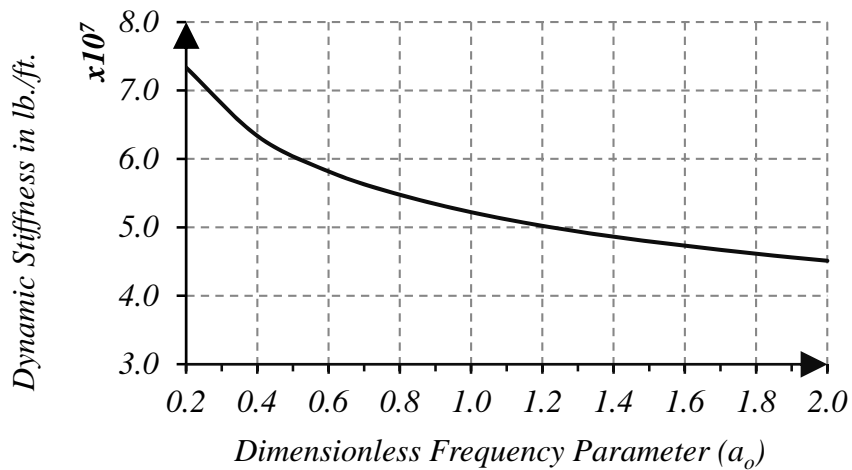


Figure 5-4: Dynamic Stiffness Based on Average Amplitude

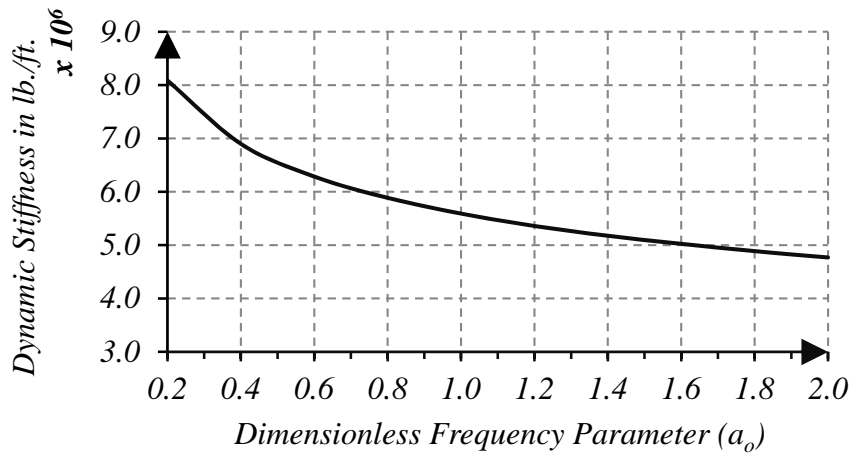


Figure 5-5: Dynamic Stiffness Based on Maximum Amplitude

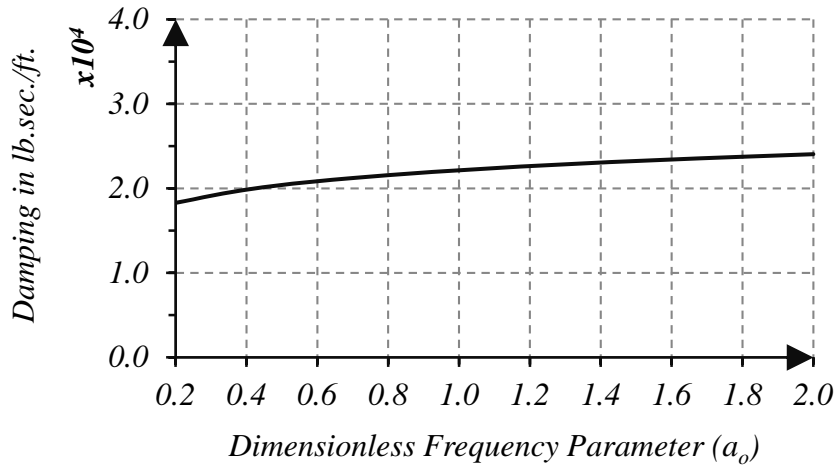


Figure 5-6: Damping of the Pile as a Function in a_0

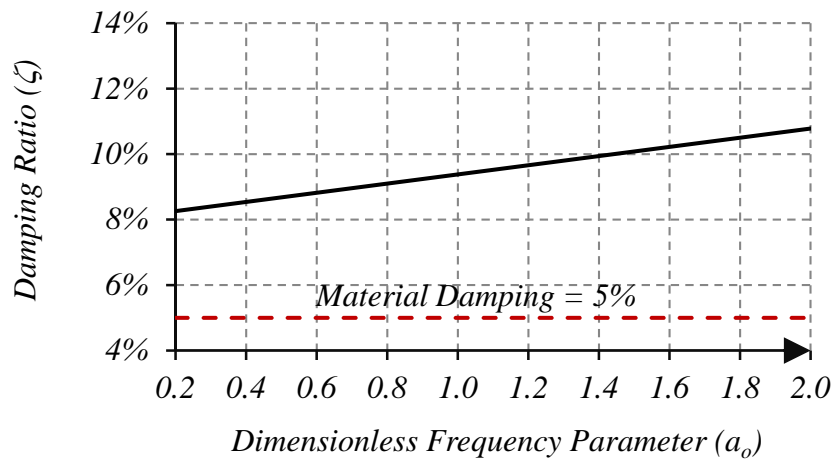


Figure 5-7: Damping Ratio of the Pile as a Function of a_0

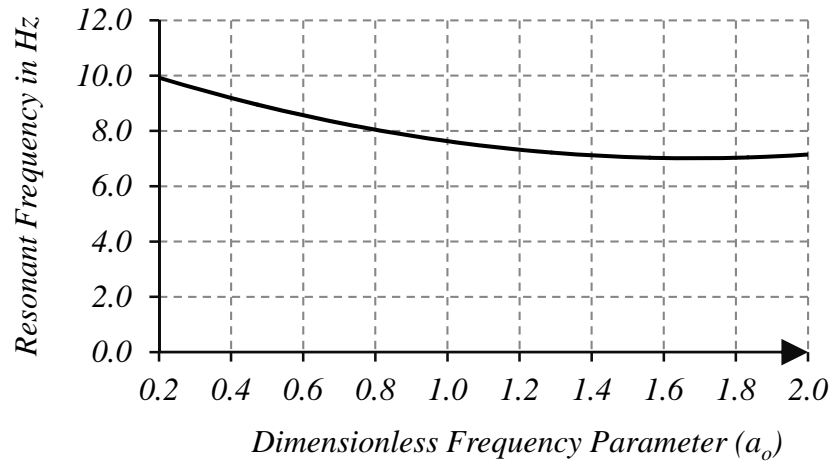


Figure 5-8: Resonant Frequency of the Pile as a Function of a_o

5.3 Vertical Static Stiffness of Pile Groups

To determine the vertical static stiffness of pile groups, the finite element models for the group of piles spaced at $2D_{pile}$, $4D_{pile}$ and $6D_{pile}$ were subjected to a vertical static unit load acting at the center of the pile cap. The vertical deflection at the pile cap center was determined for the different pile group configurations and for pile groups having different concrete compressive strengths. The results are shown in Figure 5-9 shows that the vertical static stiffness of the pile group as a function of the soil shear modulus (G_{soil}).

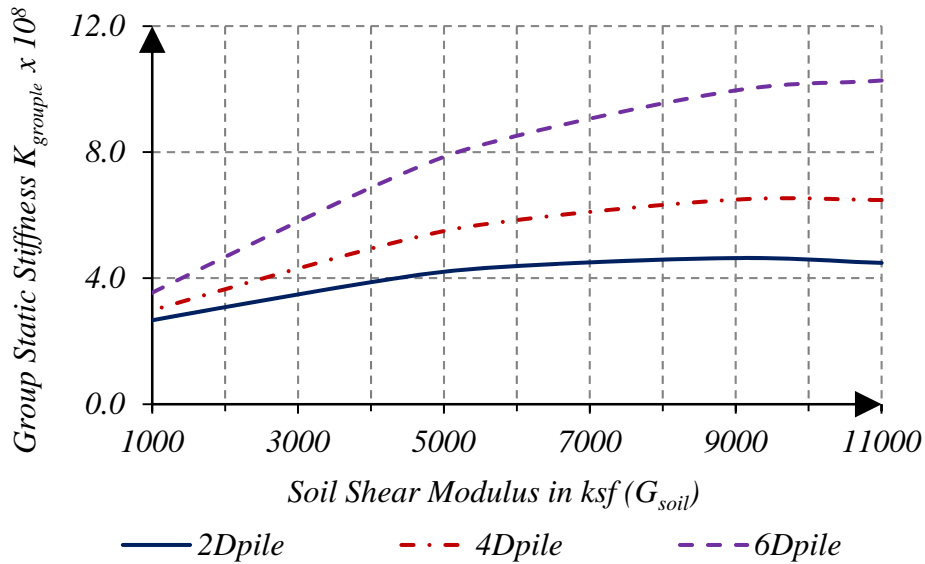


Figure 5-9: Vertical Static Stiffness for Pile Groups with $f_c = 3000$ psi

The results shown in the figure shows that the vertical static stiffness of the pile groups increases with the increase in the soil shear modulus. This increase in the pile group static stiffness is attributed to the increased soil stiffness, which resulted in more load sharing between the pile and soil. This led to a reduction in the group vertical displacement and thus increased the soil pile system stiffness. Figures 5-10 , 5-11 and 5-12 show the vertical static stresses for a group of piles spaced at $2D_{pile}$ and embedded in a soil continuum having a soil shear modulus of 1000 ksf, 6000 ksf and 11000 ksf, respectively. For the group of piles embedded in weak soils (soil shear modulus, G_{soil} , equal to 1000 ksf), as show in Figure 5-10, the axial stiffness of the soil-pile system is governed by the stiffness of the bearing layer and the axial stiffness of the group of piles. This is shown by the high stress concentration field at the pile tip. Also, the axial load in the pile elements along its length is constant (0.1 lbs. at the pile head all the way to the pile tip), which means that no load is transferred to the soil elements by friction along the pile length, thus the group of piles acted as end bearing piles. As the soil shear

modulus increases to 6000 ksf, as shown in Figure 5-11, part of the load on the pile cap is transferred to the soil elements by friction between the soil and the pile, and part of the load is transferred by bearing at the pile tip. This is shown by the stress field along the pile shaft and the concentration of the stress field at the pile tip. The axial load at the pile tip is reduced by approximately 50% from the axial load at the pile head. This indicates that approximately 50% of the load is transferred to the surrounding soil elements. For this soil condition, the stiffness of the soil-pile system is governed by the friction resistance between the pile and the soil element, the stiffness of the soil material at the pile tip and the axial stiffness of the pile elements. As the soil shear modulus increases to 11000 ksf, the soil is defined as strong soil deposit and the stiffness of the soil pile system is governed by the frictional resistance along the pile elements. This is shown in Figure 5-12 where the stress field is greater along the pile shaft with a little stress concentration at the pile tip. Figure 5-12 shows that the load on the pile elements is very little at the pile tip and most of the axial load on the pile cap is transferred to the soil element by friction along the pile shaft. Thus, the piles are acting as friction piles.

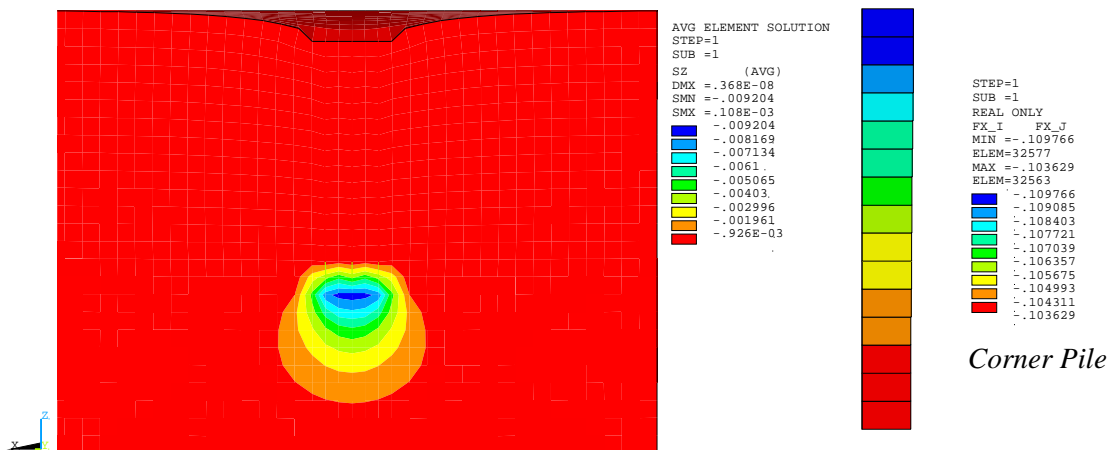


Figure 5-10: Vertical Soil Stresses for a Group of Piles and Axial Pile Forces in Soil with Shear Modulus (G_s) = 1000 ksf

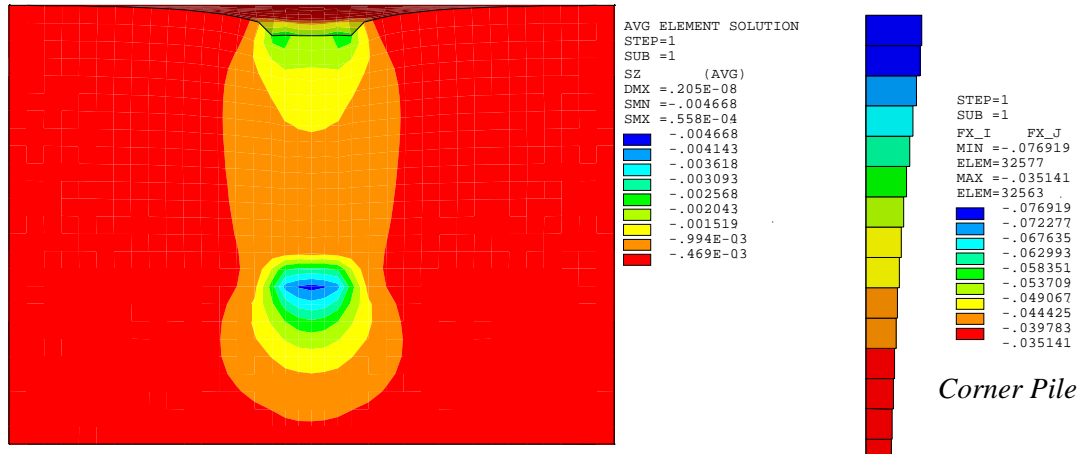


Figure 5-11: Vertical Soil Stresses for a Group of Piles and Axial Pile Forces in Soil with Shear Modulus (G_s) = 6000 ksf

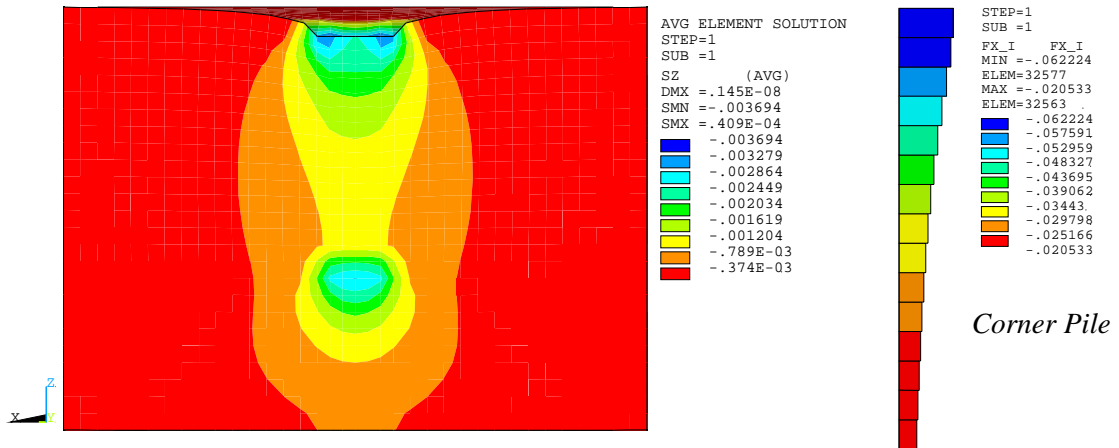
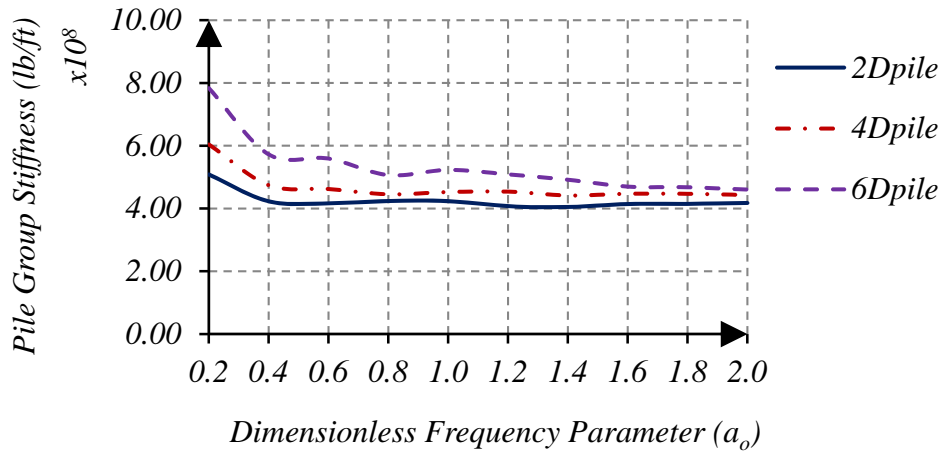


Figure 5-12: Vertical Soil Stresses for a Group of Piles and Axial Pile Forces in Soil with Shear Modulus (G_s) = 11000 ksf

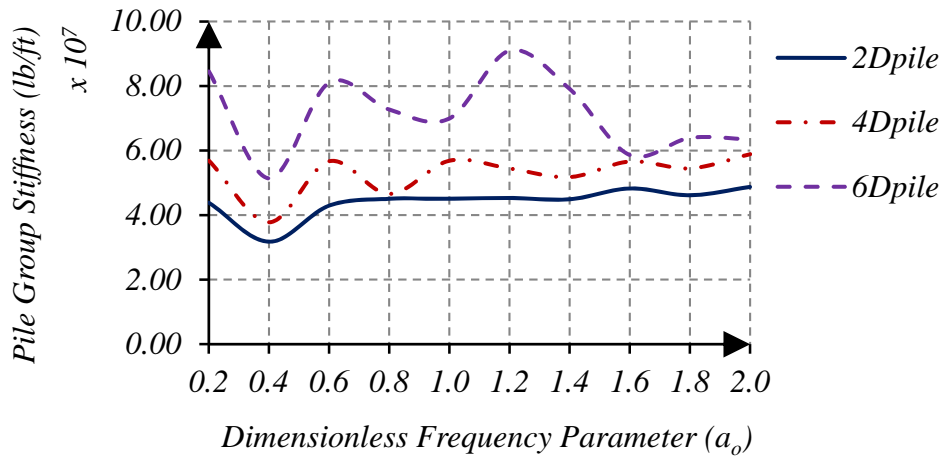
5.4 Dynamic Stiffness, Damping and Resonant Frequency of Pile Groups

The three finite element models for the pile foundation soil system shown in Figures 3-13, 3-14 and 3-15 were excited by vertical constant amplitude harmonic excitation forces. The maximum amplitude response at different values of the dimensionless frequency parameter (a_0) of the pile foundation system were measured at the centerline of the pile cap and the vertical dynamic stiffness for the pile groups was determined as the inverse of the vertical amplitude. Figures 5-13 to 5-16 show the

average and minimum vertical dynamic stiffness for a 3 x 3 group of piles having concrete compressive strength of 3000 psi, 4000 psi, 5000 psi and 6000 psi. These figures show the dynamic stiffness for a group of piles that are spaced at $2D_{pile}$, $4D_{pile}$ and $6D_{pile}$, i.e., spaced at 3, 6 and 9 ft. respectively, as a function of the dimensionless frequency parameter (a_o).

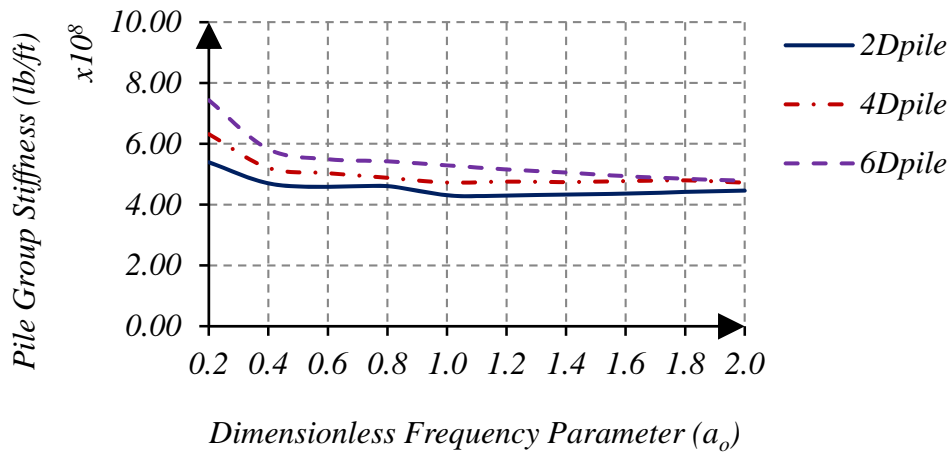


(a)

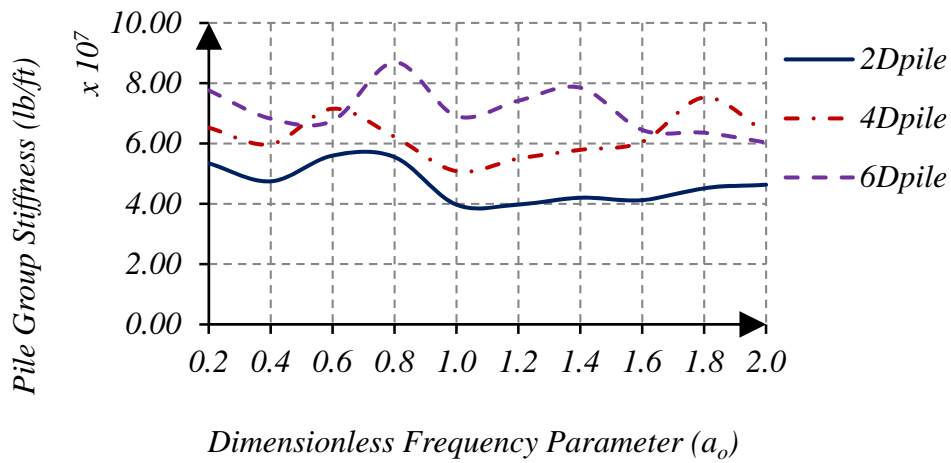


(b)

Figure 5-13: Dynamic Stiffness for a 3 x 3 Group of Piles with $f_c = 3000$ psi
 (a) Pile Group Stiffness Based on Average Amplitude
 (b) Pile Group Stiffness Based on Maximum Amplitude

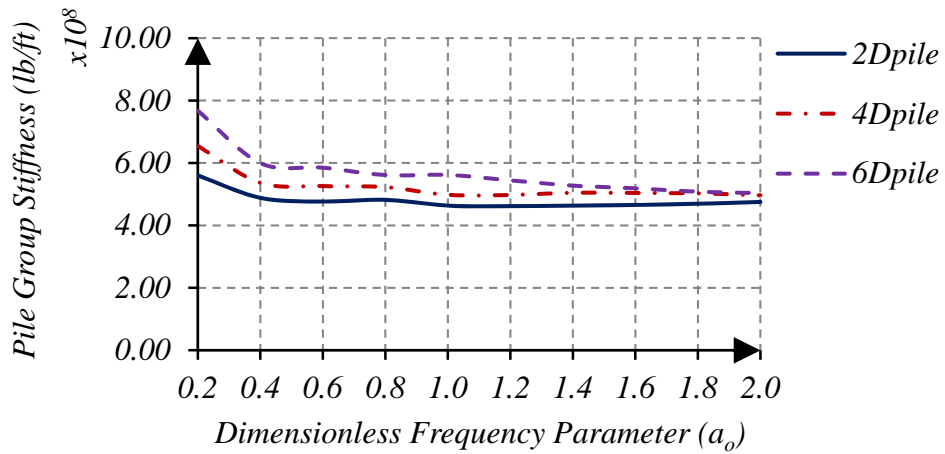


(a)

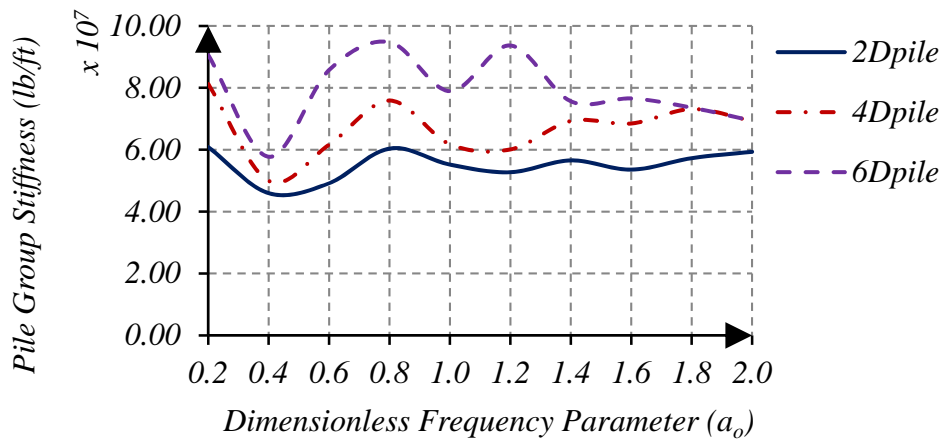


(b)

Figure 5-14: Dynamic Stiffness for a 3 x 3 Group of Piles with $f_c = 4000$ psi
 (a) Pile Group Stiffness Based on Average Amplitude
 (b) Pile Group Stiffness Based on Maximum Amplitude



(a)

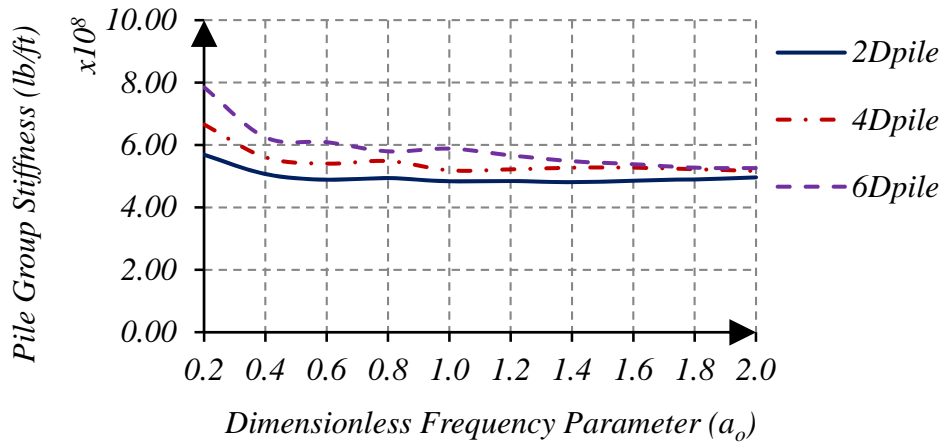


(b)

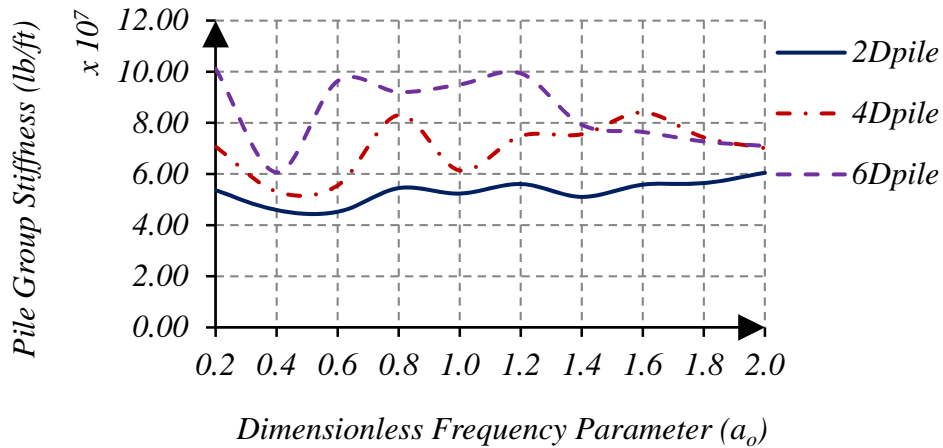
Figure 5-15: Dynamic Stiffness for a 3 x 3 Group of Piles with $f_c = 5000$ psi

(a) Pile Group Stiffness Based on Average Amplitude

(b) Pile Group Stiffness Based on Maximum Amplitude



(a)



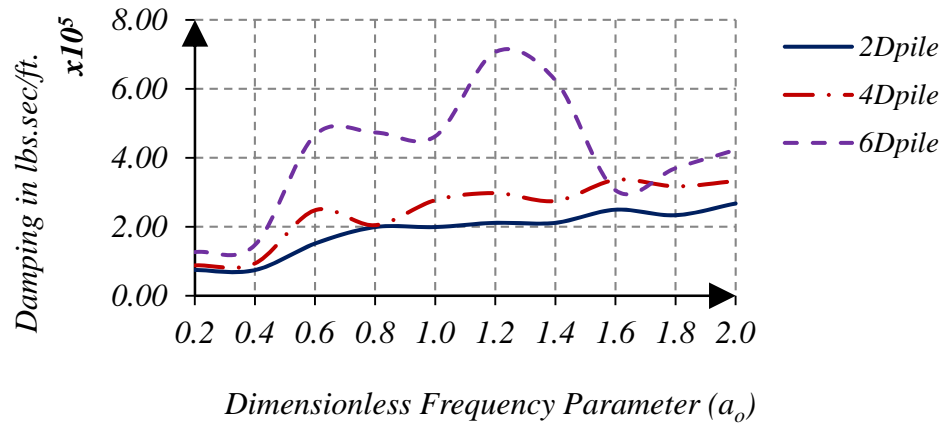
(b)

Figure 5-16: Dynamic Stiffness for a 3 x 3 Group of Piles with $f_c = 6000$ psi

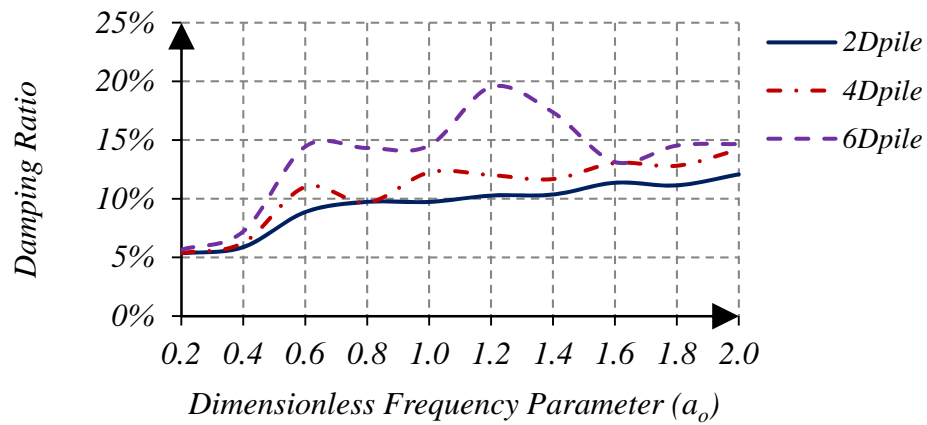
(a) Pile Group Stiffness Based on Average Amplitude

(b) Pile Group Stiffness Based on Maximum Amplitude

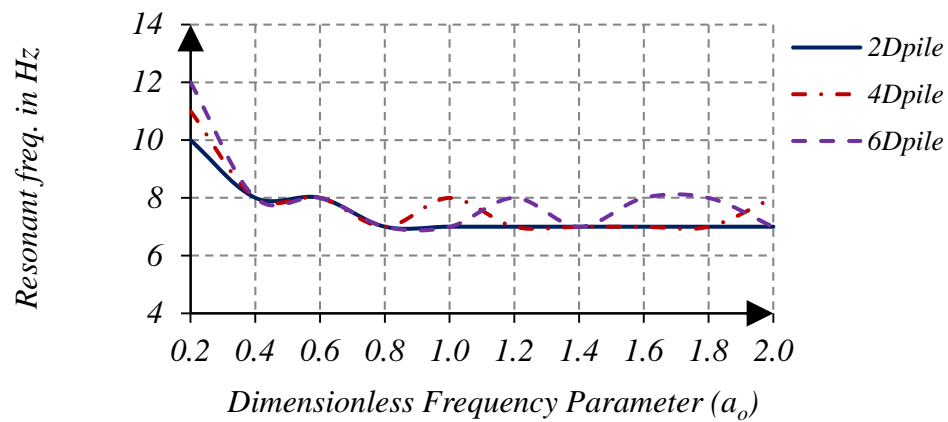
Figures 5-17 to 5-20 show the damping, damping ratio and resonant frequency for a 3 x 3 group of piles spaced at $2D_{pile}$, $4D_{pile}$ and $6D_{pile}$ as a function of the dimensionless frequency parameter (a_o). These figures show the results for a group of piles having concrete compressive strengths of 3000, 4000, 5000 and 6000 psi.



(a)

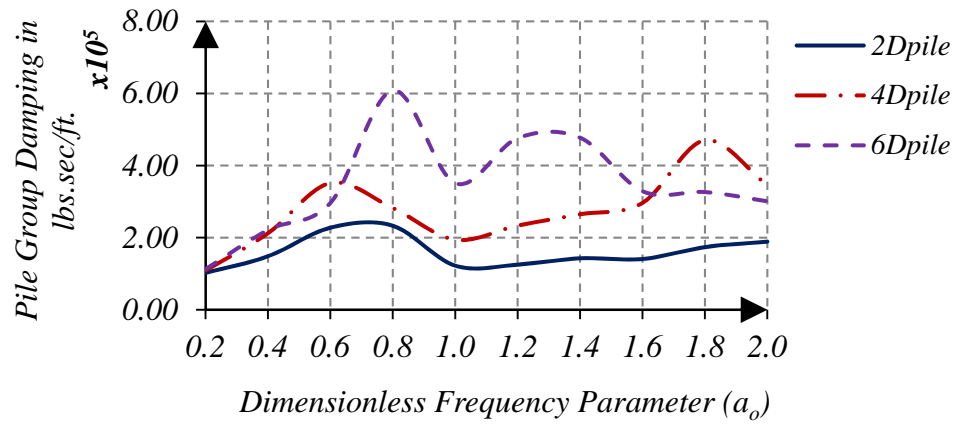


(b)

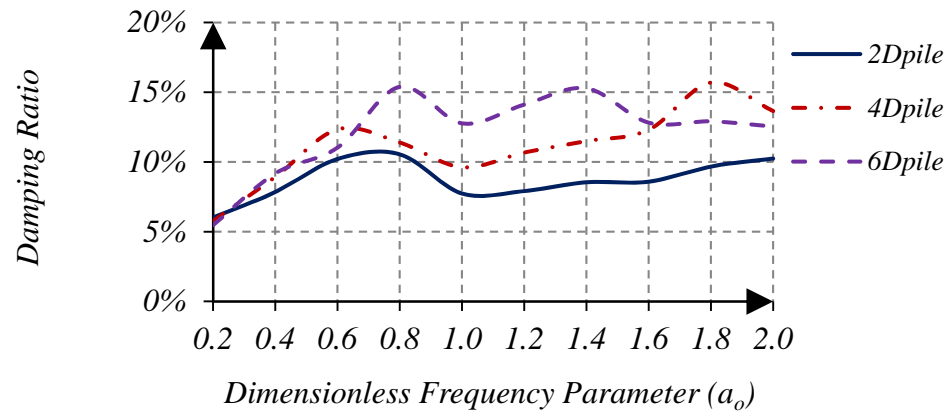


(c)

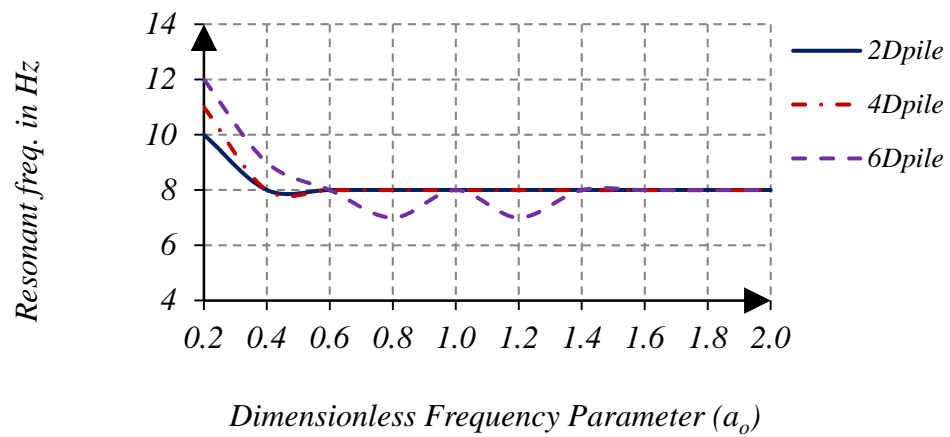
Figure 5-17: Response of a Group of Piles with $f_c = 3000$ psi
 (a) Damping of a 3 x 3 Group of Piles
 (b) Damping Ratio of a 3 x 3 Group of Piles
 (c) Resonant Frequency of a 3 x 3 Group of Piles



(a)

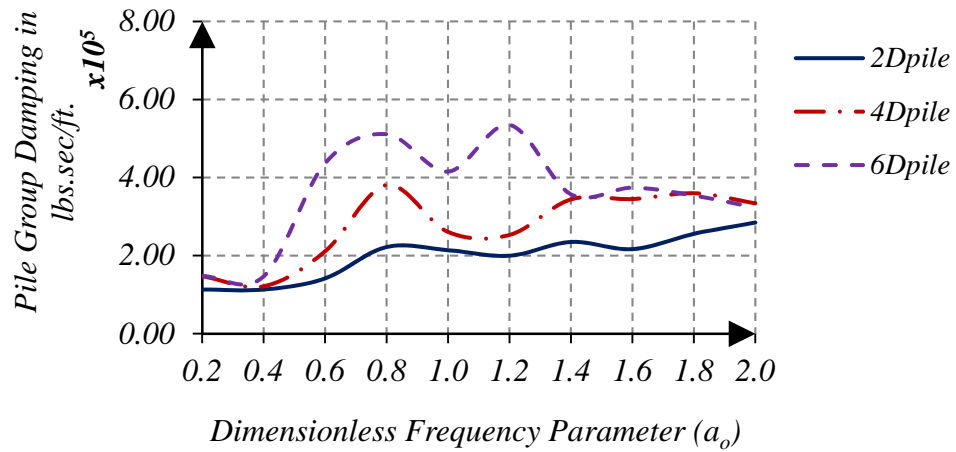


(b)

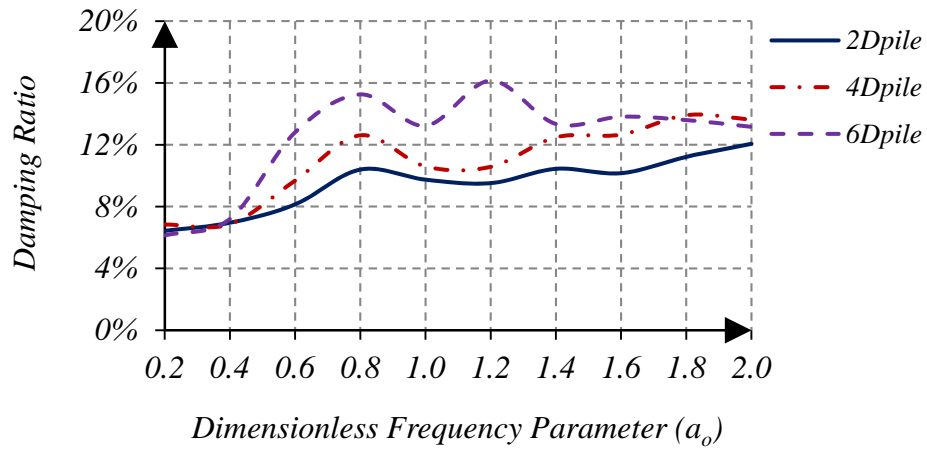


(c)

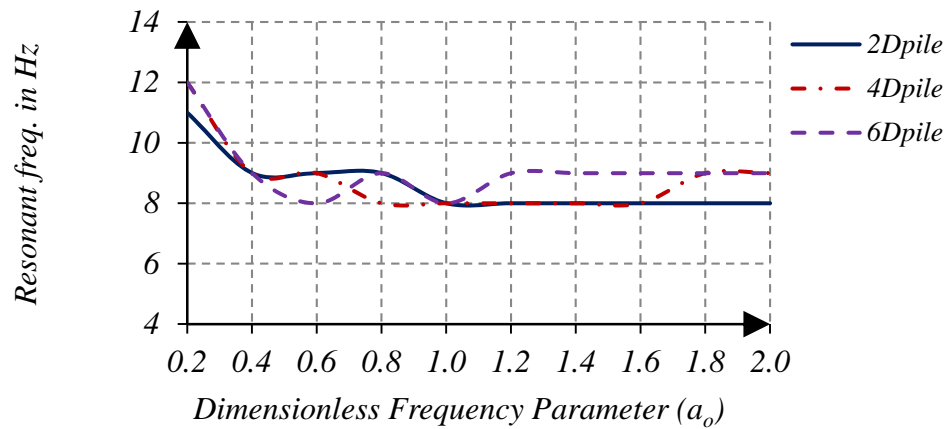
Figure 5-18: Response of a Group of Piles with $f_c = 4000$ psi
 (a) Damping of a 3 x 3 Group of Piles
 (b) Damping Ratio of a 3 x 3 Group of Piles
 (c) Resonant Frequency of a 3 x 3 Group of Piles



(a)

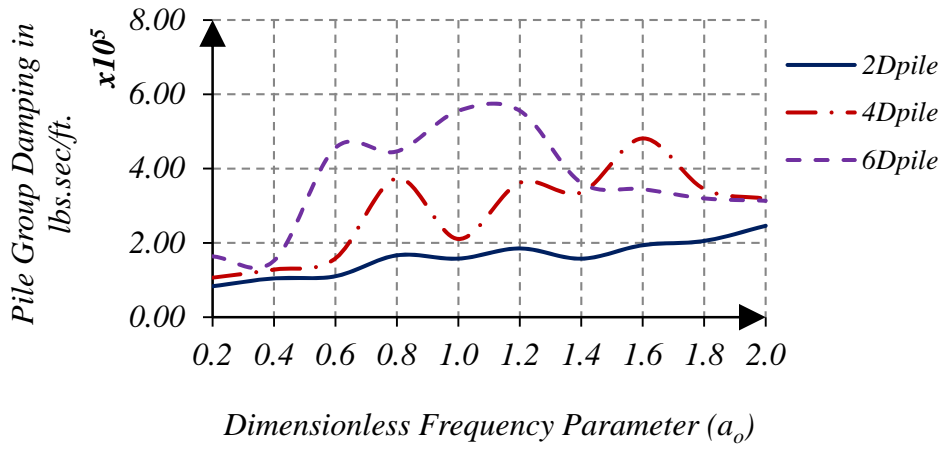


(b)

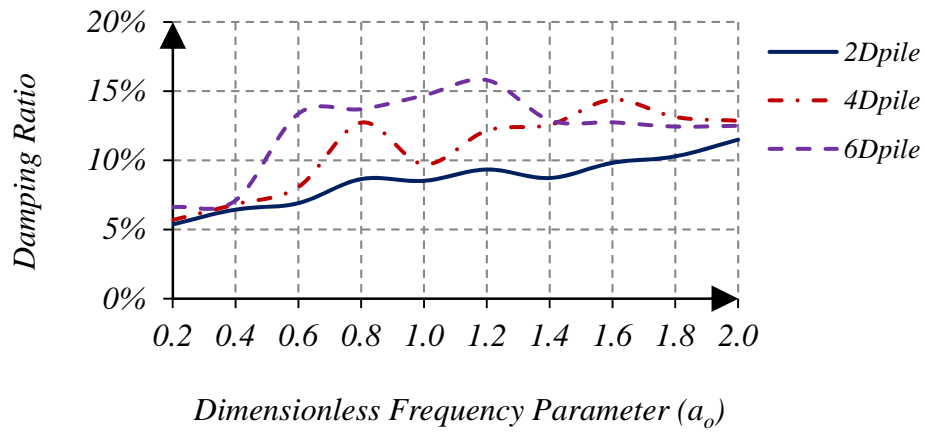


(c)

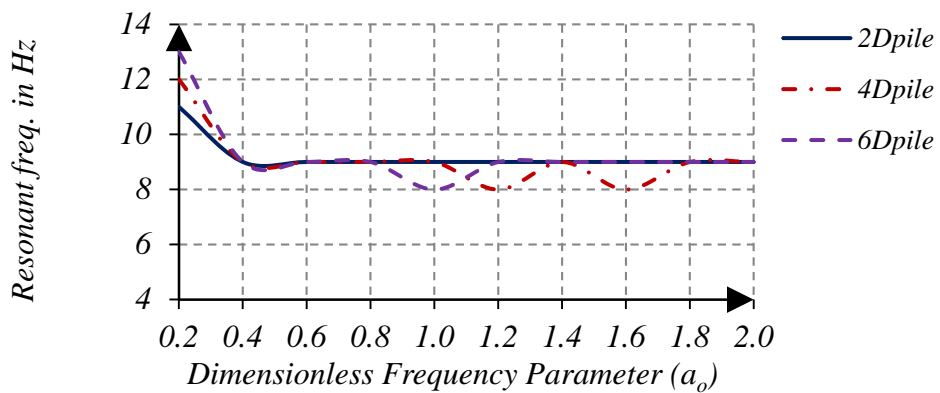
Figure 5-19: Response of a Group of Piles with $f_c = 5000$ psi
 (a) Damping of a 3 x 3 Group of Piles
 (b) Damping Ratio of a 3 x 3 Group of Piles
 (c) Resonant Frequency of a 3 x 3 Group of Piles



(a)



(b)



(c)

Figure 5-20: Response of a Group of Piles with $f_c = 6000$ psi
 (a) Damping of a 3 x 3 Group of Piles
 (b) Damping Ratio of a 3 x 3 Group of Piles
 (c) Resonant Frequency of a 3 x 3 Group of Piles

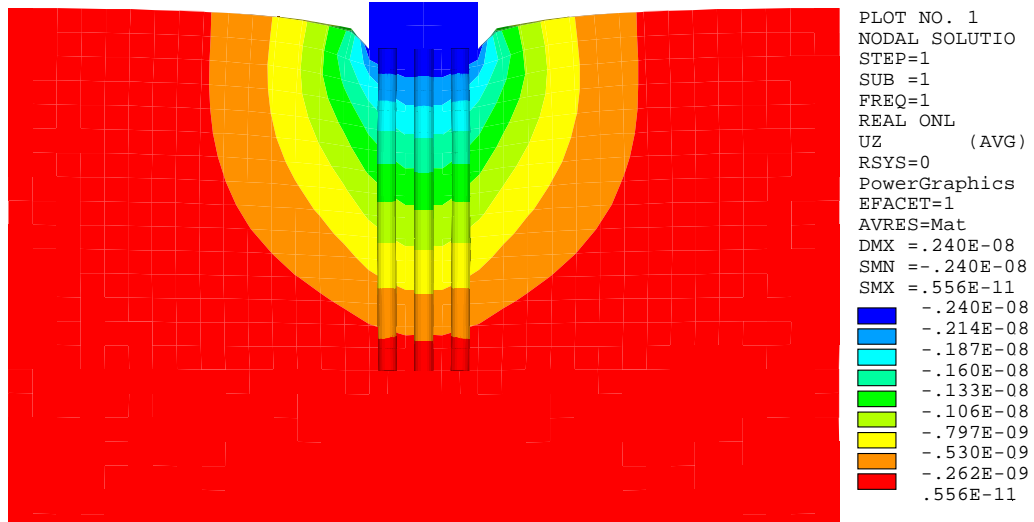
To explain the oscillatory behavior of the stiffness, damping, resonant frequency and damping ratio as a function of the dimensionless frequency parameter (a_0), the following discussion is presented. Along the length of each pile at all points on the pile, and in our case for a homogenous medium, cylindrical waves propagate radially outwards in the horizontal direction due to the vertical vibration. These stress waves are generated from each pile in the pile group. The waves emitted from each pile will be subject to attenuation with distance, and when encountering a pile in the group will result in refraction, reflection and change in phase. Such wave interaction will affect the dynamic response of the pile group. The results of such interaction, as shown in Figures 5-13 to 5-20 show such strong oscillatory behavior, i.e., the curves are having peaks and valleys. The case of peaks and valleys were also shown in Dobry and Gazetas (1988) study and their explanation is that the change in the value of (a_0), causes interference of the shear waves originating along the pile length and such interference can be constructive where peaks will occur or destructive where a valley will occur.

It is important to note that the response of the pile group is influenced by the soil shear modulus, the machine frequency and the pile spacing. The difference response between the cases of the $2D_{pile}$, $4D_{pile}$ and $6D_{pile}$ in all figures is that the values for the $6D_{pile}$ are higher than the $4D_{pile}$ and the case of $2D_{pile}$ are the smallest. The reason the pile group spaced at $6D_{pile}$ has higher stiffness than the pile group spaced at $4D_{pile}$ and $2D_{pile}$ is attributed to the largest contribution of the soil between the piles to the group. With the large soil volume in the case of the pile group spaced at $6D_{pile}$, the stiffness increases as well as the damping. Also for the same frequency, when $a_0 = 0.2$. the stiffness is higher than the stiffness at $a_0 = 2.0$ when the soil is weak. Thus, as the

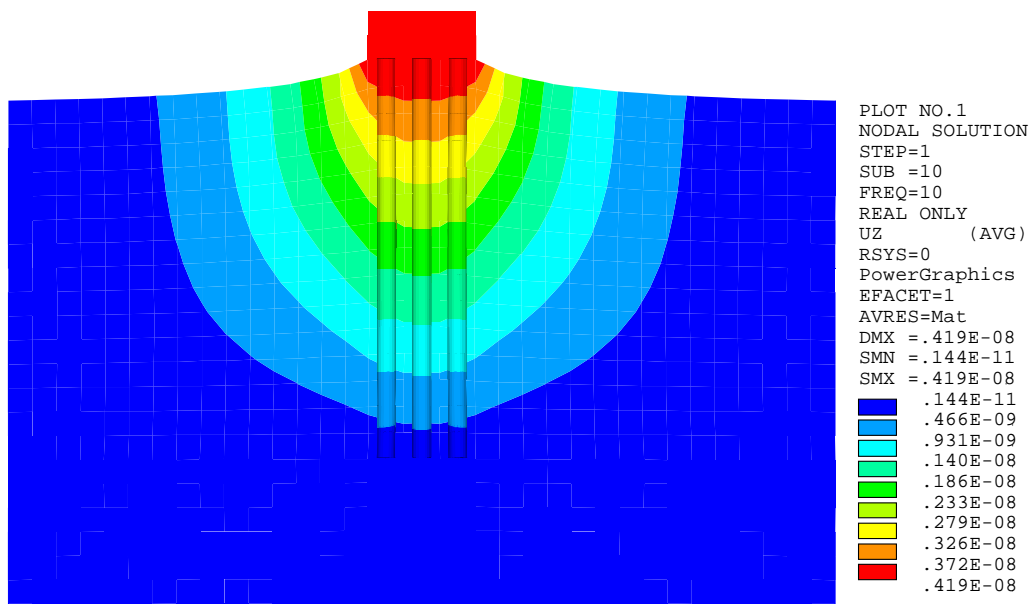
dimensionless frequency parameter (a_0) increases indicating weak soil material, the effect of the soil in the vertical dynamic stiffness of the pile group is reduced and the pile group vertical dynamic stiffness is mainly influenced by the structural stiffness of the pile groups. Also for the case of close spacing, i.e., $2D_{pile}$, the response of all figures exhibit a smother variation with (a_0) compared to the bigger variation in the $4D_{pile}$ and the much bigger variation in the case of pile group spaced at $6D_{pile}$. The explanation is that with the close spacing, the pile group behaves like an isolated embedded foundation, i.e., the soil mass between the piles tends to vibrate in phase with the piles and so the pile groups-soil system respond as a block.

Figures 5-21 to 5-26 show the vertical displacement fields of the soil-pile system for pile groups spaced at $2D_{pile}$, $4D_{pile}$ and $6D_{pile}$. The vertical displacement field for each pile spacing is shown at low frequency range (1.0 Hz), quasi static, and at the soil-pile group resonant frequency. The displacement fields are shown for two soil conditions. The first soil condition is for strong soils, identified by a dimensionless frequency parameter, a_0 of 0.2, and the second soil condition is for weak soils, identified by a dimensionless frequency parameter, a_0 of 2.0. For strong soils at low and at resonant frequencies, the displacement fields between the piles show a uniform displacement distribution in the soil continuum. At this dimensionless frequency parameter, the soil displacement field is well defined around the foundation and both the soil and the pile move as a block. This in-phase motion of the soil pile elements is because the cylindrical waves emitted along the pile element are uniform and coherent resulting in uniform displacement fields. For weak soil deposits as shown in Figures 5-22, 5-24, and 5-26 the displacement fields at low frequency range show a uniform

displacement distribution in the soil elements between the pile group since at such low frequency there are no cylindrical waves emitted from the piles and the displacement of the soil pile elements is quasi static. At resonant frequency, on the other hand, the displacement field between the pile elements are not uniform and show considerable wave interference. Such wave interference is the cause of the oscillatory behavior of the stiffness, damping, resonant of the soil-pile response. As the cylindrical waves travel away from the pile into the soil continuum, and depending on the soil type, waves attenuate, refract and change in phase. When these cylindrical waves meet another cylindrical wave from an adjacent pile, they either become amplified, if both traveling waves have the same frequency and phase, or attenuate when the two traveling waves have different frequencies and phase angles.

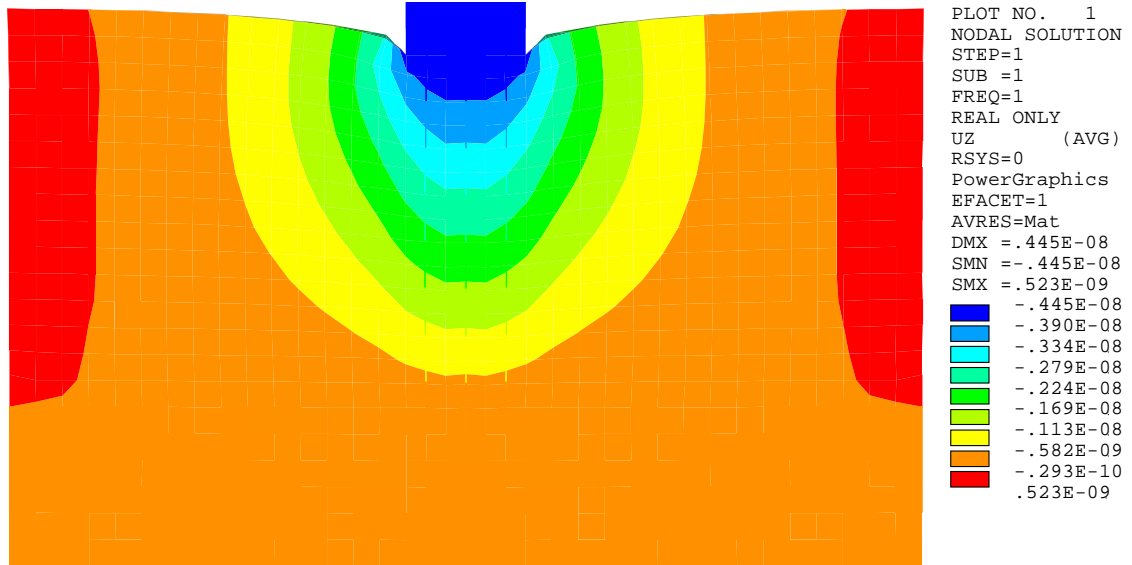


(a)

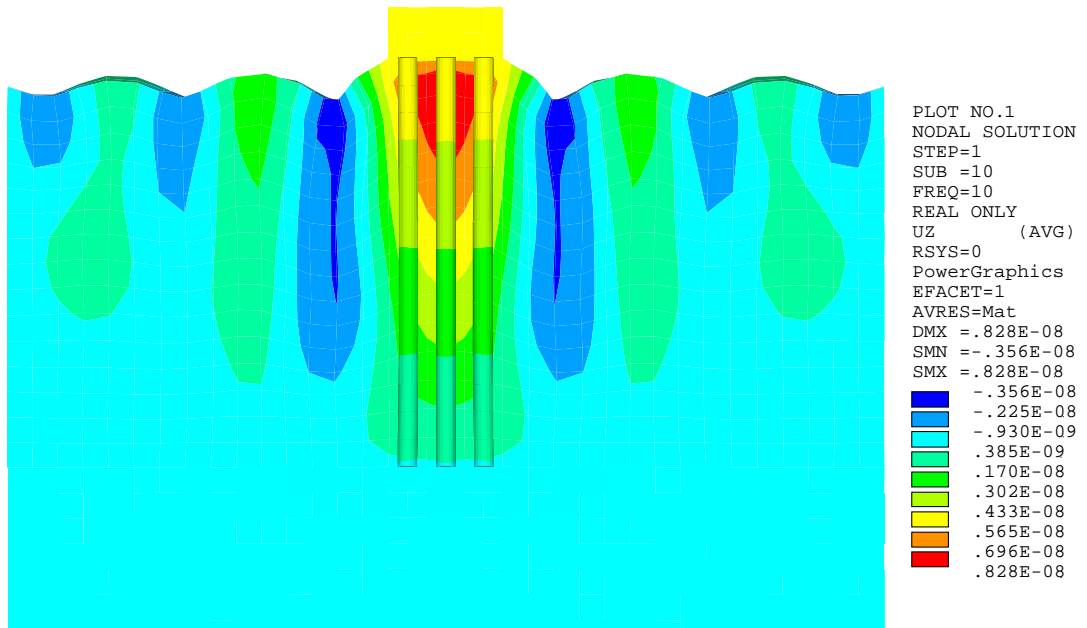


(b)

Figure 5-21: Displacement of Pile Groups Spaced at $2D_{pile}$ in Strong Soil ($a_0 = 0.2$)
 (a) Vertical displacement response at 1.0 Hz and $f_c = 3000$ psi
 (b) Vertical displacement response at 10 Hz (Resonance) and $f_c = 3000$ psi

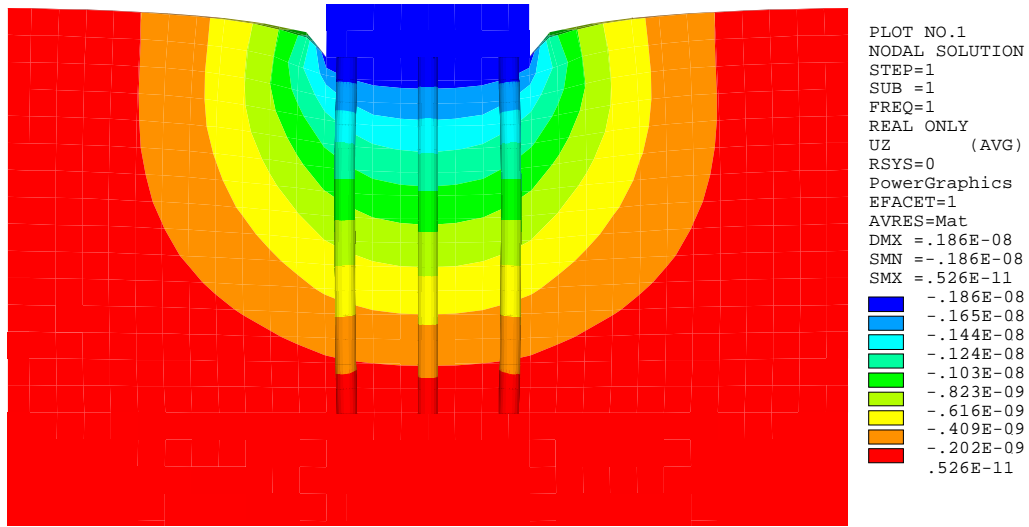


(a)

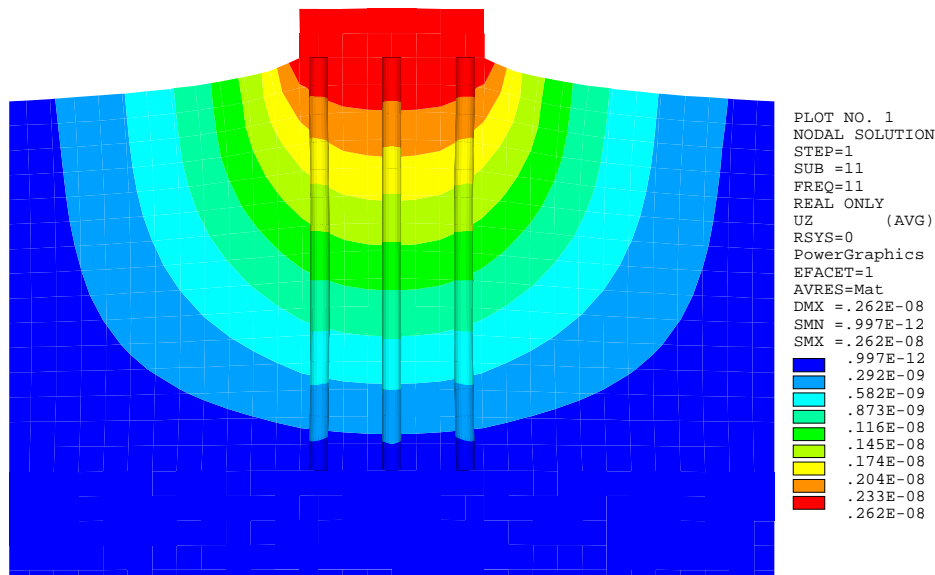


(b)

Figure 5-22: Displacement of Pile Groups Spaced at $2D_{pile}$ in Weak Soil ($a_0 = 2.0$)
 (a) Vertical displacement response at 1.0 Hz and $f_c = 3000$ psi
 (b) Vertical displacement response at 10 Hz (Resonance) and $f_c = 3000$ psi

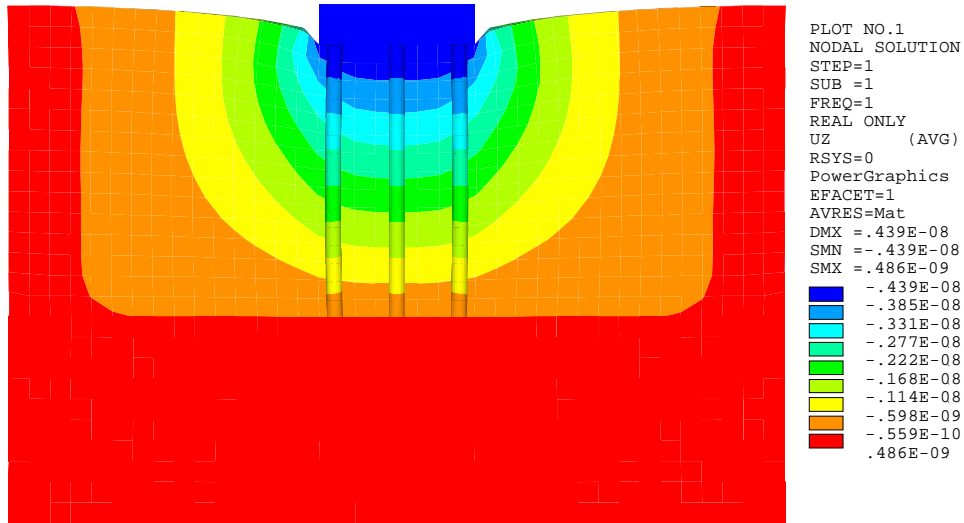


(a)

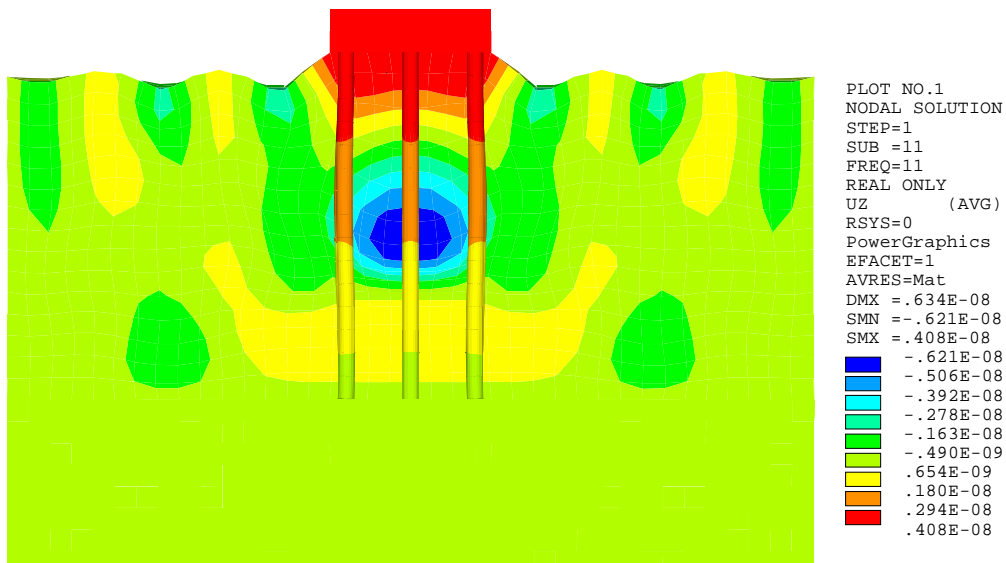


(b)

Figure 5-23: Displacement of Pile Groups Spaced at $4D_{pile}$ in Strong Soil ($a_0 = 0.2$)
 (a) Vertical displacement response at 1.0 Hz and $f_c = 3000$ psi
 (b) Vertical displacement response at 11 Hz (Resonance) and $f_c = 3000$ psi

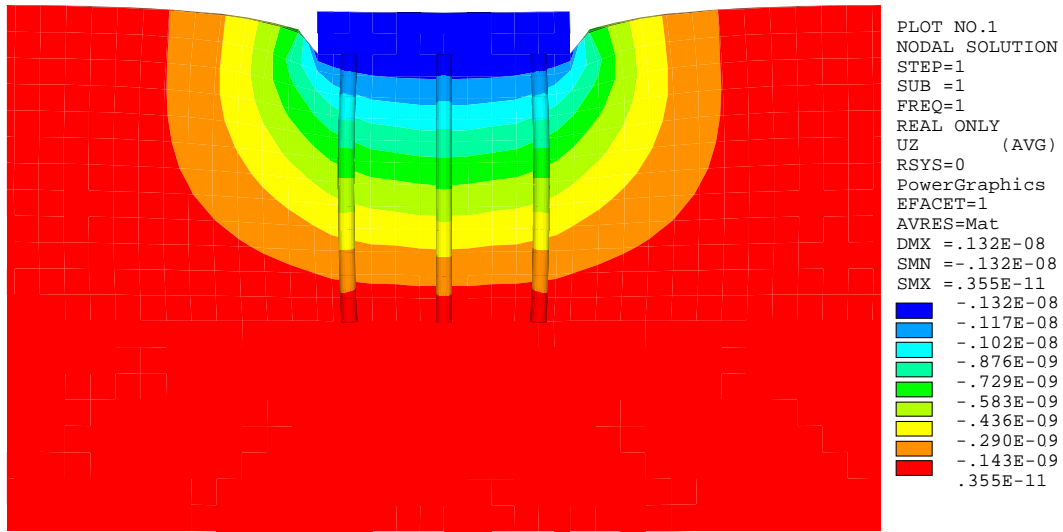


(a)

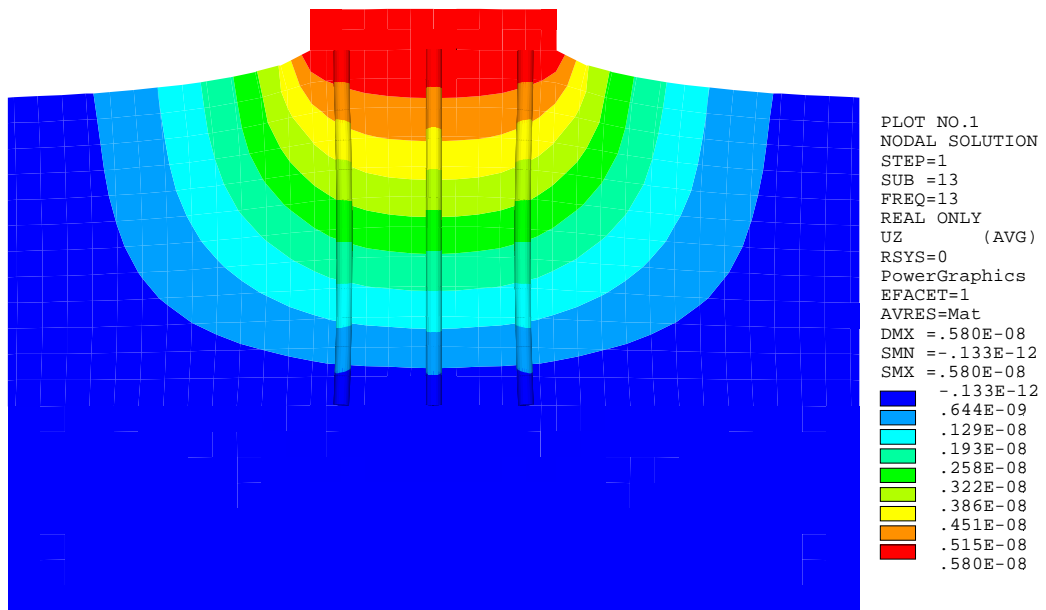


(b)

Figure 5-24: Displacement of Pile Groups Spaced at $4D_{pile}$ in Weak Soil ($a_0 = 2.0$)
 (a) Vertical displacement response at 1.0 Hz and $f_c = 3000$ psi
 (b) Vertical displacement response at 11 Hz (Resonance) and $f_c = 3000$ psi

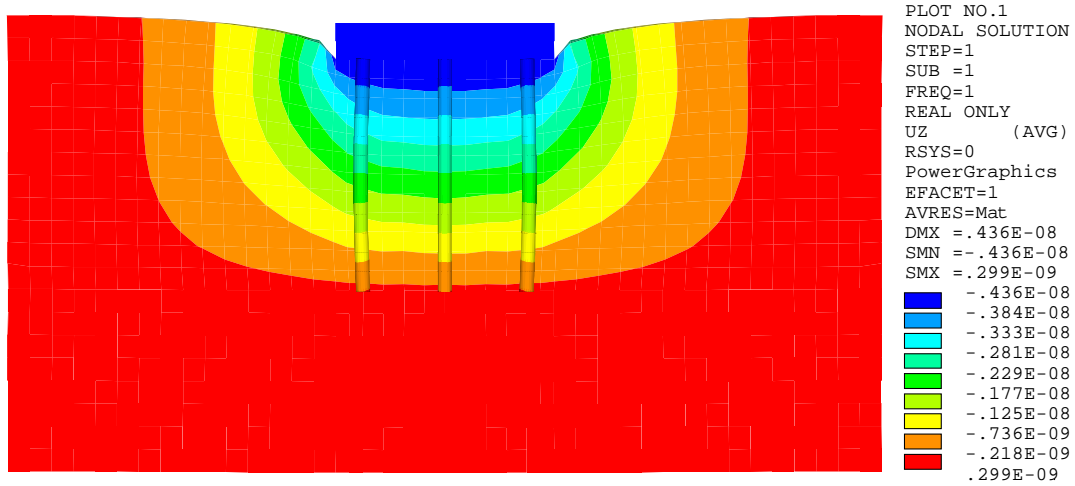


(a)

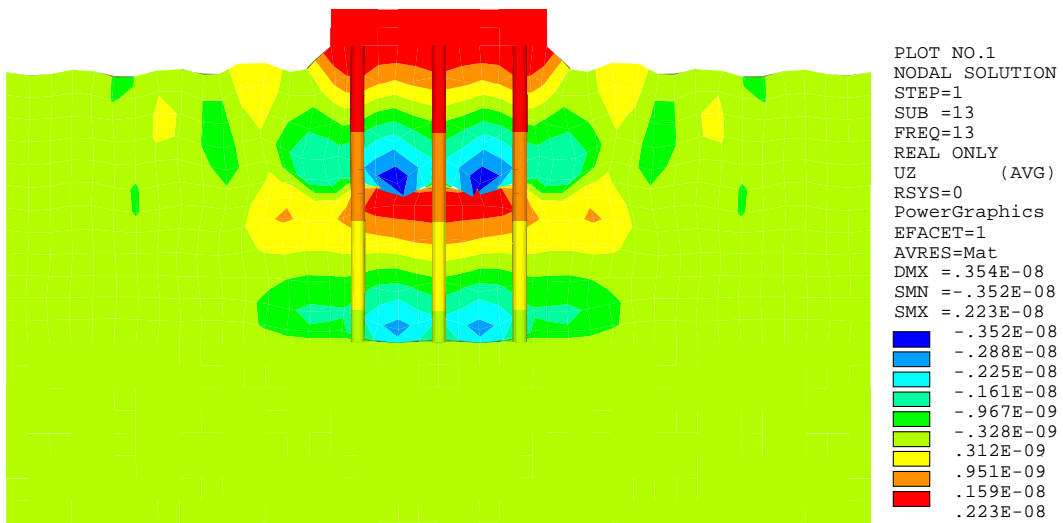


(b)

Figure 5-25: Displacement of Pile Groups Spaced at $6D_{pile}$ in Strong Soil ($a_0 = 0.2$)
 (a) Vertical displacement response at 1.0 Hz and $f_c = 3000$ psi
 (b) Vertical displacement response at 13 Hz (Resonance) and $f_c = 3000$ psi



(a)



(b)

Figure 5-26: Displacement of Pile Groups Spaced at $6D_{pile}$ in Weak Soil ($a_0 = 2.0$)
 (a) Vertical displacement response at 1.0 Hz and $f_c = 3000$ psi
 (b) Vertical displacement response at 13 Hz (Resonance) and $f_c = 3000$ psi

5.5 Effect of the Ratio G_{soil}/E_{pile} on the Dynamic Stiffness and Damping

The effect of the ratio of the soil's shear modulus and the pile's Young's modulus on the vertical dynamic stiffness and damping of a group of piles spaced at $2D_{pile}$, $4D_{pile}$ and $6D_{pile}$ are presented in Figures 5-27 to 5-34.

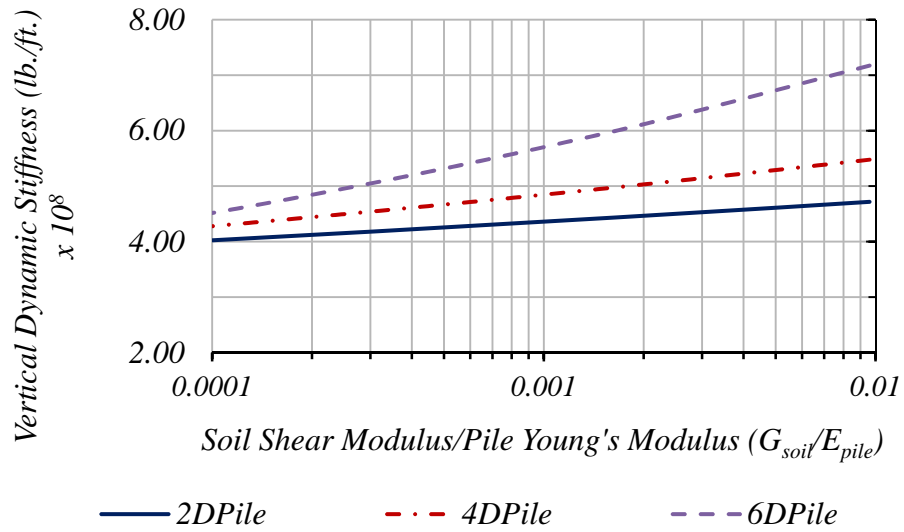


Figure 5-27: Effect of G_{soil}/E_{pile} on Group Stiffness for Piles with $f_c = 3000$ psi.

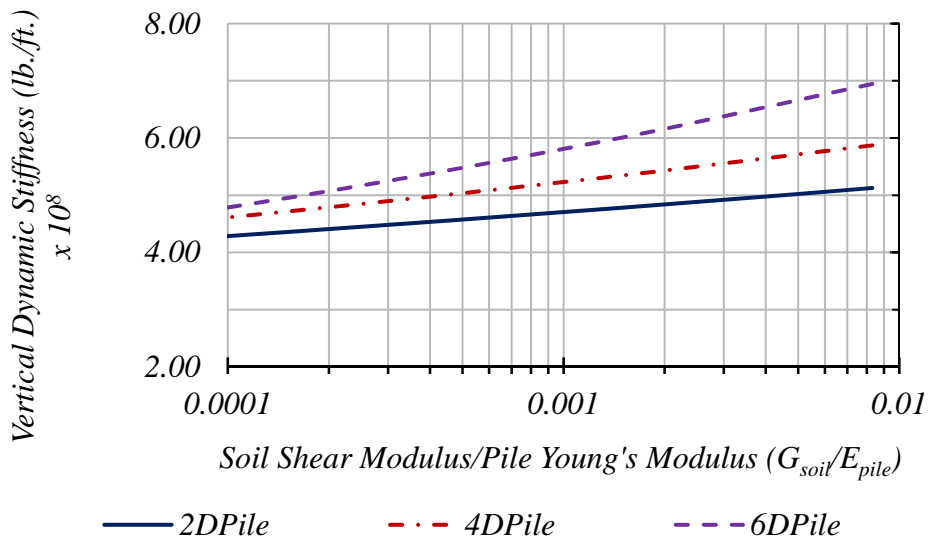


Figure 5-28: Effect of G_{soil}/E_{pile} on Group Stiffness for Piles with $f_c = 4000$ psi.

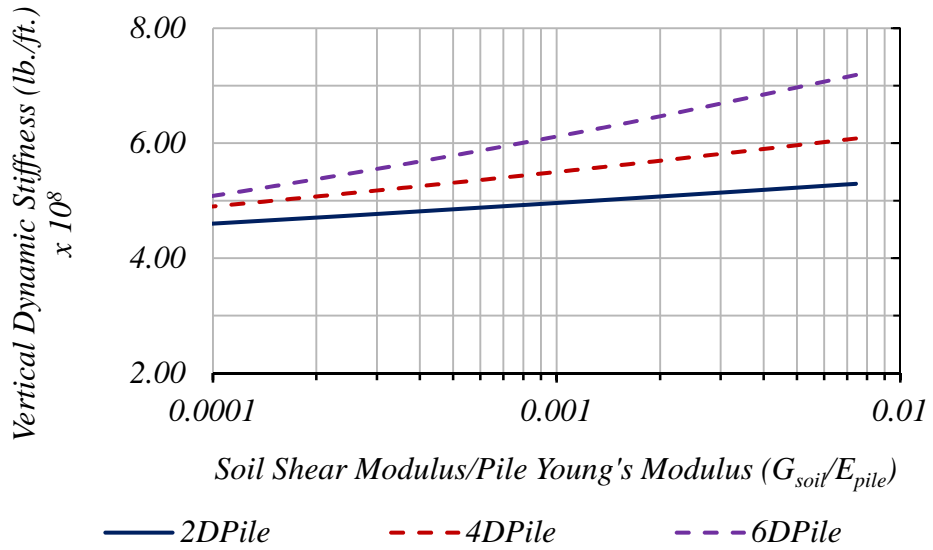


Figure 5-29: Effect of G_{soil}/E_{pile} on Group Stiffness for Piles with $f_c = 5000$ psi.

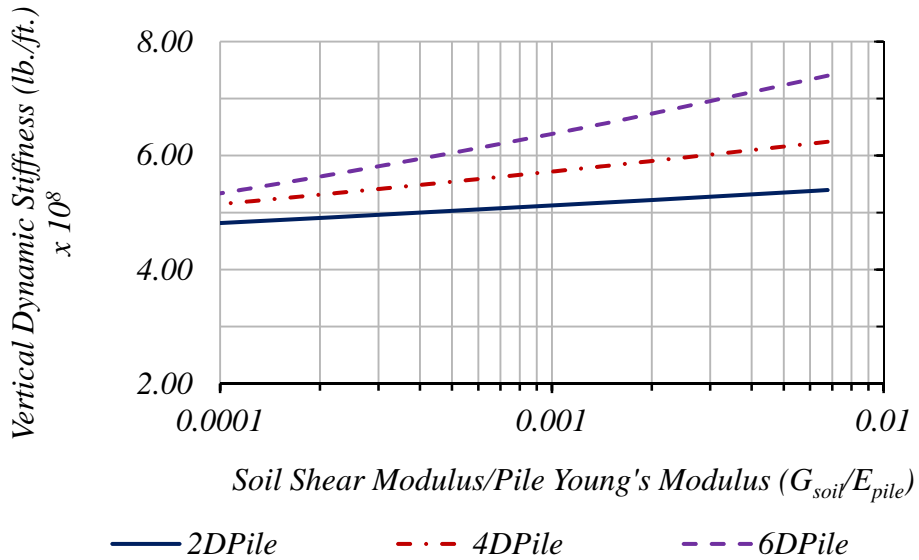


Figure 5-30: Effect of G_{soil}/E_{pile} on Group Stiffness for Piles with $f_c = 6000$ psi.

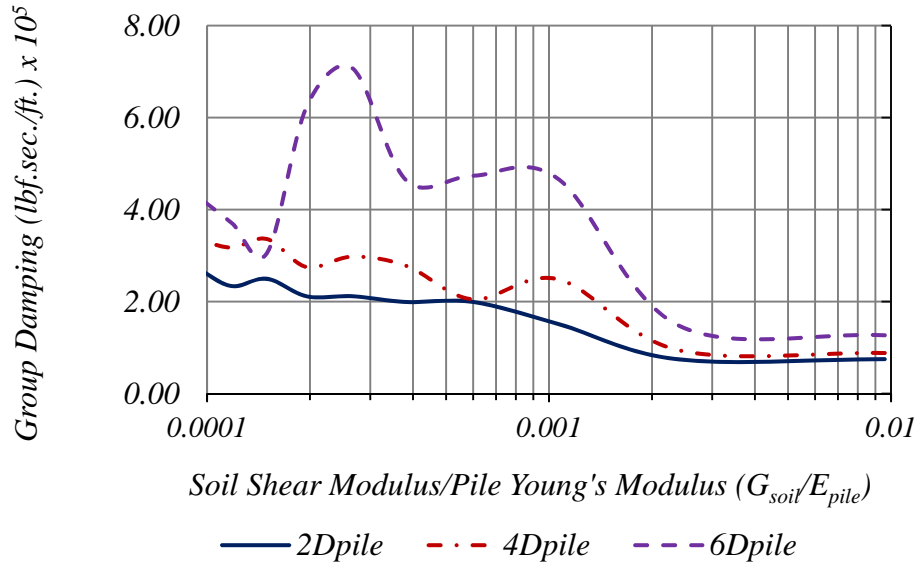


Figure 5-31: Effect of G_{soil}/E_{pile} on Group Damping for Piles with $f_c = 3000$ psi.

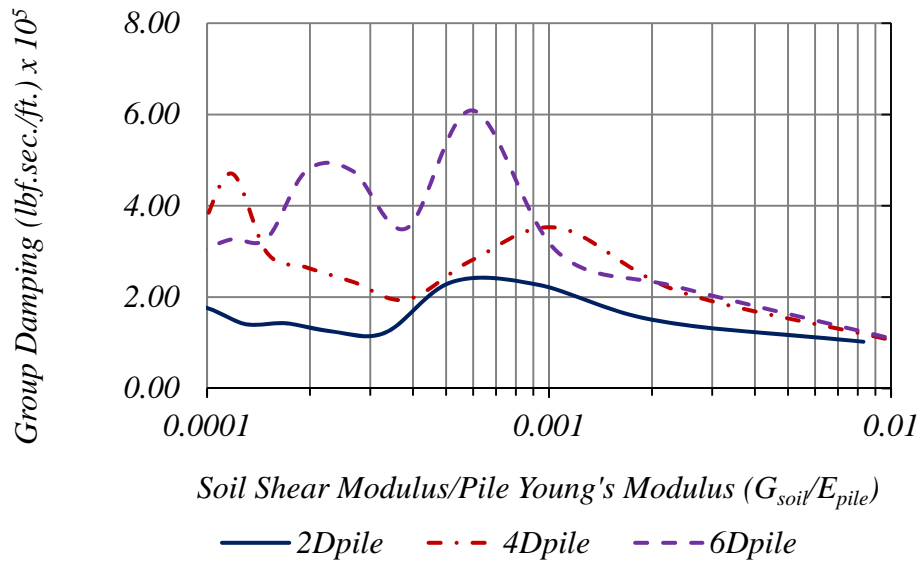


Figure 5-32: Effect of G_{soil}/E_{pile} on Group Damping for Piles with $f_c = 4000$ psi.

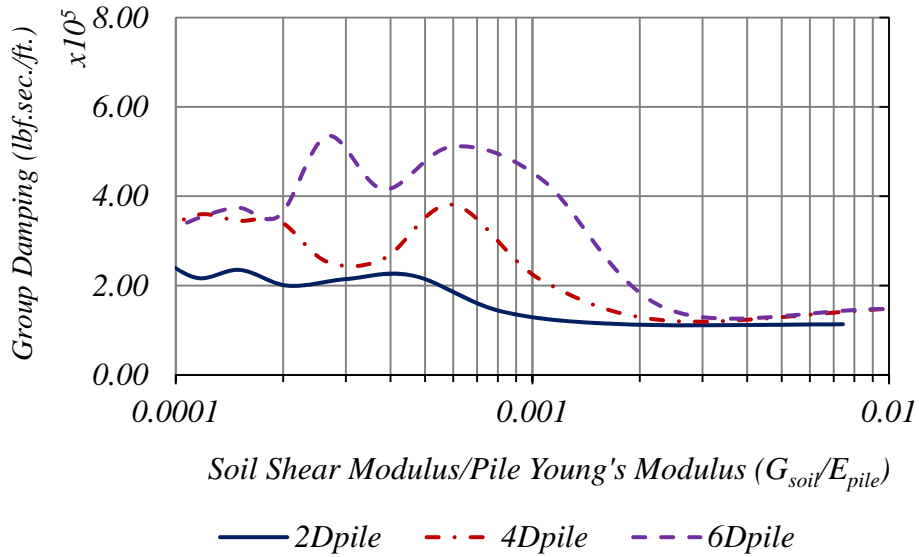


Figure 5-33: Effect of G_{soil}/E_{pile} on Group Damping for Piles with $f_c = 5000$ psi.

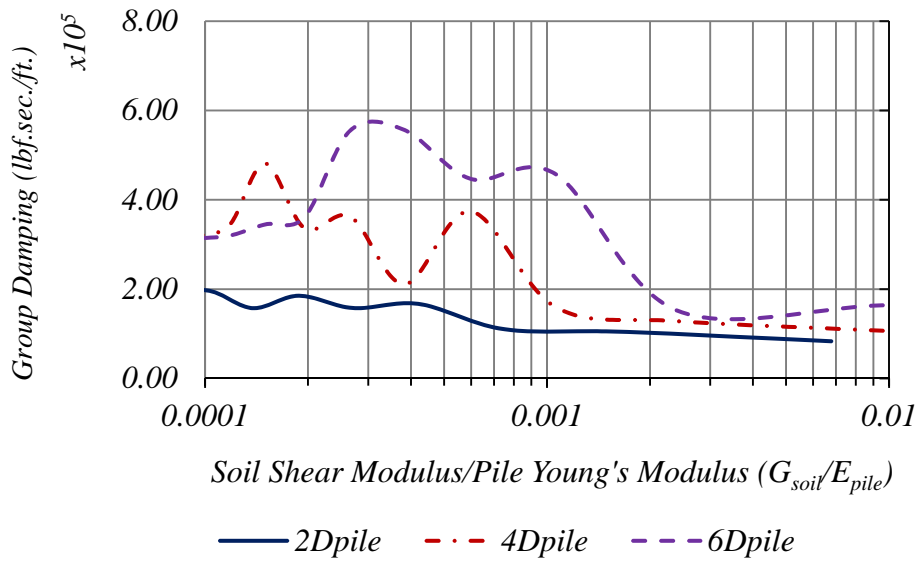


Figure 5-34: Effect of G_{soil}/E_{pile} on Group Damping for Piles with $f_c = 6000$ psi.

As shown in Figure 5-27, the vertical dynamic stiffness for pile groups spaced at $2D_{pile}$, $4D_{pile}$ and $6D_{pile}$ was increased by approximately 17%, 28% and 59% respectively, when the ratio of G_{soil}/E_{pile} was increased from 10^{-4} to 10^{-2} . For pile groups having concrete strength of 4000 psi, the dynamic stiffness was increased by 20%, 28% and 47 % for pile groups spaced at $2D_{pile}$, $4D_{pile}$ and $6D_{pile}$ respectively, as shown in

Figure 5-28. The increase in the dynamic stiffness for pile groups with concrete strength of 5000 psi and spaced at $2D_{pile}$, $4D_{pile}$ and $6D_{pile}$ was 16%, 26% and 44%, respectively when the ratio of G_{soil}/E_{pile} was increased from 10^{-4} to 10^{-2} , as shown in Figure 5-29. Finally, the dynamic stiffness for pile groups having strength of 6000 psi and was increased by was 13%, 26% and 43 % for pile groups spaced at $2D_{pile}$, $4D_{pile}$ and $6D_{pile}$, respectively, as shown in Figure 5-30.

The increase in the soil shear modulus to pile Young's modulus indicates an increase in the densification of the soil material indicating a strong soil deposit. Therefore, as the ratio of the soil shear modulus to the pile young's modulus increases, the soil deposit between the pile elements becomes stronger soils and reduces the displacement of the soil-pile system, thus increasing the stiffness of the pile groups.

The vertical dynamic stiffness of pile groups spaced at $6D_{pile}$ was approximately 1.5 times higher than the vertical dynamic stiffness of pile groups spaced at $2D_{pile}$ at ratio of G_{soil}/E_{pile} of 0.01. The increase in the dynamic stiffness for piles spaced at $6D_{pile}$ is due to the effect of increased soil volume between the piles within the group which resulted in an increase of the load sharing between the piles and the soil. Thus increasing the stiffness of the pile groups spaced at $6D_{pile}$ than the pile groups spaced at $2D_{pile}$.

The effect of the increase in the soil shear modulus to the pile Young's modulus on the pile groups damping depends on the soil pile system minimum stiffness (K_{min}), and the resonant frequency of the soil pile system. The increase in the ratio of the soil shear modulus to the pile Young's modulus might increase or decrease the damping of the pile groups system, i.e., the curves will have peaks and valleys. For example, as

shown in Figure 5-27, when the ratio of the soil shear modulus to pile Young's modulus was 3.83×10^{-4} and 2.6×10^{-4} which is equivalent to dimensionless frequency parameter (a_o) of 1.0, and 1.2 respectively, the damping of pile groups at $6D_{pile}$ showed a valley at G_{soil}/E_{pile} of 3.83×10^{-4} and a peak at G_{soil}/E_{pile} 2.6×10^{-4} . At the same values of dimensionless frequency parameter the minimum stiffness of the pile groups spaced at $6D_{pile}$ showed a valley at a_o of 1.0 and a peak at a_o of 1.2, as shown in Figure 5-13 (b).

Depending on the soil medium between the piles, the stress waves generated from each pile in the pile group will be subject to attenuation with distance and when encountering a pile in the group will result in refraction, reflection and change in phase. When the cylindrical stress waves generated from one pile in the group have the same frequency and phase as the cylindrical stress waves generated from another pile within the group, the damping of the soil pile system will decrease due to the amplification of the resulting waves. On the other hand, the damping of the soil pile system will increase when these stress waves are out of phase due to the de-amplification of the resulting wave. Thus resulting in the oscillatory behavior of the damping.

5.6 Forces and Displacements of Pile Groups

5.6.1 Static Forces and displacement in Piles

To determine the static forces and displacement of the individual piles within the pile group, a static unit load equals to 1.0 lb. was applied at the center of the pile cap as shown in Figure 5-35.

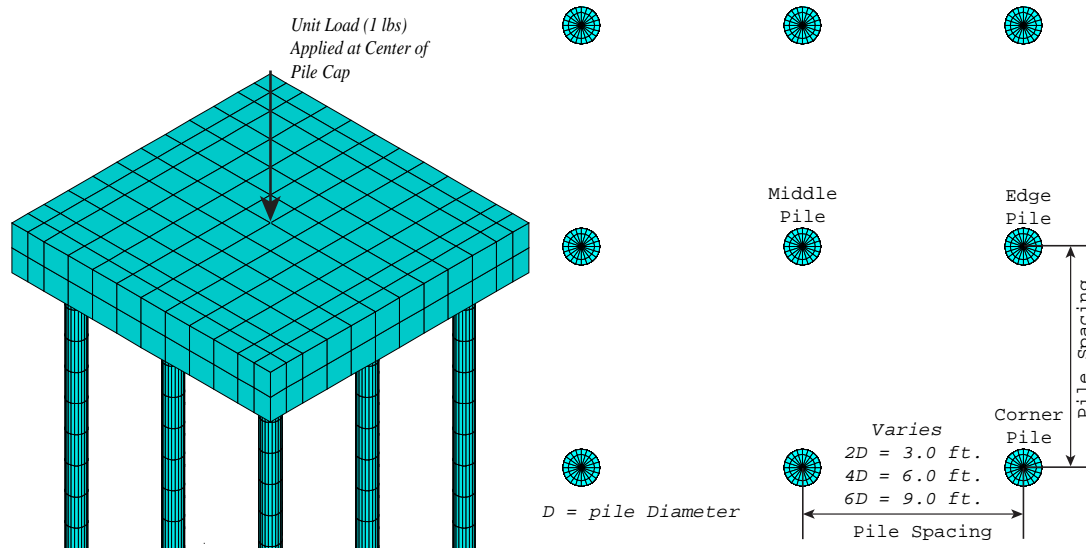


Figure 5-35: Unit Load Applied to Pile Cap

The static force in each pile within the pile groups are determined for two soil cases. Soil case 1 is for strong soils ($G_{soil}=17.20 \times 10^3$ ksf) and soil case 2 is for weak soils ($G_{soil}=0.172 \times 10^3$ ksf). The forces in the piles are determined for pile groups spaced at the $2D_{pile}$ (pile spacing = 3.0 ft.), $4D_{pile}$ (spacing = 6.0 ft.) and $6D_{pile}$ (spacing = 9.0 ft.). For each pile group spacing, the distribution of the static force along the pile length is also determined for a middle, corner and edge pile.

5.6.1.1 Forces in Pile Embedded in Strong Soils

Figures 5-36, 5-37 and 5-38 show the force distribution along the pile length for middle, corner and edge piles for the pile groups spaced at $2D_{pile}$, $4D_{pile}$ and $6D_{pile}$ in strong soils. The horizontal axis of the figures show the static vertical load acting on each pile while the vertical axis is the pile depth. The loads on the piles decreased with the pile depth. The decreased portion of the load is being carried by the surrounding soils. The decreased force along the pile length for a pile spaced at $2D_{pile}$ is larger than the decreased force along the pile length for piles spaced at $4D_{pile}$ and $6D_{pile}$. For example, the static force acting at the head of the pile and at the pile tip of the middle

pile spaced at $2D_{pile}$, shown in Figure 5-36, is 7.01×10^{-2} lbs. and 5.02×10^{-2} lbs. respectively. The percent variation between the force at the pile tip and the force at the pile head is 40%. This percent is reduced to 20% for the pile spaced at $6D_{pile}$, indicating a larger load being transmitted to the soil. i.e., more soil-pile load sharing.

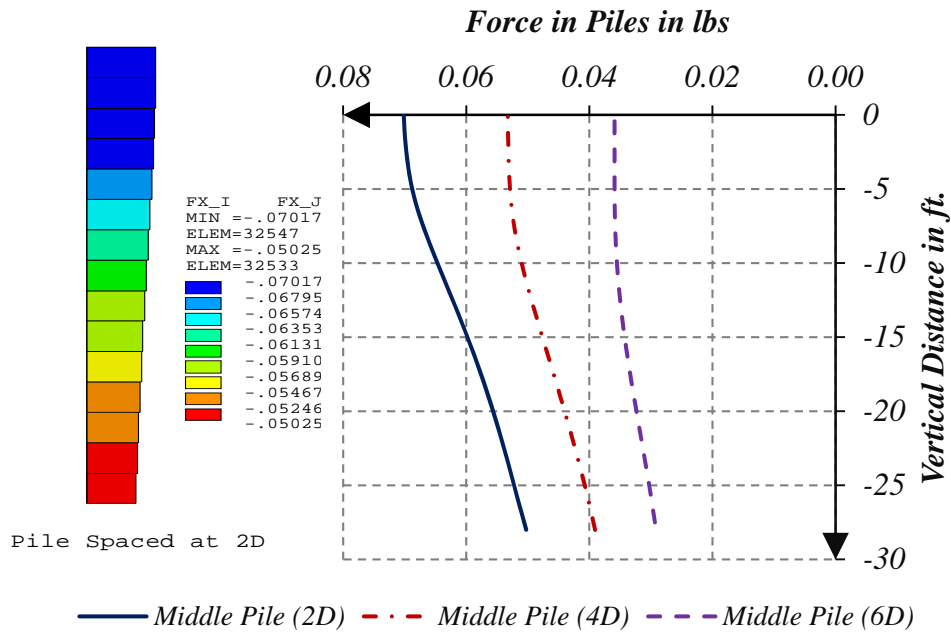


Figure 5-36: Static Force in Middle Pile for Pile Groups in Strong Soils ($G_{soil}=17.20 \times 10^3$ ksf and $f_c = 3000$ psi)

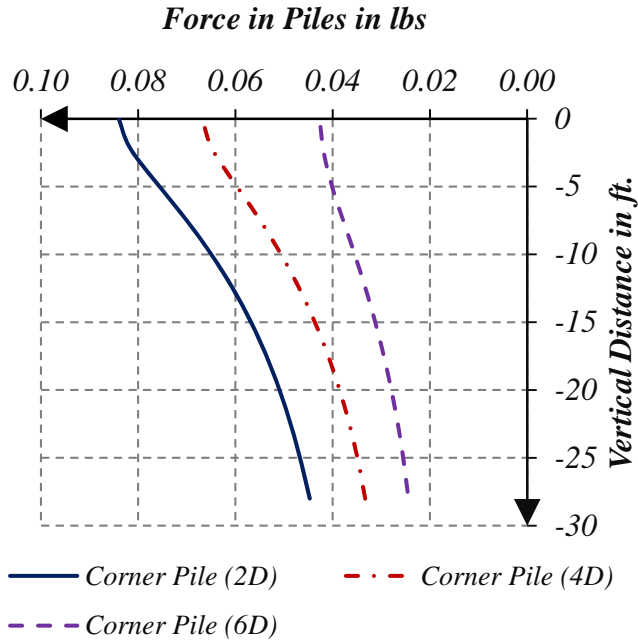


Figure 5-37: Static Force in Corner Pile for Pile Groups in Strong Soils ($G_{soil} = 17.20 \times 10^3$ ksf and $f_c = 3000$ psi)

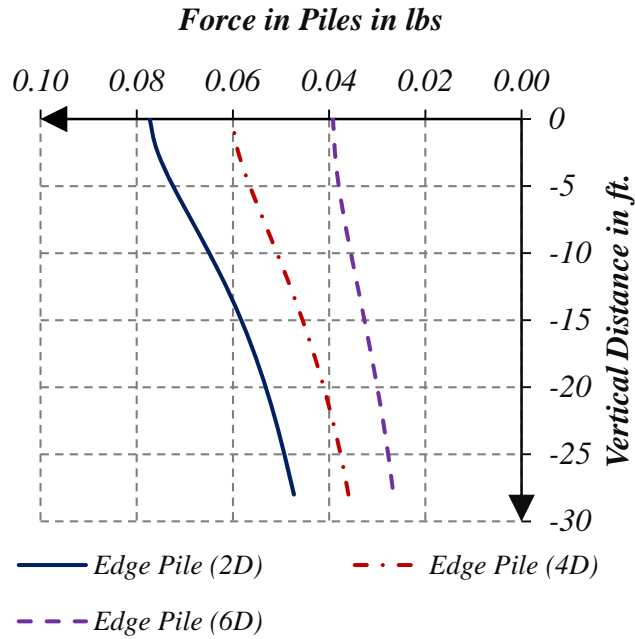


Figure 5-38: Static Force in Edge Pile for Pile Groups in Strong Soils ($G_{soil} = 17.20 \times 10^3$ ksf and $f_c = 3000$ psi)

The forces in the middle, corner and edge piles for pile groups spaced at $2D_{pile}$ is higher than piles spaced at $4D_{pile}$ as well as piles spaced at $6D_{pile}$, as shown in Table 5-1.

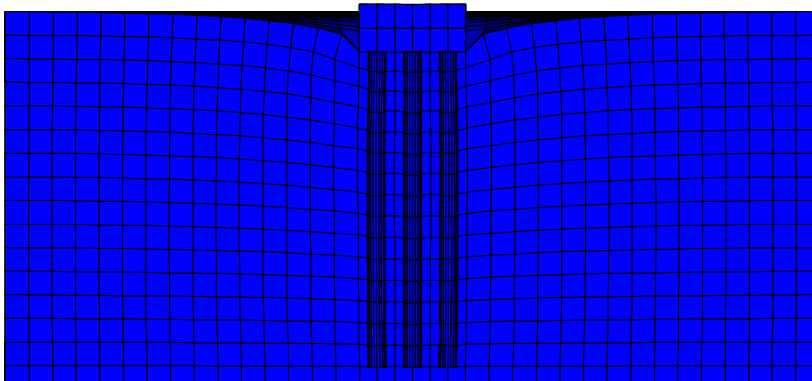
Table 5-1: Static Loads on Piles Embedded in Strong Soils

	<i>Max. Load on Middle Pile in lbs.</i>	<i>Max. Load on Edge Pile in lbs.</i>	<i>Max. Load on Corner Pile in lbs.</i>
<i>Piles Spaced at $2D_{pile}$</i>	7.02×10^{-2}	7.73×10^{-2}	8.40×10^{-2}
<i>Piles Spaced at $4D_{pile}$</i>	5.33×10^{-2}	6.01×10^{-2}	6.68×10^{-2}
<i>Piles Spaced at $6D_{pile}$</i>	3.59×10^{-2}	3.92×10^{-2}	4.27×10^{-2}

For pile groups spaced at $2D_{pile}$, the total loads on the piles is $(7.02 \times 10^{-2} + 4 \times 7.73 \times 10^{-2} + 4 \times 8.40 \times 10^{-2} = 0.72 \text{ lbs}$, i.e., 72% of the load is resisted by the piles and 28% of the load is resisted by the soil. The percent of the load resisted by the piles is reduced to 56% for piles spaced at $4D_{pile}$ ($5.33 \times 10^{-2} + 4 \times 6.01 \times 10^{-2} + 4 \times 6.68 \times 10^{-2} = 0.56 \text{ lbs}$.) and 36% for piles spaced at $6D_{pile}$. The increase in pile forces for piles spaced at $2D_{pile}$ is attributed to the effect of the load sharing between the soil and the pile, which increases as the spacing between the piles increases since the inter-pile soil volume increases. This results in higher load sharing between the soils and the pile and thus reduces the load on the piles. The effect of soil load sharing is also shown for the portion of the load being transmitted to middle, corner and edge piles within the pile groups having the same pile spacing. For the same piles spacing, the load on the middle pile is less than the load on the edge pile, which is also less than the load on the corner pile. The tributary area of the soil around the middle, edge and corner pile is s^2 , $\frac{1}{2} s^2$ and $\frac{1}{4} s^2$ (where s is the pile spacing). Thus the load sharing is higher for the middle pile than the edge pile and the load sharing between the soil and edge pile is higher than the soil and the corner pile. Thus the load on the middle pile is less than the load on the edge pile, and the load on the edge pile is less than the load on the corner pile, as shown in Table 5-1.

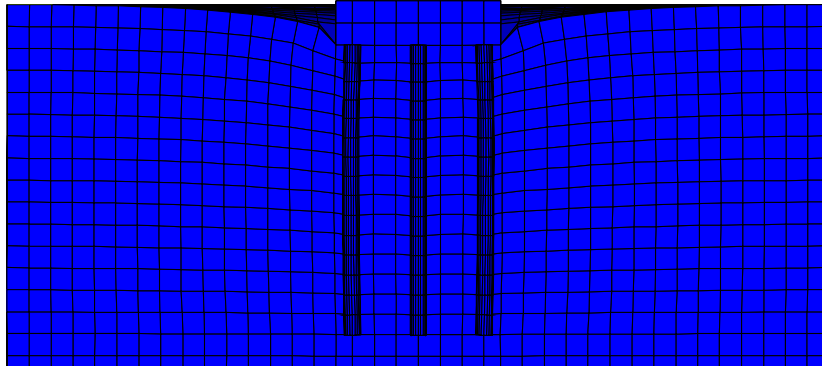
5.6.1.2 Static Displacement of Pile Groups in Strong Soils

The effect of soil pile load sharing is also shown to reduce the pile group vertical displacement, and consequently increases the group static stiffness as the pile spacing increases. Figure 5-39 shows the vertical displacement for pile groups spaced at the $2D_{\text{pile}}$, $4D_{\text{pile}}$ and $6D_{\text{pile}}$ in strong soils ($G_{\text{soil}} = 17.2 \times 10^3$ ksf). The displacement of pile groups spaced at the $2D_{\text{pile}}$ is $0.242\text{e-}8$ ft. which is 28% higher than the displacement of pile groups spaced at the $4D_{\text{pile}}$ ($0.188\text{e-}8$ ft.), and 82% higher than the pile groups spaced at the $6D_{\text{pile}}$ ($0.133\text{e-}8$ ft.). Thus the static stiffness of pile groups spaced at the $2D_{\text{pile}}$ is less than pile groups spaced at $4D_{\text{pile}}$ and $6D_{\text{pile}}$. The increase in the stiffness for pile groups at $6D_{\text{pile}}$ and $4D_{\text{pile}}$ in strong soils is due to the effect of load sharing between the piles within the groups and soils around the piles, which increases as the spacing of the pile increases, thus resulting in reducing the vertical displacement and increasing the stiffness of the pile group.



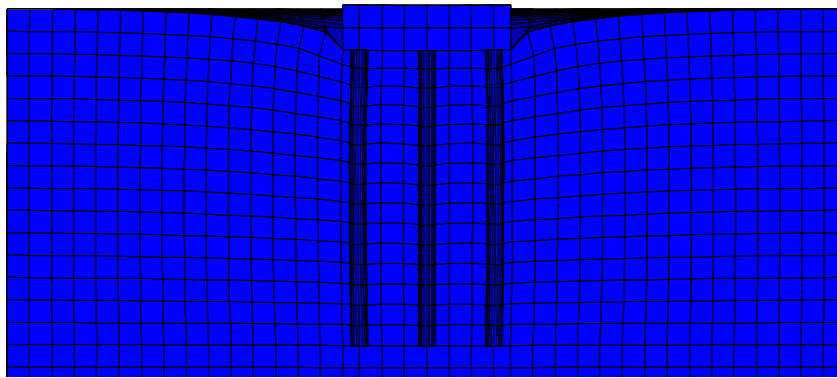
Maximum
Displacement
at the center of
the pile cap =
 $0.242\text{e-}8$ ft.

(a) Pile Groups Spaced at $2D_{\text{pile}}$



Maximum Displacement at the center of the pile cap = $0.188e-8$ ft.

(b) Pile Groups Spaced at $4D_{pile}$



Maximum Displacement at the center of the pile cap = $0.133e-8$ ft.

(c) Pile Groups Spaced at $6D_{pile}$

Figure 5-39: Static Displacement of Pile Groups in Strong Soils

5.6.1.3 Forces in Piles Embedded in Weak Soils

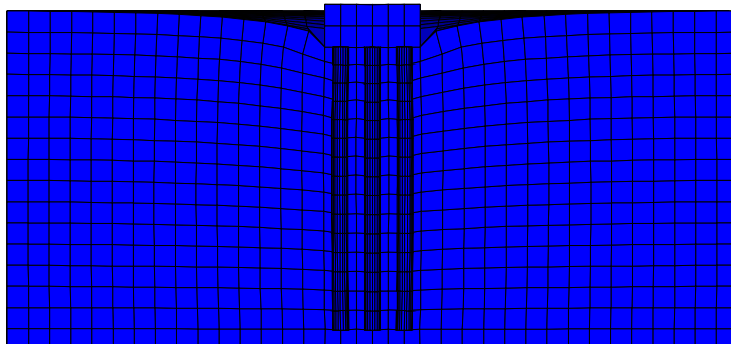
The effect of soil in load sharing is reduced when the piles are embedded in weak soil. This is shown in Table 5-2 where the load is equally distributed among the piles within the group and all the piles carry the same load as shown in Table 5-2.

Table 5-2: Static Loads on Piles Embedded in Weak Soils

	<i>Load on Middle Pile in lbs.</i>	<i>Load on Edge Pile in lbs.</i>	<i>Load on Corner Pile in lbs.</i>
<i>Piles Spaced at $2D_{pile}$</i>	<i>-0.11072</i>	<i>-0.11072</i>	<i>-0.11072</i>
<i>Piles Spaced at $4D_{pile}$</i>	<i>-0.11072</i>	<i>-0.11072</i>	<i>-0.11072</i>
<i>Piles Spaced at $6D_{pile}$</i>	<i>-0.11072</i>	<i>-0.11072</i>	<i>-0.11072</i>

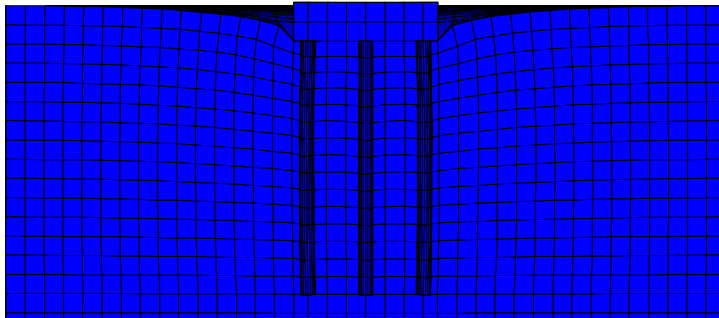
5.6.1.4 Static Displacement of Pile Groups in Weak Soils

Figure 5-40 shows the vertical static displacement of pile groups in weak soil ($G_{\text{soil}} = 0.172 \times 10^3$ ksf). The vertical displacements were the same for pile groups with different spacing due to the reduction of the load sharing effect between the pile and soil and thus the system stiffness being totally governed by the axial stiffness of the pile groups.



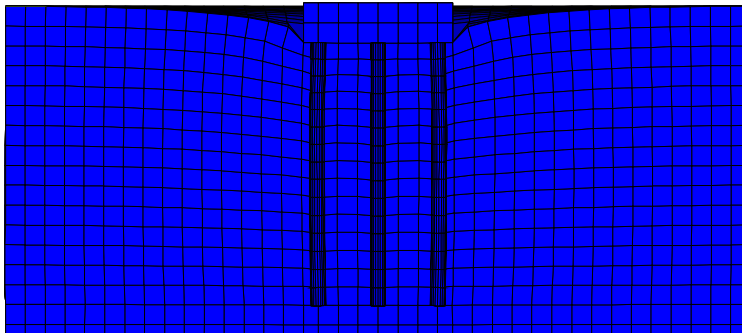
Maximum Displacement at the center of the pile cap. = $0.447\text{e-}8$ ft.

(a) Pile Groups Spaced at $2D_{\text{pile}}$



Maximum Displacement at the center of the pile cap = $0.447\text{e-}8$ ft.

(b) Pile Groups Spaced at $4D_{\text{pile}}$



Maximum Displacement at the center of the pile cap. = $0.447\text{e-}8$ ft.

(c) Pile Groups Spaced at $6D_{\text{pile}}$

Figure 5-40: Static Displacement of Pile Groups in Weak Soils

5.6.2 Dynamic Forces and Displacement in Piles

Novak (1974) stated that the load on each pile in the pile group is not equal when their displacements are equal. Dobry and Gazetas (1988) in a group of nine piles (three by three grouping) stated that the rigidity of the pile cap produces the same vertical displacement of all the piles and thus the force in each pile will then differ. Three cases were analyzed as follows:

Case 1: A group of 2 x 2 piles as shown in Figure 5-41. The force time history was found to be the same for all piles, thus the forces on the piles were the same.

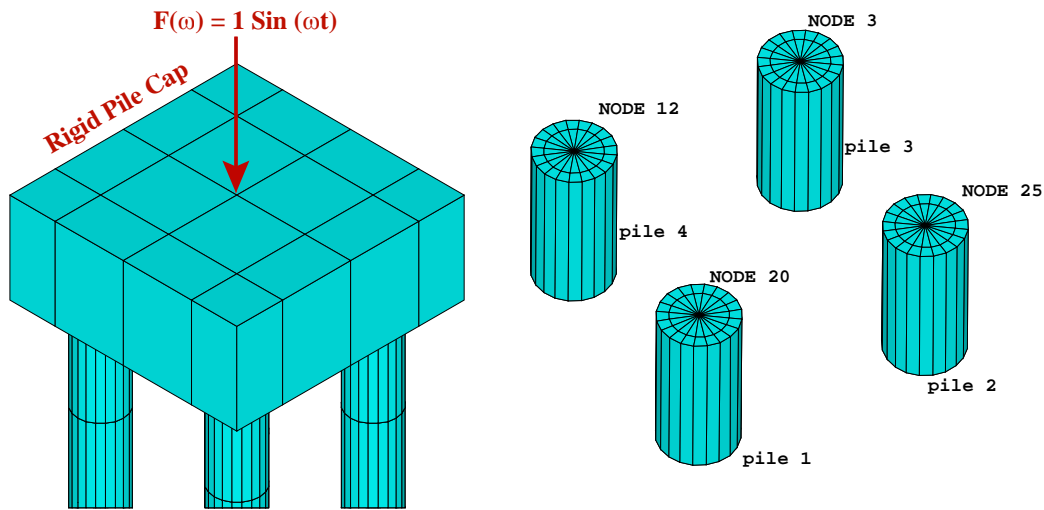


Figure 5-41: Case 1-a 2 x 2 group of pile

Case 2: A group of 3 x 3 piles were analyzed for a dimensionless frequency parameter $a_0 = 0.2$, i.e. $G_{soil} = 17.2 \times 10^3$ ksf as shown in Figure 5-42. In this case, it was found that the force in the corner pile (Pile 1) was greater than the force in the edge pile (Pile 2), which in turn was greater than the force in the middle pile. The larger increase in the pile force for the corner pile than for the edge pile and middle pile are attributed to the effect of the soil load sharing for the middle pile and edge pile. In the middle pile,

the area of soil around the pile is s^2 , where s is the pile spacing, as the soil deposit gets stronger, the soil shares the load with the pile and part of the force is transmitted to the soil, which reduces the force on the piles. For corner piles and edge piles, on the other hand, the effective soil area contributing to the load sharing is $\frac{1}{4} s^2$ and $\frac{1}{2} s^2$ respectively, thus the contribution to the load sharing is less than the middle pile and the load on the corner pile and edge pile increases. The load sharing between the soil pile elements is shown in Figure 5-43, which shows the vertical force distribution on a vertical cut of the soil pile system in strong soils. The figure shows a large portion of the load is transmitted to the soil elements (identified by the dark blue color) under the foundation which leads to a reduction in the load on the middle pile. At a further increase in distance from the pile-soil foundation the load dissipates within the soil elements until the load completely dissipates at a distance approximately equal to the pile cap length. The force amplitude in each pile is shown in Table 5-3.

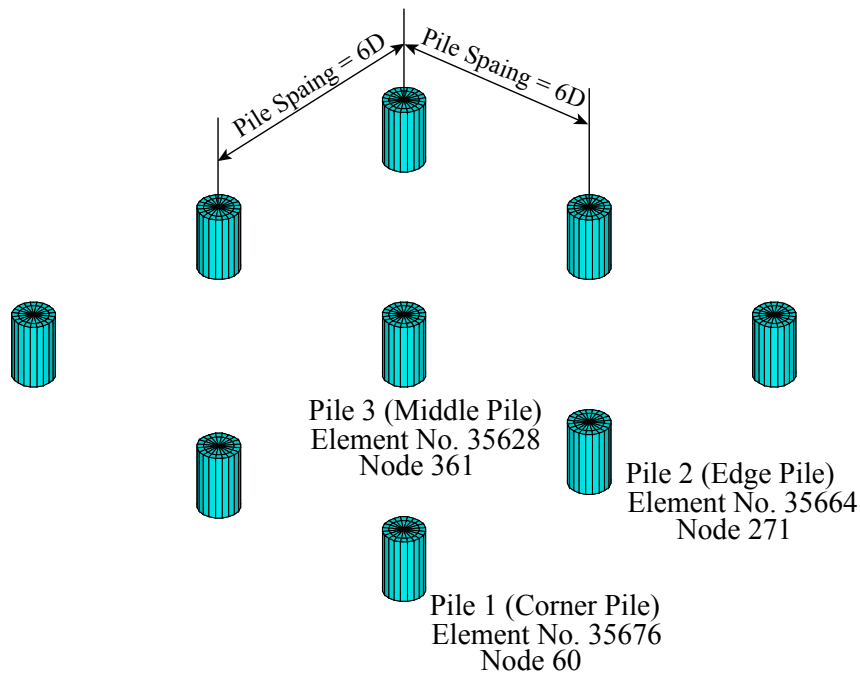


Figure 5-42: A Group of Piles 3 x 3 Spaced at 9 ft.

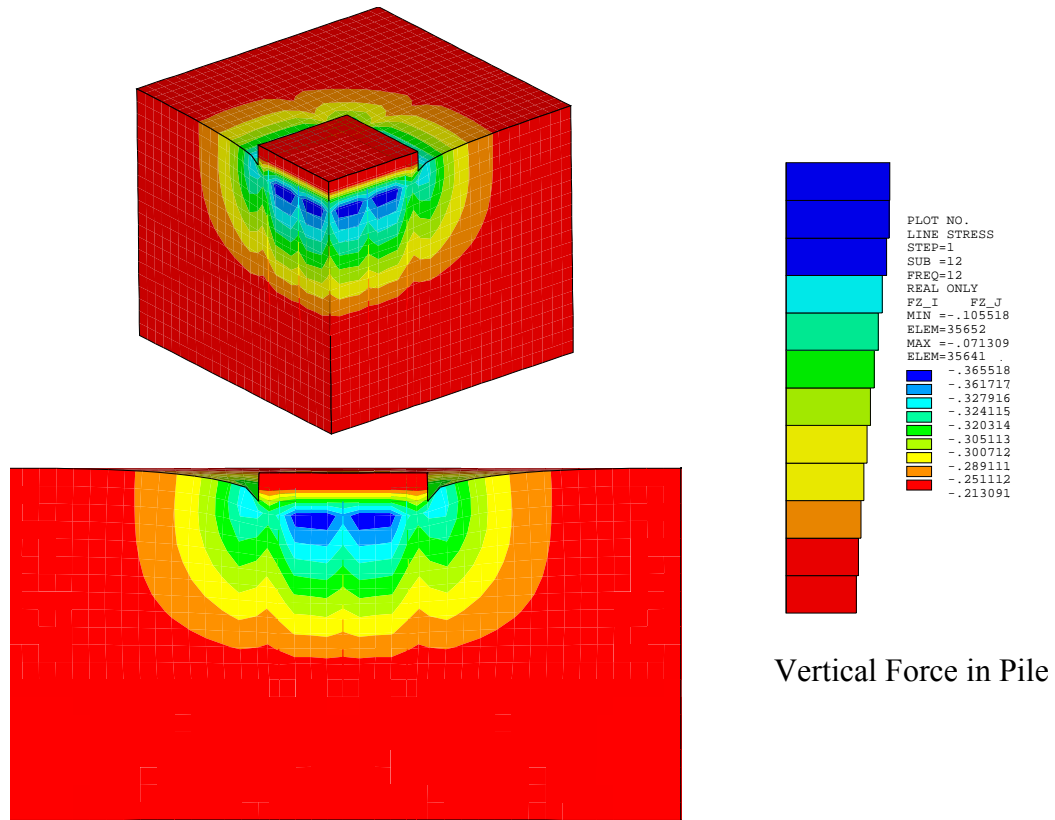


Figure 5-43: Vertical Force Distribution in the Soil Pile System in Strong Soil
 ($a_0 = 0.2$ and $G_{soil} = 17.2 \times 10^3$ ksf)

Table 5-3: Forces Amplitude for Piles in Strong Soils at Resonance (12Hz)

	<i>Forces in Pile in lbs.</i>	<i>% of the load</i>
<i>Pile 1 (Corner Pile)</i>	0.36 lbs.	$\frac{0.36lbs}{0.36 + 4 \times 0.31 + 4 \times 0.27} \cong 13\%$
<i>Pile 2 (Edge Pile)</i>	0.31 lbs.	$\frac{0.31lbs}{0.36 + 4 \times 0.31 + 4 \times 0.27} \cong 11.5\%$
<i>Pile 3 (Middle Pile)</i>	0.27 lbs.	$\frac{0.27lbs}{0.36 + 4 \times 0.31 + 4 \times 0.27} \cong 10\%$

As shown in Table 5-3, the total force in the pile groups is $0.36 \text{ lbs.} \times 4 + 0.31 \text{ lbs.} + 0.27 \text{ lbs.} \times 4 = 2.83 \text{ lbs.}$ This force is almost double the applied force amplitude. This increase in the total pile force is due to the effect of the additional inertia loads resulting from the vibrating soil continuum at resonance.

Case 3: A group of 3 x 3 piles were analyzed for a dimensionless frequency parameter $a_0 = 2.0$, i.e., $G_{soil} = 0.172 \times 10^3$ ksf. In this case, the soil deposit is characterized as a weak soil deposit and the effect of load sharing between the soil and the pile element is diminished. The pile cap moves as a rigid body under the effect of dynamic excitation emitting harmonic waves within the soil medium and exciting the whole soil continuum, as shown in Figure 5-44. For this case, the rigid body motion of the pile cap generates an equal force distributed among the pile elements and maintaining an equal displacement at the connection node between the pile head and the pile cap.

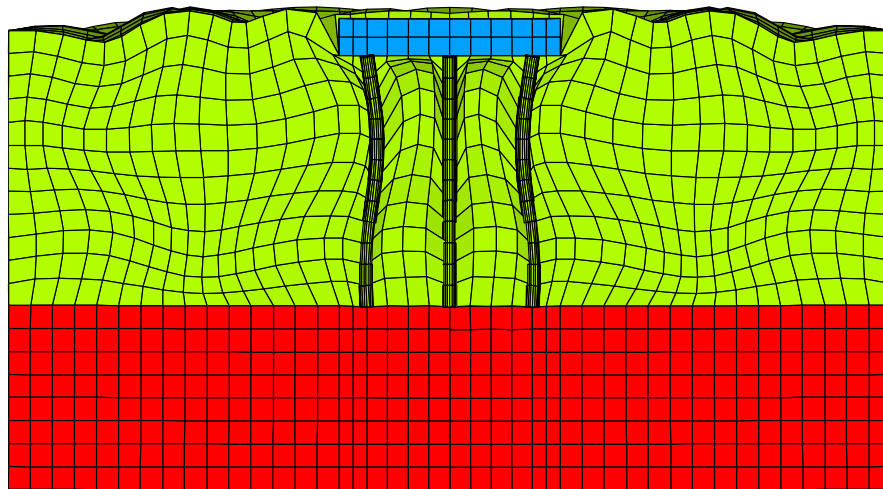


Figure 5-44: Displacement of Pile Group for Weak Soil
($a_0 = 2.0$ and $G_{soil} = 0.172 \times 10^3$ ksf)

Figure 5-45 shows the force time history for corner, middle and edge piles. The force amplitude at each pile is summarized in Table 5-4.

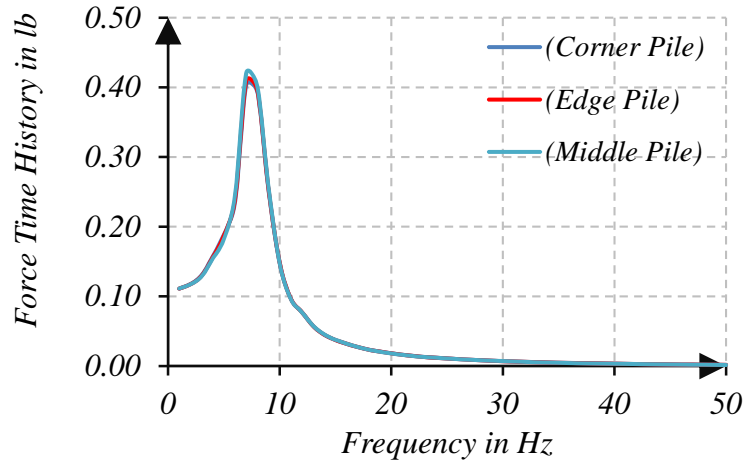


Figure 5-45: Force Time History for Pile Group in for Weak Soil
 $(a_0 = 2.0$ and $G_{soil} = 0.172 \times 10^3$ ksf)

Table 5-4: Forces amplitude in the piles for weak soil at resonance (7.0Hz)

	<i>Forces in Pile in lbs.</i>	<i>% of the load</i>
<i>Pile 1 (Corner Pile)</i>	0.42 lbs.	$\frac{0.42lbs}{0.42 + 4 \times 0.42 + 4 \times 0.42} \cong 11\%$
<i>Pile 2 (Edge Pile)</i>	0.42 lbs.	$\frac{0.42lbs}{0.42 + 4 \times 0.42 + 4 \times 0.42} \cong 11\%$
<i>Pile 3 (Middle Pile)</i>	0.42 lbs.	$\frac{0.42lbs}{0.42 + 4 \times 0.42 + 4 \times 0.42} \cong 11\%$

Shown from Table 5-4, the total force in the pile groups is $0.42 \text{ lbs.} \times 9 = 3.78 \text{ lbs.}$ The increase in the total pile force is due to the effect of the additional inertia loads resulting from the vibrating soil continuum at resonance.

5.6.3 Summary

In the static case, the distribution of forces among the 3×3 pile group is dependent on the variation of the soil shear modulus and the pile spacing. In a weak soil, soil sharing of the load is minimum and for all pile spacing $2D_{pile}$, $4D_{pile}$ and $6D_{pile}$, the displacement of the pile cap in all cases is the same and the load carried by the individual piles were also the same, i.e., $1/9$ of the applied load (0.11 lbs.). For the case

of strong soils, the displacement of the pile cap was larger for the case of a pile group spacing at $2D_{\text{pile}}$ and smallest for the case of a pile group spacing at $6D_{\text{pile}}$. The distribution of the forces among the piles showed that the corner piles carried the largest portion of the applied load, followed by the edge pile, and the middle pile carried the smallest load. All loads decreased with the increase of the pile spacing. At a spacing of $2D_{\text{pile}}$, the forces on the piles were almost double the forces in the case of a spacing of $6D_{\text{pile}}$.

In the dynamic case, the case of the 2 x 2 pile group, due to the symmetry the four piles equally shared the applied load. For the case of 3 x 3 pile groups, similar to the static case, the rigidity of the pile cap produced the same vertical displacement of the piles but the forces transmitted by each pile differed. At resonance, for weak soils, all piles carried the same load and for strong soils, the corner pile carried the largest load followed by the edge pile and the smaller load was carried by the middle pile. In the dynamic case, the total load on the piles were amplified to 3.78 in weak soil and 2.83 for strong soil relative to the 1 lbs. load applied.

5.7 Pile Interaction and Group Efficiency

5.7.1 Static Efficiency Factors

Under a static load, the group of piles experienced an increase in settlement in comparison to the settlement of an individual pile. This was because the displacement of the pile increased if the pile was located within the deformation field of a neighboring pile, as a result the overall displacement of a group of piles was greater than the displacement of an individual pile. Another factor in the static interaction was that with the use of a rigid cap, a redistribution of the forces in the piles would occur

as discussed in section 5.6.1. To determine the static efficiency factor, a single pile as well as a group of piles were subjected to a 1 lb. axial load. The vertical displacement for the single pile and pile groups spaced at $2D_{pile}$, $4D_{pile}$ and $6D_{pile}$ were determined as shown in Figure 5-39. The displacement of piles spaced at $2D_{pile}$, $4D_{pile}$ and $6D_{pile}$ were 0.242×10^{-8} , 0.188×10^{-8} and 0.133×10^{-8} , respectively. i.e., the displacement of piles spaced at $2D_{pile}$ was higher than the displacement of piles spaced at $4D_{pile}$ and $6D_{pile}$. The increase in the group displacement resulted in a decrease in the group stiffness. Figures 5-46 and 5-47 show the axial stiffness for a single pile and for a pile group respectively.

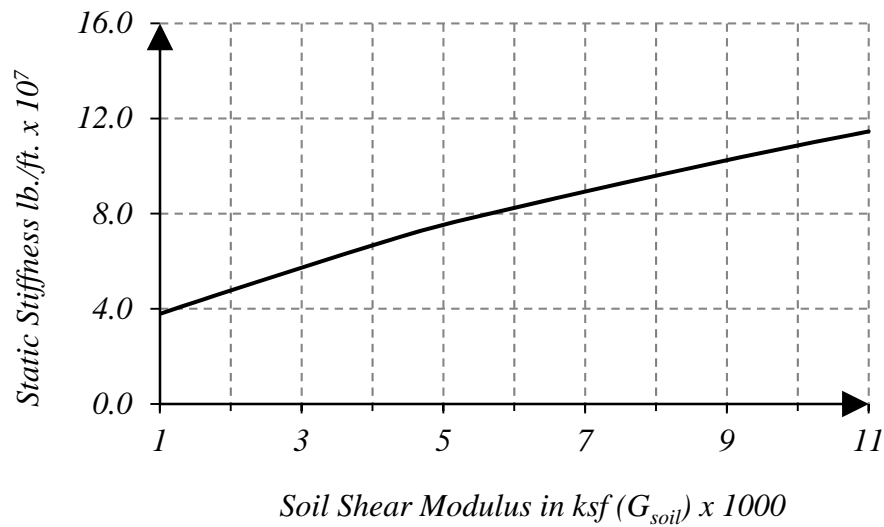


Figure 5-46: Static Stiffness for Single Pile for Pile Diameter = 1.50 ft. and Concrete Strength = 3000 psi

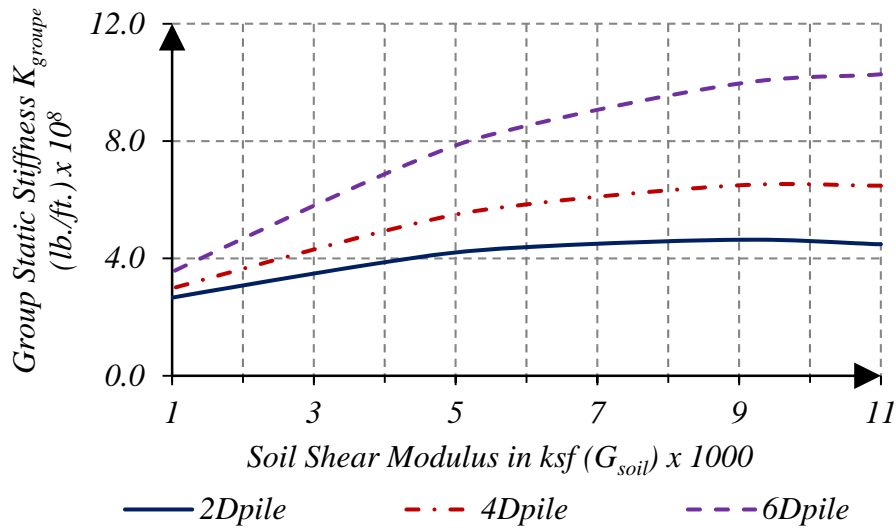


Figure 5-47: Static Stiffness for Pile Groups Spaced at 2D_{pile}, 4D_{pile} and 6D_{pile} for a Pile Diameter = 1.50 ft. and Concrete Strength = 3000 psi

As shown in Figure 5-47, the group stiffness for piles spaced at 6D_{pile} was higher than the stiffness of a group of piles spaced at 2D_{pile}. This increase in the group stiffness was due to the contribution of the load sharing between the soil and the piles.

The static efficiency factors were determined based on equation (5-2).

$$\alpha_{static} = \frac{K_{group}}{N_{pile}K_{single}} \quad (5-2)$$

where: $\alpha_{stiffness}$ was the static efficiency factor, N_{pile} was the number of piles within the group, K_{single} was the static stiffness of a single pile, K_{group} was the pile group static stiffness.

The static efficiency factor as a function in the soil shear modulus is shown in Figure 5-48.

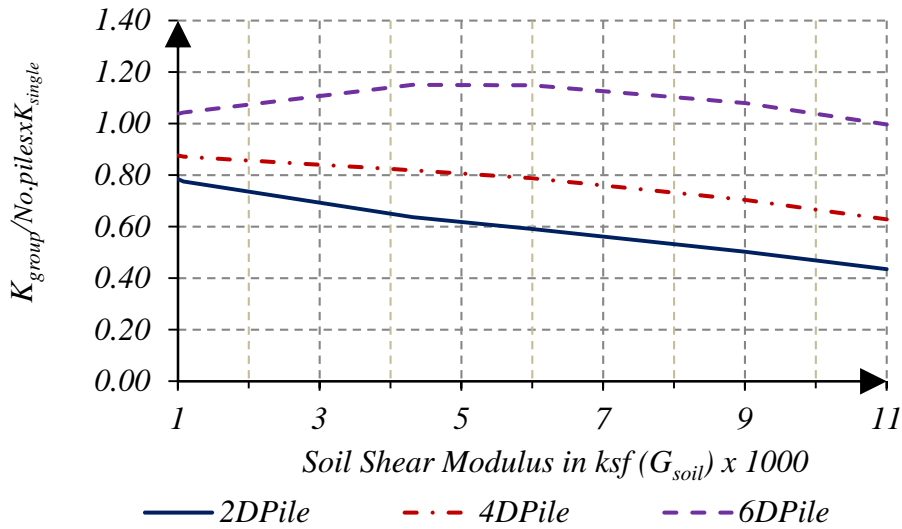


Figure 5-48: Static Efficiency Factors

As shown in Figures 5-46 and 5-47, the static stiffness of a single pile and of a pile groups increased with the increase in the soil shear modulus, however, the static efficiency of the pile group decreased with the increase in the soil shear modulus, as shown in Figure 5-48. Also shown in Figure 5-48, that the efficiency factor for the case of pile spaced at $6D_{pile}$ was larger than piles spaced at $4D_{pile}$ and $2D_{pile}$ and was slightly larger than 1.0. This is because the piles are farther apart and the increase in efficiency is due to the contribution of the load sharing between the soil and the piles.

For piles spaced at $2D_{pile}$ and $4D_{pile}$, at low values of shear modulus, the piles acted as end bearing and thus the efficiency was close to one. For strong soils, i.e., for higher values of shear modulus, the piles act as a friction piles. Thus in the case of friction piles, the interference of the stress field of each pile with the adjacent pile caused the efficiency to be reduced. With the increase in the shear modulus of the soils, the more interference of the stress field occurs.

If we compare the results with the static efficiency factors presented by Randolph and Poulos (1982), they showed an average value of 0.6 for spacing of the $6D_{pile}$ and 0.5 for the $4D_{pile}$ and 0.4 for the $2D_{pile}$ (see Appendix C). Whereas AASHTO (2012), for a pile group in clay, if the soil at the surface was soft an efficiency factor of 0.65 was proposed for a pile spacing at a $2.5D_{pile}$ and it increased to 1.0 for a pile spacing of a $6D_{pile}$. Figure 5-49 shows a comparison between the FE solution for different values of soil shear modulus (G_{soil}) and AASHTO. The figure shows good correlation between them.

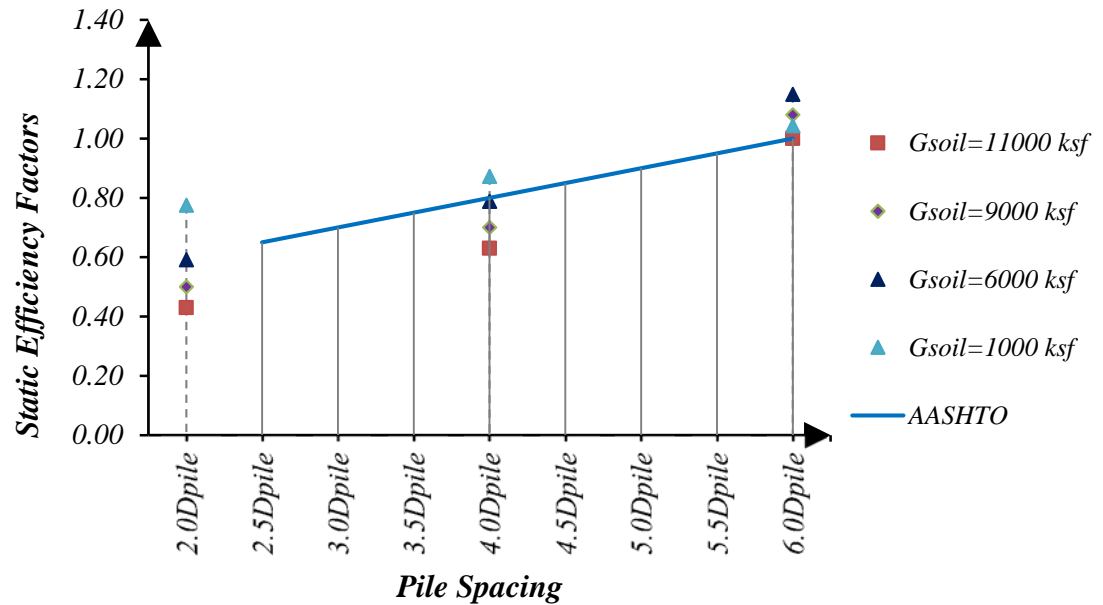


Figure 5-49: Static Efficiency Factors Based on AASHTO and FE

5.7.2 Dynamic Efficiency Factor

The dynamic stiffness and damping efficiency factors were determined from equations (5-3) and (5-4).

$$\alpha_{stiffness} = \frac{K_{group}}{N_{pile}K_{single}} \quad (5-3)$$

$$\alpha_{damping} = \frac{C_{group}}{N_{pile}C_{single}} \quad (5-4)$$

Where: $\alpha_{stiffness}$ and $\alpha_{damping}$ were the stiffness and damping efficiency factor, N_{pile} was the number of piles within the group, K_{single} was the dynamic stiffness of a single pile, K_{group} was the dynamic stiffness for a group of piles, C_{single} was the vertical damping of a single pile and C_{group} was the damping for a group of piles.

The vertical dynamic stiffness efficiency factors were determined for piles having a concrete compressive strength of 3000 psi and spaced at $2D_{pile}$, $4D_{pile}$ and $6D_{pile}$. The results of the stiffness and damping efficiency factors are shown in Figures 5-50 and 5-51 as a function in the dimensionless frequency parameter (a_o).

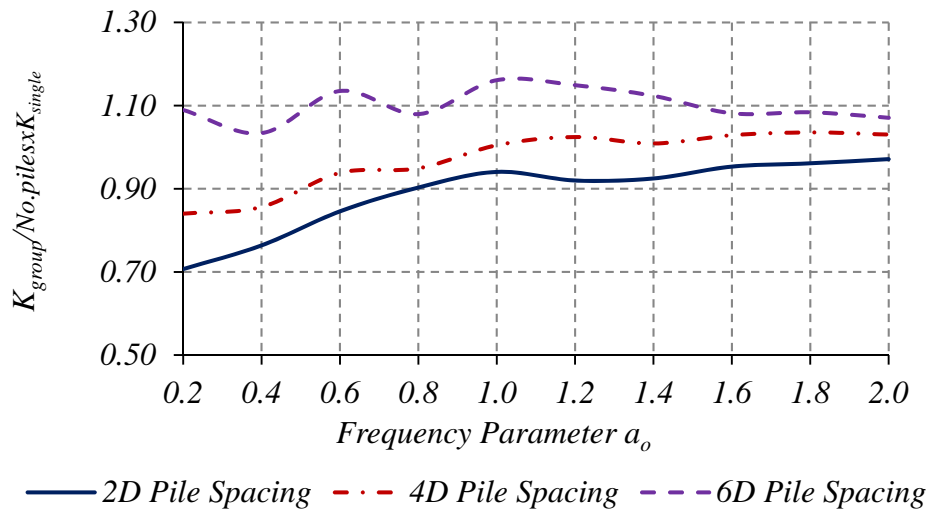


Figure 5-50: Stiffness Efficiency Factors

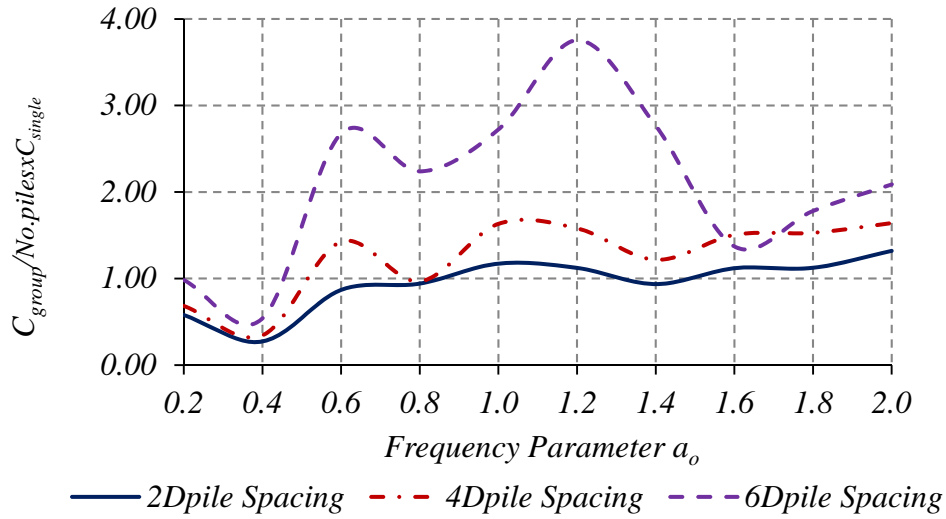


Figure 5-51: Damping Efficiency Factors

As shown in Figures 5-50 and 5-51, the pile group efficiency factors for the stiffness and damping also show an oscillatory behavior. The dynamic efficiency of the pile group differ considerably from the static efficiency of the pile group as they are a function of a_0 , and a_0 is a function of the machine frequency, pile diameter and soil shear modulus. The figures show that the efficiency factors for stiffness can be as high as 1.15 at a_0 equal to 1.0 and the efficiency factor for the damping can be as high as 3.75 for a_0 equal to 1.2. For a machine frequency of 50 Hz, both the dynamic stiffness and damping efficiency factors were plotted as a function of the soil shear modulus (G_{soil}) in Figures 5-52 and 5-53, respectively.

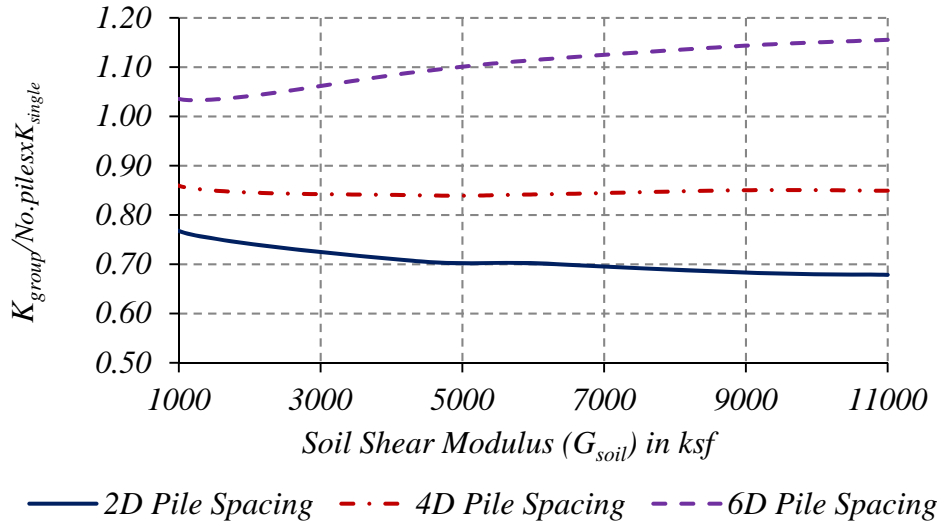


Figure 5-52: Group Stiffness Efficiency Factors as Function in (G_{soil}) (Piles Concrete Compressive Strength, $f_c = 3000$ psi)

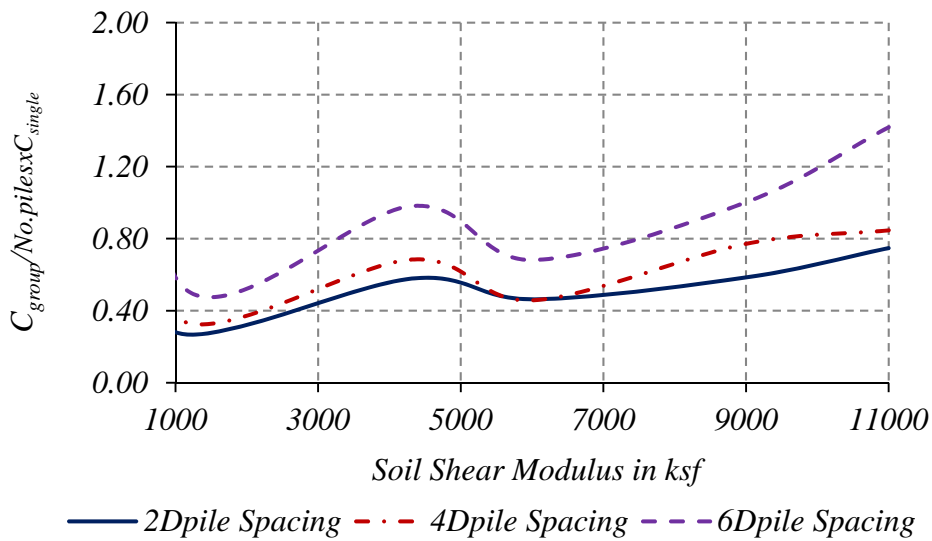


Figure 5-53: Group Damping Efficiency Factors as Function in (G_{soil}) (Piles Concrete Compressive Strength, $f_c = 3000$ psi)

As noted in Figures 5-52 and 5-53, the efficiency factors are much smoother when plotted against the shear modulus of the soil in comparison to the plots 5-50 and 5-51 against a_0 . Table 5-5 shows the wave length determined for soils with different shear modulus and for frequency of 50Hz. As shown in the table, the wavelength (λ) is greater than the pile spacing with the ratio of λ over the spacing is greater than 1.0 for

all cases. Thus the soil mass between the piles tended to vibrate in phase with the piles so the pile group soil system responded as a block.

Table 5-5: Wave Length in Soils with Different Shear Modulus

Shear Modulus (G_{soil}) in ksf	Wave length (λ) in ft.	$\lambda/2D_{pile}$	$\lambda/4D_{pile}$	$\lambda/6D_{pile}$
1,000	11.34	3.78	1.89	1.26
3,000	19.66	6.55	3.28	2.18
5,000	25.37	8.64	4.23	2.82
7,000	30.03	10.01	5.01	3.34
9,000	34.05	11.35	5.68	3.78
11,000	37.64	12.54	6.27	4.18

The stiffness efficiency factors for of the pile group spaced at $6D_{pile}$ increased by 12% as the soil shear modulus increased from 1,000 to 11,000 ksf. Changes in the soil pile system stiffness efficiency factors were almost constant for pile groups spaced at $4D_{pile}$, while the efficiency factors were reduced by 10% for pile groups spaced at $2D_{pile}$ when the soil shear modulus was increased from 1,000 to 11,000 ksf. For pile groups spaced at $6D_{pile}$, the effect of load sharing between the pile and soil resulted in an increase of the overall soil pile system stiffness. The effect of the load sharing was reduced when the piles were closely spaced and the interference of the soil shear stress field around the pile element resulted in a reduction of the soil pile system stiffness efficiency factors similar to the static case. In the case of the damping efficiency factor, it exhibited a more complicated behavior with the curves having peaks and valleys. When the spacing became smaller such as the spacing of $2D_{pile}$, the curve became smoother.

Figures 5-54 to 5-56 show the vertical shear stress within the continuum at a frequency of 50Hz and soil shear modulus of 1,000, 6,000 and 11,000 ksf, respectively. The figures show that for the static case, at a low shear modulus, the piles acted as end bearings and at a high shear modulus, the piles acted as friction piles.

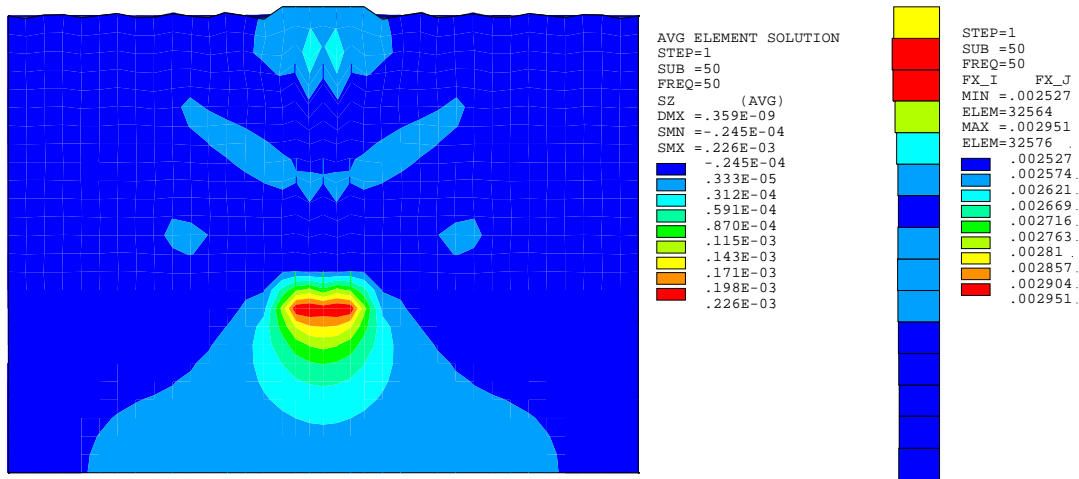


Figure 5-54: Vertical Stress in Soil-Pile Elements and Axial Load in Piles (Frequency = 50 Hz and $G_{soil} = 1,000$ ksf)

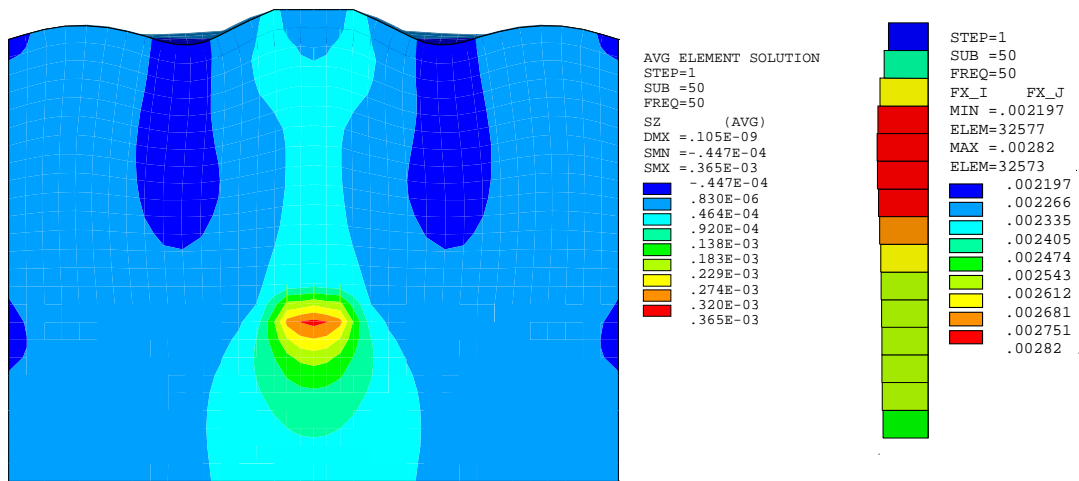


Figure 5-55: Vertical Stress in Soil-Pile Elements and Axial Load in Piles (Frequency = 50 Hz and $G_{soil} = 6,000$ ksf)

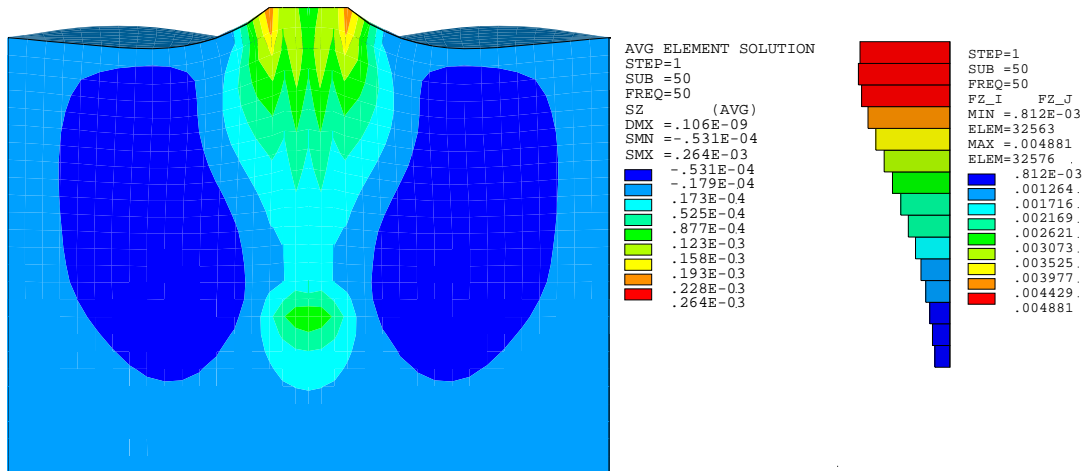


Figure 5-56: Vertical Stress in Soil-Pile Elements and Axial Load in Piles
(Frequency = 50 Hz and $G_{\text{soil}} = 11,000$ ksf)

The results provided showed efficiency factors that are less than or greater than one. This is in agreement with ACI 351 (2004), which states that “Group stiffness and damping can be either reduced or increased by pile-soil-pile interaction”. However, if we used the dynamic interaction equation provided by Dobry and Gazetas (1988), the results showed that the efficiency factor for the stiffness was about 0.3 for all pile spacings and the damping was 0.4 for all pile spacings (see Appendix C). Thus such an equation is not valid.

Chapter 6: Model Comparison

6.1 Comparison of Pile Static Stiffness with Mylonakis and Gazetas Solution

Mylonakis and Gazetas (1992) defined the vertical static stiffness of a single pile in a homogenous soil as follows:

$$K_{\text{pile}} = E_{\text{pile}} A_{\text{pile}} \lambda \frac{\Omega + \tanh(L_p \lambda)}{1 + \Omega \tanh(L_p \lambda)} \quad (6-1)$$

$$\text{where } \lambda = \sqrt{\frac{\delta G_{\text{soil}}}{E_{\text{pile}} A_{\text{pile}}}} \quad (6-2)$$

$$\text{and } \delta = \frac{2\pi}{\ln \frac{(2\chi_1 \chi_2 L_p [1 - \nu_{\text{soil}}])}{d_{\text{pile}}}} \quad (6-3)$$

χ_1 and χ_2 are constants defined by Gazetas equal to 2.5 and 1.0 respectively, Ω is a parameter which depend on the factor λL_p , G_{soil} is the soil shear modulus, E_{pile} is the pile Young's modulus, A_{pile} is the pile cross sectional area, L_p is the pile length, d_{pile} is the pile diameter and ν_{soil} is the soil's Poisson's ratio.

The vertical static stiffness determined from the finite element solution was compared to the results obtained using Mylonakis and Gazetas closed form solution for different values of the soil shear modulus and is shown in Figure 6-1.

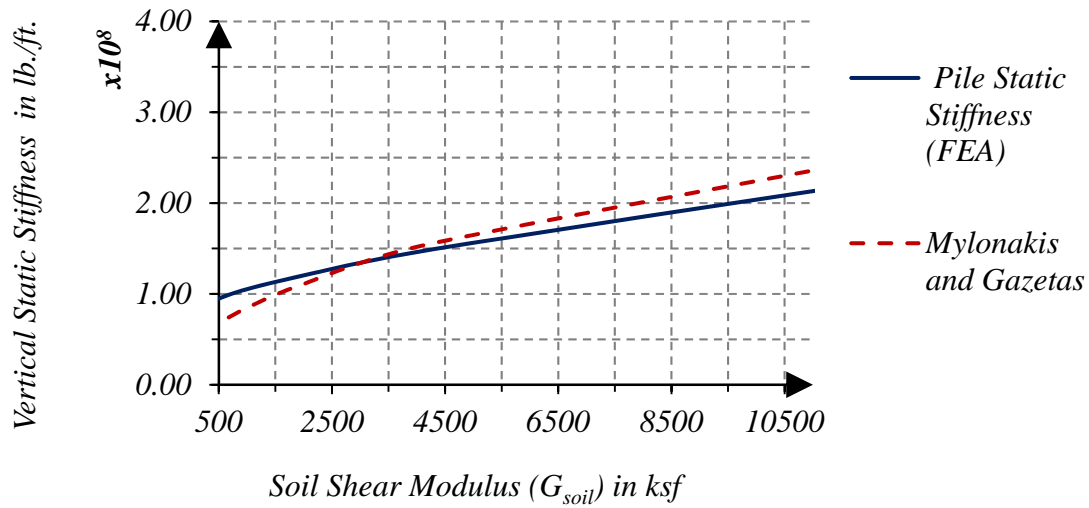


Figure 6-1: Comparison between Mylonakis and Gazetas and FEA Solution for Static Stiffness

From Figure 6-1 the difference between the pile vertical static stiffness calculated using Mylonakis and Gazetas and the one determined from the finite element solution is within 2%.

6.2 Comparison of the Pile Stiffness with DYNA5

Petrash et al. (2011), determined the impedance (dynamic stiffness and damping) for a 2 x 2 pile group, spaced at 3.0 ft. center to center using the DYNA5 program. The method used in DYNA5 for calculating the pile impedance is based on the plane strain method where elastic waves are assumed to propagate in a horizontal direction, similar to Novak's elasto-dynamic solution. In their calculation, the piles were assumed to be concrete and floating tip having a modulus of elasticity (E_p) of 804,230,000 lb./ft². The pile diameter and embedment was set equal to 1.0 ft. and 30 ft., respectively. The soil shear wave velocity and Poisson's ratio used in the DYNA5 model were 300 ft./s and 0.35. A constant material damping ratio of 5% was used for the soil elements while a material damping ratio of 10% was used for the pile element.

To verify the ANSYS model, the soil pile impedance determined by ANSYS were compared with the soil pile impedance determined using DYNA. The inputs to the ANSYS model were modified to match the input parameter used by Petrash et al. in the DYNA5 model. Figure 6-2 shows the ANSYS finite element model of the pile groups.

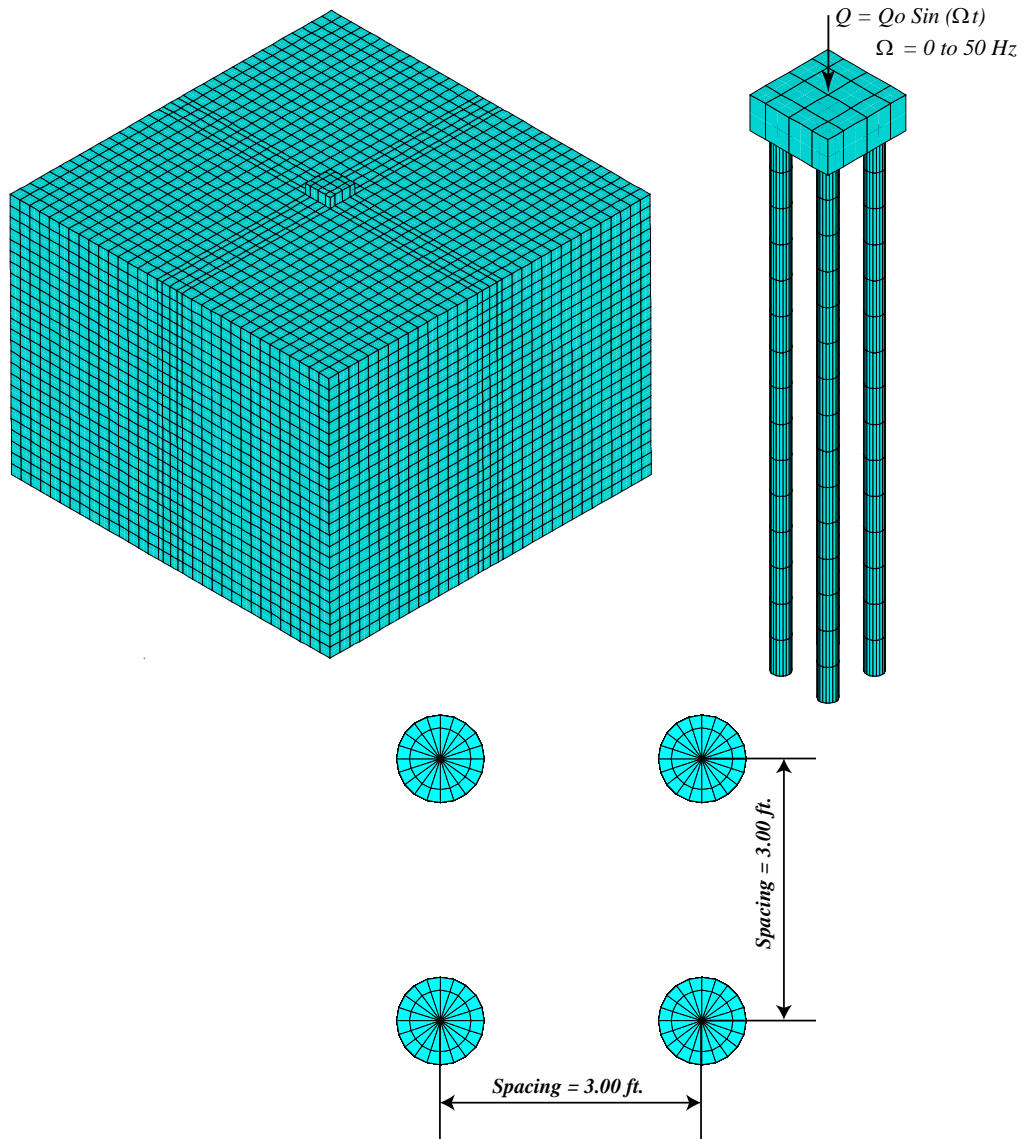


Figure 6-2: Modified ANSYS Finite Element Model

The ANSYS model was excited using a constant amplitude harmonic excitation force. The dynamic stiffness and damping of the pile-soil system was determined using

equation (4-2) and equation (4-6). Figure 6-3 shows the vertical displacement of the soil pile system at resonance as determined from the ANSYS model, while Figure 6-4 shows the vertical amplitude of the soil pile system as a function of the exciting frequency.

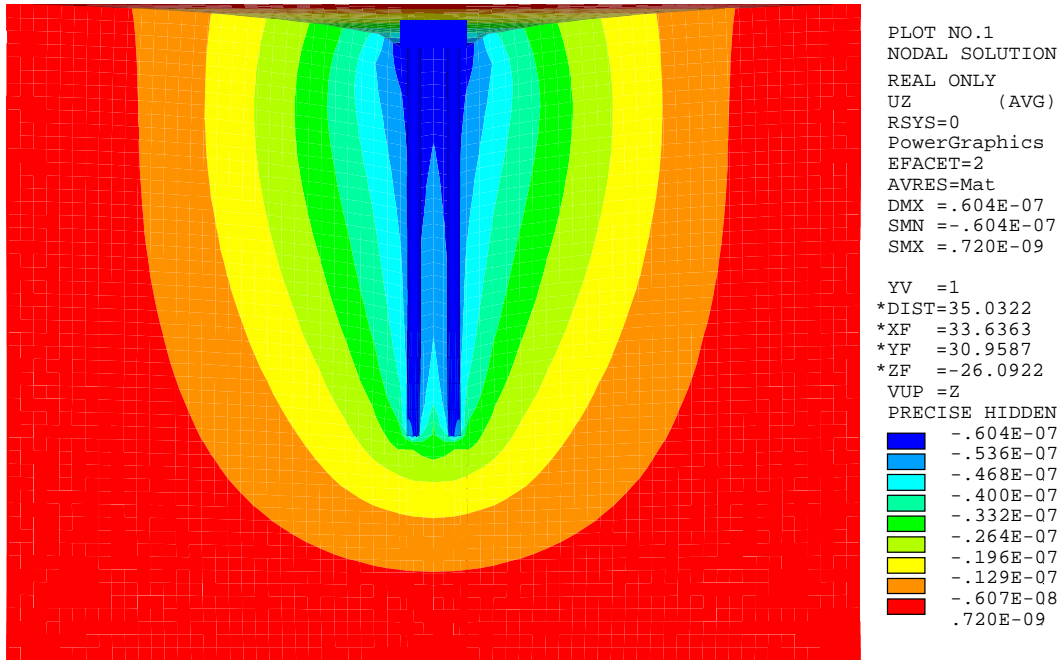


Figure 6-3: Vertical Displacement for Pile Group 2x2 and Spacing = 3.0 ft. at Resonance

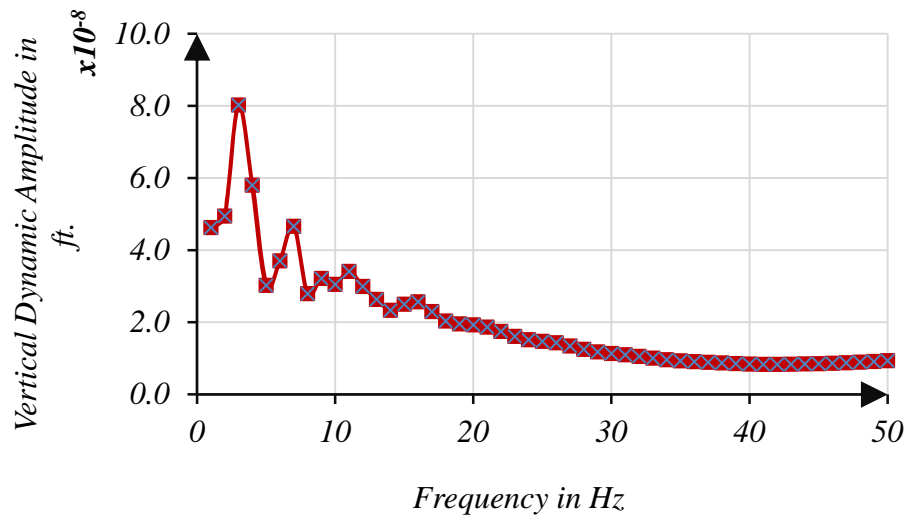


Figure 6-4: Vertical Displacement Amplitude of the Piles

The dynamic stiffness and damping determined from the finite element solution were summarized in Table 6-1. Also shown in the table are the results of the dynamic stiffness and damping determined using the DYNA5 solution.

Table 6-1: Comparison of Stiffness and Damping between ANSYS and DYNA5.

	ANSYS Solution	DYNA5 Solution	% Difference
Vertical Stiffness (lb. /ft.)	1.25E+7	1.50E+7	20 %
Damping (lb. sec/ft.)	3.81E+5	3.98E+5	4.46 %

The difference in the stiffness between the ANSYS solution and the DYNA5 solution is contributed to the three dimensional effects of the soil pile interaction considered in ANSYS while the DYNA5 solution is based on two dimension plane strain solution.

6.3 Comparison of the Pile Stiffness with Novak (1974) and Chowdhury & DasGupta (2009)

A comparison between the vertical dynamic amplitude response of a single pile obtained using the finite element solution (FEA) and using Novak (1974) closed form continuum solution and Chowdhury and DasGupta (2009) closed form solution was performed. A rectangular concrete foundation having a dimension of 2.0 ft. x 2.0 ft. and a 1.0 ft. thickness supporting a machine with a total mass of 10^5 lb. was used in the comparison. The foundation was assumed to be supported on a single pile having a diameter of 3.0 ft. and a pile length selected to be 30 ft. The soil material properties used in the model were defined based on the dimensionless frequency parameter (a_0).

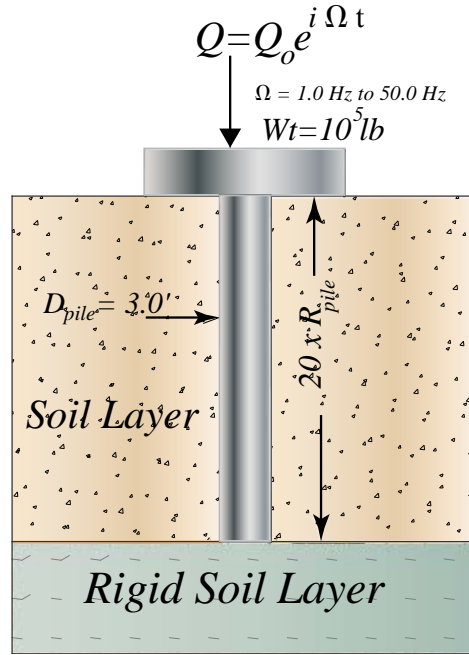


Figure 6-5: Block Foundation Supported on Piles

The pile material properties used in the model are as follows:

Young's modulus of pile material

$$E_{pile} = 57000\sqrt{f_c} \quad (6-4)$$

Shear Modulus of Pile Material

$$G_{pile} = \frac{E_{pile}}{2(1 + \nu)} \quad (6-5)$$

Where: f_c = pile concrete compressive strength = 3000 psi and ν = Poisson's ratio of concrete = 0.17.

The foundation was subjected to a vertical harmonic excitation force acting at the foundation center of gravity equal to the following equation:

$$Q = Q_0 \sin(\Omega t) = Q_0 e^{i\Omega t} \quad (6-6)$$

Where Ω = Applied frequency of the forcing function = 1 to 50 Hz and $Q_0 = 1.0 \text{ lb}$.

The amplitude response of the pile foundation system at different frequencies of excitation was computed based on the following equation:

$$A = \frac{Q_o}{K_{pile}} \frac{1}{\sqrt{\left(1 - \left(\frac{\omega_n}{\Omega}\right)^2\right)^2 + \left(2\zeta\left(\frac{\omega_n}{\Omega}\right)\right)^2}} \quad (6-7)$$

Based on Novak, the pile dynamic stiffness is computed as follows:

$$K_{pile} = \left[\frac{E_{pile} A_{pile}}{r_o} \right] \left(3.75 \left(\frac{V_s}{V_c} \right)^2 - 0.05 \left(\frac{V_s}{V_c} \right) + 0.0501 \right) \quad (6-8)$$

Chowdhury and DasGupta defined the pile dynamic stiffness as:

$$K_{pile} = \left[\frac{\pi^2 E_{pile} A_{pile}}{8L_{pile}} \right] + \left[\frac{2.7 G_{soil} L_{pile}}{2} \right] \quad (6-9)$$

Where: V_s = soil shear wave velocity, V_c = compression wave velocity of the pile material, G_{soil} , ρ_{soil} is the soil shear modulus and mass density, r_o = pile radius, A_{pile} is the pile cross sectional area, and ω_n = pile natural frequency.

Figures 6-6 to 6-8 shows the amplitude response of the pile foundation system presented in Figure 6-5. The presented results are based on the solution using the finite element model, Novak and Chowdhury and DasGupta closed form continuum solution for a range of frequency dependent parameter $a_o = 0.25$ to $a_o = 0.35$.

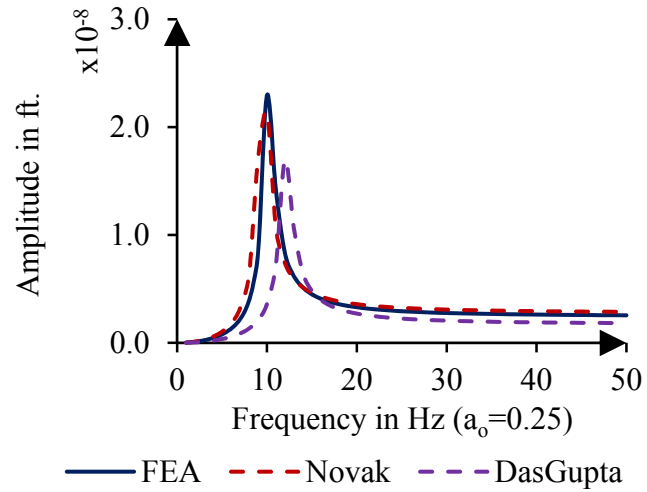


Figure 6-6: Comparison of Response between FEA and Novak at $a_0 = 0.25$

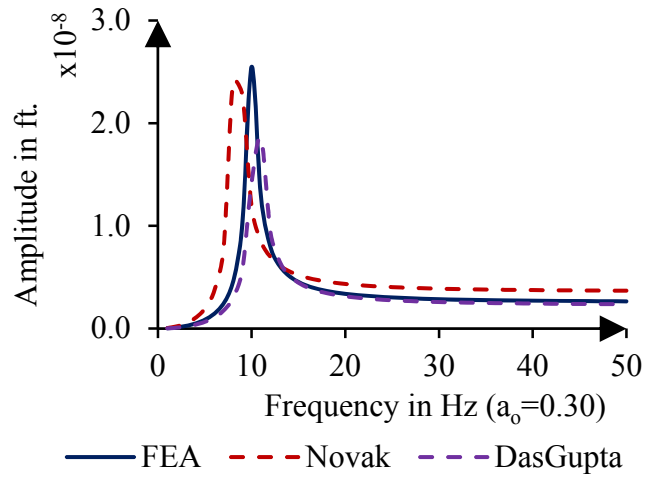


Figure 6-7: Comparison of Response between FEA and Novak at $a_0 = 0.30$

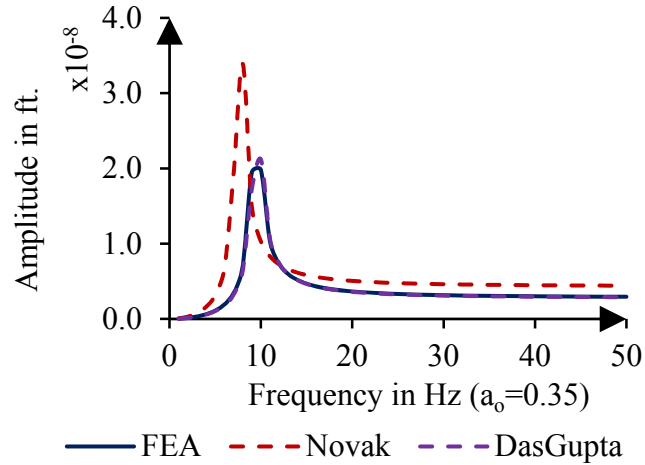


Figure 6-8: Comparison of Response between FEA and Novak at $a_0 = 0.35$

The percent differences between the finite element solution maximum amplitude and resonant frequency and Novak (1974) and Chowdhury & DasGupta (2009) closed form solutions of the soil pile system are shown in Table 6-2 to Table 6-3 for different values of the soil dimensionless frequency parameter (a_0).

Table 6-2: Comparison between FEA Solution and Novak Closed Solution

(a_0)	Novak Closed Form Solution		Finite Element Analysis		Percent Different in Amp.	Percent Different in Freq.
	Maximum Amplitude in ft.	Resonant Frequency in Hz	Maximum Amplitude in ft.	Resonant Frequency in Hz		
0.25	2.13×10^{-8}	9.54	2.29×10^{-8}	7.00	7.76%	26.65%
0.30	2.40×10^{-8}	8.41	2.55×10^{-8}	6.00	6.14%	28.68%
0.35	3.39×10^{-8}	7.66	1.982×10^{-8}	6.00	41.6%	21.63%

Table 6-3: Comparison between FEA and Chowdhury and DasGupta Solution

Soil Dimensionless Frequency Parameter (a_0)	Chowdhury and Dasgupta Closed Form Solution		Finite Element Analysis		Percent Different in Amp.	Percent Different in Freq.
	Maximum Amplitude in ft.	Resonant Frequency in Hz	Maximum Amplitude in ft.	Resonant Frequency in Hz		
0.25	1.69×10^{-8}	12.10	2.29×10^{-8}	7	35.44%	42.15%
0.30	1.85×10^{-8}	10.57	2.55×10^{-8}	6	37.91%	43.25%
0.35	2.12×10^{-8}	9.53	1.98×10^{-8}	6	6.33%	37.07%

As shown in the tables above, within the recommended range of $a_0 = 0.3$, the amplitude results determined using the finite element solution and Novak closed form solution was within 8%. Above this value when $a_0 = 0.35$, the difference between both solution was 40%. The difference between the results of the finite element solution and Chowdhury & DasGupta closed form solution was within 35% for a_0 of 0.3.

6.4 Comparison of the Pile Damping with Gazetas and Dobry

Gazetas and Dobry (1984), and Dobry (2014) assumed that in an axially loaded pile, the waves generated along the pile-soil interface propagated mainly in the horizontal direction, under essentially plane strain conditions. The shear waves propagate with a wave speed of V_s . Thus a radiation of energy at the contact between the soil and the pile surface would have a value of $\rho \times V_s \times A$. Where A is the total area of the pile surface. In addition to this was the damping lost at the base of the pile. Because of the small diameter of the pile, the values at the base could be quite small. Since $C = \rho \times V_s \times A$, for the case when $a_0 = 0.2$, the whole length of the pile vibrates, and $V_s = 235.3$ ft./sec. thus $C = (100/32.2) \times 235.3$ ft./sec $\times 2 \times \pi \times 1.50$ ft. $\times 30$ ft. = 2.06×10^5 lb.sec/ft. (In Figure 4-16, at $a_0 = 2.0$, the damping was 1.6×10^5 lb. sec/ft.

Chapter 7: Conclusion and Recommendation

7.1 Single Pile

To design pile-supported structures, the stiffness and damping of the soil-pile system at the level of the pile head are needed. The interaction of the pile with the surrounding soils under vibratory loading will modify the pile stiffness and influence its damping. The results of a finite element 3D model with viscous boundaries to determine the dynamic stiffness and damping are presented. The pile embedded in the soils was modeled as beam elements while the linearly elastic soil with material damping was modeled as eight-node brick elements and the pile was supported on a rigid soil layer. The parametric study undertaken to determine the major factors that affect the dynamic characteristics of the soil-pile system under a vertical harmonic loading showed the following:

7.1.1 Static Response

1. The axial stiffness of the single pile increased with the increase in the soil shear modulus. The increase in static stiffness for the pile in strong soil was due to the effect of the soil in increasing the overall pile-soil static stiffness.
2. The difference in the vertical static stiffness between the finite element model and the axial stiffness, assuming the pile as an axially loaded member for a pile in strong soil, was 61% for a pile having a concrete compressive strength equal to 3000 psi, 58% for a pile having a concrete compressive strength equal to 4000 psi, 55% for a pile having a concrete compressive strength equal to 5000 psi, and 54% for a pile having a concrete compressive strength equal to 6000

psi. The increase in static stiffness for the pile in a strong soil was due to the effect of the soil in increasing the overall pile-soil static stiffness.

7.1.2 Dynamic Response

1. Pile stiffness decreased with the increase in the dimensionless frequency parameter (a_0). Use of the average displacement amplitude produced a stiffness almost 10 times the use of the maximum amplitude. The stiffness of the soil pile system was reduced by approximately 50% when a_0 changed from 0.20 to 2.0.
2. Damping increased with the increase in the dimensionless frequency a_0 . At a high value of a_0 , when the soil was weak, the pile vibration would emanate simultaneous waves along the whole pile length whereas for the low value of a_0 , where the soil was strong, the waves emanated from a limited length of the pile. Thus, more geometrical damping would occur with the high values of a_0 than with the low values of a_0 .
3. For soil with lower values of shear modulus (1.9×10^3 kip/ft²), when a_0 was 0.60 or less, its contribution to the system frequency was negligible. The frequency of the soil-pile system could be attributed to the frequency of the piles only.
4. The increase in the ratio of $G_{\text{soil}}/E_{\text{pile}}$ increased the dynamic stiffness and decreased the damping of the soil-pile system.
5. With an increase of the soil shear modulus from 1×10^3 kip/ft² to 12×10^3 kip/ft², the pile vertical dynamic stiffness increased by 25% and the damping decreased by 20%.

6. The effect of the increase in the static load on the pile was that both the stiffness and damping would be affected, with the stiffness and damping increasing, however, the resonant frequency was reduced.
7. Pile length affected the dynamic stiffness and damping. For piles in strong soils, the stiffness and damping was not changed with the increase in the length of the pile. For piles in weak soils, both the stiffness and damping decreased with increasing the length of the pile.
8. An increase in the pile strength increased the stiffness and reduced the damping. The strength increased from 3000 psi to 6000 psi, increasing the stiffness by 15% and reducing the damping by 11%.
9. With higher values of shear wave velocity, indicating a strong soil material, the soil pile system was stiffer and consequently the system resonant frequency was increased.
10. The dynamic stiffness was about three times higher than the static stiffness. At a low value of the shear modulus the static stiffness was almost the same as the stiffness of the pile treated as a compression member, thus there was no soil contribution toward the static stiffness.

7.2 Pile Groups

The interaction between the piles within the group as well as the interaction between the group of piles and the soil modify the stiffness and damping characteristics of the pile foundation. The elastic waves transmitted from each pile interacted with each other modifying the response of the pile foundation system and affecting its performance. The results of a finite element 3D finite element model with viscous

boundaries to determine the dynamic stiffness and damping of a group piles 3 x 3 and spaced at $2D_{pile}$, $4D_{pile}$ and $6D_{pile}$ (3.0 ft., 6.0ft. and 9.0 ft.) were presented. The piles embedded in the soils were modeled as beam elements while the linearly elastic soil with material damping was modeled as eight-noded brick elements. The pile groups were connected with a rigid massless pile cap for uniform distribution of the excitation force on the pile groups without adding additional masses or stiffness to the pile groups. The pile was supported on a rigid soil layer. The parametric study undertaken to determine the major factors that affect the dynamic characteristics of the soil-pile system under a vertical harmonic loading showed the following:

7.2.1 Static Response

1. The vertical static stiffness of pile groups increased with the increase in the soil shear modulus. This increase in the pile group static stiffness was due to the effect of increased soil stiffness between the piles within the groups, thus increasing the overall pile-soil system rigidity.
2. The static stiffness of pile groups spaced at the $2D_{pile}$ was less than pile groups spaced at $4D_{pile}$ and $6D_{pile}$. The increase in the stiffness for pile groups at $6D_{pile}$ and $4D_{pile}$ in strong soils was due to the effect of load sharing between the piles within the groups and soils around the piles, which increased as the spacing of the pile increased.
3. For a group of piles embedded in weak soils, the group of piles acted as an end bearing piles. As the soil shear modulus increased the load was transferred to the surrounding soil and thus in strong soils, the piles were acting as friction piles.

4. The vertical displacement of a pile group in weak soils was the same for pile groups with different spacing, whereas in strong soils the displacement of the groups with $2D_{\text{pile}}$ spacing was the largest and the displacement for the $6D_{\text{pile}}$ spacing was the smallest.
5. In weak soils, the forces in the middle, edge and corner piles were the same for all spacings. In strong soils, the forces in the piles were not the same although the cap produced the same vertical displacement of all piles. The middle pile carried the smallest load and the corner pile carried the largest load. The load on the piles decreased with depth and with the increase in spacing.
6. In the case of a two by two pile group, due to the symmetry, the four piles shared the applied load equally.
7. The efficiency factor for piles spaced at $6D_{\text{pile}}$ was larger than spaced at $4D_{\text{pile}}$ and $2D_{\text{pile}}$. At low values of the shear modulus, the piles acted as end bearing piles, thus the efficiency was closer to 1.0. For stronger soils the piles acted as friction piles thus the efficiency decreased.

7.2.2 Dynamic Response

1. The vertical dynamic stiffness and damping of the pile groups were found to be dependent on the pile spacing and the dynamic properties of the soil deposit between the piles. The dynamic stiffness of the pile groups were reduced by 50%, 33% and 25% for pile groups spaced at $2D_{\text{pile}}$, $4D_{\text{pile}}$ and $6D_{\text{pile}}$ respectively when the dimensionless frequency parameter was increased from 0.20 to 2.0.

2. The stiffness, damping, resonant frequency and damping ratio showed oscillatory behavior with the dimensionless frequency (a_0). This oscillatory behavior was attributed to the effect of the attenuation, reflection, refraction, and phase changes of the cylindrical waves that propagated radially outwards in the horizontal direction along the length of each pile at all points on the pile.
3. The pile group spaced at $6D_{pile}$ had higher stiffness and damping than the pile groups spaced at $4D_{pile}$ and $2D_{pile}$ due to the larger contribution of the soil between the piles to the groups. With the larger soil volume in the case of the pile group spaced at $6D_{pile}$, the stiffness increased as well as the damping.
4. As the dimensionless frequency parameter (a_0) increased indicating weak soil material, the effect of the soil in the vertical dynamic stiffness of the pile group was minimal and the pile group vertical dynamic stiffness was governed by the structural stiffness of the pile groups.
5. For a closely spaced pile group, i.e., $2D_{pile}$ the response pile group exhibited a smoother variation with (a_0) compared to the bigger variation in the $4D_{pile}$ and the much bigger variation in the pile group spaced at $6D_{pile}$. As the spacing between the piles was reduced, the pile group behaved like an isolated embedded foundation, i.e., the soil mass between the piles tended to vibrate in phase with the piles and so the pile groups-soil system responded as a block.
6. For a 3 x 3 pile group embedded in strong soils, the dynamic force in the corner pile was found to be greater than the force in the edge pile, which in turn was greater than the force in the middle pile. The increase in the pile force for the

corner pile compare to the edge pile and middle pile was attributed to the effect of the soil load sharing for the middle pile and edge pile.

7. For a 3 x 3 pile group embedded in weak soils, the effect of soil in load sharing was reduced and the load was equally distributed among the piles within the group and thus all the piles carried the same load.
8. The behavior of a pile group under dynamic loading was similar to one under the static loading. The rigidity of the pile cap produced the same vertical displacement of the piles but the forces transmitted to each pile differed. At resonance, for weak soils, all piles carried the same load and for strong soils, the corner pile carried the largest load followed by the edge pile and the smaller load was carried by the middle pile. The total load on the piles were amplified to 3.78 lb. in weak soils and 2.83 lb. in strong soils relative to the 1.0 lb. load applied.
9. The pile group efficiency under dynamic loading differed considerably from the pile group effect under static loads as they were a function of a_0 , and a_0 was a function of the machine frequency, pile diameter and soil shear modulus. The efficiency factors for stiffness could be as high as 1.15 at a_0 equal to 1.0 and the efficiency factor for the damping could be as high as 3.75 for a_0 equal to 1.2.
10. The efficiency factor showed a much smoother plots when drawn as a function in the shear modulus. Also, as for the static factors, for weak soils the dynamic factor was close to 1.0 and decreased with the increase in the shear modulus except for the spacing of the $6D_{\text{pile}}$ which kept increasing.

Appendix A: Tables of Single Pile and Pile Groups Analysis

A.1. Results of Vertical Static Stiffness for Single Pile

Table: A-1: Vertical Static Stiffness of a Single Pile

Shear Modulus in ksf	Vertical Static Stiffness in lb./ft.			
	Fc = 3000 psi	Fc = 4000 psi	Fc = 5000 psi	Fc = 6000 psi
17241	2.72×10^8	2.92×10^8	3.09×10^8	3.24×10^8
4310	1.49×10^8	1.64×10^8	1.77×10^8	1.89×10^8
1916	1.19×10^8	1.33×10^8	1.45×10^8	1.56×10^8
1078	1.07×10^8	1.20×10^8	1.31×10^8	1.40×10^8
690	9.94×10^7	1.12×10^8	1.22×10^8	1.31×10^8
479	9.44×10^7	1.06×10^8	1.15×10^8	1.23×10^8
352	9.04×10^7	1.01×10^8	1.10×10^8	1.17×10^8
269	8.71×10^7	9.69×10^7	1.05×10^8	1.11×10^8
213	8.41×10^7	9.31×10^7	1.00×10^8	1.06×10^8
172	8.13×10^7	8.96×10^7	9.61×10^7	1.01×10^8

A.2. Results of Vertical Dynamic Stiffness for Single Pile

Table: A-2: Average Vertical Dynamic Stiffness for a Single Pile in lb. /ft.

a_0	Fc = 3000 psi	Fc = 4000 psi	Fc = 5000 psi	Fc = 6000 psi
0.2	4.1×10^8	4.2×10^8	4.3×10^8	4.51×10^8
0.4	3.7×10^8	3.9×10^8	4.0×10^8	4.15×10^8
0.6	3.4×10^8	3.7×10^8	3.8×10^8	3.95×10^8
0.8	3.3×10^8	3.5×10^8	3.7×10^8	3.82×10^8
1.0	3.1×10^8	3.4×10^8	3.6×10^8	3.71×10^8
1.2	3.0×10^8	3.3×10^8	3.5×10^8	3.63×10^8
1.4	3.0×10^8	3.3×10^8	3.4×10^8	3.57×10^8
1.6	2.9×10^8	3.2×10^8	3.4×10^8	3.51×10^8
1.8	2.8×10^8	3.2×10^8	3.3×10^8	3.46×10^8
2.0	2.8×10^8	3.1×10^8	3.3×10^8	3.42×10^8

Table: A-3: Minimum Vertical Dynamic Stiffness for a Single Pile in lb. /ft.

a_o	$F_c = 3000\text{psi}$	$F_c = 4000\text{psi}$	$F_c = 5000\text{psi}$	$F_c = 6000\text{psi}$
0.2	3.6×10^7	3.2×10^7	3.31×10^7	3.85×10^7
0.4	2.9×10^7	3.1×10^7	3.26×10^7	3.55×10^7
0.6	2.6×10^7	3.1×10^7	3.23×10^7	3.38×10^7
0.8	2.4×10^7	3.0×10^7	3.21×10^7	3.27×10^7
1.0	2.3×10^7	3.0×10^7	3.19×10^7	3.18×10^7
1.2	2.2×10^7	3.0×10^7	3.18×10^7	3.12×10^7
1.4	2.1×10^7	2.9×10^7	3.16×10^7	3.06×10^7
1.6	2.0×10^7	2.9×10^7	3.15×10^7	3.01×10^7
1.8	1.9×10^7	2.9×10^7	3.15×10^7	2.97×10^7
2.0	1.9×10^7	2.9×10^7	3.14×10^7	2.94×10^7

A.3. Effect of $G_{\text{soil}}/E_{\text{pile}}$ on Vertical Dynamic Stiffness of Single Pile

Table: A-4: Effect of $G_{\text{soil}}/E_{\text{pile}}$ Ratio on Dynamic Stiffness of a Single Pile

Concrete Strength = 3000 psi		Concrete Strength = 4000 psi	
$G_{\text{soil}}/E_{\text{pile}}$	Vertical Dynamic Stiffness in lb./ft.	$G_{\text{soil}}/E_{\text{pile}}$	Vertical Dynamic Stiffness in lb./ft.
3.84×10^{-2}	4.133×10^8	3.32×10^{-2}	4.218×10^8
9.60×10^{-3}	3.672×10^8	8.31×10^{-3}	3.856×10^8
4.26×10^{-3}	3.427×10^8	3.69×10^{-3}	3.659×10^8
2.40×10^{-3}	3.263×10^8	2.08×10^{-3}	3.525×10^8
1.54×10^{-3}	3.141×10^8	1.33×10^{-3}	3.425×10^8
1.07×10^{-3}	3.045×10^8	9.23×10^{-4}	3.345×10^8
7.83×10^{-4}	2.966×10^8	6.78×10^{-4}	3.279×10^8
6.00×10^{-4}	2.899×10^8	5.19×10^{-4}	3.223×10^8
4.74×10^{-4}	2.841×10^8	4.10×10^{-4}	3.174×10^8
3.84×10^{-4}	2.791×10^8	3.32×10^{-4}	3.131×10^8

Table: A-5: Effect of G_{soil}/E_{pile} Ratio on Dynamic Stiffness of a Single Pile

Concrete Strength = 5000 psi		Concrete Strength = 6000 psi	
G_{soil}/E_{pile}	Vertical Dynamic Stiffness in lb./ft.	G_{soil}/E_{pile}	Vertical Dynamic Stiffness in lb./ft.
2.97×10^{-2}	4.338×10^8	2.71×10^{-2}	4.511×10^8
7.43×10^{-3}	3.994×10^8	6.79×10^{-3}	4.149×10^8
3.30×10^{-3}	3.805×10^8	3.02×10^{-3}	3.950×10^8
1.86×10^{-3}	3.677×10^8	1.70×10^{-3}	3.815×10^8
1.19×10^{-3}	3.580×10^8	1.09×10^{-3}	3.714×10^8
8.26×10^{-4}	3.503×10^8	7.54×10^{-4}	3.633×10^8
6.07×10^{-4}	3.439×10^8	5.54×10^{-4}	3.566×10^8
4.65×10^{-4}	3.385×10^8	4.24×10^{-4}	3.509×10^8
3.67×10^{-4}	3.338×10^8	3.35×10^{-4}	3.460×10^8
2.97×10^{-4}	3.296×10^8	2.71×10^{-4}	3.416×10^8

A.4. Results of Vertical Damping of Single Pile

Table: A-6: Vertical Damping for Single Pile with $f_c=3000$ psi

a_o	$f_c = 3000$ psi				
	DMF	K_{pile} lb./ft. (Min)	Freq. (Hz)	Damping Ratio	Pile Damping
0.20	6.08	4.88×10^7	7.00	8%	1.825×10^5
0.40	5.74	2.18×10^7	6.00	9%	1.009×10^5
0.60	5.42	2.53×10^7	5.00	9%	1.485×10^5
0.80	5.12	2.03×10^7	5.00	10%	1.261×10^5
1.00	4.84	2.01×10^7	5.00	10%	1.322×10^5
1.20	4.58	2.11×10^7	5.00	11%	1.462×10^5
1.40	4.35	2.18×10^7	5.00	12%	1.598×10^5
1.60	4.13	2.10×10^7	5.00	12%	1.619×10^5
1.80	3.94	2.02×10^7	5.00	13%	1.633×10^5
2.00	3.76	2.21×10^7	5.00	13%	1.872×10^5

Table: A-7: Vertical Damping for Single Pile with $f_c=4000$ psi

a_o	$f_c = 4000$ psi				
	DMF	K_{pile} lb./ft. (Min)	Freq. (Hz)	Damping Ratio	Pile Damping.
0.20	7.70	3.88×10^7	8.00	6%	1.003×10^5
0.40	6.09	2.55×10^7	6.00	8%	1.111×10^5
0.60	4.94	2.67×10^7	6.00	10%	1.436×10^5
0.80	4.15	3.17×10^7	5.00	12%	2.432×10^5
1.00	3.66	2.99×10^7	5.00	14%	2.597×10^5
1.20	3.39	3.02×10^7	5.00	15%	2.828×10^5
1.40	3.28	3.11×10^7	5.00	15%	3.018×10^5
1.60	3.23	3.04×10^7	5.00	15%	2.994×10^5
1.80	3.19	2.83×10^7	5.00	16%	2.826×10^5
2.00	3.07	2.97×10^7	5.00	16%	3.081×10^5

Table: A-8: Vertical Damping for Single Pile with $f_c=5000$ psi

a_o	$f_c = 5000$ psi				
	DMF	K_{pile} lb./ft. (Min)	Freq. (Hz)	Damping Ratio	Pile Damping
0.20	7.42	3.92×10^7	8.00	7%	1.052×10^5
0.40	6.17	3.58×10^7	6.00	8%	1.539×10^5
0.60	5.25	2.41×10^7	6.00	10%	1.217×10^5
0.80	4.59	2.74×10^7	6.00	11%	1.581×10^5
1.00	4.13	3.03×10^7	6.00	12%	1.946×10^5
1.20	3.81	3.14×10^7	6.00	13%	2.185×10^5
1.40	3.55	2.99×10^7	6.00	14%	2.238×10^5
1.60	3.29	3.23×10^7	6.00	15%	2.609×10^5
1.80	2.96	3.52×10^7	6.00	17%	3.150×10^5
2.00	2.50	3.72×10^7	6.00	20%	3.947×10^5

Table: A-9: Vertical Damping for Single Pile with $f_c=6000$ psi

a_o	$f_c = 6000$ psi				
	DMF	K_{pile} lb./ft. (Min)	Freq. (Hz)	Damping Ratio	Pile Damping.
0.20	6.62	4.80×10^7	8.00	8%	1.44×10^5
0.40	5.88	3.41×10^7	7.00	8%	1.32×10^5
0.60	5.32	2.84×10^7	6.00	9%	1.42×10^5
0.80	4.88	2.75×10^7	6.00	10%	1.50×10^5
1.00	4.54	2.94×10^7	6.00	11%	1.72×10^5
1.20	4.25	3.05×10^7	6.00	12%	1.91×10^5
1.40	3.97	2.85×10^7	6.00	13%	1.90×10^5
1.60	3.65	3.01×10^7	6.00	14%	2.19×10^5
1.80	3.26	3.36×10^7	6.00	15%	2.73×10^5
2.00	2.76	3.64×10^7	6.00	18%	3.50×10^5

A.5. Results of Vertical Static Stiffness for Pile Groups

Table: A-10: Vertical Static Stiffness for Pile Groups with $f_c=3000$ psi

Soil Shear Modulus in ksf	Vertical Static Stiffness in lb./ft.		
	2D _{Pile} Spacing	4D _{Pile} Spacing	6D _{Pile} Spacing
11000	4.57×10^8	6.62×10^8	1.05×10^8
9000	4.50×10^8	6.26×10^8	9.56×10^7
6000	4.34×10^8	5.82×10^8	8.54×10^7
4314	4.10×10^8	5.30×10^8	7.46×10^7
1078	2.70×10^8	3.02×10^8	3.56×10^7
479	2.42×10^8	2.57×10^8	2.80×10^7
270	2.32×10^8	2.41×10^8	2.54×10^7
173	2.32×10^8	2.32×10^8	2.41×10^7
120	2.21×10^8	2.26×10^8	2.33×10^7
88	2.17×10^8	2.22×10^8	2.28×10^7
67	2.12×10^8	2.17×10^8	2.24×10^7
53	2.07×10^8	2.12×10^8	2.20×10^7
43	2.02×10^8	2.07×10^8	2.17×10^7

Table: A-11: Vertical Static Stiffness for Pile Groups with $f_c=4000$ psi

Soil Shear Modulus in ksf	Vertical Static Stiffness in lb./ft.		
	$2D_{Pile}$ Spacing	$4D_{Pile}$ Spacing	$6D_{Pile}$ Spacing
11000	4.99×10^8	7.10×10^8	9.95×10^8
9000	4.89×10^8	6.70×10^8	9.04×10^8
6000	4.71×10^8	6.20×10^8	8.07×10^8
4314	4.44×10^8	5.64×10^8	7.08×10^8
1078	3.02×10^8	3.35×10^8	3.71×10^8
479	2.74×10^8	2.90×10^8	3.06×10^8
270	2.63×10^8	2.73×10^8	2.82×10^8
173	2.57×10^8	2.64×10^8	2.71×10^8
120	2.51×10^8	2.57×10^8	2.63×10^8
88	2.46×10^8	2.52×10^8	2.57×10^8
67	2.40×10^8	2.46×10^8	2.52×10^8
53	2.34×10^8	2.40×10^8	2.46×10^8
43	2.26×10^8	2.33×10^8	2.40×10^8

Table: A-12: Vertical Static Stiffness for Pile Groups with $f_c=5000$ psi

Soil Shear Modulus in ksf	Vertical Static Stiffness in lb./ft.		
	$2D_{Pile}$ Spacing	$4D_{Pile}$ Spacing	$6D_{Pile}$ Spacing
11000	5.32×10^8	7.48×10^8	1.04×10^9
9000	5.22×10^8	7.05×10^8	9.42×10^8
6000	5.02×10^8	6.53×10^8	8.41×10^8
4314	4.73×10^8	5.94×10^8	7.38×10^8
1078	3.31×10^8	3.63×10^8	4.00×10^8
479	3.02×10^8	3.18×10^8	3.35×10^8
270	2.90×10^8	3.01×10^8	3.11×10^8
173	2.83×10^8	2.91×10^8	2.98×10^8
120	2.77×10^8	2.84×10^8	2.90×10^8
88	2.71×10^8	2.77×10^8	2.83×10^8
67	2.64×10^8	2.70×10^8	2.77×10^8
53	2.55×10^8	2.63×10^8	2.71×10^8
43	2.46×10^8	2.54×10^8	2.64×10^8

Table: A-13: Vertical Static Stiffness for Pile Groups with $f_c=6000$ psi

Soil Shear Modulus in ksf	Vertical Static Stiffness in lb./ft.		
	2D _{Pile} Spacing	4D _{Pile} Spacing	6D _{Pile} Spacing
11000	5.62×10^8	7.82×10^8	1.07×10^9
9000	5.51×10^8	7.37×10^8	9.76×10^8
6000	5.30×10^8	6.83×10^8	8.71×10^8
4314	5.00×10^8	6.21×10^8	7.64×10^8
1078	3.56×10^8	3.89×10^8	4.26×10^8
479	3.27×10^8	3.44×10^8	3.60×10^8
270	3.15×10^8	3.26×10^8	3.36×10^8
173	3.07×10^8	3.16×10^8	3.23×10^8
120	3.00×10^8	3.08×10^8	3.14×10^8
88	2.93×10^8	3.00×10^8	3.07×10^8
67	2.84×10^8	2.92×10^8	3.00×10^8
53	2.74×10^8	2.83×10^8	2.92×10^8
43	2.63×10^8	2.73×10^8	2.84×10^8

A.6. Results of Vertical Dynamic Stiffness for Pile Groups

Table: A-14: Average and Minimum Dynamic Stiffness for Pile Groups with $f_c=3000$

a _o	Vertical Dynamic Stiffness in lb./ft. For Piles With $f_c=3000$ psi					
	Average Dynamic Stiffness			Minimum Dynamic Stiffness		
	2D _{Pile}	4D _{Pile}	6D _{Pile}	2D _{Pile}	4D _{Pile}	6D _{Pile}
0.20	5.08×10^8	6.04×10^8	7.84×10^8	4.39×10^7	5.69×10^7	8.45×10^7
0.40	4.23×10^8	4.74×10^8	5.73×10^8	3.17×10^7	3.78×10^7	5.14×10^7
0.60	4.17×10^8	4.62×10^8	5.59×10^8	4.29×10^7	5.67×10^7	8.11×10^7
0.80	4.24×10^8	4.46×10^8	5.07×10^8	4.50×10^7	4.66×10^7	7.27×10^7
1.00	4.24×10^8	4.53×10^8	5.23×10^8	4.50×10^7	5.69×10^7	7.00×10^7
1.20	4.07×10^8	4.54×10^8	5.09×10^8	4.53×10^7	5.45×10^7	9.10×10^7
1.40	4.05×10^8	4.42×10^8	4.92×10^8	4.49×10^7	5.18×10^7	7.91×10^7
1.60	4.14×10^8	4.47×10^8	4.70×10^8	4.83×10^7	5.66×10^7	5.86×10^7
1.80	4.15×10^8	4.47×10^8	4.68×10^8	4.61×10^7	5.45×10^7	6.40×10^7
2.00	4.18×10^8	4.43×10^8	4.60×10^8	4.87×10^7	5.89×10^7	6.35×10^7

Table: A-15: Average and Minimum Dynamic Stiffness for Pile Groups with $f_c=4000$

a_o	Vertical Dynamic Stiffness in lb./ft. For Piles With $f_c=4000$ psi					
	Average Dynamic Stiffness			Minimum Dynamic Stiffness		
	2DPile	4DPile	6DPile	2DPile	4DPile	6DPile
0.20	5.4×10^8	6.3×10^8	7.4×10^8	5.3×10^7	6.5×10^7	7.8×10^7
0.40	4.7×10^8	5.2×10^8	5.8×10^8	4.7×10^7	6.0×10^7	6.8×10^7
0.60	4.6×10^8	5.0×10^8	5.5×10^8	5.6×10^7	7.2×10^7	6.8×10^7
0.80	4.6×10^8	4.9×10^8	5.4×10^8	5.5×10^7	6.2×10^7	8.7×10^7
1.00	4.3×10^8	4.7×10^8	5.3×10^8	4.0×10^7	5.1×10^7	6.9×10^7
1.20	4.3×10^8	4.8×10^8	5.2×10^8	4.0×10^7	5.5×10^7	7.4×10^7
1.40	4.3×10^8	4.7×10^8	5.1×10^8	4.2×10^7	5.8×10^7	7.9×10^7
1.60	4.4×10^8	4.8×10^8	4.9×10^8	4.1×10^7	6.1×10^7	6.5×10^7
1.80	4.4×10^8	4.8×10^8	4.9×10^8	4.5×10^7	7.5×10^7	6.4×10^7
2.00	4.5×10^8	4.7×10^8	4.8×10^8	4.6×10^7	6.4×10^7	6.0×10^7

Table: A-16: Average and Minimum Dynamic Stiffness for Pile Groups with $f_c=5000$

a_o	Vertical Dynamic Stiffness in lb./ft. For Piles With $f_c=5000$ psi					
	Average Dynamic Stiffness			Minimum Dynamic Stiffness		
	2DPile	4DPile	6DPile	2DPile	4DPile	6DPile
0.20	5.6×10^8	6.5×10^8	7.7×10^8	6.1×10^7	8.1×10^7	9.1×10^7
0.40	4.9×10^8	5.4×10^8	6.0×10^8	4.6×10^7	5.0×10^7	5.8×10^7
0.60	4.8×10^8	5.3×10^8	5.9×10^8	4.9×10^7	6.2×10^7	8.6×10^7
0.80	4.8×10^8	5.2×10^8	5.6×10^8	6.0×10^7	7.6×10^7	9.5×10^7
1.00	4.6×10^8	5.0×10^8	5.6×10^8	5.5×10^7	6.2×10^7	7.9×10^7
1.20	4.6×10^8	5.0×10^8	5.4×10^8	5.3×10^7	6.0×10^7	9.4×10^7
1.40	4.6×10^8	5.0×10^8	5.3×10^8	5.7×10^7	6.9×10^7	7.6×10^7
1.60	4.7×10^8	5.0×10^8	5.2×10^8	5.4×10^7	6.8×10^7	7.7×10^7
1.80	4.7×10^8	5.0×10^8	5.1×10^8	5.7×10^7	7.3×10^7	7.4×10^7
2.00	4.8×10^8	5.0×10^8	5.0×10^8	5.9×10^7	6.9×10^7	6.9×10^7

Table: A-17: Average and Minimum Dynamic Stiffness for Pile Groups with $f_c=6000$

a_o	Vertical Dynamic Stiffness in lb./ft. For Piles With $f_c=6000$ psi					
	Average Dynamic Stiffness			Minimum Dynamic Stiffness		
	2DPile	4DPile	6DPile	2DPile	4DPile	6DPile
0.20	5.69×10^8	6.66×10^8	7.85×10^8	5.37×10^7	7.07×10^7	1.01×10^8
0.40	5.07×10^8	5.61×10^8	6.25×10^8	4.58×10^7	5.31×10^7	6.06×10^7
0.60	4.89×10^8	5.41×10^8	6.09×10^8	4.51×10^7	5.56×10^7	9.64×10^7
0.80	4.94×10^8	5.49×10^8	5.80×10^8	5.45×10^7	8.30×10^7	9.21×10^7
1.00	4.84×10^8	5.19×10^8	5.89×10^8	5.23×10^7	6.14×10^7	9.50×10^7
1.20	4.85×10^8	5.22×10^8	5.67×10^8	5.61×10^7	7.49×10^7	9.94×10^7
1.40	4.81×10^8	5.28×10^8	5.48×10^8	5.10×10^7	7.56×10^7	7.93×10^7
1.60	4.86×10^8	5.28×10^8	5.39×10^8	5.58×10^7	8.41×10^7	7.65×10^7
1.80	4.90×10^8	5.23×10^8	5.28×10^8	5.64×10^7	7.43×10^7	7.27×10^7
2.00	4.96×10^8	5.17×10^8	5.26×10^8	6.05×10^7	7.02×10^7	7.10×10^7

A.7. Effect of G_{soil}/E_{pile} on Pile Group Dynamic Stiffness

Table: A-18: Effect of G_{soil}/E_{pile} Ratio on Stiffness for Pile Groups with $f_c=3000$ psi

G_{soil}/E_{pile}	Vertical Dynamic Stiffness (K_v) in lb./ft.		
	2DPile	4DPile	6DPile
9.59×10^{-3}	4.72×10^8	5.48×10^8	7.17×10^8
2.40×10^{-3}	4.49×10^8	5.08×10^8	6.23×10^8
1.07×10^{-3}	4.37×10^8	4.86×10^8	5.74×10^8
5.99×10^{-4}	4.28×10^8	4.71×10^8	5.42×10^8
3.83×10^{-4}	4.22×10^8	4.60×10^8	5.18×10^8
2.66×10^{-4}	4.16×10^8	4.51×10^8	4.99×10^8
1.96×10^{-4}	4.12×10^8	4.44×10^8	4.83×10^8
1.50×10^{-4}	4.08×10^8	4.37×10^8	4.71×10^8
1.18×10^{-4}	4.05×10^8	4.32×10^8	4.59×10^8
9.59×10^{-5}	4.02×10^8	4.27×10^8	4.50×10^8

Table: A-19: Effect of G_{soil}/E_{pile} Ratio on Stiffness for Pile Groups with $f_c=4000$ psi

G_{soil}/E_{pile}	Vertical Dynamic Stiffness (K_v) in lb./ft.		
	$2D_{Pile}$	$4D_{Pile}$	$6D_{Pile}$
8.30×10^{-3}	5.13×10^8	5.87×10^8	6.95×10^8
2.08×10^{-3}	4.85×10^8	5.44×10^8	6.18×10^8
9.23×10^{-4}	4.69×10^8	5.21×10^8	5.77×10^8
5.19×10^{-4}	4.58×10^8	5.05×10^8	5.50×10^8
3.32×10^{-4}	4.50×10^8	4.93×10^8	5.30×10^8
2.31×10^{-4}	4.43×10^8	4.83×10^8	5.14×10^8
1.69×10^{-4}	4.38×10^8	4.75×10^8	5.00×10^8
1.30×10^{-4}	4.33×10^8	4.68×10^8	4.89×10^8
1.03×10^{-4}	4.29×10^8	4.62×10^8	4.80×10^8
8.30×10^{-5}	4.25×10^8	4.57×10^8	4.71×10^8

Table: A-20: Effect of G_{soil}/E_{pile} Ratio on Stiffness for Pile Groups with $f_c=5000$ psi

G_{soil}/E_{pile}	Vertical Dynamic Stiffness in lb./ft.		
	$2D_{Pile}$	$4D_{Pile}$	$6D_{Pile}$
7.43×10^{-3}	5.29×10^8	6.08×10^8	7.19×10^8
1.86×10^{-3}	5.06×10^8	5.67×10^8	6.43×10^8
8.25×10^{-4}	4.93×10^8	5.45×10^8	6.02×10^8
4.64×10^{-4}	4.84×10^8	5.29×10^8	5.75×10^8
2.97×10^{-4}	4.77×10^8	5.18×10^8	5.55×10^8
2.06×10^{-4}	4.71×10^8	5.08×10^8	5.39×10^8
1.52×10^{-4}	4.66×10^8	5.00×10^8	5.26×10^8
1.16×10^{-4}	4.62×10^8	4.94×10^8	5.15×10^8
9.17×10^{-5}	4.59×10^8	4.88×10^8	5.05×10^8
7.43×10^{-5}	4.56×10^8	4.83×10^8	4.96×10^8

Table: A-21: Effect of G_{soil}/E_{pile} Ratio on Stiffness for Pile Groups with $f_c=6000$ psi

G_{soil}/E_{pile}	Vertical Dynamic Stiffness in lb./ft.		
	2D _{Pile}	4D _{Pile}	6D _{Pile}
6.78×10^{-3}	5.39×10^8	6.24×10^8	7.40×10^8
1.69×10^{-3}	5.20×10^8	5.86×10^8	6.65×10^8
7.53×10^{-4}	5.08×10^8	5.65×10^8	6.24×10^8
4.24×10^{-4}	5.01×10^8	5.50×10^8	5.97×10^8
2.71×10^{-4}	4.95×10^8	5.39×10^8	5.77×10^8
1.88×10^{-4}	4.90×10^8	5.30×10^8	5.61×10^8
1.38×10^{-4}	4.86×10^8	5.23×10^8	5.47×10^8
1.06×10^{-4}	4.82×10^8	5.16×10^8	5.36×10^8
8.37×10^{-5}	4.79×10^8	5.11×10^8	5.26×10^8
6.78×10^{-5}	4.77×10^8	5.06×10^8	5.18×10^8

A.8. Damping of a Group of Piles

Table: A-22: Damping, Damping Ratio and Resonant Frequency for a Group of Piles with $f_c=3000$ psi

a_o	Damping			Damping Ratio			Res Frequency		
	2D _{pile}	4D _{pile}	6D _{pile}	2D _{pile}	4D _{pile}	6D _{pile}	2D	4D	6D
0.20	7.47×10^4	8.84×10^4	1.27×10^5	5.3%	5.4%	5.7%	10	11	12
0.40	7.41×10^4	9.42×10^4	1.48×10^5	5.9%	6.3%	7.2%	8	8	8
0.60	1.51×10^5	2.48×10^5	4.66×10^5	8.9%	11.0%	14.5%	8	8	8
0.80	1.99×10^5	2.05×10^5	4.74×10^5	9.7%	9.7%	14.3%	7	7	7
1.00	1.99×10^5	2.77×10^5	4.63×10^5	9.7%	12.3%	14.5%	7	8	7
1.20	2.11×10^5	2.98×10^5	7.07×10^5	10.3%	12.0%	19.5%	7	7	8
1.40	2.11×10^5	2.75×10^5	6.24×10^5	10.4%	11.7%	17.4%	7	7	7
1.60	2.50×10^5	3.36×10^5	3.06×10^5	11.4%	13.1%	13.1%	7	7	8
1.80	2.33×10^5	3.18×10^5	3.70×10^5	11.1%	12.8%	14.5%	7	7	8
2.0	2.67×10^5	3.33×10^5	4.23×10^5	12.1%	14.2%	14.7%	7	8	7

Table: A-23: Damping, Damping Ratio and Resonant Frequency for a Group of Piles with $f_c=4000$ psi

a_o	Damping			Damping Ratio			Res Frequency		
	$2D_{pile}$	$4D_{pile}$	$6D_{pile}$	$2D_{pile}$	$4D_{pile}$	$6D_{pile}$	2D	4D	6D
0.20	1.02×10^5	1.09×10^5	1.13×10^5	6.0%	5.8%	5.5%	10	11	12
0.40	1.48×10^5	2.13×10^5	2.22×10^5	7.8%	8.9%	9.2%	8	8	9
0.60	2.28×10^5	3.52×10^5	2.97×10^5	10.2%	12.4%	11.0%	8	8	8
0.80	2.33×10^5	2.82×10^5	6.09×10^5	10.5%	11.4%	15.4%	8	8	7
1.00	1.22×10^5	1.95×10^5	3.51×10^5	7.7%	9.6%	12.8%	8	8	8
1.20	1.25×10^5	2.34×10^5	4.77×10^5	7.9%	10.7%	14.1%	8	8	7
1.40	1.43×10^5	2.65×10^5	4.78×10^5	8.5%	11.5%	15.3%	8	8	8
1.60	1.41×10^5	2.97×10^5	3.29×10^5	8.6%	12.3%	12.8%	8	8	8
1.80	1.74×10^5	4.70×10^5	3.27×10^5	9.7%	15.7%	12.9%	8	8	8
2.0	1.89×10^5	3.46×10^5	3.01×10^5	10.2%	13.7%	12.5%	8	8	8

Table: A-24: Damping, Damping Ratio and Resonant Frequency for a Group of Piles with $f_c=5000$ psi

a_o	Damping			Damping Ratio			Res Frequency		
	$2D_{pile}$	$4D_{pile}$	$6D_{pile}$	$2D_{pile}$	$4D_{pile}$	$6D_{pile}$	2D	4D	6D
0.20	1.13×10^5	1.47×10^5	1.48×10^5	6.4%	6.8%	6.1%	11	12	12
0.40	1.13×10^5	1.22×10^5	1.47×10^5	7.0%	6.9%	7.2%	9	9	9
0.60	1.42×10^5	2.11×10^5	4.37×10^5	8.1%	9.7%	12.8%	9	9	8
0.80	2.22×10^5	3.81×10^5	5.11×10^5	10.4%	12.6%	15.3%	9	8	9
1.00	2.14×10^5	2.61×10^5	4.16×10^5	9.7%	10.6%	13.2%	8	8	8
1.20	2.00×10^5	2.53×10^5	5.35×10^5	9.5%	10.6%	16.1%	8	8	9
1.40	2.35×10^5	3.44×10^5	3.57×10^5	10.4%	12.5%	13.3%	8	8	9
1.60	2.16×10^5	3.45×10^5	3.74×10^5	10.2%	12.7%	13.8%	8	8	9
1.80	2.56×10^5	3.60×10^5	3.54×10^5	11.2%	13.9%	13.6%	8	9	9
2.0	2.85×10^5	3.34×10^5	3.23×10^5	12.1%	13.6%	13.2%	8	9	9

Table: A-25: Damping, Damping Ratio and Resonant Frequency for a Group of Piles with $f_c=6000$ psi

a_o	Damping			Damping Ratio			Res Frequency		
	$2D_{pile}$	$4D_{pile}$	$6D_{pile}$	$2D_{pile}$	$4D_{pile}$	$6D_{pile}$	2D	4D	6D
0.20	8.33×10^4	1.07×10^5	1.64×10^5	5.4%	5.7%	6.6%	11	12	13
0.40	1.04×10^5	1.28×10^5	1.53×10^5	6.4%	6.8%	7.1%	9	9	9
0.60	1.10×10^5	1.59×10^5	4.56×10^5	6.9%	8.1%	13.4%	9	9	9
0.80	1.67×10^5	3.74×10^5	4.47×10^5	8.6%	12.7%	13.7%	9	9	9
1.00	1.58×10^5	2.11×10^5	5.56×10^5	8.5%	9.7%	14.7%	9	9	8
1.20	1.85×10^5	3.62×10^5	5.56×10^5	9.3%	12.2%	15.8%	9	8	9
1.40	1.57×10^5	3.36×10^5	3.62×10^5	8.7%	12.6%	12.9%	9	9	9
1.60	1.94×10^5	4.82×10^5	3.45×10^5	9.8%	14.4%	12.8%	9	8	9
1.80	2.05×10^5	3.45×10^5	3.20×10^5	10.3%	13.1%	12.4%	9	9	9
2.0	2.46×10^5	3.19×10^5	3.14×10^5	11.5%	12.9%	12.5%	9	9	9

Appendix B: Derivation of Compliance Functions

B.1. Vertical Vibration of Foundation on Elastic Half Space

Lamb studied the problem of vibration of single vibrating force acting at a point on the surface of an elastic half-space. This study included cases in which the oscillating force equal $Q = Q_0 e^{i\omega t}$ acts in the vertical direction as shown in Figure B-1 which is generally referred to as the dynamic Boussinesq problem. Shekter, corrected a mistake in Reissner's work and she presented a solution for the dynamic response of a uniformly loaded circular footing.

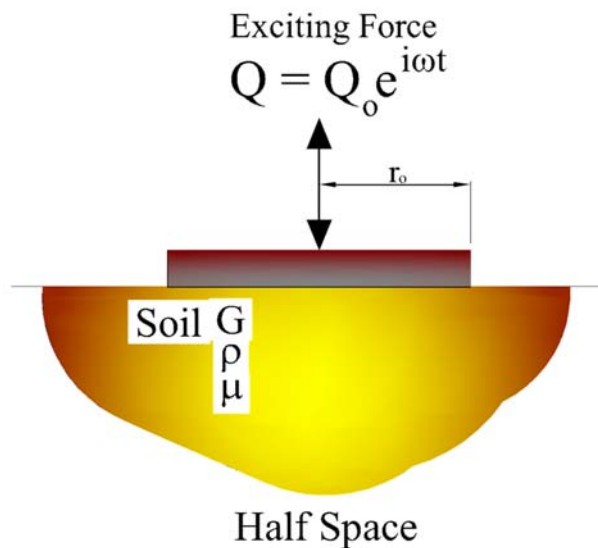


Figure B-1: Vertically Loaded Foundation

The vertical displacement of the center of a uniformly loaded circular disc ($Q_0 e^{i\omega t} = \pi r_0^2 q_0 e^{i\omega t}$) resting on the surface of an elastic half space obtained by Reissner is given by

$$z(t) = \frac{Q_0 e^{i\omega t}}{Gr_0} \times (f_1 + if_2) \quad (B-1)$$

Where

Q_0 = amplitude of the exciting force acting on the foundation

z = periodic displacement at the center of the loaded area

ω = circular frequency of the applied load

r_0 = radius of loaded area

G = Shear modulus of the soil

Q = Excitation force which has an amplitude of Q_0

f_1 and f_2 = Reissner's displacement functions

The displacement compliance functions f_1 and f_2 are related to the Poisson's ratio of the medium and the frequency of the exciting force.

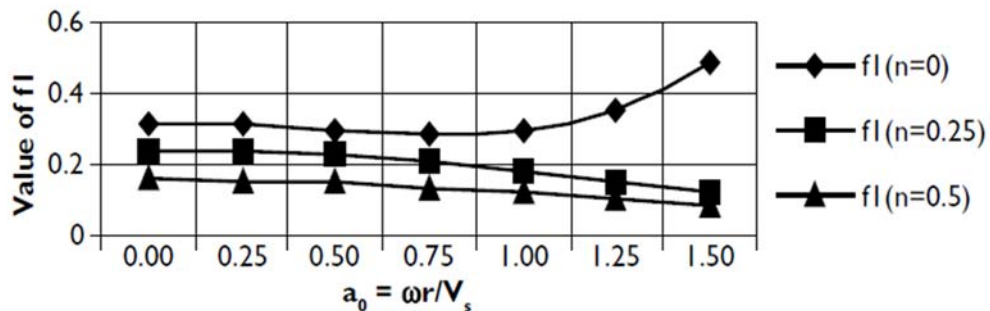


Figure B-2: Coefficient f_1 for Flexible Foundation (Reissner1936)

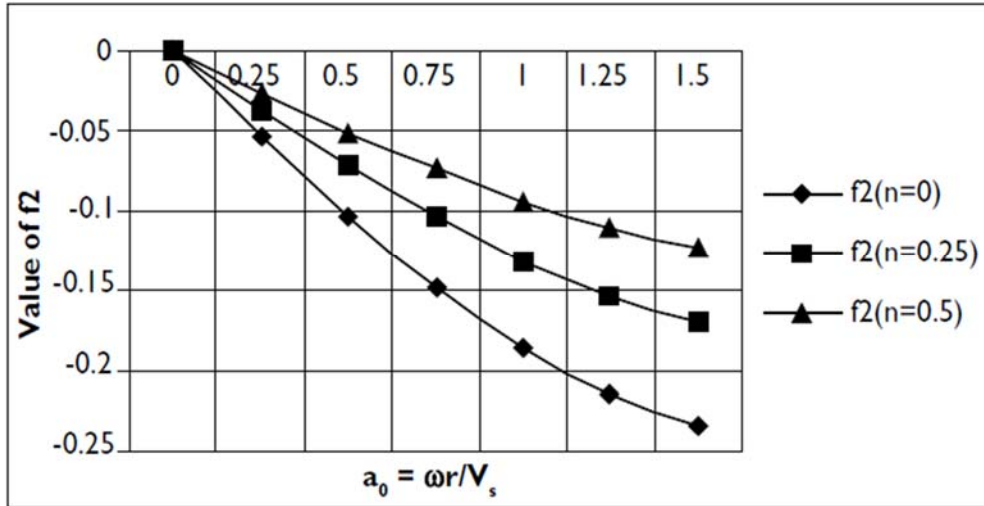


Figure B-3: Coefficient f_2 for Flexible Foundation (Reissner1936)

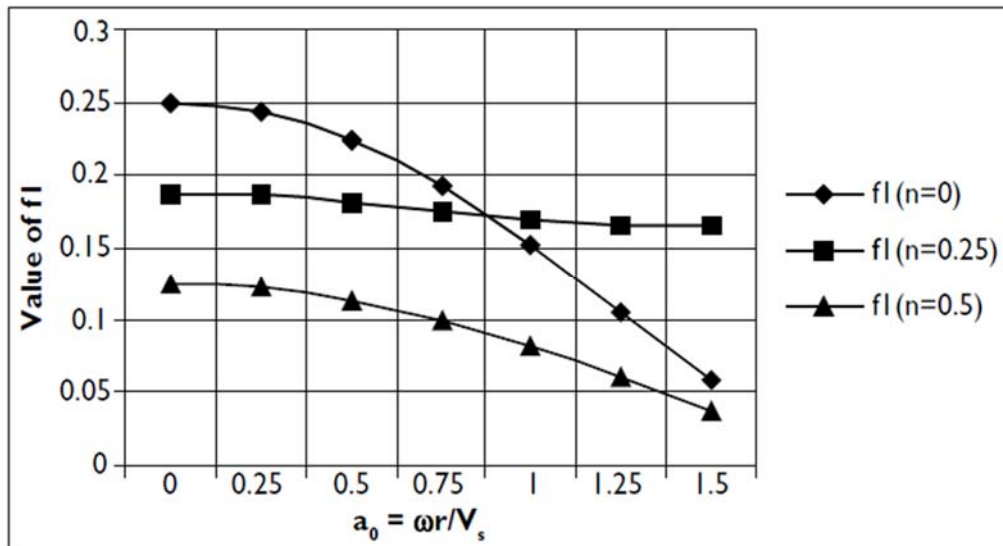


Figure B-4: Coefficient f_1 for Rigid Foundation (Reissner1936)

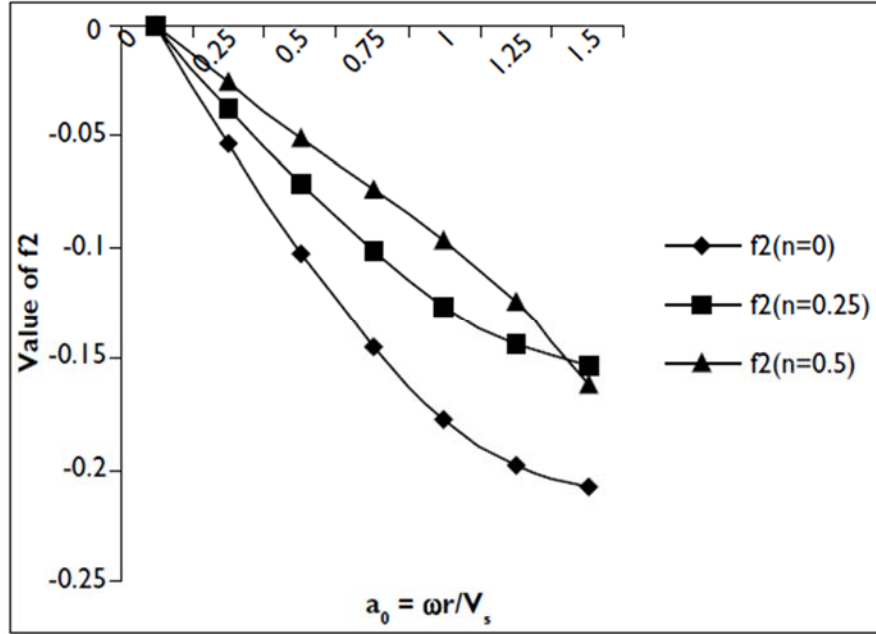


Figure B-5: Coefficient f_2 for Rigid Foundation (Reissner1936)

For flexible circular foundation of weight W (mass = $m = W/g$) resting on an elastic half-space and subjected to an exciting force of magnitude of $Q_0 e^{i\omega t}$ Using the displacement relation given in equation.A-2 and solving the equation of equilibrium of force, Reissner obtained the following relationships.

$$A_z = \text{Amplitude of the vibration} = \frac{Q_0}{Gr_0} Z \quad (\text{B-2})$$

$$Z = \text{Dimensionless amplitude} = \sqrt{\frac{f_1^2 + if_2^2}{(1 - ba_0^2 f_1)^2 + (ba_0^2 f_2)^2}} \quad (\text{B-3})$$

Where

$$b = \text{Dimensionless mass ratio} = \frac{m}{\rho r_o^2} = \left(\frac{W}{g}\right) \left[\frac{1}{\left(\frac{\gamma}{g}\right) r_o^3} \right] = \frac{W}{\gamma r_o^3}$$

γ = Unit weight of the elastic soil

$$a_o = \text{Dimensionless frequency} = \omega r_o \sqrt{\frac{\rho}{G}} = \frac{\omega r_o}{v_s}$$

v_s = Soil shear wave velocity

The work of Reissner was further extended by Quinlan (1953) and Sung (1953). Reissner's work was related only to the case of flexible circular foundations where the soil reaction is uniform over the entire area. Quinlan and Sung considered the cases of rigid circular foundations where the contact pressure of is as shown in Figure B-6, flexible foundations with contact pressure is as shown in Figure B-7 and the types of foundations for which the contact pressure distribution is parabolic, as shown in Figure B-8. The distribution of contact pressure for all three cases may be expressed as follows.

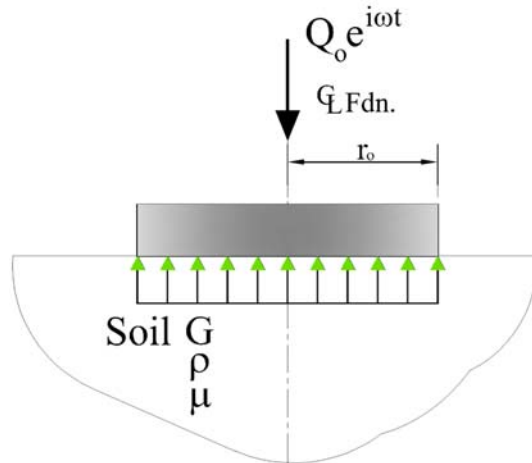


Figure B-6: Uniform Pressure Distribution

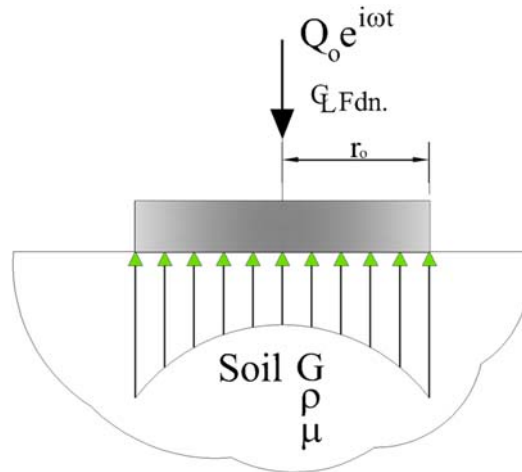


Figure B-7: Pressure Distribution under Rigid Foundation

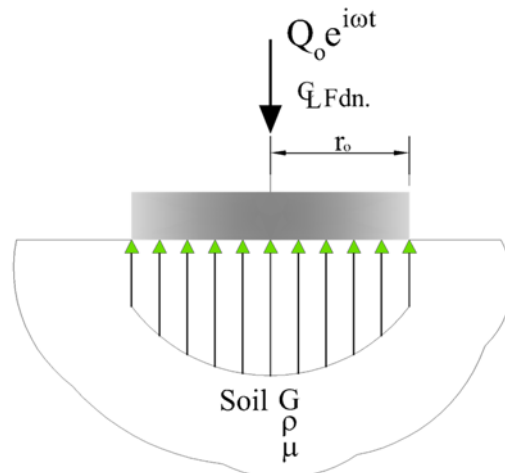


Figure B-8: Parabolic Pressure Distribution

For flexible circular foundations the contact pressure at a distance r measured from the center of the foundation is given by

$$q = \frac{Q_0 e^{i(\omega t + \alpha)}}{\pi r_0^2} \text{ for } (r < r_0) \quad (\text{B-4})$$

For rigid circular foundations the contact pressure at a distance r measured from the center of the foundation is given by

$$q = \frac{Q_0 e^{i(\omega t + \alpha)}}{2\pi r_0 \sqrt{r_0^2 - r^2}} \text{ for } (r < r_0) \quad (\text{B-5})$$

For foundations with parabolic contact pressure distribution, the contact pressure at a distance r measured from the center of the foundation is given by

$$q = \frac{2(r_0^2 - r^2)Q_0 e^{i(\omega t + \alpha)}}{\pi r_0^4} \text{ for } (r < r_0) \quad (\text{B-6})$$

Quinlan and Sung defined the displacement at the center of the contact area resting on the half space as

$$z = \frac{Q_0 e^{i\omega t}}{Gr_0} (f_1 + if_2) \quad (\text{B-7})$$

Where: f_1 and f_2 are the compliance function

Quinlan and Sung also proposed the compliance functions f_1 and f_2 are as shown in Figures B-9, B-10 and B-11.

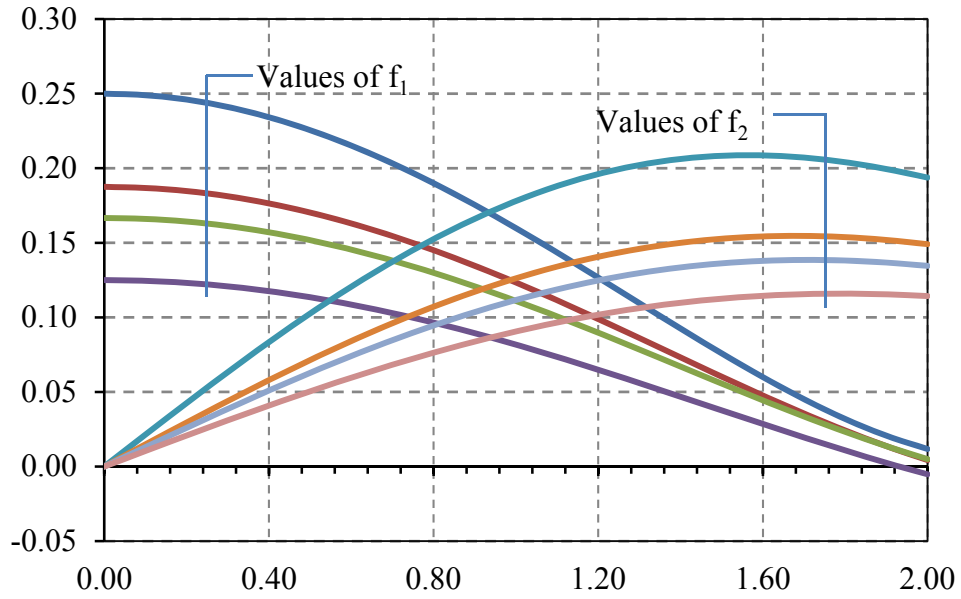


Figure B-9: Compliance Functions f_1 and f_2 for Rigid Base

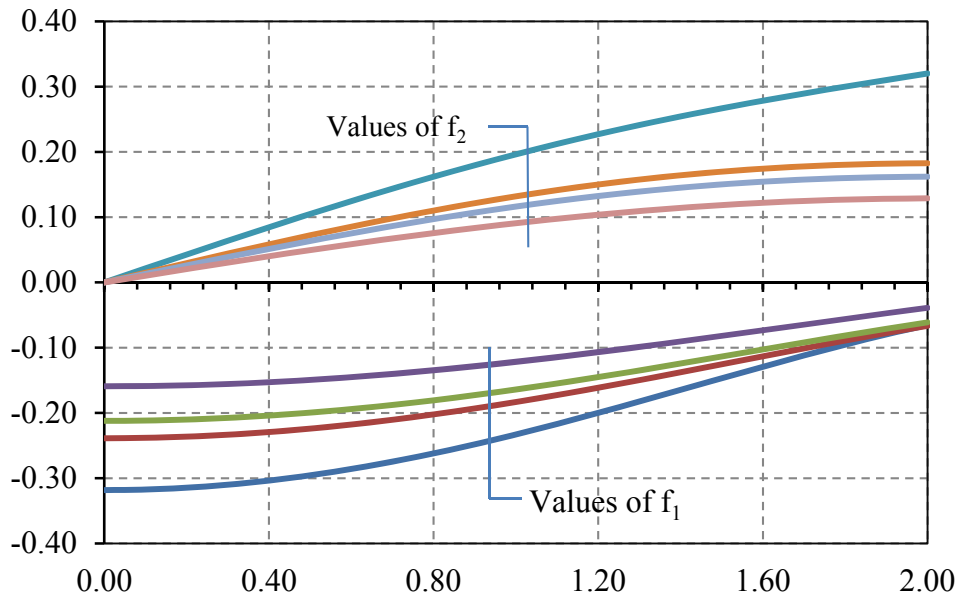


Figure B-10: Compliance Functions f_1 and f_2 for Uniform Loading

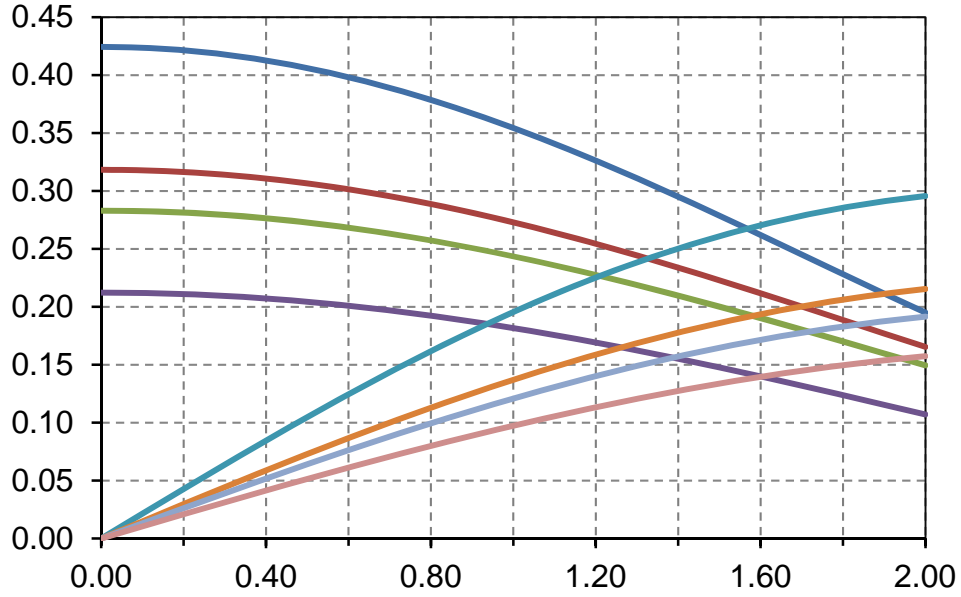


Figure B-11: Compliance Functions f_1 and f_2 for Parabolic Loading

For machine foundation, the foundations are subjected to a frequency dependent excitation, in contrast to the constant-force excitation. The amplitude of the exciting force can be given as:

$$Q = 2m_e e \omega = m_1 e \omega^2 \quad (B-8)$$

Where:

m_1 = Total of the rotating mass

ω = Circular frequency of the rotating mass

The amplitude of vibration A_z is given by:

$$A_z = \frac{Q_o}{Gr_o} Z = \frac{m_1 e \omega^2}{Gr_o} \sqrt{\frac{f_1^2 + if_2^2}{(1 - ba_o^2 f_1)^2 + (ba_o^2 f_2)^2}} \quad (B-9)$$

$$a_o = \omega r_o \sqrt{\frac{\rho}{G}} \quad \text{or} \quad \omega^2 = \frac{a_o^2 G}{\rho r_o^2} \quad (\text{B-10})$$

$$A_z = \frac{m_1 a_o^2}{\rho r_o^3} \sqrt{\frac{f_1^2 + i f_2^2}{(1 - b a_o^2 f_1)^2 + (b a_o^2 f_2)^2}} = \frac{m_1}{\rho r_o^3} Z' \quad (\text{B-11})$$

$$Z' = \text{dimensionless amplitude} = a_o^2 \sqrt{\frac{f_1^2 + i f_2^2}{(1 - b a_o^2 f_1)^2 + (b a_o^2 f_2)^2}} \quad (\text{B-12})$$

The variation of the dimensionless Z amplitude with a_o (Richart, 1962) for rigid circular foundations ($\mu = \text{Poisson's ratio} = 0.25$ and $b = 5, 10, 20,$ and 40) is shown in Figure B-12 and Figure B-13.

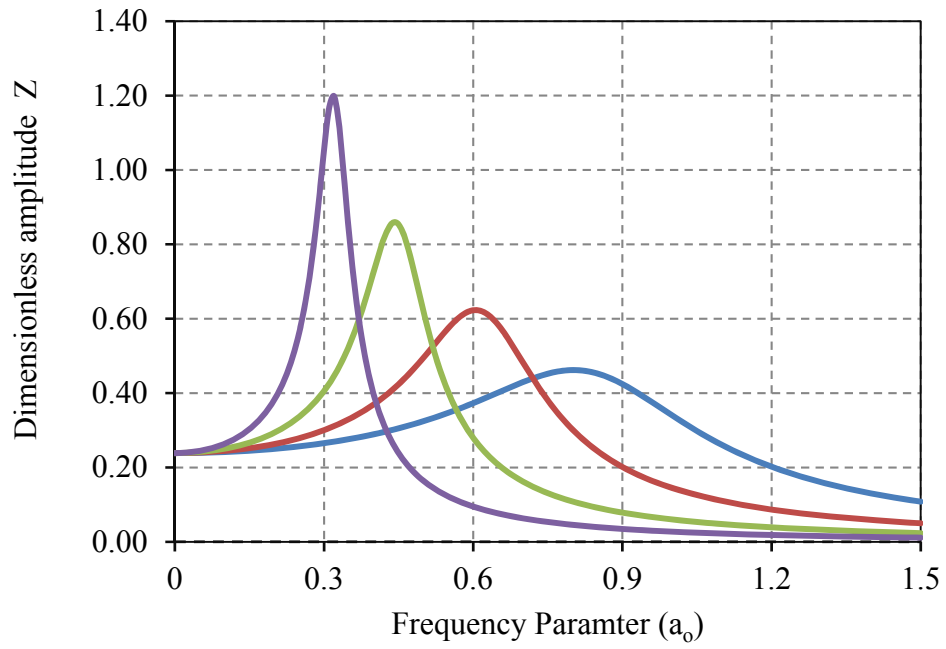


Figure B-12: Plot of Z Versus a_0 for Flexible Circular Foundation

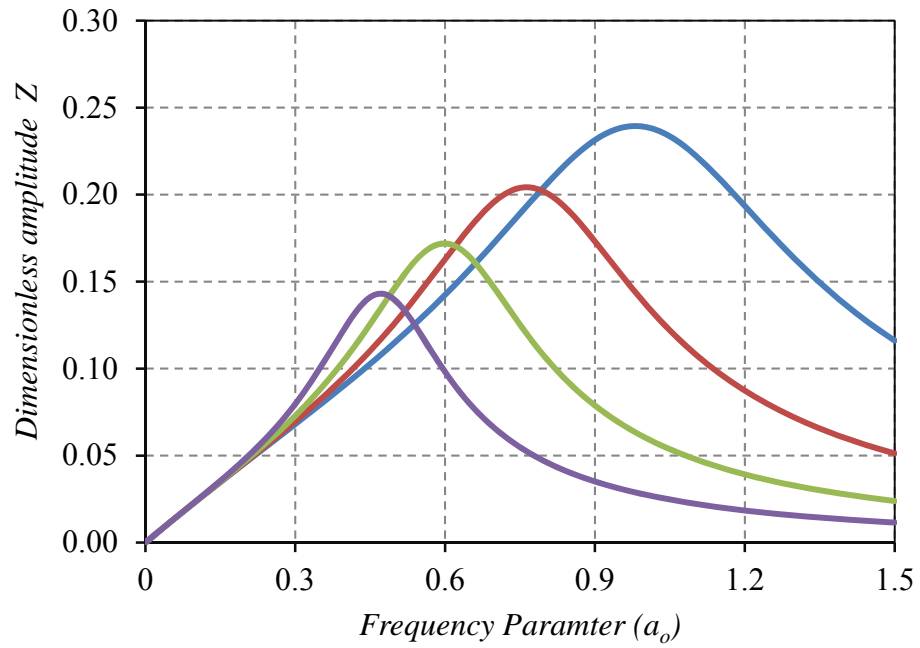


Figure B-13: Plot of Z Versus a_0 for Rigid Circular Foundation

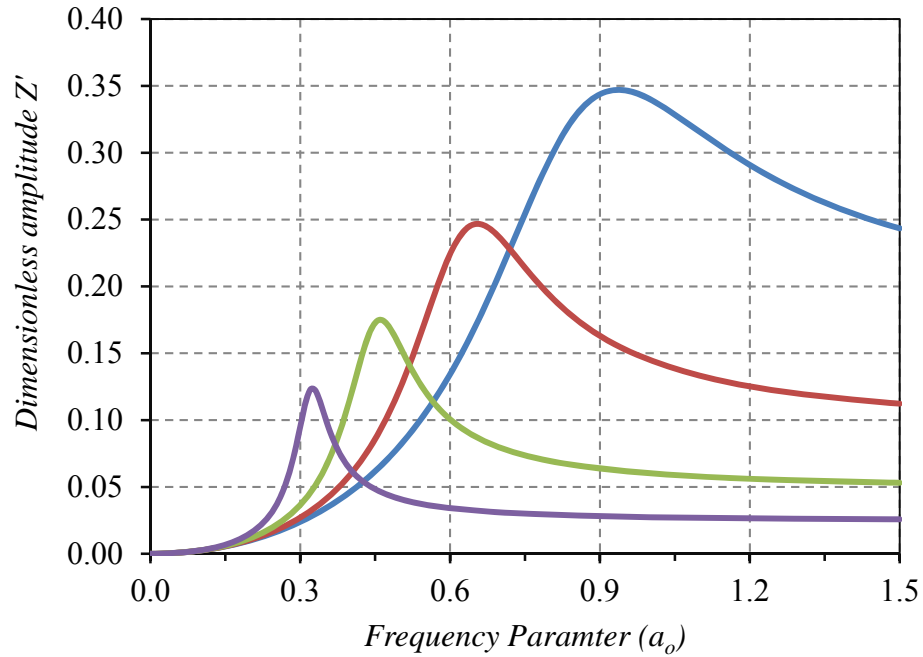


Figure B-14: Variation of Z' with a_0 for Flexible Circular Foundation

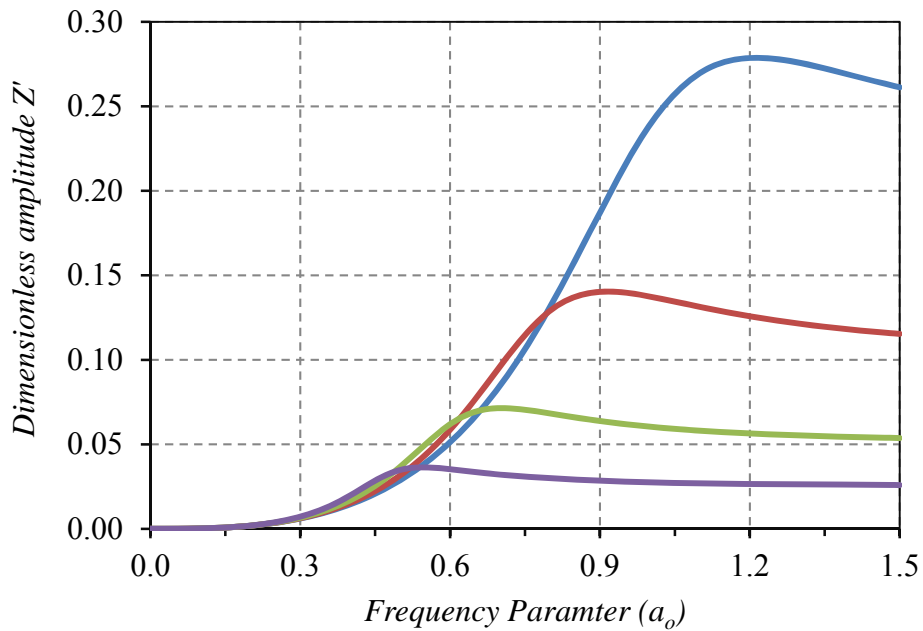


Figure B-15: Variation of Z' with a_0 for Rigid Circular Foundation

Displacement functions (f_1 and f_2) are related to the dimensionless frequency a_0 and Poisson's ratio μ . In Sung's original study, it was assumed that the contact pressure

distribution remains the same throughout the range of frequency considered; however, for dynamic loading conditions, the rigid-base pressure distribution does not produce uniform displacement under the foundation.

The dynamic response of a rigid circular foundation on an elastic half-space in the vertical, rocking and sliding modes of vibration was studied by Bycroft considering the same contact pressures used by Quinlan and Sung. Since the equivalent dynamic pressure in rigid base a uniform dynamic displacement beneath the footing is not always true as it varies with frequency of the applied dynamic loads, Bycroft used the weighted average of displacement under the footing and an average magnitude of displacement functions. The weighted average solution corresponds to applying the total dynamic force $Q = \int \rho dA$, where ρ and A are the contact pressure and area, to a rigid block such that the work done by the dynamic applied force is just equal to the work done by the contact pressure. He calculated the weighted average of the displacements beneath the footing to obtain the values of the compliance functions f_1 and f_2 . All these solutions are valid for small frequency ratios ($a_0 < 1.5$), and it was shown by Richart (1962) that this range includes the operational frequencies of most of the practical problems. However the solution of Bycroft extended to rigid circular plate subjected to high frequency exciting forces

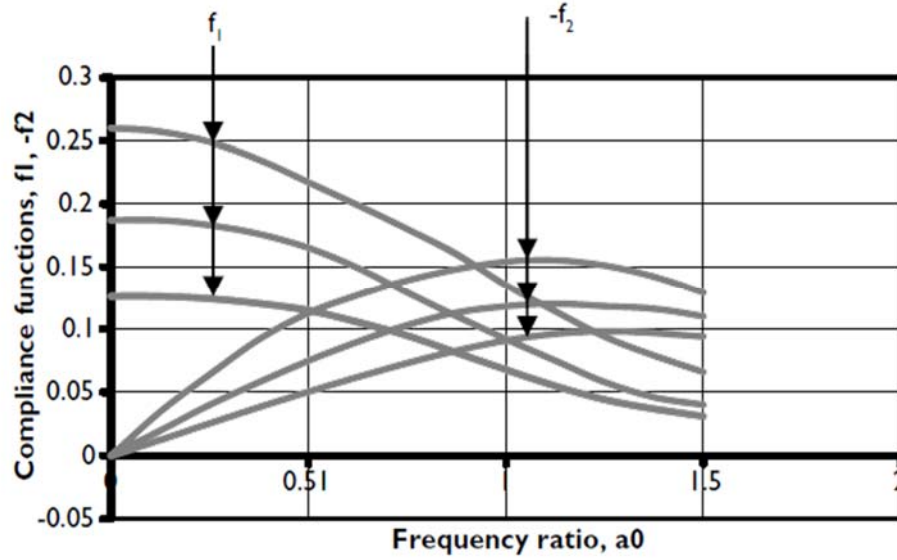


Figure B-16: Variation of the Displacement Functions with a_0 and Poisson's Ratio

Hsieh (1962) attempted to modify the original solution of Reissner in order to develop an equation similar to that for damped vibrations of single-degree free system. Hsieh's considered a rigid circular weightless disc on the surface of an elastic half space. The disc is subjected to a vertical vibration by a force

$$P = P_0 e^{i\omega t} \quad (B-13)$$

The vertical displacement of the disk can be given by

$$z = \frac{P_0 e^{i\omega t}}{Gr_0} (f_1 + if_2) \quad (B-14)$$

$$\frac{dz}{dt} = \frac{P_0 \omega e^{i\omega t}}{Gr_0} (if_1 - f_2) \quad (B-15)$$

$$f_1 \omega z - f_2 \frac{dz}{dt} = \frac{P_0 \omega}{Gr_0} (f_1^2 + f_2^2) e^{i\omega t} \quad (B-16)$$

Therefore:

$$P = P_o e^{i\omega t} \xrightarrow{\text{yields}} f_1 \omega z - f_2 \frac{dz}{dt} = \frac{P_o \omega}{Gr_o} (f_1^2 + f_2^2) e^{i\omega t} \quad (\text{B-17})$$

$$P = \left[Gr_o \left(\frac{f_1}{f_1^2 + f_2^2} \right) \right] z + \left[\frac{Gr_o}{\omega} \left(\frac{-f_2}{f_1^2 + f_2^2} \right) \right] \frac{dz}{dt} = k_z z + c_z \dot{z}$$

Hsieh (1962) was able to modify the original solution of Reissner developed an equation similar to the single degree of freedom system. Therefore, for a rigid circular foundation rested on a half space subject having a mass (m) and radius (r_o) and subject to periodic force = Q_oe^{iωt}, the response of the soil system is governed by the following equation

$$m\ddot{z} + c_z \dot{z} + k_z z = Q_o e^{i\omega t} \quad (\text{B-18})$$

$$m\ddot{z} + c_z \dot{z} + k_z z = Q_o e^{i\omega t}$$

Where:

$$c_z = \text{frequency dependent damping ratio} = \left[\frac{Gr_o}{\omega} \left(\frac{-f_2}{f_1^2 + f_2^2} \right) \right]$$

$$k_z = \text{frequency dependent stiffness} = \left[Gr_o \left(\frac{f_1}{f_1^2 + f_2^2} \right) \right]$$

Lysmer and Richart (1966) proposed simplified expressions for the soil vertical stiffness (**k_z**) and damping ratio (**c_z**) which were frequency independent. They considered a of elastic systems typical consists of a linear elastic system S that is excited by a periodic vertical force P(t),of frequency ω and amplitude P_o. The system may or may not contain viscous damping and it may have finite or infinite dimension

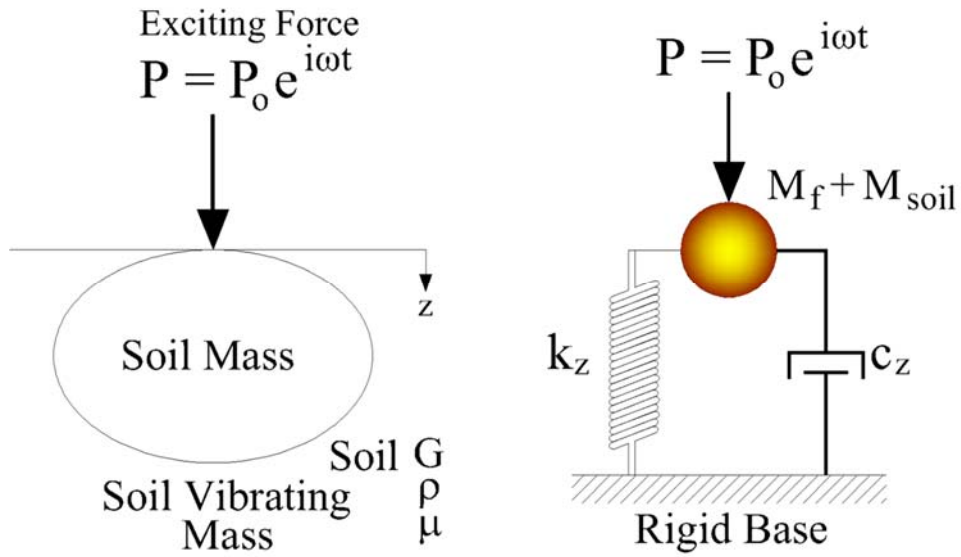


Figure B-17: Soil Idealization as Determined by Lysmer and Richart

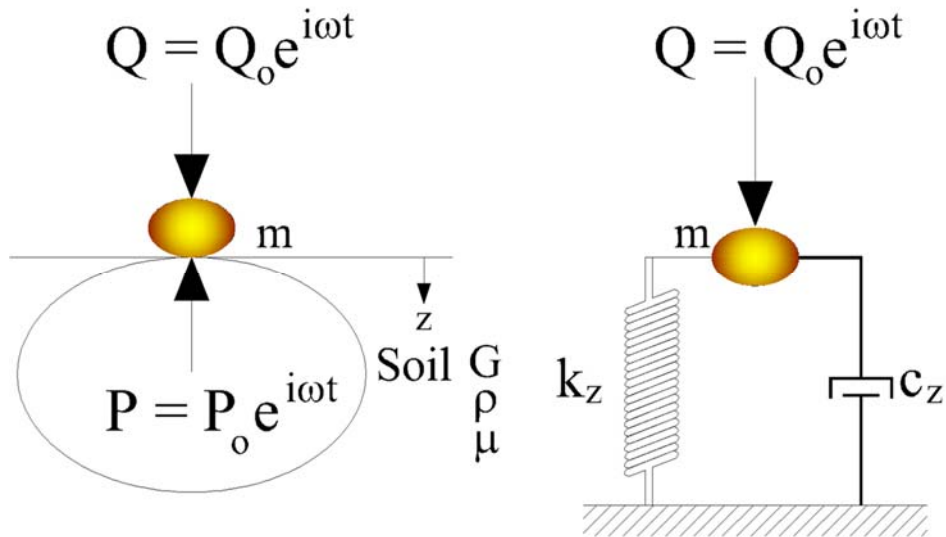


Figure B-18: Soil and Foundation Idealization as Determined by Lysmer and Richart

They redefined the displacement compliance functions in the form $f_1 + if_2$. However, Lysmer and Richart noticed that if they multiplied the compliance function by $\frac{4}{1-\mu}$, that compliance function become independent to Poisson's ratio and the compliance curves developed by Bycroft merge into the curves shown in Figure B-19.

$$\mathbf{F} = \frac{\mathbf{f}}{\left[\frac{1-\mu}{4}\right]} = \frac{\mathbf{f}_1 + i\mathbf{f}_2}{\left[\frac{1-\mu}{4}\right]} = \mathbf{F}_1 + i\mathbf{F}_2 \quad (\text{B-19})$$

Function F_1 and F_2 are independent from Poisson's ratio and as show below

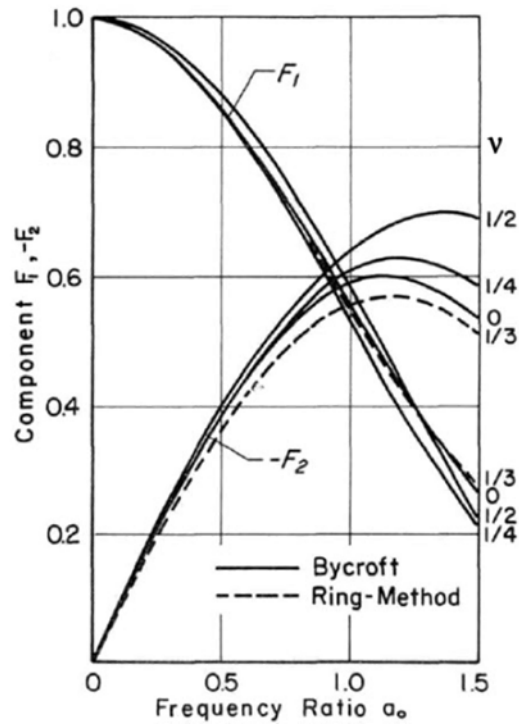


Figure B-19: Plot of F_1 - F_2 Versus a_0 for Rigid Circular Foundation Subjected to Vertical Vibration (Lysmer and Richart)

Lysmer and Richart also modified the mass ratio to

$$B_z = \left(\frac{1-\mu}{4}\right) b = \left(\frac{1-\mu}{4}\right) \left(\frac{m}{\rho r_o^2}\right) \quad (\text{B-20})$$

$$b = \text{dimensionless mass ratio} = \frac{m}{\rho r_o^2} = \left(\frac{W}{g}\right) \left[\frac{1}{\left(\frac{Y}{g}\right) r_o^3}\right] = \frac{W}{\gamma r_o^3}$$

Based on Lysmer and Richart, a for rigid circular foundation under vibration in the form of

$$m\ddot{z} + c_z\dot{z} + k_z z = Q_0 e^{i\omega t} \quad (\text{B-21})$$

Satisfactory results are obtained by defining the static spring constant for the rigid circular foundation as

$$k_z = \frac{4G}{1 - \mu} \quad (\text{B-22})$$

And the damping ratio of the soil is given by

$$c_z = \frac{3.4r_0}{1 - \mu} \sqrt{G\rho} \quad (\text{B-23})$$

B.2. Rocking Vibration of Foundation on Elastic Half Space

Arnold, Bycroft, and Wartburton provided the theoretical solutions for foundations subjected to rocking vibration for rigid circular foundations where the contact pressure (q) at any point in the plan subject to exciting moment ($M_y = M_y e^{i\omega t}$) is given by:

$$q = \frac{3M_y r \cos \alpha}{2\pi r_o^3 \sqrt{r_o^2 - r^2}} e^{i\omega t} \quad (\text{B-24})$$

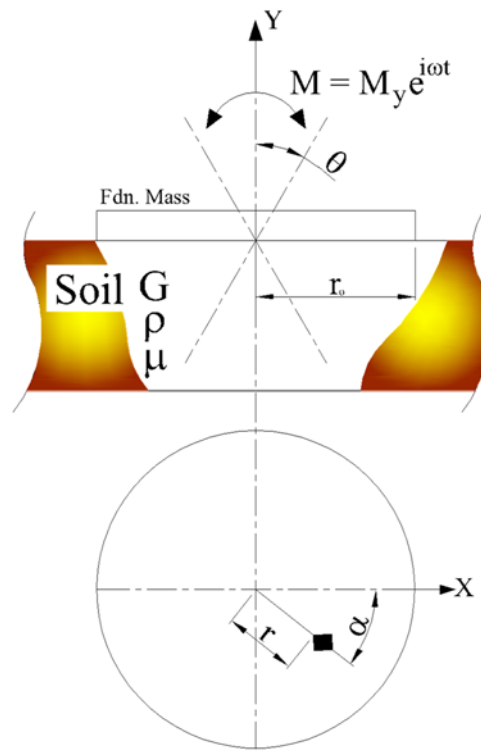


Figure B-20: Foundation Rocking Mode of Vibration

The mass-spring-dashpot model for the rigid circular foundation was developed by Hall in the same as Lysmer and Richart developed for vertical vibration. Based on Hall, the equation of motion for a rocking vibration can be given as follows:

$$I_o \ddot{\theta} + c_\theta \dot{\theta} + k_\theta \theta = M_y e^{i\omega t} \quad (\text{B-25})$$

Where:

θ = rotation of the foundation vertical axis

$$I_o = \text{mass moment of inertia of the foundation} = \frac{W_o}{g} \left(\frac{r_o^2}{4} + \frac{h^2}{3} \right)$$

W_o = Weight of the foundation

h = Height of the foundation

g = Acceleration due to gravity

The rocking stiffness coefficient and the damping ratio is given as

$$k_\theta = \text{static spring constant} = \frac{8Gr_o^3}{3(1 - \mu)} \quad (\text{B-26})$$

$$c_\theta = \text{dashpot coefficient} = \frac{0.8r_o^4\sqrt{G}}{(1 - \mu)(1 + B_\theta)} \quad (\text{B-27})$$

Where

$$B_\theta = \text{inertia ratio} = \frac{3(1 - \mu)}{8} \frac{I_o}{\rho r_o^5}$$

B.3. Sliding Vibration of Foundation on Elastic Half Space

Hall followed an approach similar to that developed by Lysmer's and Richart in developing an equivalent mechanical analog for elastic half space theory in vertical mode, He developed equivalent static springs for sliding and rocking by using the solution to the motion of a rigid circular plate on the surface of an elastic half space given by Bycroft (1956), Hall developed coupled rocking and sliding motion for all Poisson's ratios (μ).

As Shown in Figure B-21, the horizontal displacement of a weightless disc on the surface of an elastic half space with shear modulus G , Poisson's ratio ν and mass density ρ . Is given by the following equation

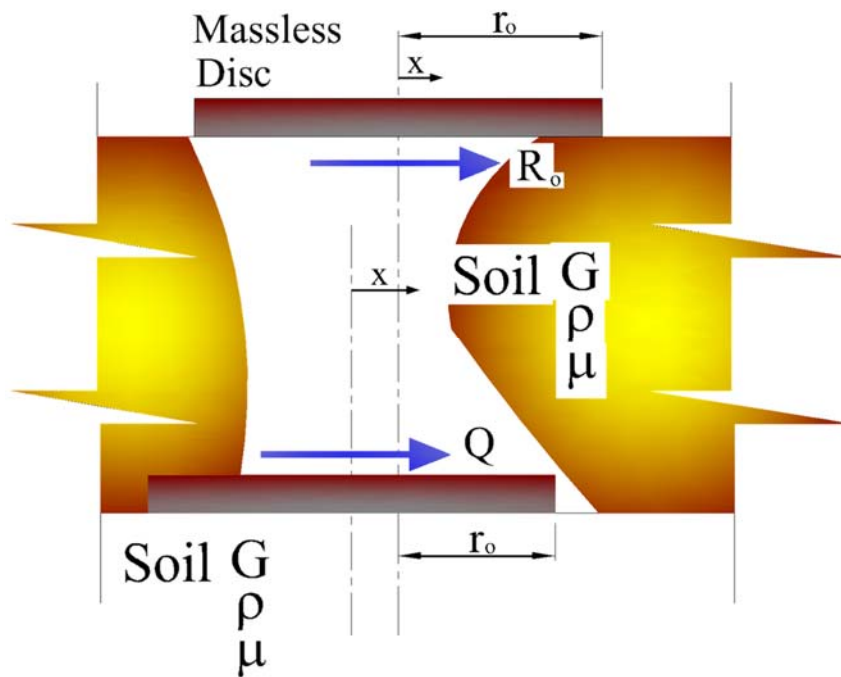


Figure B-21: Foundation Sliding Mode of Vibration

$$x = x_0 e^{i\omega t} \quad (B-28)$$

where:

x_o = motion amplitude,

ω = circular frequency

The reaction at the base of the disc is given by

$$R = R_o e^{i\omega t} \quad (\text{B-29})$$

And the displacement and reaction relation is described by the following reaction

$$x = \frac{R_o}{Gr_o} (f_1 + if_2) \quad (\text{B-30})$$

where:

f_1 and f_2 are the compliance function of Poisson's ratio (μ) and the

Dimensionless frequency $a_o = \omega r_o \sqrt{\frac{\rho}{G}}$.

Following Hsieh's, Hall took the soil reaction

$$R_o = -\frac{Gr_o}{\omega} \frac{f_2}{f_1^2 + f_2^2} \frac{dx}{dt} + Gr_o \frac{f_1}{f_1^2 + f_2^2} x \quad (\text{B-31})$$

Hall also the compliance function by introducing the notation

$$\mathbf{F}_1 = \frac{-f_1}{f_1^2 + f_2^2} \quad \text{and} \quad \mathbf{F}_2 = \frac{f_2}{a_o(f_1^2 + f_2^2)} \quad (\text{B-32})$$

Where the function F_1 and F_2 was defined by Hall as

$$F_1 = 4.573 - 0.02004a_o - 0.2122a_o^2$$

And

$$F_2 = 2.610 - 0.012574a_o - 0.1025a_o^2 \quad (\text{B-33})$$

Therefore, theoretical solutions for sliding vibration of rigid circular foundation subjected to frequency dependent dynamic force equals to $Q = Q_0 e^{i\omega t}$. Using to the mass-spring-dashpot analog solution developed by Hall, the equation of motion of the foundation is be given in the form

$$m\ddot{x} + r_0^2 \sqrt{G\rho} F_2 \dot{x} + Gr_0 F_1 x = Q_0 e^{i\omega t} \quad (B-34)$$

Where :

m = mass of the foundation system

$$k_x = Gr_0 F_1, \text{ for static case } a_0 = 0 \text{ and } \mu = 0 \xrightarrow{\text{yields}} F_1 = 4.537, \text{ and } k_x \\ = 4.537 Gr_0$$

$$\text{for } \mu \neq 0, \text{ the value of } k_x \text{ is expressed as } = \frac{32(1 - \mu)Gr_0}{7 - 8\mu}$$

$$\text{Damping Coefficient} = c_x = r_0^2 \sqrt{G\rho} F_2 = r_0^2 \sqrt{G\rho} \frac{F_2}{F_1} F_1$$

For static case, where $a_0=0$, and Poisson's = 0 the damping coefficient is expressed as

$$c_x = r_0^2 \sqrt{G\rho} F_1 \frac{2.61}{4.573} = 0.5707 F_1 r_0^2 \sqrt{G\rho}$$

For Poisson's ratio $\mu \neq 0$, the damping expression is approximated as

$$c_x = \frac{18.4(1 - \mu)}{7 - 8\mu} r_0^2 \sqrt{\rho G}$$

The foundation circular frequency is calculated as

$$\omega_x = \sqrt{\frac{k_x}{m}} = \sqrt{\frac{32(1 - \mu)Gr_o}{(7 - 8\mu)m}} \quad (B-35)$$

And the critical damping in sliding is given by

$$c_{cr} = 2\sqrt{k_x m} = 2\sqrt{\frac{32m(1 - \mu)Gr_o}{7 - 8\mu}} \quad (B-36)$$

The foundation damping ratio is given as

$$D_x = \frac{c_x}{c_{cr}} = \frac{0.288}{B_x} \quad (B-37)$$

$$B_x = \text{mass ratio} = \frac{7 - 8\mu}{32(1 - \mu)} \frac{m}{\rho r_o^3}$$

The amplitude of the foundation under constant force excitation is calculated

$$A_x = \frac{Q_o}{k_x} \frac{1}{\sqrt{\left(1 - \left(\frac{\omega^2}{\omega_x^2}\right)^2\right)^2 + \left(2D_x \frac{\omega}{\omega_x}\right)^2}} \quad (B-38)$$

where

ω = frequency of excitation

B.4. Torsional Vibration of Foundation

Reissner (1937) solved the vibration problem of a flexible circular foundation of radius r_o subjected to a torque $T = T_o e^{i\omega t}$ about axis z - z . by considering a linear distribution of shear stress where the shear stress is considered zero at center and maximum at the periphery of the foundation, as shown in Figure B-22 Reissner and Sagoli solved the same problem for the case of a rigid foundation considering a linear variation of displacement from the center to the periphery of the foundation.

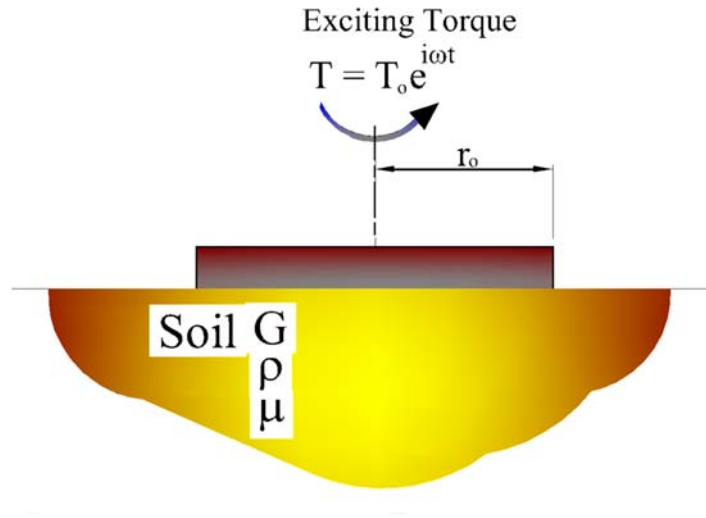


Figure B-22: Foundation Torsional Vibration

The shear stress is given as

$$\tau_{\theta} = \frac{3}{4\pi r_o^3} \frac{Tr}{\sqrt{r_o^2 - r^2}} \quad \text{for } 0 < r < r_o \quad (\text{B-39})$$

The rigid circular foundation subject to frequency dependent torsional load, using Hall analogy for the mass-spring-dashpot system, the equation of motion is given as

$$J_{zz}\alpha + c_{\alpha}\alpha + k_{\alpha}\alpha = T_o e^{-i\omega t} \quad (\text{B-40})$$

Where:

J_{zz} = Mass moment of inertia of the foundation about axis zz

c_α = dashpot coefficient for torsional vibration

k_α = static spring constant = $\frac{16}{3}Gr_o^3$

α = rotation angle due to application of the torque load

Appendix C: Static and Dynamic Efficiency Calculation

C.1. Comparison of Static Efficiency Factors between FE Solution and Randolph and Poulos

Randolph and Poulos (1986) defined the static efficiency factors as follows:

$$\alpha_a(G_{\text{soil}}, s) := \frac{0.5 \ln\left(\frac{L_{\text{pile}}}{s}\right)}{\ln\left(\frac{L_{\text{pile}}}{\text{ft}} \cdot \frac{D_{\text{pile}}}{\text{ft}} \cdot \frac{G_{\text{soil}}}{G_{\text{base}}}\right)} \quad (\text{C-1})$$

Where:

- L_{pile} is the pile length = 30 ft.
- D_{pile} is the pile diameter = 1.50 ft.
- G_{soil} is the soil shear modulus
- s is the pile spacing = 2D, 4D and 6D
- G_{base} is the base soil shear modulus = $E_{\text{pile}}/500$,
- E_{pile} is the pile Young's Modulus = 3.122×10^6 psi

Using equation (C-1) and for different values of range of soil shear modulus shown below, the following Mathcad program was created to compute the efficiency factors using Randolph and Poulos equation

	0
0	$1.1 \cdot 10^4$
1	$9 \cdot 10^3$
2	$6 \cdot 10^3$
3	$4.314 \cdot 10^3$
4	$1.078 \cdot 10^3$
5	479.307
6	269.61
7	172.551
8	119.827
9	88.036
10	67.403
11	53.256
12	43.138

$$G := \begin{pmatrix} 1100\text{ksf} \\ 900\text{ksf} \\ 600\text{ksf} \\ G_{\text{soil}}(0.20) \\ G_{\text{soil}}(0.40) \\ G_{\text{soil}}(0.60) \\ G_{\text{soil}}(0.80) \\ G_{\text{soil}}(1.00) \\ G_{\text{soil}}(1.20) \\ G_{\text{soil}}(1.40) \\ G_{\text{soil}}(1.60) \\ G_{\text{soil}}(1.80) \\ G_{\text{soil}}(2.00) \end{pmatrix} = \text{Table} \cdot \text{ksf}$$

$$\alpha_{\text{int}} := \begin{cases} \text{for } z \in 0, 1.. \text{rows}(G) - 1 \\ \quad \text{for } i \in 0, 1.. 8 \\ \quad \quad \text{for } j \in 0, 1.. 8 \\ \quad \quad \quad K_{i,j} \leftarrow \begin{cases} \alpha_a(G_z, S_{i,j}) & \text{if } S_{i,j} > 0 \\ 1 & \text{otherwise} \end{cases} \\ \quad \quad M_{z,0} \leftarrow \frac{G_z}{\text{ksf}} \\ \quad \quad M_{z,1} \leftarrow \text{mean} \left(\sum_{m=0}^{\text{rows}(K)-1} K^{(m)} \right) \end{cases}$$

The results obtained from Randolph and Poulos static efficiency equation was compared against the results determined from the FE solution for pile groups at spacing of 2D, 4D and 6D. The results are shown in Figures C-1 to C-3.

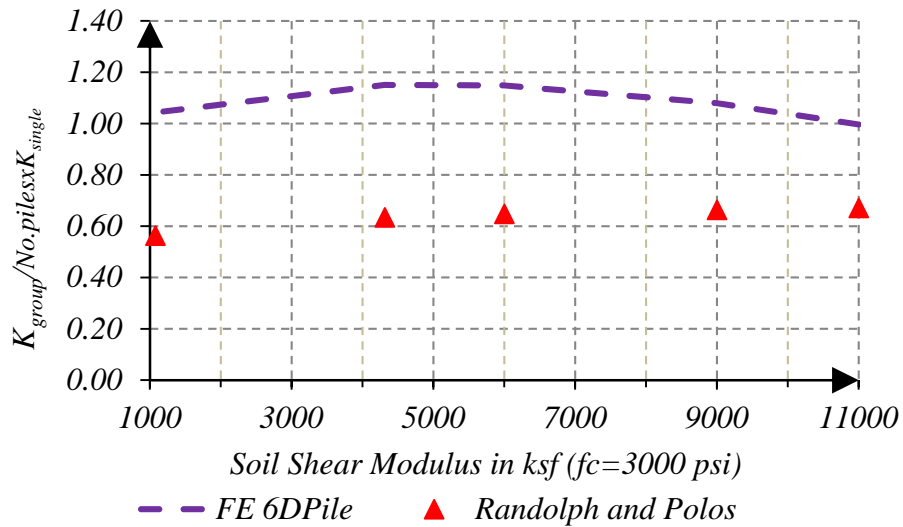


Figure C-1: Comparison of Efficiency Factors Between FE and Randolph and Poulos for Piles Spaced at $6D_{\text{pile}}$

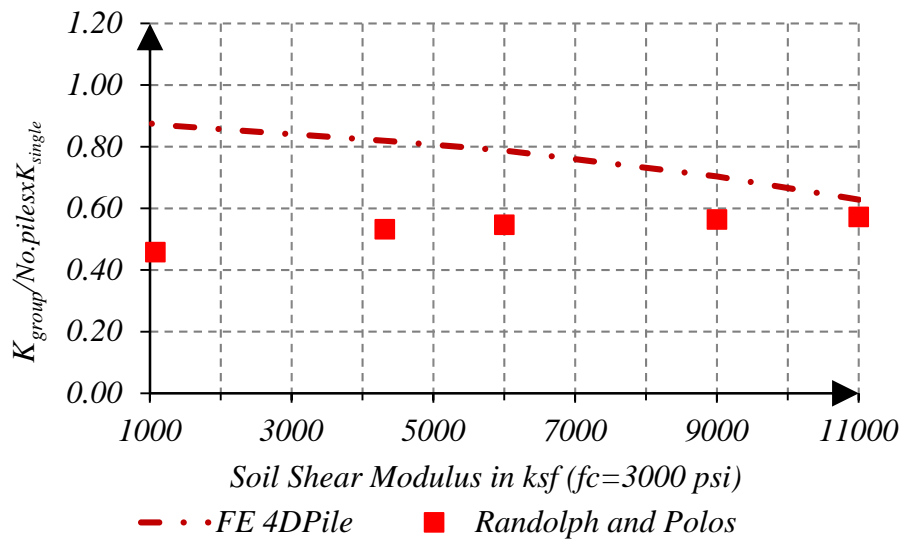


Figure C-2: Comparison of Efficiency Factors Between FE and Randolph and Poulos for Piles Spaced at 4D_{pile}

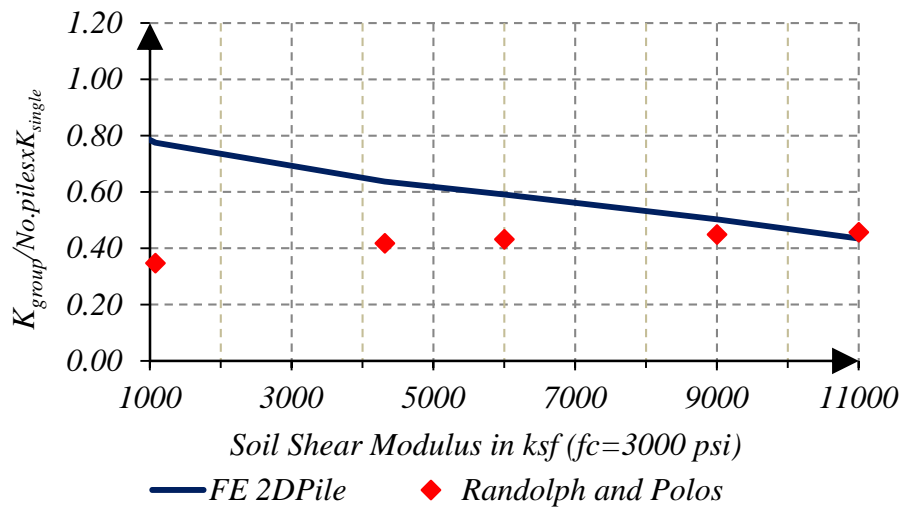


Figure C-3: Comparison of Efficiency Factors Between FE and Randolph and Poulos for Piles Spaced at 2D_{pile}

C.2. Comparison of Dynamic Efficiency Factors between FE Solution and Dobry and Gazetas.

Dobry and Gazetas (1988) defined the dynamic stiffness and damping efficiency as follows:

The dynamic stiffness efficiency

$$\alpha_{v.stiffness} = \left(\frac{S}{r_o} \right)^2 \cdot e^{\frac{-1}{V_s} (\beta \cdot \omega \cdot S)} \quad (C-2)$$

The damping efficiency

$$\alpha_{v.damping} = \left(\frac{S}{r_o} \right)^2 \cdot e^{\frac{-1}{V_s} (i \cdot \omega \cdot S)} \quad (C-3)$$

Where:

- β is the material damping = 5%
- ω is the operating frequency in rad/sec
- S is the pile spacing
- V_s is the soil shear modulus

For the range of soil shear modulus used in this study

References

1. AASHTO (2014). LRFD Bridge Design Specifications 7th Ed., Washington, D.C.
2. ACI 318 (2002). Building Code Requirements for Reinforced Concrete. ACI.
3. ACI Committee 351 (2004). Foundations for Dynamic Equipment. ACI 351.34-04.
4. American Petroleum Institute (2003). Recommended Practice for Planning, Designing and Constructing Fixed Offshore Platforms-Working Stress Design. RP 2A-WSD.
5. ANSYS Inc. (2011). General Finite Element Program, Version 13. Canonsburg, PA.
6. Ashkinadze, K., and Fang, L. (2014). A Statistical Approach to Dynamic Response of Pile Groups in Foundation for Vibrating Machinery, Vulnerability, Uncertainty and Risk. American Society of Civil Engineers, Reston, 465-474.
7. Baranov, V.A. (1967). On the Calculation of Excited Vibrations of an Embedded Foundation. Polytechnic Institute of Riga, 195-209.
8. Barkan, D.D. (1962). Dynamics of Bases and Foundations. McGraw-Hill Book Co., NY.
9. Barton, Y.O. (1982). Laterally loaded model piles in sand: Centrifuge tests and finite element analysis. Ph.D. Thesis, University of Cambridge, GB.
10. Bea, R.G., and Audibert, J.M.E. (1979). Performance of Dynamically Loaded Pile Foundations. Proc., 2nd Int. Conf. on Behavior of Offshore Structures, BOSS'79, Imperial College, London, GB, 477-490.
11. Broms, B. (1964a). The Lateral Resistance of Piles in Cohesive Soils. Journal of the Soil Mechanics and Foundation Division. American Society of Civil Engineers, 90(2): 27-63.

12. Broms, B. (1964b). The Lateral Resistance of Piles in Cohesive Soils. *Journal of the Soil Mechanics and Foundation Division. American Society of Civil Engineers*, 90(3), 123-156.
13. Bycroft, G. N. (1956). Forced Vibration of a Rigid Circular Plate on a Semi-Infinite Elastic Space and an Elastic Stratum, *Philosophical Transactions of the Royal Society. London, Series A* 248, 327-386.
14. Chowdhury, I. and Dasgupta, P.S (2006). Dynamic Response of Piles Under Vertical Loads. *Indian Geotechnical Journal*, 36(2).
15. Chowdhury, I. and Dasgupta, P.S. (2009). *Dynamic of Structures and Foundations, A Unified Approach, I. Fundamentals*, CRC Press.
16. Chowdhury, I. and Dasgupta, P.S. (2009). *Dynamic of Structures and Foundations, A Unified Approach, II. Applications*, CRC Press.
17. Das, B.M. and Ramana, G.V. (2011). *Principals of Soil Dynamics*, 2nd edition. CENGAGE Learning.
18. Davisson, M.T. and Gill H.L. (1963). Laterally Loaded Piles in a Layered Soil System. *Journal of the Soil Mechanics and Foundations Engineering, ASCE*, 89(3), pp 63-94.
19. Deeks, A.J. and Randolph, M.F. (1995). A Simple Model for Inelastic Footing Response to Transient Loading. *International Journal for Numerical and Analytical Methods in Geomechanics*, 19(5), 307-329.
20. Dobry, R. and Gazetas, G. (1985). Dynamic Stiffness and Damping of Foundations by Simple Methods, *Vibration Problems in Geotechnical Engineering* (G. Gazetas and E.T. Selig, eds.), ASCE, 77-107.

21. Dobry, R. and Gazetas, G. (1986). Dynamic Response of Arbitrarily Shaped Foundations, *Journal of Geotechnical Engineering*, ASCE, 112(2), 109-135.
22. Dobry, R. and Gazetas, G. (1988). Simple Method for Dynamic Stiffness and Damping of Floating Pile Groups, *Geotechnique*, 38(4), 557-574.
23. Dobry, R. (2014). Simplified Methods in Soil Dynamics. *Soil Dynamics and Earthquake Engineering*, 61-62, 246-268.
24. Erden, S.M. and Stokoe, K.H. (1975). Effects of Embedment on Foundation Response. *Shock and Vibration Problems in Geotechnical Engineering*, ASCE National Convention, Denver, CO.
25. Fan, K., Gazetas, G., Kaynia, A., Kausel, E., and Ahmad, S. (1991). Kinematic Seismic Response of Single Piles and Pile Groups. *J. Geotech. Engrg.*, 117(12), 1860–1879
26. Forehand, P.W. and Reese, J.L. (1964). Prediction of Pile Capacity by the Wave Equation. *Journal, Soil Mechanics and Foundations Division*, 90(SM 2), 1-25.
27. Gazetas, G. and Roesset, J. M. (1979). Vertical Vibrations of Machine Foundations, *Journal of the Geotechnical Engineering Division*, ASCE, 105(GT12), 1435-1454.
28. Gazetas, G. (1984). Seismic Response of End-Bearing Single Piles, *Soil Dynamics and Earthquake Engineering*, 3(2).
29. Gazetas, G. and Dobry, R. (1984). Horizontal Response of Piles in Layered Soils, *Journal of Geotechnical Engineering*, ASCE, 110(1), 20-40.
30. Gazetas, G. (1991). Foundation Vibrations. *Foundation Engineering Handbook*, 2nd edition, Van Nostrand Reinholds, 553-593.

31. Gazetas, G. (1991). Formulas and Charts for Impedances of Surface and Embedded Foundations, *Journal of Geotechnical Engineering*, ASCE, 117(9), 1363-1381.
32. Gazetas, G. and Makris, N. (1991). Dynamic Pile-Soil-Pile Interaction Part 1, Analysis of Axial Vibration. *Earthquake Engineering and Structural Dynamics* 20(2), 115-132.
33. Gazetas, G., Fan, K. and Kaynia, A. (1992). Dynamic Response of Pile Groups with Different Configurations. *Soil Dynamics and Earthquake Engineering*, 239-257.
34. Gupta, B.N. (1972). Effect of Foundation Embedment on the Dynamic Behavior of Foundation of the foundation—Soil System. *Geotechnique*, 22(1), 129–137.
35. Han, Y.C. (2010). Dynamic Analysis for Foundation of Vibrating Equipments Considering Soil Structure Interaction. *Soil Dynamics and Earthquake Engineering*, ASCE, pp 71-76
36. Hardin, B.O. and Richart, F.E., Jr. (1963). Elastic Wave Velocities in Granular Media. *JSMFD*, ASCE, 89 (SM1).
37. Hardin, B.O. (1965). The Nature of Damping in Sands. *J. Soil Mechanics Foundation Division*. ASCE, 91(SM-1), 63–97.
38. Hardin, B.O. and Drnevich, V.P. (1973). Shear Modulus and Damping in Soils, Design Equations and Curves. *JSMFD*, ASCE, Vol. 98, No. SM7.
39. Hetenyi, M. (1946). *Beams on Elastic Foundation; Theory with Applications in the Fields of Civil and Mechanical Engineering*. University of Michigan Press.
40. Holeyman, A.E. (1985). Dynamic Non-Linear Skin Friction of Piles. *Proceedings of the International Symposium on Penetrability and Driveability of Piles*, 173-176.

41. Holeyman, A.E. (1988). Modeling of Dynamic Behavior at the Pile Base. Proceedings of the 3rd International Conference on the Application of Stress-Wave Theory to Piles, 174-185.
42. Holeyman, A., Legrand, C., and Van Rompaey, D. (1996). A Method to Predict the Drivability of Vibratory Driven Piles. Proceedings of the 5th International Conference on the Application of Stress-Wave Theory to Piles, 1101-1112.
43. Hsieh, T.K. (1962). Foundation Vibrations. Proceedings of Institute of Civil Engineers, 22, 211–226.
44. .Hu, Y., Randolph, M.F. and Watson, P.G. (1999). Bearing Response of Skirted Foundation on Nonhomogeneous Soil. Journal of Geotechnical and Geoenvironmental Engineering, ASCE, 125(11), 924-935.
45. .Kagawa, T., Kraft, L. M. (1980). Soil-Pile-Structure Interaction of Offshore Structures During an Earthquake. Proceedings of 12th Annual Offshore Technological Conference, 3, 235–245.
46. Kausel, E. and Roesset. J. M. (1975). Dynamic Stiffness of Circular Foundations. Journal of Engineering Mechanics Division. ASCE, 101(6), 771-785.
47. Kavvadas, M. and Gazetas, G. (1993). Kinematic Seismic Response and Bending of Free-Head Piles in Layered Soil. Geotechnique, 43, 2, pp207-222.
48. Kuhlemeyer, R.L. and Lysmer, J. (1973). Finite Element Method Accuracy for Wave Propagation Problems. Journal of Soil Mechanics and Foundations, ASCE 99 (SM5).
49. Lambe, T. W. and Whitman, R. V. (1969). Soil Mechanics. John-Wiley and Sons, NY.

50. Lok, T., Pestana, J. and Seed, R. (1998). Numerical Modeling and Simulation of Coupled Seismic Soil-Pile-Structure Interaction. ASCE, Geotechnical Earthquake Eng. and Soil Dynamics, Vol. II, 1211-1222.
51. Lysmer, J. (1965). Vertical Motions of Rigid Footings. Ph.D. thesis, University of Michigan, Ann Arbor.
52. Lysmer, J. and Richart, F. E. (1966). Dynamic Response of Footings to Vertical Loading. Journal of the Soil Mechanics and Foundations Division. ASCE, 92(1), 65-91.
53. Lysmer, J., (1978). Finite Element Analysis of Soil-Structure Interaction. Report No. UCB/EERC-78/29, University of California, Berkeley, CA.
54. Luco, J. E., and Westmann, R.A. (1968). Dynamic Response of a Rigid Footing Bonded to an Elastic Half-Space. Journal of Applied Mechanics, ASME, 35E, 697.
55. Luco, J.E. and Westmann, R.A. (1971). Dynamic Response of Circular Footings. Journal of Engineering Mechanic Division, ASCE, 97, EMS, 138.
56. Luco, J.E. (1974). Impedance Functions for a Rigid Foundation on a Layered Medium. Nuclear Engineering. Design, 31, 204.
57. Manna, B. and Baidya, D. (2009). "Vertical Vibration of Full-Scale Pile—Analytical and Experimental Study." J. of Geotech. and Geoenviron. Eng., ASCE, 135(10), 1452–1461.
58. Makris, N. and Gazetas, G. (1992). Dynamic Pile-Soil-Pile Interaction. Part II: Lateral and Seismic Response. Earthquake Engineering and Structural Dynamics, 21, 145-162.

59. Matlock, H. and Reese, L.C. (1960). Generalized Solutions for Laterally Loaded Piles. *Journal of Soil Mechanics and Foundation Division, ASCE*, 86, 63-91.
60. Matlock, H. (1970). Correlations for Design of Laterally Loaded Piles in Soft Clay. 2nd Annual Offshore Technology Conference, Houston, Texas, 577 - 594.
61. Mylonakis, G. and Gazetas G. (1996). Settlement and Additional Internal Forces of Grouped Piles in Layered Soil. City College of City University of New York, National Technical University, Athens
62. Naggar, M.H.EI. and Novak, M. (1995). Nonlinear Lateral Interaction in Pile Dynamics. *Journal of Soil Dynamics and Earthquake Engineering*, 14, 141-157.
63. Naggar, M.H.EI. and Novak, M. (1996). Nonlinear Analysis for Dynamic Lateral Pile Response. *Journal of Soil Dynamics and Earthquake Engineering*, 15(4), 233-244.
64. Nogami, T., Otani, J., Konagai, K. and Chen, H. (1992). Nonlinear Soil-Pile Interaction Model for Dynamic Lateral Motion. *Journal of Geotechnical Engineering*, 118(1).
65. Novak, M. and Beredugo, Y.O. (1972). Vertical Vibration of Embedded Footings. *Journal of the Soil Mechanics and Foundations Division, ASCE*, 98(SM12), 1291-1310.
66. Novak, M. and Sachs, K. (1973). Torsional and Coupled Vibrations of Embedded Footings. *International Journal of Earthquake Engineering and Structural Dynamics*, 2(1), 11-33.
67. Novak, M. (1974). Dynamic Stiffness and Damping of Piles. Faculty of Engineering Science, University of Western Ontario, London, Ontario.

68. Novak, M. (1976). Vertical Vibration of Floating Piles. Faculty of Engineering Science, University of Western Ontario, London, Ontario.
69. Novak, M. and El Sharnouby, B. (1983). Stiffness Constants of Single Piles. *Journal of Geotechnical Engineering, Division, ASCE*, 109, 961–974.
70. Penzien, J., Scheffey, C.F. and Parmelee, R.A. (1964). Seismic Analysis of Bridges on Long Piles, *Journal Engineering Mechanics Division, ASCE*, EM3, 223-254.
71. Petrash1, A., Bounds, W. and Wong, S. (2011). Designing Foundations for Vibrating Machinery: Dealing With Soil and Software Issues. ASCE Structures Congress, ASCE.
72. Poulos, H. G. and Davis, E. (1980). *Pile Foundation Analysis and Design*. New York: Wiley and Sons.
73. Quinlan, P.M. (1953). The Elastic Theory of Soil Dynamics, *Symp. on Dyn. Test of Soils. ASTM STP No. 156*, 3-34.
74. Randolph, M.F. and Murphy, B.S. (1985). Shaft Capacity of Driven Piles in Clay. *OTC4883*, 371-378.
75. Randolph, M.F. and Simons, H.A. (1986). An Improved Soil Model for One Dimensional Pile Driving Analysis. *Proceedings of the 3rd International Conference of Numerical Methods in Offshore Piling*, 3-17.
76. Randolph, M.F. and H.G. Poulos (1986). Estimating the flexibility of off shore pile groups. *Proceedings of the 2rd International Conference of Numerical Methods in Offshore Piling, Austin*, 318-328.

77. Reissner, E. (1936). Stationäre, Axialsymmetrische, Durch Eine Schut-Telnde Masse Erregte Schwingungen Eines Homogenen Elastischen Halbraumes. Ing. Arch., 7, 381.
78. Reissner, E. and Sagochi, H.F. (1944). Forced Torsional Oscillations of an Elastic Half Space. Journal of Applied Physics, 15, 652-662.
79. Richart, F.E., Jr. (1962). Foundation Vibrations. Transaction, ASCE, 127, Part I, 863-898.
80. Richart, F. and Whitman, R.V. (1967). Comparison of Footing Foundation Tests with Theory. Journal of the Soil Mechanics and Foundations, ASCE, 93 (SM6), 143-167.
81. Richart, F.E., Hall, J.R., and Woods, R.D. (1970). Vibration of Soils and Foundations. Prentice-Hall, Inc., Englewood Cliffs, NJ.
82. Seidel, M. and Coronel, M. (2011). A New Approach for Assessing Offshore Piles Subjected to Cyclic Axial Loading. Geotechnik, 34.
83. Sheta, M. and Novak, M. (1982). Vertical Vibration of Pile Groups. Journal of Geotechnical Engineering Division, ASCE 108 (GT4), 570-590.
84. Smith, E.A.L. (1960). Pile-Driving Analysis by the Wave Equation. Journal of Soil Mechanics and Foundations Division, 86(EM 4), 35-61.
85. Sung, T.Y. (1953). Vibration in Semi-Infinite Solids Due to Periodic Surface Loading. Sc.D. Thesis, Harvard University.
86. Swane, I.C. and Poulos, H.G. (1982). A Theoretical Study of the Cyclic Shakedown of Laterally Loaded Piles. Research Report R415, University of Sydney, School of Civil and Mining Engineering.

87. Tajimi H. (1966). Earthquake Response of Foundation Structures Report. Faculty of Science and Engineering, Nihon University Tokyo 1.1-3.5.
88. Tazoh, T., Wakahara, T., Shimizu, K. and Matsuzaki, M. (1988). Effective Motion of Group Pile Foundations. Proceedings of the 9th World Conference on Earthquake Engineering, Tokyo, 3, 587-592.
89. Waas, G. and Hartmann, H.G. (1981). Piles Subjected to Dynamic Horizontal Loads. European Simulation Meeting on Modeling and Simulation of Large Scale Structural Systems, Capri, 17.
90. Weissmann, G.F. and Hart, R.R. (1961). Damping Capacity of Some Granular Soils. ASTM STP 305, 45-54.
91. Whitman, R.V. and Richart, F.E., Jr. (1967). Design Procedures for Dynamically Loaded Foundations. Journal of the Soil Mechanics and Foundations Division, ASCE, 93(SM6), 169-193.
92. Whitman, R.V. (1970). Soil Structure Interaction—Seismic Design for Nuclear Power Plants, The MIT Press, Cambridge, Massachusetts.
93. Whitman, R.V. (1972). Analysis of Soil-Structure Interaction—A State of the Art Review. Soil Publications No-300, M.I.T.
94. Wilson, E.L. (2002). Three-Dimensional Static and Dynamic Analysis of Structures, 3rd Edition. Computer and Structure, Inc., Berkeley, CA.
95. Wolf, J.P. and Von Arx, G, A. (1978). Impedance Functions of a Group of Vertical Piles. Proceedings of the ASCE Specialty Conference on Earthquake Engineering and Soil Dynamics, 11, 1024-1041.

96. Wolf, J.P. (1994). Foundation Vibration Analysis: Using a Simple Physical Model. Prentice-Hall, Englewood-Cliffs, NJ.
97. Woods, R.D. (1968). Screening of Surface Waves in Soils. Journal of the Soil Mechanics and Foundations Division, ASCE, 94, (SM4), 951-979.
98. Woods, R.D., Barnett, N.E. and Sagesser, R. (1974). Holography – A New Tool for Soil Dynamics. Journal of Geotechnical Engineering Division, ASCE, 100(GT11), 1231-1247.